



HAL
open science

Influence of the solvent sorption, additivition, and chemical modification on the molecular mobility dynamics of Polyamide 6,6 amorphous phase and its consequences on the tensile and impact strength properties of this polymer

Agustin Rios de Anda

► **To cite this version:**

Agustin Rios de Anda. Influence of the solvent sorption, additivition, and chemical modification on the molecular mobility dynamics of Polyamide 6,6 amorphous phase and its consequences on the tensile and impact strength properties of this polymer. Other. Université Claude Bernard - Lyon I, 2012. English. NNT : 2012LYO10259 . tel-00933978

HAL Id: tel-00933978

<https://theses.hal.science/tel-00933978>

Submitted on 21 Jan 2014

HAL is a multi-disciplinary open access archive for the deposit and dissemination of scientific research documents, whether they are published or not. The documents may come from teaching and research institutions in France or abroad, or from public or private research centers.

L'archive ouverte pluridisciplinaire **HAL**, est destinée au dépôt et à la diffusion de documents scientifiques de niveau recherche, publiés ou non, émanant des établissements d'enseignement et de recherche français ou étrangers, des laboratoires publics ou privés.

N° d'ordre 259-2012

Année 2012

THESE DE L'UNIVERSITE DE LYON

Délivrée par

L'UNIVERSITE CLAUDE BERNARD LYON 1

ECOLE DOCTORALE MATERIAUX

DIPLOME DE DOCTORAT

(arrêté du 7 août 2006)

soutenue publiquement le 5 décembre 2012

par

M. Agustín RIOS DE ANDA

Influence of the solvent sorption, additivation, and chemical modification on the molecular mobility dynamics of Polyamide 6,6 amorphous phase and its consequences on the tensile and impact strength properties of this polymer.

Directeur de thèse : M. Paul SOTTA

Encadrant Rhodia-Solvay : Mme. Louise-Anne FILLOT

JURY

Mme. Valérie MIRI	Rapporteur
M. Stéphane MARAIS	Rapporteur
Mme. Eliane ESPUCHE	Examineur
M. Jean-Louis HALARY	Examineur
M. Ángel ALEGRÍA	Examineur
M. Paul SOTTA	Directeur de thèse
Mme. Louise-Anne FILLOT	Encadrant Rhodia-Solvay

Remerciements

Je tiens tout d'abord remercier Paul Sotta et Louise-Anne Fillot, mes encadrants de thèse et les meilleurs encadrants qu'on peut avoir, pour leur temps, leur support, leur aide, leurs conseils, leur infatigable patience et leur confiance tout au long de ce travail. Je serais toujours reconnaissant envers eux pour m'avoir donné l'opportunité de travailler avec eux pendant ces trois ans (et demi avec le stage) et de toujours avoir été disponibles avec la meilleure disposition.

Je remercie Mme. Valérie Miri et M. Stéphan Marais d'avoir accepté de rapporter ce travail. Egalement je remercie Mme. Eliane Espuche, M. Jean-Louis Halary et M. Ángel Alegria d'avoir accepté de prendre part au jury de thèse.

Je voudrais remercier Ludovic Odoni et Didier Long pour m'avoir donné l'opportunité de réaliser ce projet de thèse au sein du Laboratoire Polymères et Matériaux Avancés ainsi que pour leur temps, les discussions que nous avons tenu tout au long de ce projet et leurs apports très pertinents et importants à ce travail.

Je remercie énormément Sandrine Rossi pour tout le temps et son aide qu'elle a consacré à la réalisation de ce travail de thèse et surtout pour sa bonne volonté, sa bonne humeur et sa confiance inconditionnelle. Sans Sandrine ce travail n'aurait pas pu être réalisé. Mille mercis à notre maman du LPMA.

Je tiens à remercier Caroll Vergelati, Lise Trouillet-Fonti, Olivier Sanseau, Loic Vanel, Jean-Yves Delannoy, Pierre-Yves Lahary, Cécile Corriol, et Magalie Davezac pour leurs discussions très enrichissantes autour de ce travail ou de la vie de tous les jours, notamment en géopolitique, football et rugby.

Je voudrais remercier de la même manière Cristiane Prebet, Sylvie Ghiringuelli, Vicent Curtil, Hélène Coste, Frédéric Brun, Olivier Andrès, Leo Georges, Séverine Dauffer, Didier Tupinier, Olivier Gilbain et Michel Sorin pour leur précieuse aide et leur temps consacré à la transformation de nos formulations et au développement des divers manipulations dans les laboratoires de physico-chimie, mécanique, ou de rhéologie. Je les remercie aussi pour les bons temps passés autour des cafés, des gâteaux et des trottinettes.

Egalement, je suis très reconnaissant envers Serge Henrot, Johanna Rhys, Mathias Bréhelin, Jean Claude Masteaud, Danielle Lamberet, Stéphane Jéol, et Daniel Duchêne pour leur aide précieuse et leur expertise dans des essais de DVS, de spectroscopie, dans l'étude des formulations polyamide modifiés, et de la simulation des mélanges ternaires des solvants. Je remercie de la même manière Erwan Jeanne pour son temps consacré à la caractérisation de nos échantillons par Rayons X.

Je voudrais remercier profondément mes frères d'armes thésards, post-docs, et stagiaires que j'ai pu côtoyer pendant mon séjour de 42 mois au sein du LPMA. Même si la liste est longue, je tiens à remercier à chacun d'eux pour les bons moments que nous avons partagés ensemble au sein du laboratoire et aussi à l'extérieur. Je souhaite le meilleur pour leur avenir à chacun d'eux.

Je n'ai pas de mots pour remercier infiniment Arno, Rober, Alex, Clio, Cécile, Ludi, Eddy, Pauline, Caro, Vincent, Simona, Cris, Chloé, Max, Charlotte et Naji, sans qui la vie dans le labo et surtout celle à l'extérieur n'aurait pas eu le même goût. Je garderais pour toujours les parties de billard, les tournois de foot et de volley, le squash, la découverte de la gym suédoise, les matches de la Coupe du Monde de Rugby à 9 du mat', aller de Berlin-Ouest à Berlin-Est et vice-versa à toutes heures de la journée, se déguiser pour Halloween, plonger dans les eaux Bretonnes en octobre, découvrir l'accueil chaleureux des Aveyronnais, apprendre à comment-changer-vous-même-vos-vitres-de-voiture, ou chercher les frites les plus dignes de ce nom à Bruxelles, parmi d'autres aventures plus ou moins disjonctées et tout le temps que nous avons passé ensemble. Je vous souhaite mes meilleurs vœux à chacun de vous pour vos vies professionnelles et personnelles et je vous dis sincèrement : vous êtes devenus ma famille à Lyon.

Last but not least, quisiera también agradecer a papá Nacho, a mamá Bety, a Joyce y a Ponis por darme alas, por todo el apoyo incondicional y el tiempo que siempre me han brindado, por apoyarme en todas mis decisiones, hayan sido las más cuerdas o las más locas, y por estar conmigo siempre en las buenas y en las malas. Sin ellos esta aventura no habría sido posible, y aunque la distancia es grande, nunca, nunca hemos estado lejos.

Finalmente, dedico esta tesis a dos personas muy especiales: mis abues Brígido y Lupe que siempre estuvieron y están conmigo, que me vieron crecer, y que siempre creyeron en mí aún antes de que supiera caminar. No hay día en el que no piense en ellos y en el que no los extrañe ¡Gracias por todo!

**“They say you don’t grow up, you just grow old,
it’s safe to say I haven’t done both”**

Yellowcard in *Here I am alive*

Index

Remerciements	5
Index.....	9
Introduction.....	15
I. Background Review on PA66.....	19
I.1 Structure and morphology	20
I.1.1. Molecular structure	20
I.1.2. Crystalline phase.....	21
I.1.2.1. Crystalline lattice.....	21
I.1.2.2. Crystalline lamellae	23
I.1.3. Molecular mobility of the amorphous phase	25
I.1.3.1. PA66 molecular relaxations	25
I.1.3.2. Focus on the main α relaxation.....	26
I.1.4. Heterogeneity of the amorphous phase	28
I.2. Sorption, diffusion, and pervaporation of pure solvents in PA66.....	29
I.2.1. Solvent sorption at equilibrium	29
I.2.1.1. Parameters defining polymer-solvent interactions.....	29
I.2.1.2. Influence of the crystalline phase on solubility	30
I.2.1.3. Sorption isothermal mechanisms	31
I.2.1.4. Isothermal solvent sorption in polyamides	35
I.2.2. Mechanisms of solvent diffusion in PA66	36
I.2.2.1. Fickian and Case II diffusion regimes	36
I.2.2.2. Sorption kinetics of solvents in polyamides	39
I.2.3. Solvent pervaporation	41
I.2.3.1. Pervaporation mechanisms	41
I.2.3.2. Solvent pervaporation in polyamides.....	42
I.3. Interactions of PA66 with solvent mixtures	43
I.3.1. Solvent mixtures composed of polar and non-polar molecules	43
I.3.2. Polyamides as selective membranes	44
I.4. Influence of solvents on PA66 molecular mobility.....	44
I.4.1. Effect of solvents on PA66 molecular relaxations	44
I.4.1.1. Effect of water on PA66 glass transition : experimental data	44
I.4.1.2. Effect of solvents on PA66 secondary relaxations.....	46
I.4.2. Plasticization models for a polymer-polymer or polymer-plasticizer mixture.....	47
I.5. Influence of the crystalline and amorphous phases on PA66 mechanical properties...	49
I.5.1. Influence of the crystalline phase and the temperature on the mechanical properties of polyamides.....	49
I.5.1.1. Influence of the crystalline phase.....	49
I.5.1.2. Influence of the temperature	52
I.5.2. Influence of water on polyamide mechanical properties	54
I.6. Objectives of the thesis	55
II. Materials, samples and techniques.....	61
II.1. Polymer formulations.....	61
II.1.1. Neat PA66	61

II.1.2. Modified PA66	61
II.1.2.1. Chemically-modified PA66	61
II.1.2.2. Additivated PA66	62
II.2. Polymer processing	63
II.2.1. Film-cast extrusion.....	63
II.2.2. Compounding	64
II.2.3. Injection-molding.....	65
II.2.4. Review on the processed PA6,6 samples	66
II.3. Experimental techniques.....	66
II.3.1. Structural characterization	66
II.3.1.1. Crystalline phase	66
II.3.1.1.1. Crystalline fraction	66
II.3.1.1.2. Crystalline structure	67
II.3.1.2. Molecular mobility.....	68
II.3.1.2.1. Calorimetry.....	68
II.3.1.2.2. Dynamic mechanical analyses.....	71
II.3.1.2.3. Dielectric analyses.....	72
II.3.2. Sorption and diffusion	77
II.3.2.1. Pure solvents.....	77
III.3.2.1.1. Sorption of liquid solvents	77
III.3.2.1.2. Sorption of vaporized solvents	78
II.3.2.2. Ternary mixtures.....	79
II.3.2.2.1. Measurement of the chemical activities of the ternary mixtures.....	79
II.3.2.2.1. Measurement of the composition of the absorbed species by PA6,6	81
II.3.3. Pervaporation	81
II.3.4. Mechanical properties	82
II.3.4.1. Tensile strength	82
II.3.4.2. Impact strength.....	83
III. Sorption and plasticizing effect of pure polar or non-polar solvents and mixtures of solvents in neat PA66	89
III.1. Heterogeneity of the amorphous phase	89
III.2. Sorption of pure polar and non-polar solvents	92
III.2.1. Sorption at equilibrium.....	92
III.2.2. Discussion of the results on solvent sorption in PA6,6	97
III.3. Effect of pure solvents on the molecular mobility of neat PA6,6	103
III.3.1. Effect of pure solvents on the main alpha relaxation (associated to the glass transition)	103
III.3.2. Effect of pure solvents on the secondary relaxations	110
III.3.3. Discussion of plasticization mechanisms by solvents.....	116
III.3.3.1. Case of toluene	117
III.3.3.2. Case of water	119
III.3.3.3. Case of ethanol	120
III.3.4. Relationship between solvent sorption and mesoscale simulations	121
III.3.4.1. Solvent sorption kinetics in PA6,6	121
III.3.4.2. Modeling of solvent diffusion	123
III.4. Effect of pure solvents on the crystalline phase of neat PA6,6	127
III.5. Ternary solvent mixtures.....	129
III.5.1. Thermodynamics of ternary mixtures	129

III.5.2. Sorption of ethanol-toluene-isooctane mixtures in neat PA6,6	136
III.5.3. Effect of ethanol-toluene-isooctane mixtures on PA66 molecular mobility.....	140
III.6. Conclusion	140
IV. Properties of additivated and chemically-modified PA66	147
IV.1. Effect of PA6,6 modification on its crystalline phase.....	147
IV.1.1. Effect of PA6,6 modification on crystallization and melting	147
IV.1.2. Effect on the crystalline structure	149
IV.2. Effect of PA6,6 modification on the amorphous phase molecular mobility.....	151
IV.2.1. Heterogeneity of the amorphous phase.	151
IV.2.2. Effect of PA6,6 modification on the glass transition.....	152
IV.2.3. Effect of PA6,6 modification on the secondary relaxations.....	155
IV.2.3.1. Beta relaxation.....	156
IV.2.3.2. Gamma relaxation	158
IV.3. Effect of PA6,6 modification on the barrier properties and molecular mobility.....	160
IV.3.1. Effect of PA6,6 modification on the solvent sorption at equilibrium	160
IV.3.1.1. Case of water	161
IV.3.1.2. Case of ethanol	162
IV.3.1.3. Case of toluene	163
IV.3.2. Plasticization effect of absorbed solvents in modified PA66 formulations	164
IV.3.3. Effect of PA6,6 modification on the solvent sorption kinetics.....	165
IV.3.3.1. Case of water	166
IV.3.3.2. Case of ethanol	166
IV.3.3.3. Case of toluene	167
IV.3.4. Effect of PA6,6 modification on the solvent pervaporation kinetics	168
IV.4. Effect of PA6,6 amorphous phase molecular mobility on its mechanical properties	170
IV.4.1. Effect of PA66 molecular mobility on its tensile strength properties.....	170
IV.4.1.1. Case of the Young's (tensile) modulus	170
IV.4.1.2. Case of the Yield Stress.....	172
IV.4.2. Effect of PA66 molecular mobility on its impact strength properties	173
IV.4.2.1. Case of the brittle-tough transition temperature	173
IV.4.2.2. Effect of the molecular mobility on the resilience	176
IV.5. Compromise between impact strength and pervaporation properties	178
IV.6. Conclusion	179
General conclusion	185
References.....	191
Résumé en français	i
Introduction.....	i
Chapitre I. Etude bibliographique	i
Chapitre II. Matériaux et techniques.....	ii
Chapitre III. Sorption et effet plastifiant de solvants polaires et apolaires purs et des mélanges de solvants sur du PA6,6 pur	iv
Chapitre IV. Propriétés des PA6,6 additivés ou modifiés chimiquement	x
Conclusion	xv

Introduction

This PhD thesis was carried out at the “Laboratoire Polymères et Matériaux Avancés”, a joint CNRS/Rhodia-Solvay research unit (UMR 5268). This work was done within the framework of an applicative development conducted by Rhodia, aimed to valorize Polyamide 6 or 6,6 based formulations in automotive biofuel tanks applications.

Polyamide 6,6 (PA6,6) is a good candidate for fuel tank applications since it possesses good mechanical properties relative to its weight, and it also has good barrier properties to hydrocarbons, the main components of standard gasoline. However with the increasing commercialization of biofuels, which are standard gasoline containing a certain percentage of ethanol, as well as the new environmental directives that will be more restrictive concerning the allowed gasoline permeability of a tank, new PA6,6 formulations having improved barrier properties to biofuels have to be developed. Moreover, these PA6,6 formulations need to have also good mechanical properties, specifically good impact strength behavior, and that at low temperatures since a car may be used in extreme cold conditions (ca. -40°C). It is important then to ameliorate the barrier properties and at the same time improving the impact strength of PA6,6 in order to obtain formulations having a good compromise between these two properties.

PA6,6 is a semi-crystalline polymer, which means that it is composed of a rigid, well-organized crystalline phase, and an amorphous phase in which the polymer chains are less organized and more mobile. The crystalline phase is considered to be impermeable to solvents, whereas the amorphous phase is not. The amorphous phase is thus the place in which the solvent diffusion processes occur. In addition, PA6,6 has a relatively low crystalline ratio of ca. 40%_{wt} when compared to other semi-crystalline polymers like High Density Polyethylene (HDPE) which has a crystalline ratio of ca. 70-80%_{wt}. This might mean that the properties of the amorphous phase, namely its molecular mobility, could have a major influence on the behavior of PA6,6. The amorphous phase of PA6,6 is thus expected to play a prominent role on both fuel barrier properties and impact resistance.

Polyamides possess a physical network of amide – amide hydrogen (H) bonds in both the amorphous and the crystalline phases. The existence of this network, especially in the amorphous phase, gives polyamides good mechanical and thermal properties. It is well known in the literature that water disturbs the H-bond network of the amorphous phase, leading to a modification of the polymer intrinsic properties. It is of great importance then to better understand the effects of solvents like ethanol, toluene and isooctane on the amorphous phase, polyamide-solvents interaction governing both barrier and mechanical properties.

The scientific issues of this thesis are firstly the better understanding of the molecular interactions between PA6,6 and polar or non-polar solvents, or a mixture of polar and non-polar solvents, in regard with the specific H-bonds intermolecular interactions present in polyamides. It is of interest then to study the effect of these solvents on the molecular mobility of the amorphous phase at different time scales (main and secondary relaxations of PA6,6). Finally, it is of interest to study the effect of the amorphous phase molecular mobility on the mechanical properties of PA6,6, such as tensile or impact strength properties.

In this work, neat as well as modified PA6,6 are studied, the aim of the modification being to go further in the understanding of the PA-solvent interaction / molecular mobility / mechanical properties relationship, but also to yield polyamides with improved barrier / impact strength compromise.

In the first chapter of this manuscript, a background review presents the state-of-the-art on the amorphous and the crystalline phases of polyamides, their thermo-mechanical properties, their interactions with solvents and how these molecules have an influence on polyamides thermo-mechanical properties. The conclusion of the chapter clarifies the scientific approach of this thesis. The materials and the experimental characterization techniques used in this work are further presented in the second chapter.

The third chapter of this manuscript deals with the study in neat PA6,6 of the solubility of a series of pure solvents of different sizes and polarities as well as a set of ethanol-toluene-isooctane mixtures. The solubility of these solvents and mixtures in PA6,6 are characterized and the nature of the interactions leading to their sorption by the polymer are then described by a thermodynamic approach. Later on, the effect of these solvents and mixtures on the molecular relaxations of PA6,6, i.e. the glass transition temperature T_g as well as the secondary relaxations, is characterized and discussed. Hypotheses on how the solvents are able to modify the molecular mobility of PA6,6 are further proposed.

The fourth and last chapter deals with modified PA6,6 in which intermolecular interactions have been altered. This chapter describes first the influence of the modification on PA6,6 crystalline and amorphous phases. The sorption and permeability properties of these formulations to several solvents are then studied. Finally, the mechanical properties of these formulations are assessed at various temperatures and hygrometry levels, and the relationship between amorphous phase molecular mobility and mechanical properties as well as the possibility to obtain a good compromise between fuel barrier and mechanical properties are discussed.

I. Background Review on PA66

Polyamide 6,6 (PA6,6 - commercial name Nylon 6,6) is a thermoplastic, semi-crystalline polymer belonging to the family of polyamides. It was first synthesized by Wallace Carothers, a senior researcher in DuPont, in 1935 while he was working looking for a synthetic polymer having better properties than poly-alkyl-terephthalates. Because natural resources became scarce during World War II, Nylon 6,6 found its way in the Allied military industry as the fiber used for manufacturing parachutes, flack vests, and tents, while the same applications in the Axis military camp were fulfilled by Nylon 6. Nylon 6,6 was regarded, among others, as a symbol of the Allied victory over the Axis powers in the European and Pacific Theaters and when the conflict ended, Nylon 6,6 started to be commercialized mainly as a synthetic fiber for clothing and carpets, among others, for the general public.

Although polyamides are one of the most widely used polymers, the production and consuming of polyamide-based products is not as large as that of Polyethylene, Polypropylene or Polystyrene. For example, in Europe in 2009, the consumption of polyamide accounted for roughly 2% of the total tonnage of consumed polymers [1], as it is shown in Figure 1.

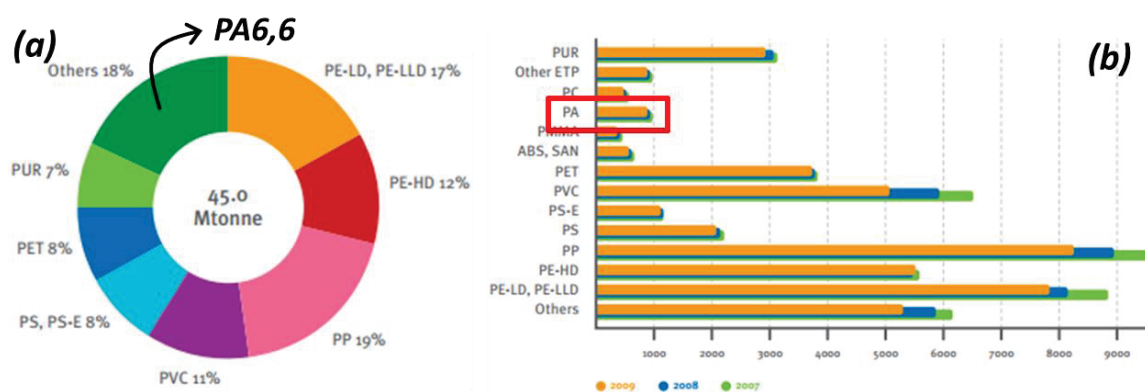


Figure 1: European polymer demand in 2009 (a) in percentage and (b) in net tons [1].

PA6,6 can be used as a technical polymer since it possesses relatively good thermomechanical properties compared to its weight. Indeed PA6,6 (density $\approx 1.13\text{g/cm}^3$) is lighter than aluminum (density $\approx 2.7\text{g/cm}^3$) and it is roughly 7 times lighter than steel (density $\approx 7.85\text{g/cm}^3$), which are two common metallic materials used for technical applications. Furthermore PA6,6 Young's modulus ($E \approx 2800\text{ MPa}$) is twice as large as that of High Density Polyethylene HDPE ($E \approx 1300\text{ MPa}$) which is one of the most produced polymers and it is comparable to those of Polystyrene and Polymethylmethacrylate ($E \approx 3000\text{ MPa}$) although it resists better to physicochemical corrosion and the attack of organic solvents.

To better understand from where these properties come from, the structural characteristics and properties of PA6,6 are now discussed, as well as its behavior in presence of solvents or at different temperatures.

I.1 Structure and morphology

I.1.1. Molecular structure

PA6,6 is a polycondensation polymer that can be obtained via two synthesis reactions. The first one involves the reaction between hexamethylenediamine, a diamine, and adipic acid, a diacid, carried out at equimolar amounts. The second mechanism involves the reaction of n moles of Nylon 6,6 salts which are no more than ionic hexamethylenediamine and adipic acid complexes. In both reactions, PA6,6 chains are obtained by the reaction of the carboxylic functions of adipic acid with the amine functions of hexamethylenediamine, water being a by-product of the reaction [2]. The polycondensation reactions and the chemical structure of PA6,6 are shown in Figure 2.

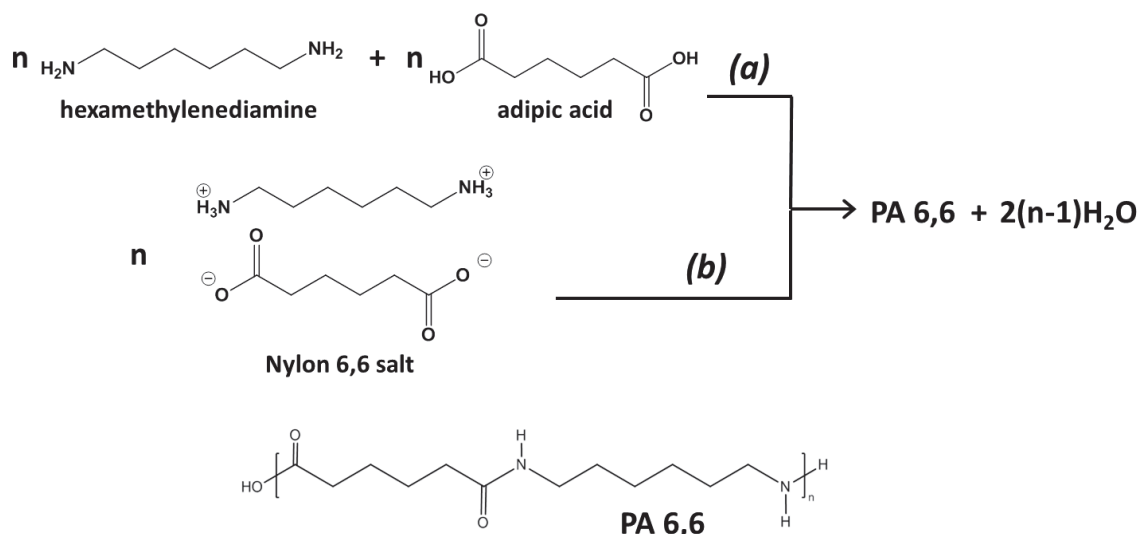


Figure 2: Polycondensation reaction yielding Polyamide 6,6 describing two mechanisms (a) the reaction of hexamethylenediamine with adipic acid and (b) the reaction of Nylon 6,6 salts.

The advantage of using Nylon salts for synthesizing PA6,6 is that the diamine and the diacid functions are always in equimolar quantities, which allows the obtaining of a reaction yield close to 100%, as well as high molar masses, the terminal groups being half amine / half acid. In the case of the synthesis involving the polycondensation of hexamethylenediamine with adipic acid, if the equimolarity of the reactants is not respected, the reaction yield and the polyamide molar masses will drop and the nature of the terminal groups will tend towards the nature of the reactant in excess [2]. Moreover, the polycondensation reaction between amines and acids is actually a reversible reaction as described in Figure 3.

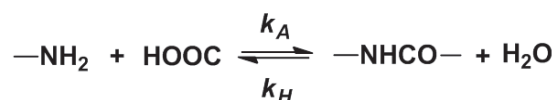


Figure 3: Amidation – hydrolysis reaction equilibrium.

In this reaction, k_A and k_H are the rate constants of the amidation and hydrolysis reactions respectively. The equilibrium constant of the overall reaction K_C is equal to the ratio of the reaction rate constants of the amidation and hydrolysis reactions as defined in Equation 1.

$$K_c = \frac{k_A}{k_H} = \frac{[NHCO][H_2O]}{[NH_2][COOH]} \quad 1$$

It is seen in Figure 3 and in Equation 1 that in order to favor the amidation reaction, water has to be extracted from the reaction medium. It is also observed that the presence of water in polyamides, at high temperatures, can lead to a scission of the polymer chains. So in the case of polyamides, the hydrolysis reaction can be considered as a form of chemical degradation. It is thus important to keep the polyamide pellets or formulations dry before processing them, since the hydrolysis of the polymer chains can lead to a decrease on the polymers molecular mass, thus provoking a modification of the polymer properties.

I.1.2. Crystalline phase

I.1.2.1. Crystalline lattice

Polyamides are semi-crystalline polymers, having a crystalline fraction of around 30 to 40%_{wt} [2]. These polymers can be considered as a two-phase material composed of a crystalline phase and an amorphous phase. In the amorphous phase the polymer chains only show a short-range order, the chains being relatively disordered at a larger scale. In the crystalline fraction, polymer chains can organize themselves following long-range, well-ordered stacking. This organization starts with crystalline lattices which at a larger scale form crystalline structures such as crystalline lamellae and at even larger scale crystalline spherulites.

Polyamides chemical structure can be considered as polymer chains containing periodically amide functions separated by an aliphatic or an aromatic backbone. As shown in Figure 2, the amide functions are formed by an amine (NH) and a carboxylic (CO) group. These groups can form strong Hydrogen-bonds (H-bonds) with amide functions belonging to other polyamide chains, i.e. the NH of one chain can bond with the CO of another chain and vice versa, as it is schematically shown in Figure 4. The presence of such bonds between polyamide chains can favor the ability of these polymers to crystallize [2].

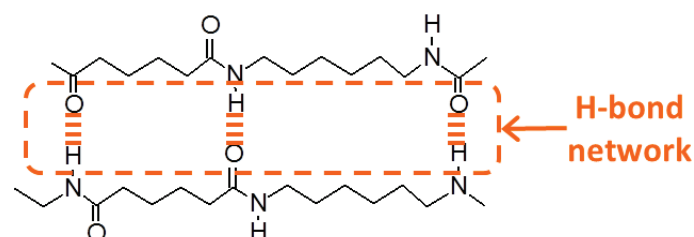


Figure 4: Schematic representation of the H-bonds formed between amide groups in PA6,6

Polyamides exhibit a crystalline polymorphism, i.e. several crystalline structures can be obtained depending on the processing conditions [2,3]. The crystalline lattice is defined by the manner in which the H-bonds formed between the chains are organized. Polyamides mainly crystallize according to two different morphologies, the α and the γ forms. Other crystalline forms, such as the β form, can be found in polyamides but there are either a variation of the two mentioned forms or they are not stable and will evolve with time towards the α or the γ forms [2-6].

I. Review

In this work, a focus on the crystalline structure of PA6,6 is made. Figure 5 shows the triclinic unit cell of PA6,6 α structure as well as the crystallographic planes of this structure described by the Miller indexes [2].

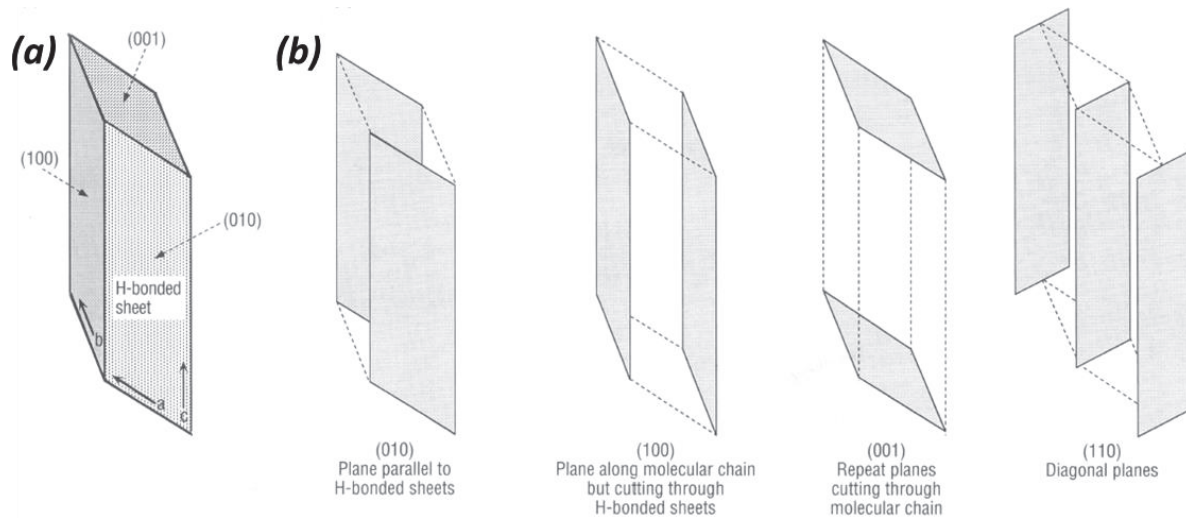


Figure 5: (a) triclinic unit cell of PA6,6 α crystalline structure and (b) individual representation of the crystal lattice planes conforming this crystalline structure [2].

The α crystalline structure is mostly found in even-even and (6-)carbon polyamides (i.e. PA6, PA6,6, PA6,10). In this structure the chains are arranged in a zigzag conformation resulting in the formation of H bonds between the amide groups in the zigzag plane, sheets of H-bonds being then formed and stacked one over the other through van der Waals interactions. Successive amide groups along a chain are rotated by 180°. Polyamides such as PA6 form monoclinic units, whereas even-even polyamides like PA6,6 form triclinic structures. Figure 6 shows a PA6,6 triclinic crystalline unit, the lattice parameters being $a=0.49$ nm, $b=0.54$ nm, $c=1.72$ nm, $\alpha=48.5^\circ$, $\beta=77.1^\circ$ and $\gamma=63.5^\circ$ [2].

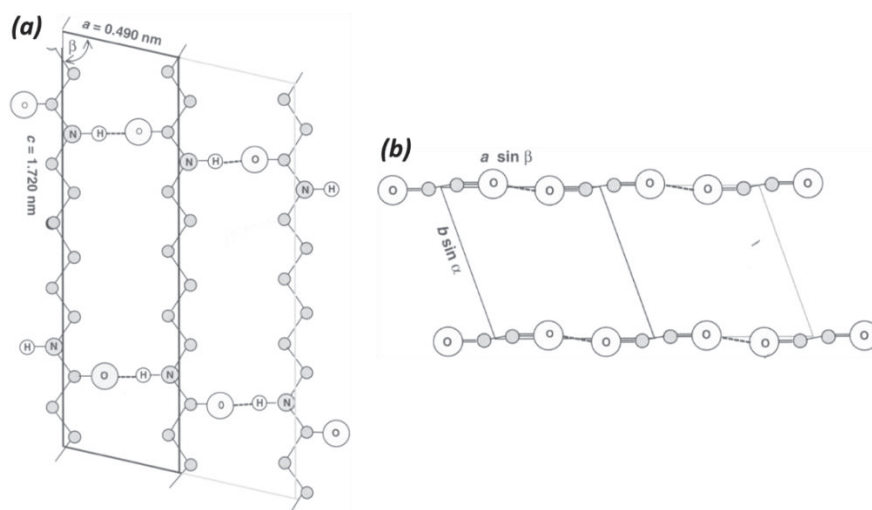


Figure 6: 2-D projection along the (a) *b* and (b) *c* axis of a PA6,6 triclinic unit cell [2].

The structure of the α crystalline phase in PA6,6 can vary depending on the processing or the crystallization method, the obtained lattice parameters varying continuously between two sets of parameters associated to the “thermodynamic” or the “kinetic” form of this phase. PA6,6 samples obtained by film-casting from a polymer solution crystallize into the α , (“thermodynamic”) form, which is characterized by a high crystalline density (1.21 g/cm³), a

I. Review

triclinic unit structure and the presence of usually two melting points at 252 and 262°C. The α_{II} (“kinetic”) form is obtained from a rapid cooling from the molten PA6,6. This form is characterized by a low crystalline density (1.16 g/cm³), by a pseudo-hexagonal unit structure and by the presence of one melting point at 262°C [7]. This form tends to evolve towards the more stable α_I form under temperature and/or a humid atmosphere [8]. Another crystalline evolution called the Brill Transition [2] occurs in PA6,6 upon heating. X-Ray diffraction experiments show that around 160°C, the (100) and (010) reflections merge into a single peak, suggesting a change from a triclinic structure to a pseudo-hexagonal structure (hexagonal symmetry in a plane perpendicular to chain axis). This evolution of PA6,6 crystalline structure upon heating implies thus that the triclinic α_I phase cannot yield a proper signature on DSC thermograms because it reorganizes far before melting.

In the case of conventional processing conditions, an intermediate α form, called α_{I-II} , is obtained, and this form evolves as well towards the α_I thermodynamic form, the evolution rate depending on the temperature and the humidity of the polymer environment. The X-Ray diffraction technique allows to determine the “degree of perfection” of the α crystalline form of PA6,6, a high perfection degree conventionally corresponding to the α_I triclinic crystalline form. The degree of perfection is given by the gap ($\Delta 2\theta$) between the Bragg diffraction peaks corresponding to the (100) and (010) planes of the crystalline structure, as shown in Figure 7. If $\Delta 2\theta$ equals 3.55° [2] the crystalline form is that of the α_I structure, if $\Delta 2\theta$ equals 0.72° the crystalline form is then that of the α_{II} structure, and if the value of $\Delta 2\theta$ is in between the latter angular values, the structure corresponds to the intermediate α_{I-II} form.

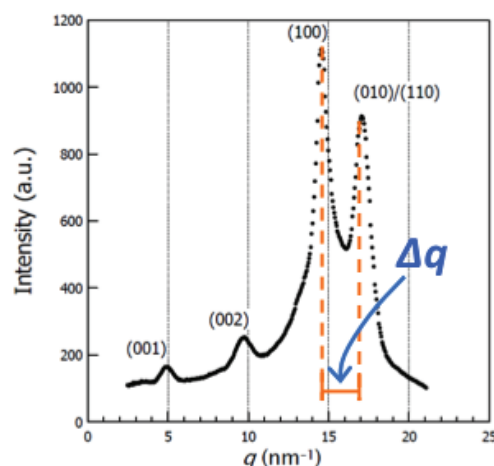


Figure 7: X-Ray diffraction spectrum for a PA6,6 sample with the $\Delta 2\theta$ value between the (100) and (010) planes indicated [9].

1.1.2.2. Crystalline lamellae

At a larger scale, polyamide crystalline units arrange themselves in lamellar structures, with a repetition period of the order of 9 nm. The morphology of this lamellar structure is somehow determined and restricted by the arrangement of the polymer chains according to the formation of H bonds between them. It has been suggested [2] that it would take three and a half monomeric repeat units to form one lamellar stern and that the polymer chain folds in the methylene backbone so as to form further lamellae as shown in Figure 8.

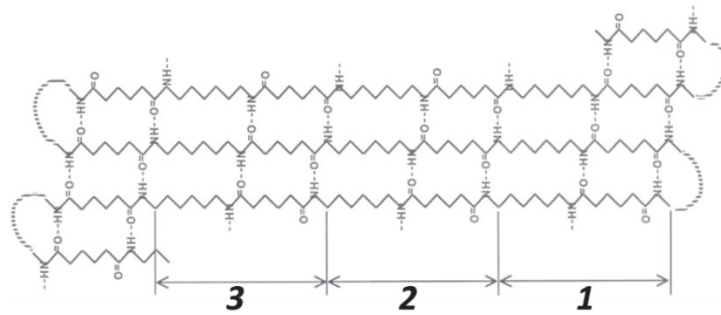


Figure 8: Ideal chain folding for PA6,6 lamellae [2].

For most semi-crystalline polymers, their crystalline morphology corresponds to a spherulitic structure, albeit that the crystallization occurred in environment free from thermal and mechanical stresses. However other crystalline morphologies can be found, for instance single crystals may be formed from solution crystallization or otherwise when thermal and/or mechanical stresses are applied to the polymer during the crystallization process fibrillar, brush, or shish-kebab morphologies can be obtained [10].

Concerning polyamides, crystallization under no external stress conducts towards the arrangement of regular chain folding on specific planes determined by the H-bond interactions between polyamide chains, forming a lamellar structure. Then this lamellar structure of polyamides grows with a certain axis to form spherulites. If the spherulite grows with its radius parallel to the major axis of its component crystals it is called a “positive” spherulite, whereas if the spherulite grows parallel to the minor axis it is called a “negative” spherulite. The growing of these “positive” and “negative” spherulites is schematically shown in Figure 9.

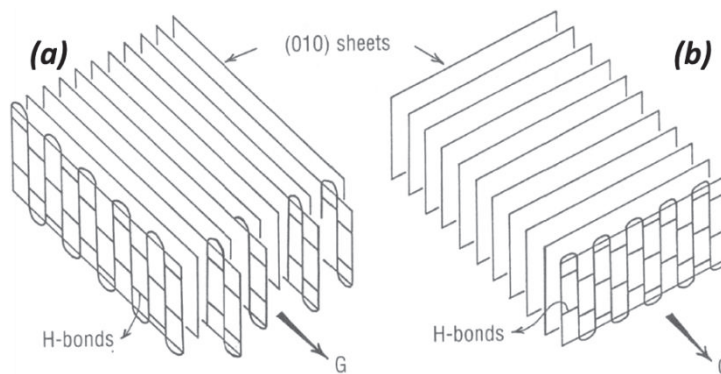


Figure 9: Schematic representation of chain folding and crystal growth in (a) positive and (b) negative spherulites. G denotes the growth direction and the planes represent H-bonded crystalline sheets [2].

The polyamides spherulites exhibit birefringence, which could be defined as the difference on the refractive indices of light when diffusing through a material. The polyamides spherulites are inherently birefringent because of the anisotropy introduced by the alignment of the H bonds in the lamellar structure. This birefringence produces the “Maltese cross” effect in polyamides spherulites when polarized light propagates through the polymers’ crystalline phase as shown in Figure 10.

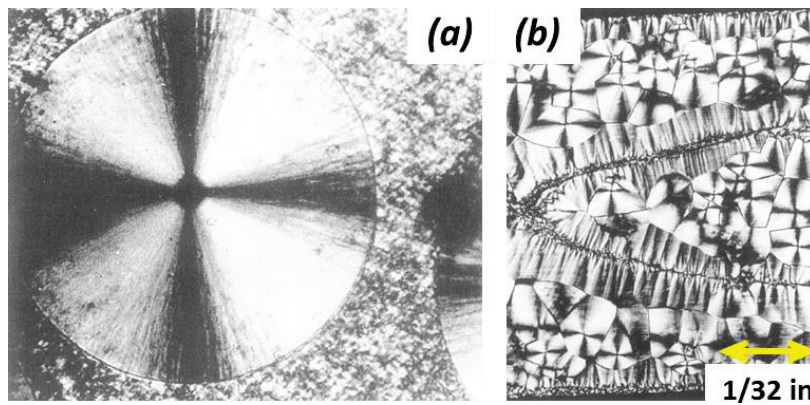


Figure 10: (a) “Maltese cross”-like polyamide characteristic spherulite and (b) compression-molded PA6,6 sample showing spherulites at a larger scale.

I.1.3. Molecular mobility of the amorphous phase

I.1.3.1. PA66 molecular relaxations

The molecular mobility of the amorphous phase is governed by molecular motions at different time scales. These motions are known as molecular relaxations. It is generally assumed that there is two types of molecular relaxations: the main relaxation (or α relaxation) corresponds to the coordinated motion of relatively long chain segments, and the secondary relaxations (namely β , γ , δ ...) correspond to the motions of small chain segments or molecular functions. The α relaxation is associated to the glass transition, the T_{α} measured at 1Hz being considered equivalent to the glass transition temperature (T_g) of the polymer.

In the case of polyamides, 3 molecular relaxations have been identified [11-14]. The α relaxation corresponds to the motion of no less than 15 monomers (determined experimentally by substituting the H bonds with covalent chemical bonds so as to effectively block the mobility of the polymer chains) and it occurs approximately at 60 – 70°C for Polyamide 6,6 (PA6,6) [11]. The β relaxation involves the rotation of the amide functions and occurs at -60°C approximately. Finally the γ relaxation corresponds to the vibrational motions of the methylene functions in the chains and it occurs at around -110°C. A schematic representation of these three relaxations for PA6,6 is given in Figure 11.

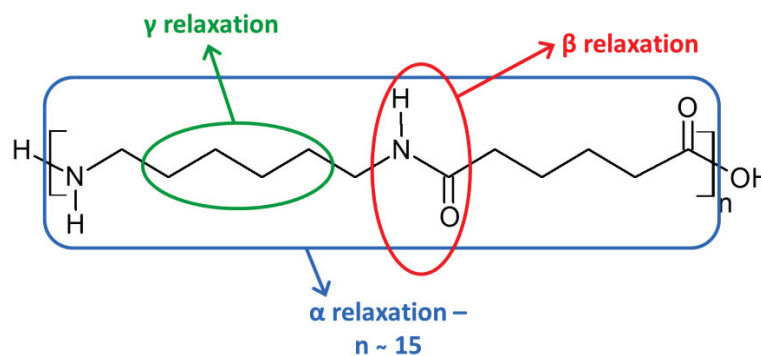


Figure 11: Schematic representation of the α , β , and γ relaxations in PA6,6.

A molecular relaxation can be characterized by its relaxation time, which is the time that describes the motions of molecular segments involved in the relaxation. The relaxation times

I. Review

depend on the temperature, and in the case of the secondary relaxations, the relaxation times can be described by an Arrhenius law [15]. This empiric law states that a certain amount of energy is needed to activate a thermally-induced phenomenon, in this case a molecular relaxation. The Arrhenius law, defined in Equation 2, is schematically plotted in Figure 12.

$$\tau(T) = \tau_{\infty} \exp\left(\frac{E_A}{RT}\right) \quad 2$$

where $\tau(T)$ is the relaxation time of a molecular motion as a function of T the temperature, τ_{∞} is the relaxation time at an infinite temperature, R is the ideal gas constant ($R=8.314$ J/mol·K), and E_A is the activation energy.

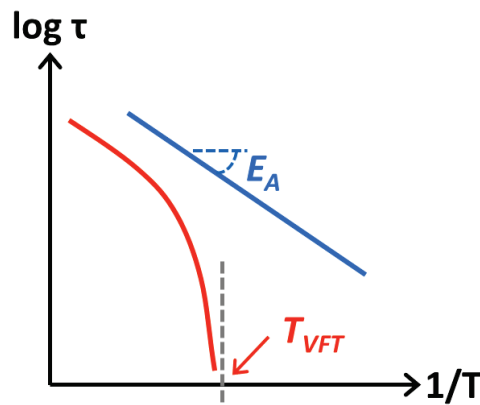


Figure 12: Schematic representation of the dependence on temperature of the relaxation time of a molecular motion described by an Arrhenius law (blue) or a VFT law (orange) [15-19].

Unlike the secondary relaxations, the characteristic relaxation time of the main α relaxation, associated to the glass transition, does not follow an Arrhenius law. Volgel [16], Fulcher [17], and Tammann [18] proposed an empiric law, named in the literature as VFT, that describes the viscosity of super-cooled liquids such as glassy polymers which combined with the time-temperature principle defined by William, Landel and Ferry [19], yields a relationship that empirically describes the dependence on the temperature of the relaxation time for the glass (or α) transition:

$$\tau(T) = \tau_{\infty} \exp\left[\frac{E_{VFT}}{R(T - T_{VFT})}\right] \quad 3$$

This relationship is similar to the Arrhenius law, but it describes a phenomenon which is only activated when the temperature is higher than a limit temperature T_{VFT} ($\approx T_g - 50^\circ\text{C}$). The VFT relationship is schematically represented in Figure 12.

1.1.3.2. Focus on the main α relaxation

The α relaxation temperature (T_α) or the glass transition temperature (T_g) depend upon several factors, the main factor being the chemical structure of polyamides themselves such as the length of the methylene backbone, the orientation in space of the polymer chains, the

I. Review

presence of rigid chemical functions like aromatic rings, and the strength of the possible interactions between chains. Indeed as it was mentioned before, polyamides can form interchain H-bonds between the amide groups within the polymer chains. Infrared Spectroscopy [20-24], Raman Spectroscopy [25], and Solid NMR [26,27] have shown that H-bonds can establish not only in the crystalline phase but also in the amorphous phase.

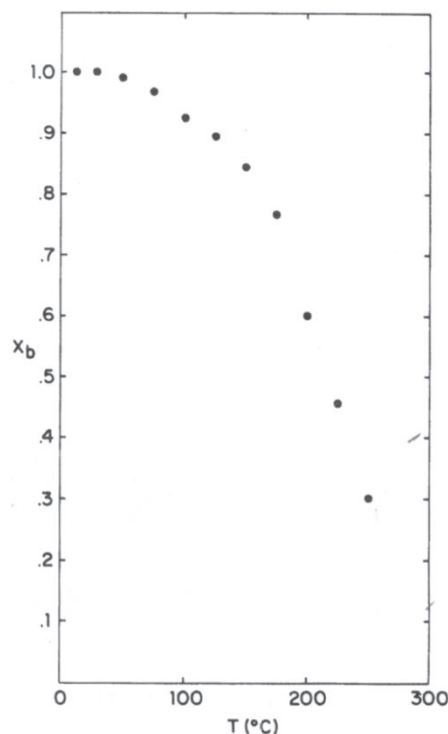


Figure 13: Plot of the total amide-amide H-bonded fraction as a function of temperature for PA6,6 as obtained by García and Starkweather [20].

In the case of PA6,6, García and Starkweather [20] showed by IR that almost all the amide functions of this polymer (in the amorphous and crystalline phases) are H-bonded at room temperature, and that a fraction of amide functions (ca. 20%) appears to be still H-bonded in the molten state (temperature higher than 260°C), as it is shown in Figure 13.

An important parameter that also determines the glass transition temperature of a given polyamide is the density of the interamide H-bonds [28]. The density of such bonds depends on the space between the amide groups, in other words, the length of the methylene backbone of polyamide chains, as well as the orientation in space of the amide groups. Globally the glass transition temperature T_g of polyamides drops when the length of the number of methylene functions between amide groups increases. Figure 14 plots for instance the glass transition temperature T_g measured by DSC for several polyamides as found in the literature [2,14] as a function of their methylene – amide function molecular ratio.

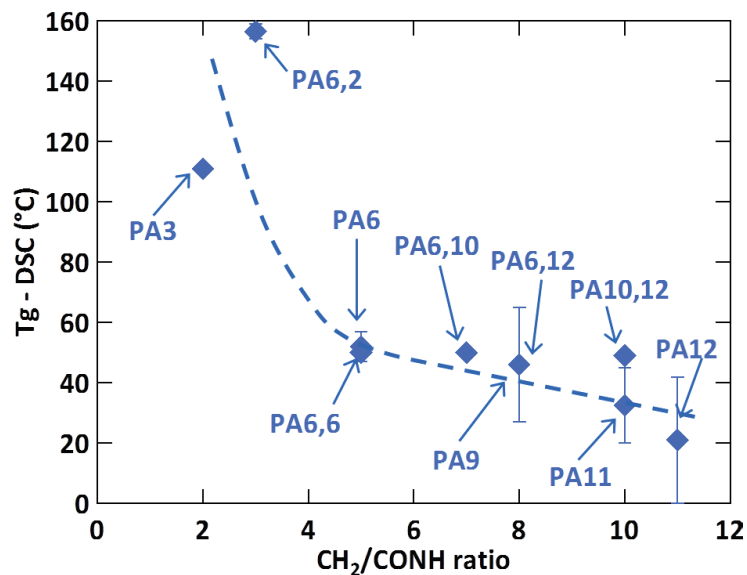


Figure 14: Glass transition temperatures T_g 's obtained by DSC for several polyamides [2,14] as a function of their methylene – amide functions molecular ratio.

I.1.4. Heterogeneity of the amorphous phase

As a semi-crystalline polymer, polyamide's morphology could be considered as a two-phase system comprising a crystalline phase and an amorphous phase. However, several authors [29-32] have proposed the existence of a third intermediate phase. In this phase, known as the Rigid Amorphous Fraction (RAF), polymer chains have a reduced mobility when compared to the chains belonging to the Mobile Amorphous Fraction (MAF) because the chains belonging to the RAF are constrained by the presence of crystallites near them. This three-phase system is schematically represented in Figure 15.

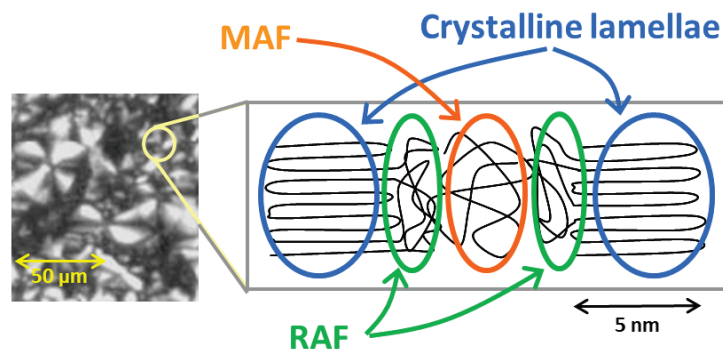


Figure 15: Schematic representation of a 3-phase polymer composed of a crystalline phase, a mobile amorphous phase and a rigid amorphous phase.

It is known that the heat capacity step ΔC_p step is directly proportional to the total amount of amorphous phase in the polymer, a consequence being that a semi-crystalline polymer exhibits a smaller ΔC_p than a 100% amorphous one. Furthermore, Wunderlich [30] observed for a series of semi-crystalline polymers that the ΔC_p measured by DSC appeared to be lower than the theoretical values expected for the semi-crystalline polymer. According to this author, this difference may originate from the presence of RAF that does not contribute to the glass transition process evidenced by DSC (only the MAF contributes). This is illustrated in Figure 16.

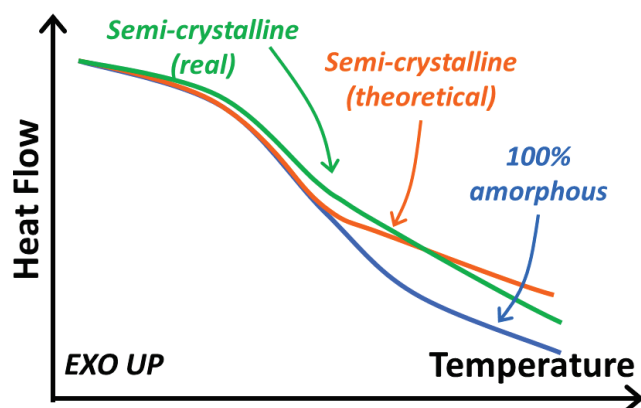


Figure 16: Schematic DSC plots at the glass transition for a completely amorphous, a theoretical semi-crystalline and an actual semi-crystalline polymer as studied by Wunderlich [30].

Moreover, Takayanagi et.al. [31] observed by DMA that the main α relaxation peak of PA6 got larger and broader at high temperatures when the crystalline fraction of the samples increased, as shown in Figure 17. Takayanagi, and later Rotter [32], attributed these phenomena to the existence and the appearance of a rigid amorphous phase whose mobility is confined by neighboring crystallites.

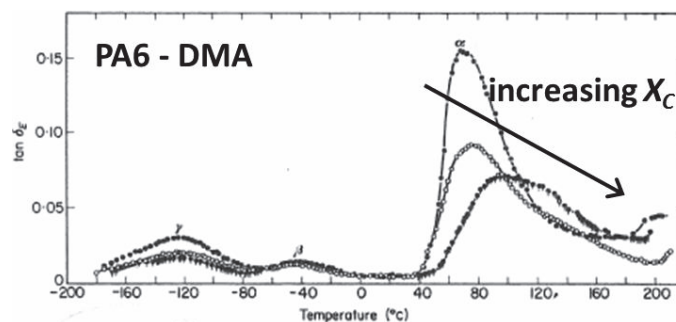


Figure 17: $\tan \delta$ spectra obtained by DMA for a series of PA6 samples having different crystalline fractions X_C as obtained by Takayanagi et.al. [31]

Cebe et.al. [33] studied semi-crystalline Poly(phenyl sulphide) (PPS) by Solid-state ^{13}C NMR. They observed three well-defined responses when analyzed by NMR. The fastest response corresponds to the motion of polymer chains within the MAF, whereas the slowest response corresponds to the chains forming the crystalline domains. The intermediate response corresponds to the chains that are found in the RAF. The intensity of this response varies accordingly with PPS crystalline ratio: if the ratio increases, the intensity of the RAF (signaling more rigid amorphous domains) increases as well.

I.2. Sorption, diffusion, and pervaporation of pure solvents in PA66

I.2.1. Solvent sorption at equilibrium

I.2.1.1. Parameters defining polymer-solvent interactions

When a polymer is put in contact with a solvent at a given temperature, the solvent will diffuse through the polymer. The solvent will be absorbed at a certain rate or amount during

I. Review

time until the sorption equilibrium is reached, that is where no more solvent is absorbed by the polymer. This is schematically shown in Figure 18.

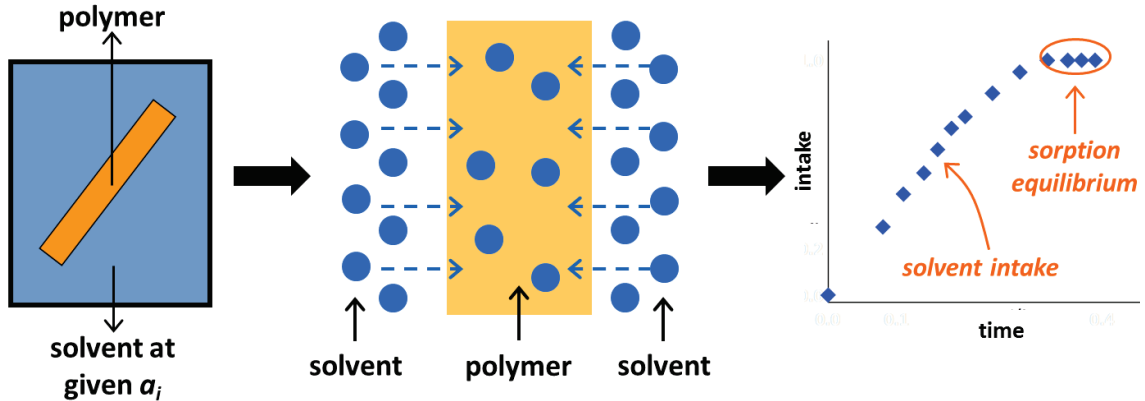


Figure 18: Schematic representation of the sorption of a solvent in a polymer.

The amount of absorbed solvent depends on the chemical activity of the solvent and on the interactions between the solvent and the polymer, as it is shown in Equation 4.

$$C_{solv} = S_{solv} \times a_{solv} \quad 4$$

where C_{solv} is the concentration of solvent in the polymer, S_{solv} is the solvent solubility parameter and a_{solv} is the chemical activity of the solvent. This relationship corresponds to the Henri sorption law.

The chemical activity a_{solv} is defined in Equation 5:

$$\ln a_{solv} = \frac{\mu_{solv} - \mu_{solv}^0}{RT} \quad 5$$

where T is the temperature, R is the ideal gas constant (8.314 J/mol·K), and μ_{solv} and μ_{solv}^0 are the chemical potentials (or the molar Gibbs free energies $(\partial G/\partial n)_{T,P}$) of the solvent in the polymer and that of the solvent in the reference state respectively, which is defined as the chemical potential of the solvent in the liquid state at the same temperature and pressure (1 atm) [34].

1.2.1.2. Influence of the crystalline phase on solubility

It is generally assumed that Crystallites, being well-organized and tight zones, do not allow solvents diffusing through their structure, so if the crystalline fraction of a polymer increases, the solvent sorption in this material decreases. The solubility coefficient for a semi-crystalline polymer S_{SC} can be estimated to vary linearly with the crystalline ratio of the polymer as shown in Equation 6:

$$S_{SC} = S_A (1 - X_C) \quad 6$$

where X_C is the crystalline ratio of the polymer.

1.2.1.3. Sorption isothermal mechanisms

By conducting solvent sorption experiments at various solvent activities, the sorption equilibrium isotherm can be obtained. This isotherm describes how the solvent sorption at equilibrium varies with solvent activity, and from the shape of the isotherm the mechanisms driving the solvent sorption can be estimated or described.

Three physical models based on a pure physical approach can describe certain sorption isotherms. These models are the Henry [37], the Langmuir [38-40], and the Flory-Huggins [35,41-49] models. There exist extensions of these models that combine two or more of these behaviors. These extensions (i.e. Dual-Mode, GAB, Park...) are presented afterwards. The shape of the sorption isotherms of the Henry, Langmuir and Flory-Huggins models are schematically plotted in Figure 19.

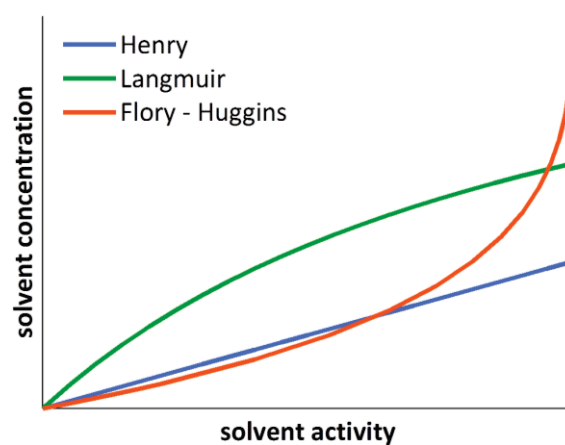


Figure 19: Henry [37], Langmuir [38-40], and Flory-Huggins [35,41-49] sorption isotherm plots.

The Henry sorption model [37] is the simplest of the three plotted in Figure 19. This model describes cases in which the sorption of a gas or solvent is small and varies linearly with the activity. The polymer-solvent interactions are then considered to be weaker than the solvent-solvent and the polymer-polymer interactions. The relationship for the Henry sorption model is given according to Equation 7:

$$\phi = S \cdot a \quad 7$$

where a is the chemical activity of the solvent, ϕ is the final concentration of solvent in the polymer and S is the solubility parameter of the solvent in the polymer which is constant in the case of the Henry sorption model. This behavior is mainly observed for solvents or gases which have a low solubility in the polymer matrix or when a solvent is absorbed in very small amounts, the sorption of this molecule tends to this behavior.

The Langmuir sorption model [38] describes the sorption of a solvent in preferential adsorption sites existing in the polymer, one molecule of solvent being at most absorbed in each site. The total amount of solvent is then governed by the concentration of adsorption sites within the polymer. In this isotherm the sorption of solvent increases rapidly with activity but at high activities the sorption is slowed down as the available absorption sites decrease. The relationship for the Langmuir sorption model is given by Equation 8:

$$\ln a = \ln \phi - \ln(1 - \phi) - E \quad 8$$

where ϕ is the fraction of occupied sites in the polymer and $E > 0$ is the gain in energy of a molecule that is absorbed by the polymer (with respect to the vapor phase). This model describes for instance the sorption of a solvent or a gas in a material containing macro voids, silica or mineral fillers [39,40].

The Flory-Huggins sorption model [35,41-49] describes the solubility of a polymer in a solvent. In this model the sorption of a solvent is driven by solvent chemical activity and by the interactions between the polymer and the solvent through the Flory-Huggins solubility parameter χ . The total free energy F for a Flory-Huggins polymer-solvent system can be then defined as:

$$\frac{F}{RT} = n_1 \ln \phi + n_2 \ln(1 - \phi) + \chi n_1(1 - \phi) \quad 9$$

where n_1 and n_2 are respectively the number of absorbed solvent molecules and the number of polymer chains of length N , ϕ is the solvent volume fraction ($\phi = n_1 / (n_1 + Nn_2)$), $1 - \phi$ is the polymer volume fraction, and χ is the Flory-Huggins interaction parameter.

During solvent sorption the number of solvent molecules absorbed by the polymer increases, while the number of polymer chains remains constant. At sorption equilibrium the free energy of the polymer-solvent system can be defined as.

$$\frac{\partial}{\partial n_1} \left(\frac{F}{RT} \right)_{n_2} = \frac{\mu - \mu_0}{RT} = \ln a \quad 10$$

By solving Equation 9 considering that the polymer chains are long ($N \gg 1$), the following relationship is obtained:

$$\ln a = \ln \phi + (1 - \phi) + \chi(1 - \phi)^2 \quad 11$$

In the case of a small sorption, the Flory-Huggins relationship (Equation 11) resumes to the Henry law sorption:

$$a_{solv} = \phi_{solv} \times \exp[1 + \chi] \quad 12$$

where ϕ_{solv} is the volumetric fraction of the solvent in the polymer and χ is the Flory-Huggins parameter for the polymer-solvent system. In this case the solubility parameter S_{solv} can be obtained by equating Equations 4 and 12:

$$S_{solv} = \frac{1}{\exp[1 + \chi]} \quad 13$$

this means that the solubility parameter S_{solv} depends on the interactions between the polymer and the absorbed solvent (i.e. the Flory-Huggins parameter χ).

In the Flory-Huggins model, when the interactions between the polymer and the solvent decrease (χ increases), the solvent intake decreases. This sorption model describes well the sorption of a solvent in a polymer with a low glass transition temperature (i.e. lower than the testing temperature).

In most cases, especially in the case of strong interactions between the polymer and the solvent, these simple models might not describe accurately the sorption of a solvent in a polymer. A combination of these models is then used to fit the sorption isotherms and to interpret the phenomena involved in the sorption process [48-53]. One of the most well-known mode is the GAB [48,49,52,53] model which is schematically plotted in Figure 20.

The GAB model can be described by the contribution of a Langmuir and Flory-Huggins sorption modes. In this mode the solvent is absorbed in preferential sites and it is able to form “clusters” of solvent around these sites, contrary to a pure Langmuir mode in which only one solvent molecule is absorbed in one absorption site.

In order to estimate the size of molecular “clusters”, several functions found in the literature are proposed. These functions calculate a mean size or amount of solvent molecules that are suspected to form clusters, which is known as Mean Cluster Size or *MCS* [52-58].

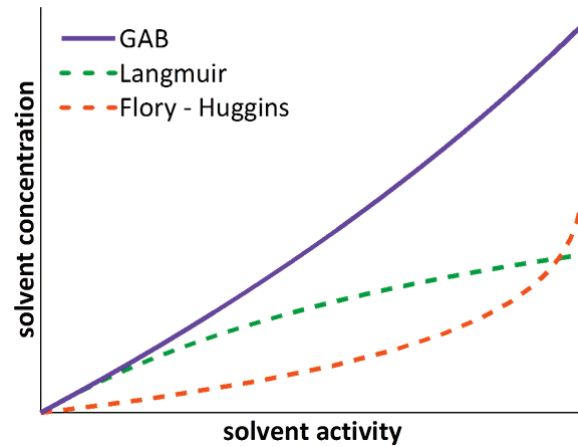


Figure 20: Typical shapes for the GAB sorption isotherm [48,49,52,53] shown as a contribution of Langmuir and Flory-Huggins isotherms.

The Mean Cluster Size (*MCS*) can be estimated according to Equation 14 [52,53]:

$$MCS = -(1 - \phi) \left[\left(\frac{\phi}{a_{GAB} c_{GAB}} \right) (-2c_{GAB}ka + 2ka + c_{GAB} - 2) - 1 \right] \quad 14$$

Where a_{GAB} is the monolayer solvent content, c_{GAB} is the Guggenheim constant, and k is a factor correcting the properties of multilayer molecules with respect to the bulk liquid.

A further example of clustering function is the Zimm – Lundberg relationship [54]. This function was developed from the assumption that polar molecules tend to aggregate. The function is derived from statistical mechanics and it states that the free energy of the polymer-solvent system depends upon the first derivative of the chemical activity of the

I. Review

solvent with respect to the volume fraction of the solvent. The Zimm – Lundberg function is given in Equation 15:

$$\frac{G}{v} = -\left(1 - \phi\right) \left(\frac{\partial \left(\frac{a}{\phi} \right)}{\partial a} \right)_{P,T} - 1 \quad 15$$

Where G is the cluster integral, v is the partial molecular volume of the solvent, ϕ is the volume fraction of the solvent absorbed by the polymer, and a is the chemical activity of the solvent. If the ratio G/v equals -1 it would mean that the solvent dissolves entirely in the polymer without forming clusters, when G/v is greater than -1 the solvents absorbed by the polymer tend to interact with themselves, forming clusters, and when G/v is smaller than -1 the interactions between the polymer and the solvent are strong and at high activities the polymer is swollen by the solvent. From the Zimm – Lundberg clustering function, the Mean Cluster Size (MCS) can be expressed according to Equation 16:

$$MCS = 1 + \phi \frac{G}{v} \quad 16$$

Finally, the *ENSIC* clustering model [55-58] (for *ENGaged Species Induced Clustering*) considers a probabilistic approach in which a solvent molecule is absorbed by a polymer-solvent system. The model is governed by the interactions between the newly absorbed molecule with polymer and with the solvent already absorbed by the material. The *ENSIC* clustering function is defined by the increase in the number of molecules dn_s for a solvent pressure (or chemical activity) increase dp . The function is given in Equation 17:

$$dn_s = (k_p n_p + k_s n_s) dp \quad 17$$

where n_p and n_s are the polymer molecules and the number of solvent molecules in the polymer respectively, and k_p and k_s are respectively the affinity parameters between a newly absorbed molecule with the polymer or with the solvent already in the polymer. By integrating Equation 17, the relationship describing the solvent intake as a function of its chemical activity in Equation 18 is obtained:

$$\phi = \frac{[\exp(a(k_s - k_p)) - 1]}{(k_s - k_p)/k_p} \quad 18$$

And thus the Mean Cluster Size (MCS) can be estimated from the *ENSIC* model according to Equation 19:

$$MCS = \frac{(1 - \phi)(1 + K\phi) \ln(1 + K\phi)}{K\phi} + \phi \quad \text{with } K = \frac{k_s - k_p}{k_p} \quad 19$$

1.2.1.4. Isothermal solvent sorption in polyamides

The sorption isotherm of water in polyamides was well studied throughout the literature [53,59-62]. When it is absorbed by polyamides, water sorption isotherm can be fitted by a GAB model isotherm, which is a Langmuir plus Flory-Huggins/multilayer clustering model. An example of this isotherm of water is shown in which was obtained by Hunt [59] at 23.5°C for PA6,6.

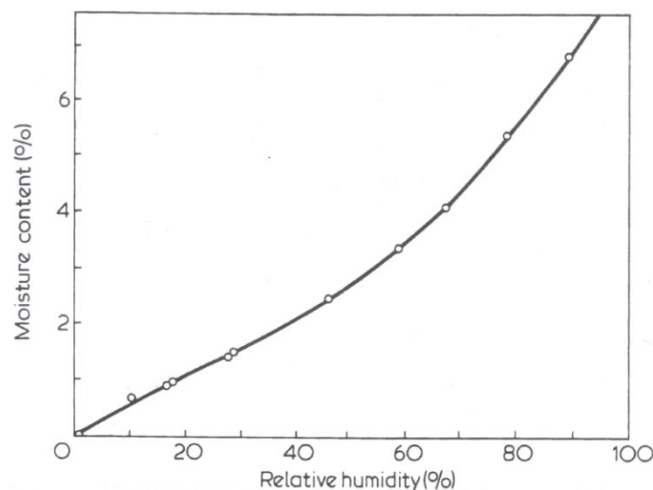


Figure 21: Sorption isotherm of water in PA6,6 at 23.5°C as obtained by Hunt [59].

Table 1 presents then some calculated Mean Cluster Size (*MCS*) values calculated from the GAB model obtained by several authors [53,61,62] for the sorption of water in PA6,6 and PA6.

Table 1: Mean Cluster Size (*MCS*) calculations following the GAB equation for PA6,6 and PA6 samples saturated in water at a chemical activity of one or close [53,61-63].

Author	Polyamide	Temperature [°C]	MCS
Starkweather et.al. [61]	PA6,6	25	3
Lim et.al. [62]	PA6,6	23	3
Picard et.al. [53]	PA6	22	1.6
Sabard et.al. [63]	PA6	40	2.3

The results shown in Table 1 show that statistically water forms clusters composed by three molecules in PA6,6 at room temperature and clusters of ca. 2 molecules in PA6, depending on the temperature. These results may certainly vary if a different sorption temperature or water chemical activity is considered, as well as a different model to calculate the *MCS* (i.e. the Zimm – Lundberg or the *ENSIC* relationships). Sabard also studied the sorption isotherms of ethanol in neat at filled PA6 formulations at 40°C at various activities [63]. Figure 22 shows the results obtained for a neat PA6.

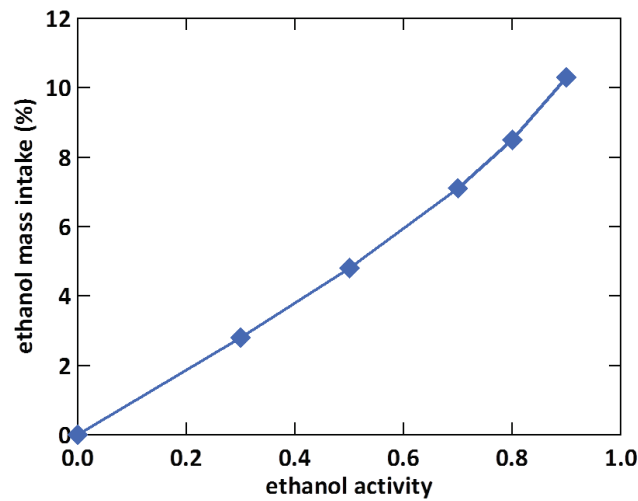


Figure 22: Sorption isotherm of ethanol in neat PA6 at 40°C as obtained by Sabard [63].

Sabard calculated the values of ethanol's *MCS* from the *ENSIC* and GAB relationships. He observed that the *MCS* obtained by the *ENSIC* model was close to the unity for all the values of ethanol activity. However he observed that the *MCS* obtained from the GAB model increased slightly with the activity to reach a value of ca. 1.5 for an ethanol activity of 0.9.

The main information obtained from the cited experiments is that water and ethanol would seem to be absorbed in polyamide in preferential sites, namely the polar amide functions borne by polyamide chains, with which water would have strong interactions. It might be possible as well that these solvents, especially water, are able to form small clusters in polyamides and this at high activity values.

1.2.2. Mechanisms of solvent diffusion in PA66

1.2.2.1. Fickian and Case II diffusion regimes

From the solvent sorption experiments schematically and briefly described in Figure 18, the sorption kinetics of this solvent can be assessed. The sorption kinetics in an amorphous polymer will be governed by the interactions between the polymer and the solvent, the molecular mobility state of the polymer, and the size of the diffusing molecules. In this work a focus is made on the two most commonly found diffusion kinetics in polymers: the Fickian and the Case II diffusions.

Concerning the Fickian diffusion [64-68], the solvent flux in the polymer is governed by the gradient of concentration of this solvent as defined by the Fick's 1st law shown in Equation 20.

$$\vec{J} = -D \text{grad } C \quad 20$$

where \vec{J} is the solvent flux in the polymer, D is the diffusion coefficient, which is constant in a Fickian regime, and C is the concentration of the solvent in the polymer.

$$\frac{\partial C}{\partial t} = -\text{div } \vec{J} \quad 21$$

From equating Fick's 1st and 2nd laws, the profile of the solvent concentration in the polymer can be obtained, as defined in Equation 22.

$$C(x) = \frac{M}{\sqrt{4Dt}} \exp\left(-\frac{x^2}{4Dt}\right) \quad 22$$

The profiles of the solvent concentration for a one-face and a two-face solvent sorption are shown schematically in Figure 23.

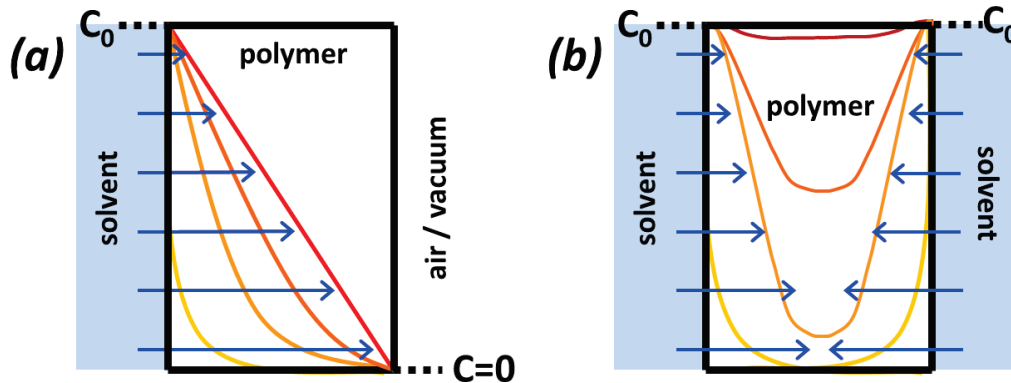


Figure 23: Graphic schematization of a solvent profile concentration following a Fickian diffusion for a (a) one-face diffusion and (b) two-face diffusion.

From Equation 22 and Figure 23 it is observed that the shapes of the solvent concentration profiles are Gaussian-like. In Fickian diffusions, the solvent intake varies linearly with the square root of time, and if the solvent intake at a given time m_t is normalized by the solvent sorption at equilibrium m_{eq} , the diffusion coefficient D of the absorbed solvent can be obtained from the slope of the obtained plot as shown in Figure 24.

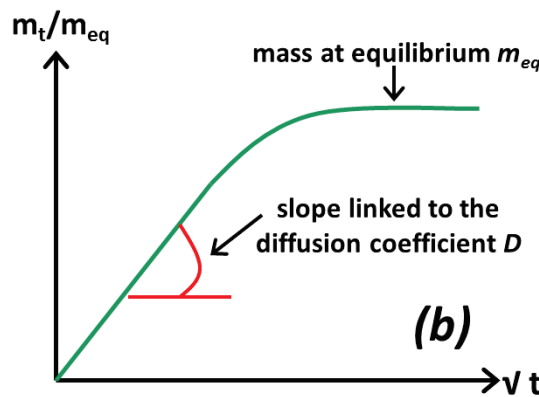


Figure 24: Graphic schematization of a sorption plot where the solvent diffuses with a Fickian regime.

In the case of a Fickian diffusion, the diffusion coefficient D is considered to be constant throughout the whole solvent diffusion. It can be then calculated from the following relationship:

$$\frac{m_t}{m_{eq}} = 1 - \frac{8}{\pi^2} \exp\left(-\frac{\pi^2 Dt}{L^2}\right) \quad 23$$

where t is the diffusion time and L is the thickness of the polymer film.

However, it is possible that a solvent is able to modify the molecular mobility of the polymer during diffusion, i.e. the glass transition temperature T_g of the polymer diminishes during diffusion and it becomes equal or inferior to the testing temperature [69]. In this case the diffusion is no longer Fickian and it is then called Case II diffusion [69-73].

In the first stages of Case II diffusion, the solvent is absorbed following a Fickian diffusion, but at some point the concentration of the polymer will be such, that locally the presence of the solvent will allow the relaxation of the polymer at the testing temperature. In this zone the diffusion of the solvent is accelerated since the polymer is plasticized and thus there is the appearance of a plasticization front. The diffusion is no longer governed by the gradient of concentration of the solvent, but rather by the ability of the solvent to modify the molecular mobility of the polymer.

In the case of a Case II diffusion, if the solvent intake is plotted as a function of the square root of time, a change in the regime of diffusion is observed when the solvent starts to locally plasticize the sample [69-75]. This is schematized in Figure 25.

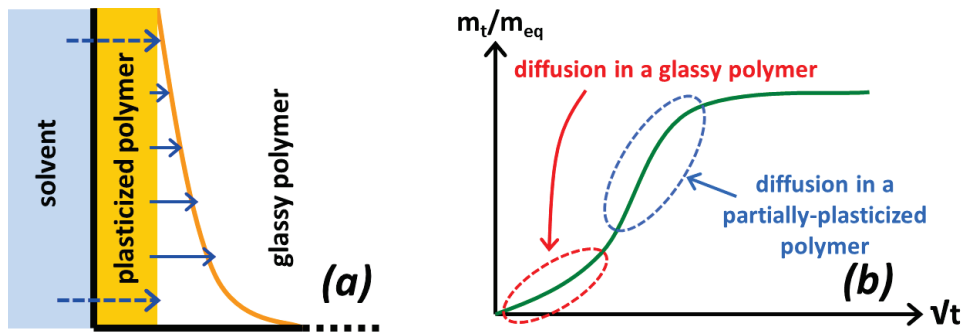


Figure 25: Graphic schematization of (a) an Case II diffusion and (b) the obtained sorption plot.

Berens et.al. [69] considered that a Case II diffusion can be described by a Fickian regime plus a relaxation process provoked by the presence of the solvent in the polymer. In this model the diffusion and plasticization processes start at the same time. However, it has been suggested however that the plasticization process would start later after the beginning of diffusion [74]. A heuristic modified diffusion-relaxation model taking into account a relaxation time-lag has been proposed in the literature [75]:

$$\frac{m_t}{m_{eq}} = \phi_F \left(1 - \sum_{n=0}^{\infty} \frac{8}{(2n+1)^2 \pi^2} \exp \left[-\frac{(2n+1)^2 \pi^2 D t}{L^2} \right] \right) + \phi_R (1 - \exp[-k_R (t - t_D)]) \quad 24$$

where $\phi_F = m_{eq-F}/m_{eq}$ and $\phi_R = m_{eq-R}/m_{eq}$ ($\phi_F + \phi_R = 1$) are the volume fractions of solvent contributing respectively to the Fickian and the relaxation processes, D is the diffusion coefficient, k_R is the relaxation constant and t_D is the time at which the polymer chain relaxation begins. As an example, Figure 26 shows the diffusion kinetics in PA6 of ethanol vapor at an activity of 0.9 obtained at 40°C and fitted by the Berens model as it was studied by Sabard [63].

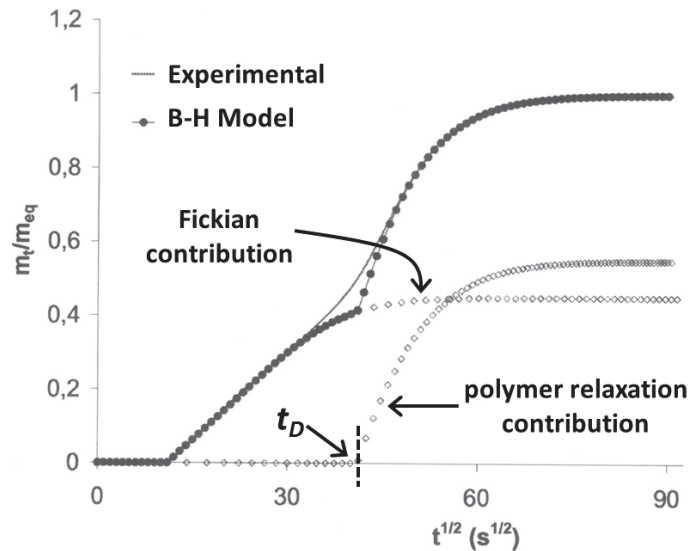


Figure 26: Case II solvent diffusion kinetics fitted by a modified Berens model [69-75] as obtained by Sabard [63].

It should be pointed out that although this relationship allows fitting the Case II diffusion regimes, this model does not consider a distribution of the polymer chains relaxation times but it rather considers that the relaxation of the polymer happens suddenly at only one time t_D .

1.2.2.2. Sorption kinetics of solvents in polyamides

Water diffusion in polyamides has been extensively studied [59,76-79]. An example is the study carried out by Hunt [59] in which the sorption kinetics of water at several hygrometry levels in PA6,6 was studied. From the total water intake the diffusion coefficients of this solvent in PA6,6 were obtained. Figure 27 shows then the sorption kinetics of water in PA6,6.

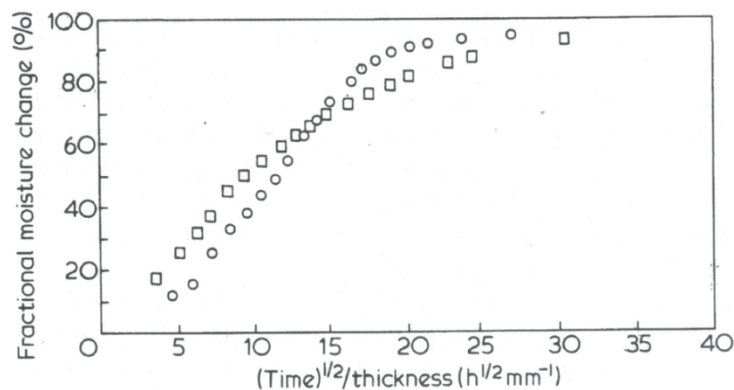


Figure 27: Sorption (○) and desorption (□) kinetics of water in a 50 μm -thick PA6,6 as reported by Hunt [59].

It is observed in Figure 27 that the sorption of water seems to follow a Fickian regime, as it seems that both the solvent sorption and desorption vary linearly with the square root of time. Hunt calculated then the diffusion coefficient D for the sorption and desorption kinetics. The values of D are plotted in Figure 28 as a function of water content.

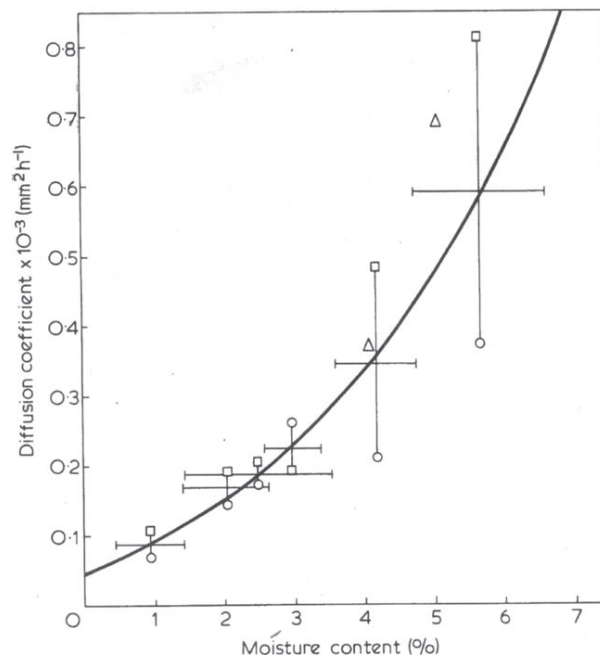


Figure 28: Calculated diffusion coefficients from the sorption (○) and desorption (□) kinetics as a function of the water content in PA6,6 as obtained by Hunt [59].

It is seen in Figure 28 that the diffusion coefficients are not constant and that their values depend on the water activity and they actually increase with the water content in the polymer.

Concerning the sorption of other kind of solvents, sorption studies have been carried out in polyamides such as PA6 filled with montmorillonite in the presence of ethanol [63]. An example of this is plotted in Figure 29.

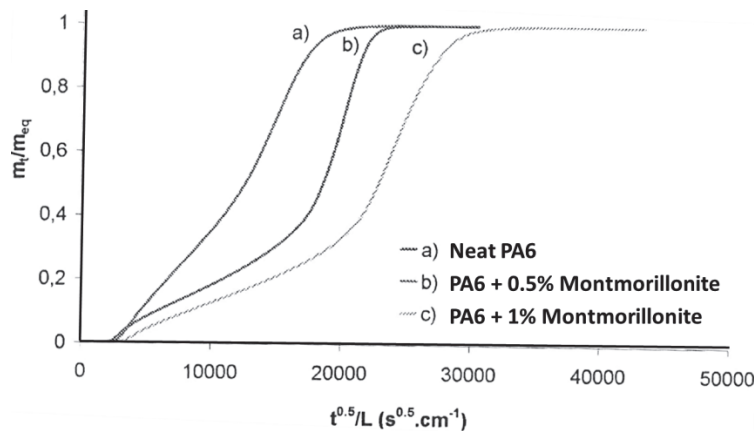


Figure 29: Ethanol sorption kinetics at a chemical activity of 0.8 for (a) neat and (b,c) charged PA6 as obtained by Sabard [63].

Sabard [63] observed that the sorption kinetics of ethanol in PA6 correspond to a Case II diffusion as it is shown in Figure 29. In this case one might think that ethanol plasticizes progressively the polymer, the diffusion starting with a Fickian regime and developing into an accelerated solvent intake.

I.2.3. Solvent pervaporation

I.2.3.1. Pervaporation mechanisms

When a polymer is placed in an atmosphere where one of the faces of the material is put in contact with a solvent and the other face is in contact with air or vacuum, the solvent will firstly diffuse through the polymer and when it reaches the face in contact with air or vacuum, the solvent molecules will start to escape or be desorbed by the polymer into the atmosphere as it is schematically shown in Figure 30a. A loss of solvent mass is then observed and if it is recorded on time, the pervaporation of the solvent through the polymer can be measured. When the solvent flux becomes constant, the solvent pervaporation steady regime is obtained as shown schematically in Figure 30b.

The diffusion and permeability coefficients can be calculated from permeability experiments. The permeability coefficient P is calculated when the solvent pervaporation steady regime is reached and it is defined as the loss of mass in a given time dm/dt normalized by the surface of the polymer in contact with the solvent A and the thickness of the polymer sample L as defined in Equation 25:

$$P = -\frac{dm}{dt} \left(\frac{L}{A} \right) \quad 25$$

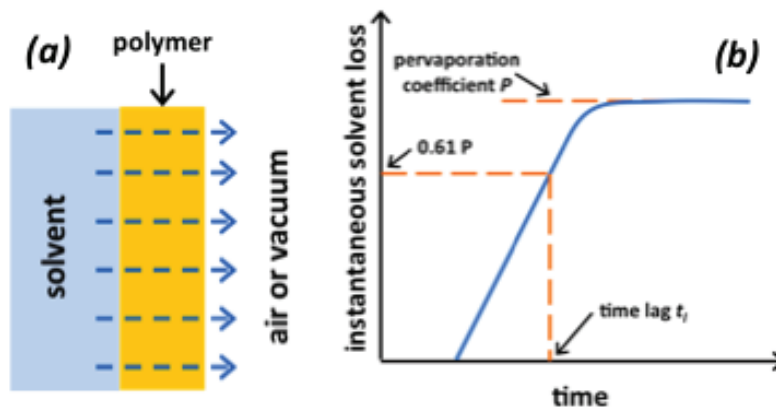


Figure 30: Schematic representation of (a) the pervaporation of a solvent through a polymer and (b) the obtained instantaneous pervaporation or solvent loss plot as a function of time.

Moreover, the diffusion coefficient D of a solvent can also be estimated from permeability tests only in the case of a Fickian diffusion regime [66]. In this case D is obtained from the pervaporation induction time or “time-lag” t_l as shown in Equation 26:

$$D = \frac{L^2}{6t_l} \quad 26$$

Finally, an equality linking the sorption, diffusion, and permeability coefficients can be established as shown in Equation 27, but this is only true if the sorption diffusion of this solvent in the studied polymer follows a Fickian regime.

$$P = D \times S \quad 27$$

1.2.3.2. Solvent pervaporation in polyamides

Polyamides, usually blended with mineral fillers or other polymers such as polyethylene or polypropylene are also studied for their permeability barrier properties to gases [80-84], water in liquid or vapor states [76,82-85], and other solvents such as ethanol and toluene [78,83,86]. Most of these studies are carried out so as to obtain a polymer blend suitable for food applications, but also studies concerning the permeability properties of PA6,6 aimed for automotive fuel tank applications are found.

Low et.al. [85] studied the influence of the temperature and of the water chemical activity on the barrier properties of PA6/nanoclay samples to this solvent. They observed that if the temperature or the relative humidity (i.e. the chemical activity of vapor water) increase, the pervaporation rate, i.e. the velocity of pervaporation, of water increases as it is shown in Figure 31.

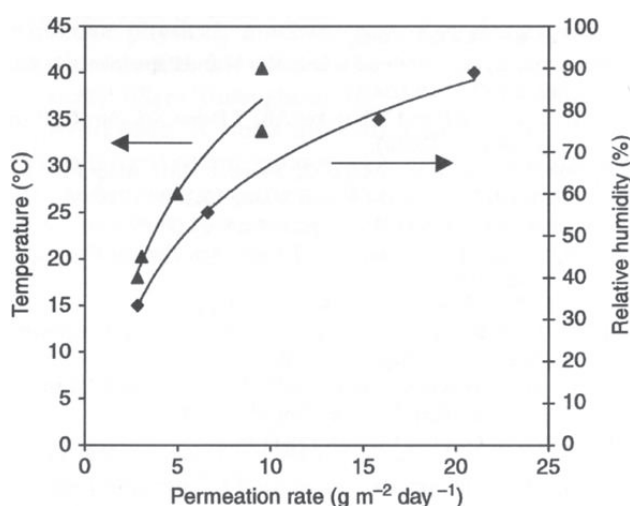


Figure 31: Steady-state pervaporation rate of the nanocomposite films as a function of temperature (Δ markers) and relative humidity (\diamond markers) as obtained by Low et.al. [85].

Moreover, Jiang et.al. [86] studied the permeability properties of PA6/nanoclay composites to ethanol and toluene. They observed globally that the PA6 samples they studied had better pervaporation properties to toluene than to ethanol, i.e. the loss of ethanol is ten times smaller than that of toluene as shown in Figure 32. These results are not surprising, as polyamides are polar polymers they would have stronger affinities with polar solvents like ethanol. On the other hand, interactions with less polar or non-polar solvents like toluene would be limited or weak. This would mean that the nature of the solvent and the possible interactions between the polymer and the solvent play a prominent role as well on the permeability properties of nylons.

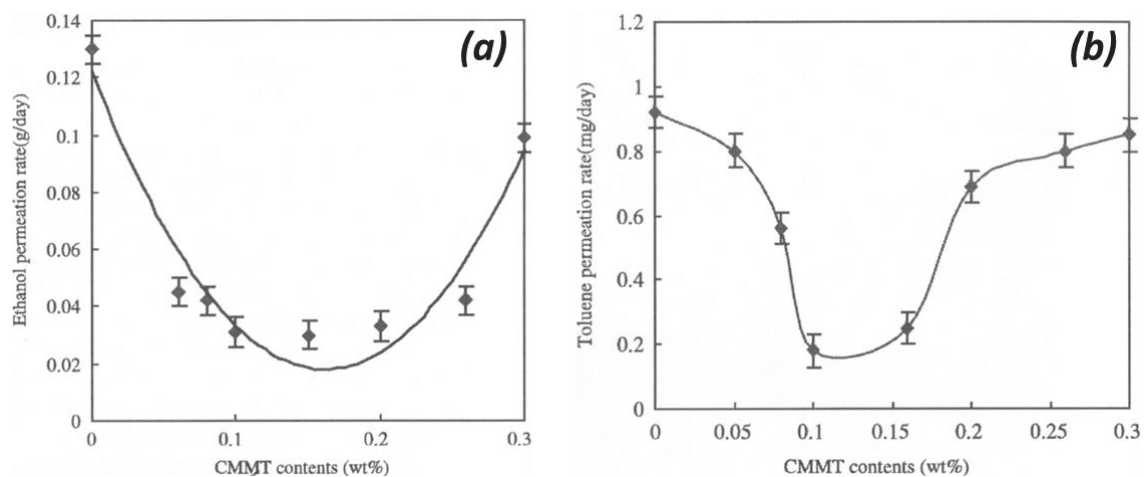


Figure 32: (a) ethanol and (b) toluene pervaporation rates of PA6/OMMT nanocomposites as a function of OMMMT content as obtained by Jiang et.al. [86].

I.3. Interactions of PA66 with solvent mixtures

I.3.1. Solvent mixtures composed of polar and non-polar molecules

There has been a growing interest in the past several years to develop cleaner and less-polluting grades of gasoline around the world. The first step towards this development was by changing the cracking and distillation processes as well as modifying or reducing the additives added to gasoline. The aim is to reduce the emissions of toxic organic pollutants such as pyridine or benzene and greenhouse-effect gases such as carbon dioxide. Furthermore, a new set of fuels, commercially known as biofuels, have been developed in the past few years. These biofuels are a blend of standard gasoline and ethanol produced by biological processes (i.e. from the fermentation of corn or cereal sugars). By adding ethanol to gasoline the octane-rate is enhanced and the polluting effects are reduced [87].

Commercially available biofuels can be modeled by ternary mixtures composed of ethanol, toluene, and isooctane. In order to assess and study the sorption and plasticization effect of these mixtures on PA66, it is important to understand well the thermodynamic properties of these mixtures in both liquid and vapor phases.

Studies on solvent mixtures carried out by Gramajo de Doz et.al. [88-91], Sandler et.al. [92,93], and others [87,94-98], have dealt with the liquid-liquid phase thermodynamic equilibrium of mixtures composed by gasoline components, ethanol, and water. However, few studies have been made concerning the vapor-liquid thermodynamic equilibriums for this sort of mixtures. Most of the studies found in the literature are for binary systems composed of alcohols and hydrocarbons [99-101] or hydrocarbons and hydrocarbons [102]. French et.al. [103] studied the vapor-liquid thermodynamic equilibrium for ethanol-fuel blends. French stated that a solvent mixture containing ethanol and several non-polar solvents is a strongly non-ideal mixture and that it could be approximated to an ethanol-hydrocarbon binary solvent mixture.

I.3.2. Polyamides as selective membranes

Polyamides, in the neat state or present in blends, filled polymers, or copolymers, are also studied for their selective separation properties [104-109]. The selective separation consists in putting a mixture of solvents of any nature (polar and/or non-polar) in contact with one side of a polymer membrane. Because these solvents may have interactive or repulsive interactions with the polymer membrane, the polymer will act as a “filter” for solvents. One or several solvents will then cross the polymer membrane and leave the liquid mixture through solvent pervaporation, which is actually the partial vaporization of a liquid solvent when it passes through a membrane. At the end the solvents able to cross the polymer membrane will be separated from solvents remaining in the liquid mixture. A schematic diagram of a pervaporation selective separation is represented in Figure 33.

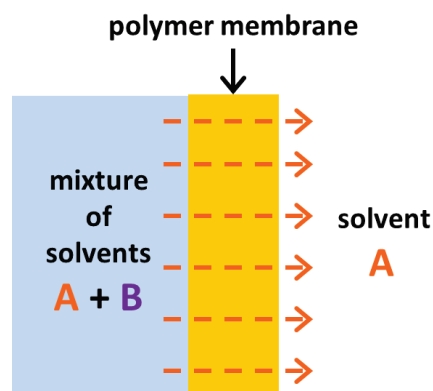


Figure 33: Schematic representation of the pervaporation selective separation of a mixture of solvents through a polymer membrane.

In the literature, several works despising the pervaporation properties of polyamide-based membranes in contact with polar/polar (i.e. water/ethanol [105]), non-polar/non-polar (i.e. benzene/cyclohexane [106-108]), and polar/non-polar (i.e. pentane/alcohols [104]) solvent mixtures can be found among others. Nevertheless, few or almost no literature data concerning the sorption of a solvent mixture in polyamides and PA6,6 is available, especially in the case of a polar/non-polar solvent mixture.

I.4. Influence of solvents on PA66 molecular mobility

I.4.1. Effect of solvents on PA66 molecular relaxations

I.4.1.1. Effect of water on PA66 glass transition : experimental data

The effect of water sorption on the main α relaxation and thus on the glass transition temperature T_g of polyamides is well documented in the literature [32,62,110-119]. It has been observed by different analytical techniques such as DSC [62,110,111], DMA [32,112-115,118,119] and Dielectric Spectroscopy [116,117] that in presence of water the relaxation is shifted towards lower temperatures and that the temperature shift increases when the concentration of water in the polymer increases. To illustrate the effect of water on the alpha relaxation, Figure 34a plots the shift in temperature of the α relaxation observed by DMA for a PA6 before and after drying [32] and Figure 34b plots the T_g drop of PA6,6 samples as a function of water concentration [62].

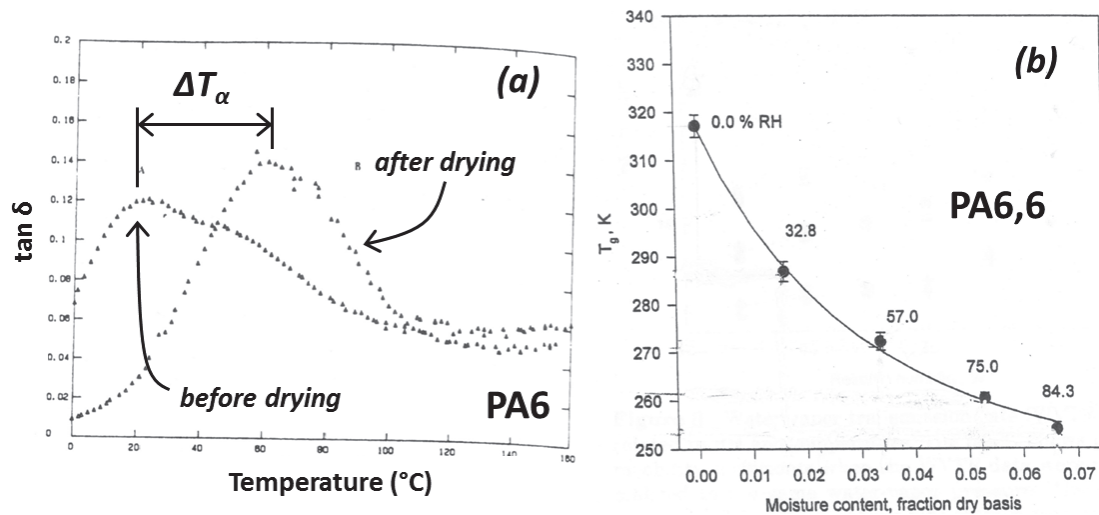


Figure 34: (a) Polyamide 6 α relaxation as observed by DMA for a dry sample and a sample containing water [32] and (b) Polyamide 6,6 T_g as a function of the fraction of absorbed water as obtained by Lim et.al. [62].

It is firstly observed in Figure 34a that the drop of T_{α} is quite large for PA6 containing water. Moreover it is shown in Figure 34b that the T_g drop provoked by water in PA6,6 can reach 60°C for a sample conditioned at a relative humidity of 85%.

It has been globally understood and accepted [120-127] that the drop of the glass transition temperature provoked by water in polyamides is due to the fact that water can form H-bonds with the amide groups present in the amorphous phase of polyamide. It has been observed by Infrared Spectroscopy [124-127] and by Solid state NMR [127] that water indeed interacts with the amide functions of polyamides. Figure 35 plots for instance the IR spectra of a PA6 at the dry state and the same sample containing water [124].

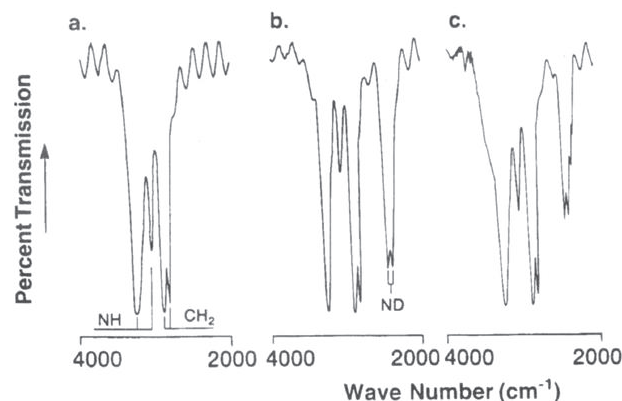


Figure 35: IR spectra for a PA6 (a) at the dry state, (b) containing 11% $_{wt}$ of D_2O , (c) after being partially dried from the (b)-state as obtained by Murthy et.al. [124].

It is observed in Figure 35, that when deuterated water D_2O is absorbed by PA6, an elongation peak related to the amide- D_2O appears (Figure 35b) and that when the sample is partially dried the intensity of this peak diminishes (Figure 35c). Puffr and Sebenda [120] have proposed a mechanism on how water binds itself to the amide groups of polyamides. This mechanism is schematically shown in Figure 36.

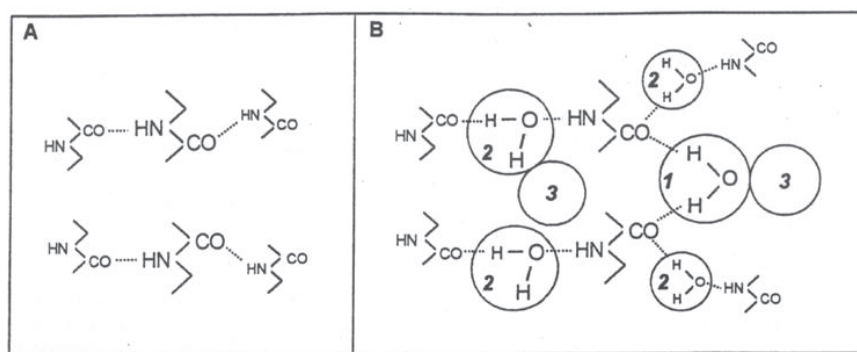


Figure 36: Mechanism of water sorption in polyamides: (1) firmly bound water, (2) loosely bound water, and (3) water clustering as proposed by Puffr and Sebenda [120].

In the water binding mechanism proposed by Puffr and Sebenda and shown in Figure 36, three “types” of bound water are considered. The firmly bound water concerns the molecules that are able to form 2 H-bonds with two different carboxylic functions, the loosely bound water concerns the molecules that also form 2 H-bonds but in this case they bind themselves to one amine and one carboxylic function. Finally, the third “type” concerns the water molecules that bind to other water molecules that are already bound with amine or carboxylic functions and that then form clusters of water or condensation sites. These observations and hypotheses on the interactions of water with polyamides are somehow correlated to the results observed for the sorption isotherm models that describe water as a solvent able to form clusters in polyamides presented before. The consideration of water forming clusters having a size of ca. 2-3 molecules corresponds well to the water-polyamide binding mechanism proposed by Puffr and Sebenda.

Few studies in the literature deal with the interactions between other types of solvents like alcohols and polyamides [128,129], however the effect of these solvents on polyamides T_g is not discussed.

1.4.1.2. Effect of solvents on PA66 secondary relaxations

Several authors have studied by either Dynamic Mechanical Analysis (DMA) or Dielectric Spectroscopy the effect of water [112-119,130] or other molecules like phenol or formic acid [119] in the secondary relaxations of different Polyamides (i.e. PA6, PA12, and PA6,6). Globally it was observed for these polyamides that their secondary relaxations temperature and amplitude are influenced by the presence of water, or other molecules such as phenol and formic acid. Let us focus in the case of the influence of water on the secondary relaxations of PA6,6 which was studied by Starkweather et.al. [130].

Concerning the β relaxation, attributed to the motions of the amide groups of the polymer chains, Starkweather observed that this relaxation was shifted towards lower temperatures and higher frequencies when in presence of water and that its intensity (i.e. value of ϵ'') of and amplitude (i.e. broadening) increased with the amount of water absorbed by PA6,6.

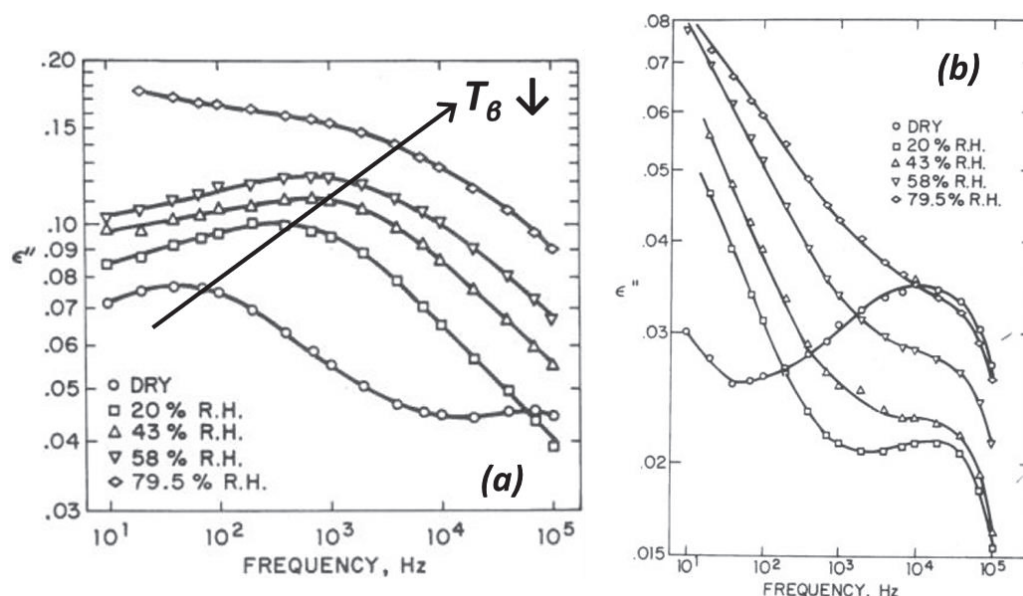


Figure 37: Loss permittivity ϵ'' as a function of frequency highlighting (a) the β and (b) the γ relaxations of PA6,6 at the dry state and in presence of water as observed by Starkweather et.al. [130].

The influence of water on the β relaxation temperature and intensity could be understood by the fact that water would preferably interact with the amide groups of PA6,6 chains. By interacting with these groups, water might make the amide functions more mobile and thus provoking a drop on the relaxation temperature. Moreover the raise in the intensity of the relaxation could be explained by the fact that water being a polar molecule will strongly respond to an applied electric field, which would provoke an increasing of the dielectric response of the polymer.

Concerning the γ relaxation, Starkweather observed that the relaxation peak position is almost unchanged with water absorption, i.e. water has a very limited influence on the γ relaxation temperature. However the shape and intensity of the relaxation is influenced by the presence of water. For dry samples the γ relaxation appears as a well-defined peak but as water is absorbed the γ relaxation shape becomes more of a shouldering, and it is furthermore seen that the β relaxation contribution and the raise in conductivity start to appear at low frequencies.

1.4.2. Plasticization models for a polymer-polymer or polymer-plasticizer mixture

Several models that predict the T_g of a polymer-polymer or a polymer-plasticizer mixture are found in the literature. The Fox [131-133] and Gordon-Taylor [134-136] equations are the most known models, among other equations such as those of Jenkel – Heusch [137], Kelley – Bueche [138], Couchman – Karasz [139,140], and Lu – Weiss [141]. For the sake of understanding in the following equations the polymer will be noted as the component 1 and the plasticizer as the component 2. As it will be seen in the following paragraphs, only the Lu – Weiss model somehow take into account the interactions between the polymer and the plasticizer, with the other models only considering their thermal properties.

I. Review

The Fox equation [131-133] is the simplest model for predicting the T_g of a polymer-plasticizer mixture, this relationship only takes into account the mass fractions and the T_g 's of each of the mixture components as shown in Equation 28 :

$$\frac{1}{T_g} = \frac{w_1}{T_{g-1}} + \frac{w_2}{T_{g-2}} \quad 28$$

where T_g is the glass transition temperature of the mixture, T_{g-1} , T_{g-2} , w_1 , and w_2 are the glass transition temperatures and the mass fractions of the mixture components 1 and 2 respectively.

The Gordon – Taylor model [134-136] is a developed Fox equation which takes into account the density and the thermal expansion coefficients of the polymer and the plasticizer, as shown in Equation 29 :

$$T_g = \frac{T_{g-1}w_1 + KT_{g-2}w_2}{w_1 + Kw_2} \quad 29$$

with K defined as:

$$K = \left(\frac{\rho_1}{\rho_2} \right) \left(\frac{\Delta\alpha_2}{\Delta\alpha_1} \right) \quad 30$$

where ρ_1 , ρ_2 , $\Delta\alpha_1$, and $\Delta\alpha_2$ are the densities and the thermal expansion coefficients of components 1 and 2 respectively.

The Jenckel – Heusch equation [137] takes into account the solvent quality of the plasticizer through the parameter ϵ , as shown in Equation 31 :

$$T_g = T_{g\epsilon 1}w_1 + T_{g\epsilon 2}w_2 + \epsilon w_1w_2(T_{g\epsilon 2} - T_{g\epsilon 1}) \quad 31$$

The Kelley – Bueche model [138] considers as well the thermal expansion coefficients of the polymer and the plasticizer but differs from the Gordon – Taylor equation in the fact that it substitutes the mass for a volume fraction as shown in Equation 32 :

$$T_g = \frac{\Delta\alpha_1 T_{g-1}v_1 + \Delta\alpha_2 T_{g-2}v_2}{\Delta\alpha_1 v_1 + \Delta\alpha_2 v_2} \quad 32$$

where v_1 and v_2 are the volume fractions of components 1 and 2.

The Couchman – Karasz model [139,140] considers instead the heat capacity at the glass transition step for the polymer and the plasticizer as shown in Equation 33 :

$$T_g = \frac{T_{g-1}w_1 + k_0 T_{g-2}w_2}{w_1 + k_0 w_2} \quad 33$$

I. Review

with k_0 defined as:

$$k_0 = \frac{\Delta C_{p-2}}{\Delta C_{p-1}} \quad 34$$

where ΔC_{p-1} and ΔC_{p-2} are the heat capacities at the glass transition step of components 1 and 2.

The Lu – Weiss model [141] is a development of the Couchman – Karasz relationship, in which the molar masses, the densities and the Flory-Huggins interaction parameter of the polymer and the plasticizer are taken into account as shown in Equation 35 :

$$T_g = \frac{T_{g-1}w_1 + k_0 T_{g-2}w_2}{w_1 + k_0 w_2} + Aw_1w_2(1 + dw_2) \quad 35$$

with A defined as:

$$A = \frac{\chi_{12} R (T_{g-1} - T_{g-2}) c}{M_1 \Delta C_{p-1}} \quad 36$$

where χ_{12} is the Flory-Huggins interaction parameter, R is the molar gas constant, M_1 is the molar mass of component 1, $c = \rho_1/\rho_2$, and finally with d defined as:

$$d = (1 - k_0) + (1 - b) + 2(1 - c) \quad 37$$

with $b = M_2/M_1$, the ratio of the molar masses of components 1 and 2.

In the literature, modeling equations and experimental results are found for miscible polymer-polymer systems (i.e. blend of atactic and isotactic PMMA's) [141], for polymer-plasticizer systems (i.e. PS-diethylbenzene and PMMA-Diethylphtalate) [138], and for some polymer-solvent systems (i.e. PS-ethylbenzene or epoxy resin-water) [140], but no data comparing a plasticizing model equation with experimental data of a polyamide-solvent system are found. These models might be used to describe such systems.

I.5. Influence of the crystalline and amorphous phases on PA66 mechanical properties

I.5.1. Influence of the crystalline phase and the temperature on the mechanical properties of polyamides

I.5.1.1. Influence of the crystalline phase

It has been observed in the literature [142-145] that the crystalline phase, specifically the crystalline ratio [142,143], the size of the crystallites [144], and the crystalline phase structure [145] have an effect on the mechanical properties of polyamides. Figure 38 presents as an example the effect of the crystalline ratio on the stiffness and the yield stress of PA6,6 as obtained by Starkweather et.al. [142].

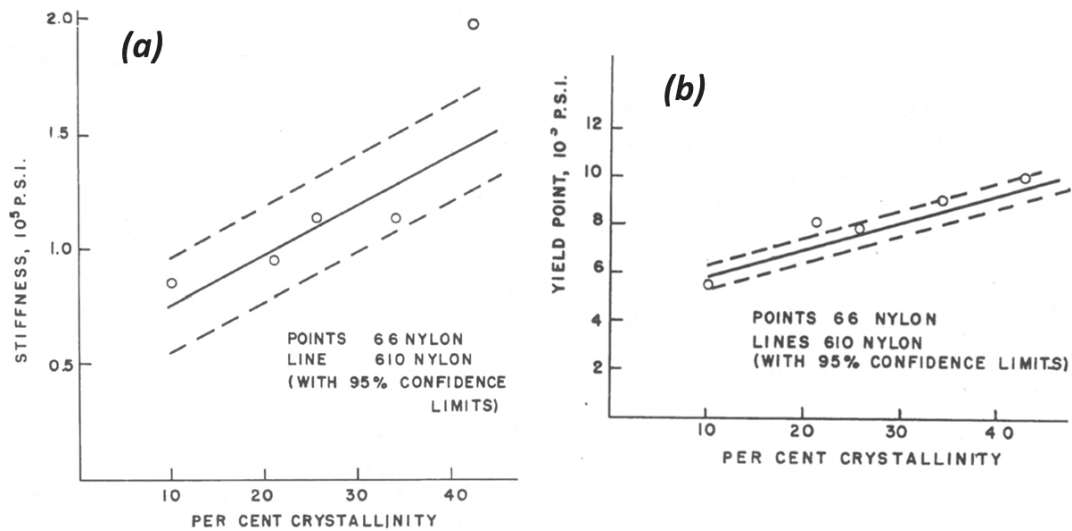


Figure 38: PA6,6 (a) stiffness and (b) yield stress as a function of the crystalline ratio as obtained by Starkweather et.al. [142].

It is observed in Figure 38 that the stiffness and the yield stress of PA6,6 increase when the crystalline ratio of this polymer increases. Moreover, Starkweather also studied the effect of the crystalline ratio on the tensile strength properties of PA6,10 [142] as it is shown in Figure 39.

Figure 39 shows that the tensile strength of PA6,10 increases when the crystalline ratio does. It is considered that the crystalline phase of a polymer acts as a reinforcement of the material and as it is observed above, when the fraction of this phase in polyamides increases, the mechanical properties of these polymers are enhanced.

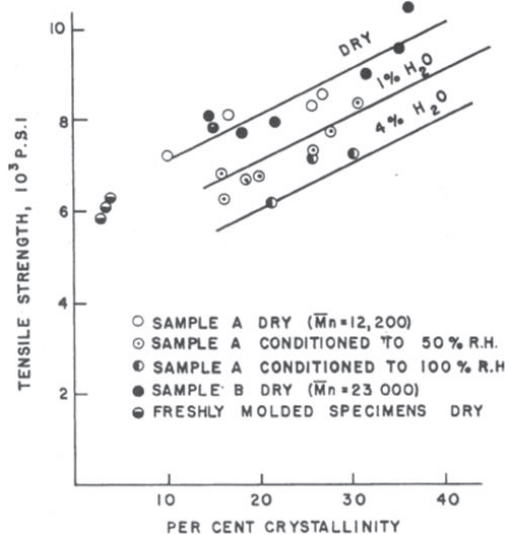


Figure 39: PA6,10 tensile strength as a function of the crystalline ratio as obtained by Starkweather et.al. [142].

Moreover, in another work, Starkweather [144] studied the influence of the size of the crystalline spherulites on the mechanical properties of PA6,6. These results are shown in Figure 40.

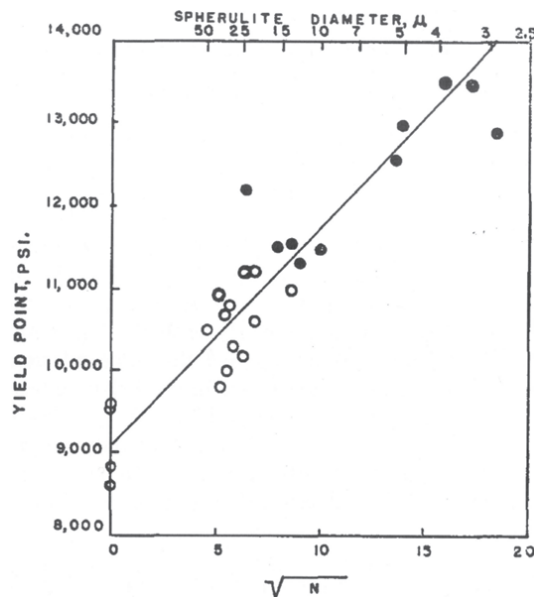


Figure 40: Effect of the spherulite diameter μ on the yield stress of PA6,6 for compression-molded films and injection-molded bars as obtained by Starkweather et.al.[144]. N is the number of spherulite boundaries per millimeter.

It is observed that when the spherulites size decreases, the yield strength of PA6,6 increases. This might be explained by the fact that the crystalline phase acts as reinforcement and when a tensional effort is applied in a polymer, having smaller spherulites allows a more uniform and a wider distribution of the loading through the spherulites, increasing the polymers tensile properties. However, the drawback of having smaller spherulites is that the polymer becomes more brittle (lower elongation at break and tensile impact strength) than other samples having larger spherulites, as it was observed by Starkweather as well. Furthermore, Miri et.al. [145] studied the effect of the α , β , and γ crystalline structures on the tensile properties of PA6, the results being shown in Figure 41.

It is observed that the stiffer samples (i.e. higher Young's modulus and yield stress, and smaller stress at failure) are those containing the α crystalline form, followed by those containing the γ form and then those containing the β form. The α form is the densest of all the three crystalline forms of PA6 and also the one where the chains in the crystalline lamellae are better organized. The presence of the α form might induce then a higher reinforcement effect on PA6 thanks to these mentioned intrinsic properties, whereas the presence of the γ form, which is stable but less organized and less dense, or the β form, which is a non-stable crystalline form, might induce a drop on the mechanical properties. In the case of PA6,6, the influence of the perfection degree of the crystalline phase on mechanical properties is little described in the literature.

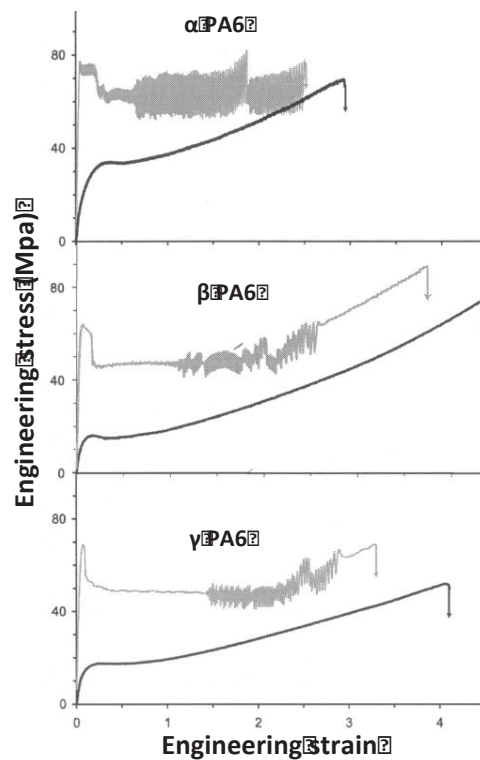


Figure 41: Effect of the crystalline structure morphology on the stress-strain properties of dry (grayish plots) and water-conditioned (blackish plots) PA6 samples as observed by Miri et.al. [145].

1.5.1.2. Influence of the temperature

The temperature also governs the mechanical behavior of polymers. Indeed if the testing temperature is modified, the molecular mobility of the polymer will vary accordingly. For instance, if the working temperature is far below the glass transition temperature T_g the polymer will be rigid (high Young's modulus E and yield stress σ_y) and brittle (low resistance upon impact) but as the temperature increases and approaches the T_g the polymer becomes more ductile (E and σ_y drop) and tough (the polymer does not fail completely upon impact). Temperature can then be considered as a parameter that can be used for studying the influence of the polymer's amorphous phase molecular mobility on its mechanical behavior.

The effect of temperature on the tensile properties of PA6 has been studied by Shan et.al. [146]. Figure 42 plots as an example the nominal stress-strain curves obtained for a dry PA6 for several draw temperatures.

It is observed in Figure 42 that when the draw temperature increases the Young's modulus E (i.e. the slope of the stress-strain curve in the elastic part) decreases, and that the value of the yield stress (maximum of the stress-strain curve) also decreases and even disappears for temperatures of 50°C and higher.

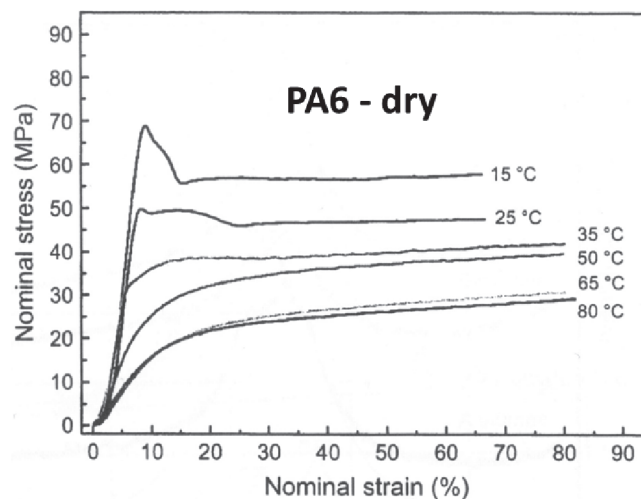


Figure 42: Nominal stress-strain curves for PA6 at various temperatures as obtained by Shan et.al. [146].

Few studies deal with the effect of temperature on the impact strength properties, namely the resilience R and the brittle-tough transition temperature $T_{B/T}$ of neat polyamides. The resilience R is the amount of energy absorbed by a defined section (linear or surface) of the polymer upon an impact test. The brittle-tough transition temperature $T_{B/T}$ is the temperature at which the polymer does not longer break completely when an impact effort is applied to it. Below $T_{B/T}$ the polymer is said to be brittle or fragile, and above $T_{B/T}$ the polymer is said to be ductile or tough.

Figure 43a shows the resilience of a dry PA6,6 obtained by Izod impact tests as a function of the temperature as described by Kohan [2], and Figure 43b shows schematically the variation of resilience as a function of temperature for a neat polyamide and for a polyamide-rubber blend, highlighting the T_g of polyamide in relation to the $T_{B/T}$ of this polymer as described by Collyer [147].

It is observed in Figure 43a that when the temperature increases, the resilience upon impact of PA6,6 increases as well. The resilience increases slightly for low temperatures (-50 to 10°C), but it rapidly increases when the temperature approaches the $T_{B/T}$ (ca. 70°C). Indeed at low temperatures the polymer is mostly rigid and will fail upon impact with a certain amount of energy but as the temperature gets closer to the $T_{B/T}$ the polymer chains will be more mobile and may then be able to better absorb the impact or in other words it would take more energy to break the polymer. It would be interesting to study in which extent the molecular mobility of PA6,6 has an influence on its impact strength properties.

I. Review

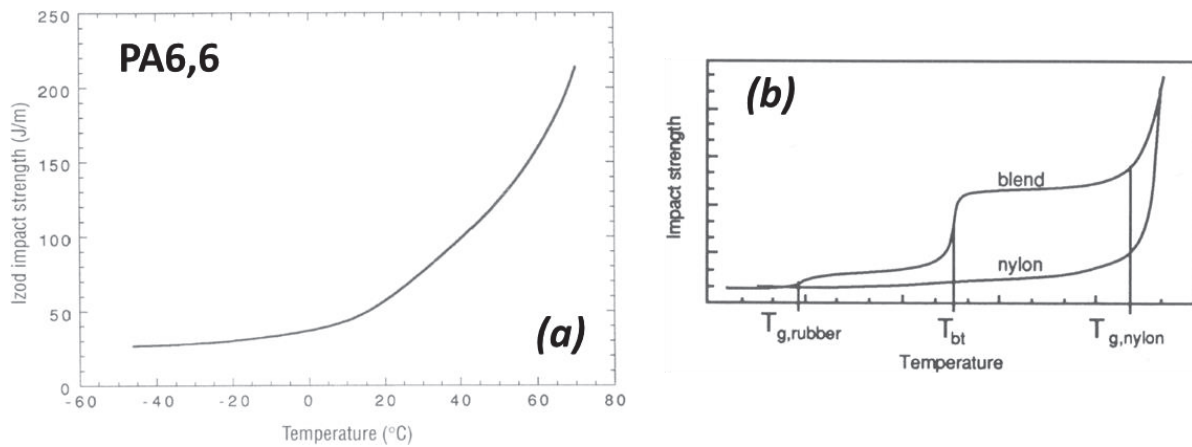


Figure 43: (a) Izod impact strength as a function of temperature for PA6,6 [2] and (b) schematic representation of the impact strength of a neat nylon and of a nylon-rubber blend as a function of the temperature [147].

1.5.2. Influence of water on polyamide mechanical properties

Studies dealing with the influence of solvent sorption in the mechanical properties of polyamides are widely found in the literature [2,145,148-151]. These studies deal actually with the effect of water on the mechanical properties of polyamides. The effect of water on polyamides properties, specifically on the Young's modulus E , the yield stress σ_Y , the elongation at break, and the flexural modulus have been studied by Miri et.al. [145] and Reimschuessel et.al. [150] and also discussed by Kohan [2]. Figure 41 shows as well the effect of water on PA6 samples studied by Miri, it was observed that water provokes a drop on the yield stress σ_Y (maximum of the stress-strain curve) as well as making the samples more ductile, i.e. the elongation at break is greater than for the dry samples. The results obtained by Reimschuessel and Kohan are shown in Figure 44.

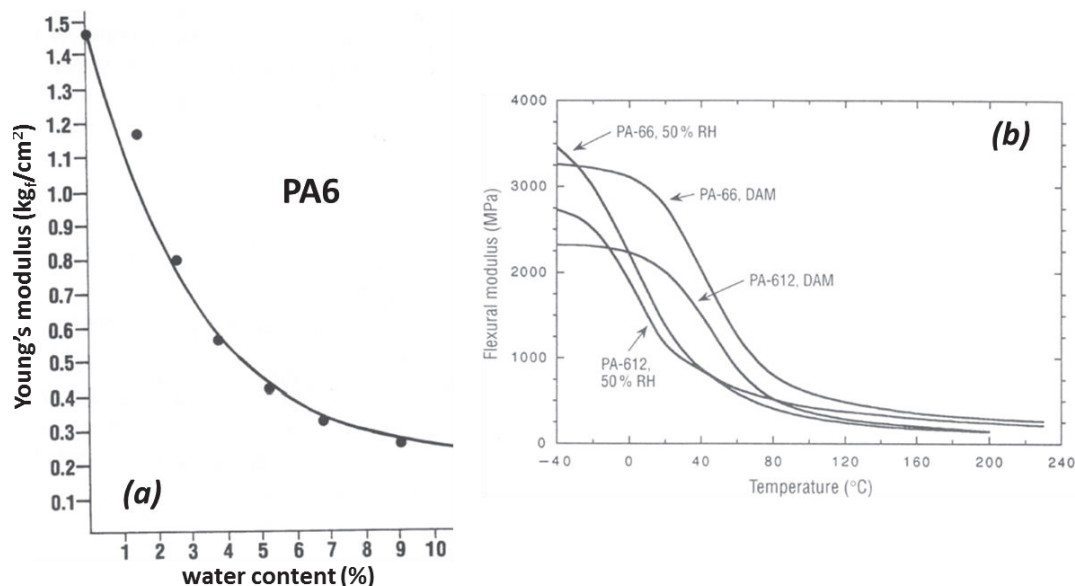


Figure 44: Effect of water sorption (a) on PA6 Young's modulus measured at 30°C [149,150] and (b) on the flexural modulus of PA6,6 and PA6,12 as described by Kohan [2].

it is observed in Figure 44a that at a given temperature of 30°C, the Young's modulus E diminishes abruptly when water is absorbed by PA6, i.e. E drops by a factor of five between

I. Review

a dry sample ($E=1.5 \text{ kg}_f/\text{cm}^2$) and a completely saturated sample containing ca. 9 %wt of water ($E=0.3 \text{ kg}_f/\text{cm}^2$). On the other hand, it is observed in Figure 44b that the flexural modulus at the glassy plateau of PA6,6 and PA6,12 increases when water is absorbed by the polymer. This rigidifying effect might come from the formation of water-amide bridges between. Thus, it is worth noticing that although water shifts the T_g of polyamide at lower temperature, it also increases the mechanical modulus in the glassy state.

Concerning the impact strength properties of polyamides, Gaymans et.al. [151] studied the effect of water on the brittle-tough transition temperature $T_{B/T}$ in Polyamide 6 (PA6) and the relationship of this transition temperature with the glass transition temperature T_g . These results are shown in Figure 45. Firstly, it is observed that for neat PA6 the $T_{B/T}$ is shifted towards lower temperatures when water is absorbed by the samples. Furthermore, Gaymans observed that the drop on the $T_{B/T}$ induced by water is similar to that of the glass transition temperature T_g and that both transitions seem to follow the same trend as shown in Figure 45b. This trend highlights the prominent role of amorphous phase on Polyamide 6 impact properties.

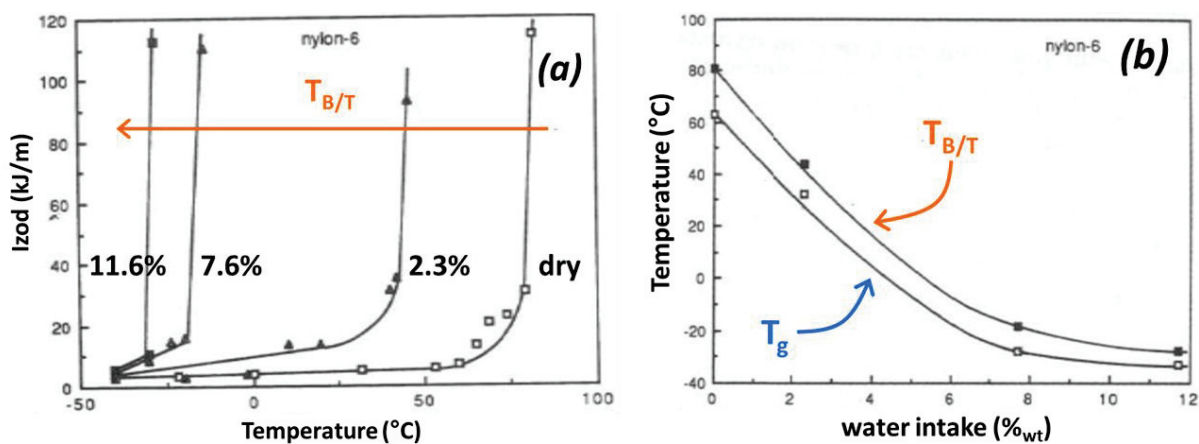


Figure 45: (a) Notched Izod impact strength as a function of temperature and (b) comparison of the T_g and the $T_{B/T}$ transitions for different water concentrations in Polyamide 6 [151].

In more crystalline polymers such as HDPE, $T_{B/T}$ is much higher than T_g , the $T_{B/T}$ being -25°C whereas the T_g is around -120°C [152]. Nevertheless, in the case of polyamides, it is also observed that there is a small gap between the T_g and the $T_{B/T}$ temperatures. This gap may come from the fact that a sample in an impact test is solicited at very high frequencies, so the main relaxation transition happens at a higher temperature when compared to the T_g . The T_α at the frequency of solicitation might then be considered as a more accurate parameter for comparing the molecular mobility with the brittle-tough transition temperature $T_{B/T}$.

I.6. Objectives of the thesis

The applicative context of this work is the development of automotive fuel tanks exhibiting good barrier properties to biofuels, while keeping good mechanical properties, notably the impact strength behavior. The scientific issues of this thesis are the better understanding of the interactions between PA6,6 and solvents, and how barrier and mechanical properties are modified when solvents of different nature are introduced in PA6,6.

The sorption at equilibrium of solvents like water and ethanol in PA6,6 is well documented. It has been observed that these solvents are absorbed in large amounts by this polymer. It would be then interesting to study the sorption at equilibrium of various solvents having different polarities and sizes, so as to better understand how the nature of a given molecule affects or enhances the interactions with PA6,6 polymer chains. In this work, the interaction between polyamide 6,6 and solvent mixtures or a series of polar and non-polar solvents exhibiting different sizes and polarities, will be studied.

Sorption isotherm models are proposed and used in the literature to describe the sorption of solvents like water or ethanol in PA6,6. Models like the GAB or Park relationships, which consider that solvents can form clusters in the polymer, describe well the sorption isotherms of water in polyamides. To further understand the interaction mechanisms between PA6,6 and solvents or solvents mixtures, we propose to not only study a wide panel of solvents, but also study PA6,6 formulations in which intermolecular interactions have been modified by additivation or chemical functionalization.

The presence of an H-bond network in PA6,6 plays a prominent role on the molecular mobility of its amorphous phase and notably on the glass transition temperature T_g . It was also shown that water interacts and disturbs this network, provoking a drop on PA6,6 T_g . Some studies in the literature deal with the interactions of polyamide with other types of solvents like alcohols [128,129], but the effect of these solvents on polyamides T_g is not discussed. In this work, it is proposed to study the effect of polar and non-polar molecules on PA6,6 amorphous phase molecular mobility (glass transition process and secondary relaxations), and to compare the plasticization effect of the different molecules, introduced as pure solvents or as solvent mixtures. Empirical and theoretical models that describe the T_g drop of a polymer in presence of plasticizers were detailed in this chapter. In this work, it is proposed to check if these models can predict the effect of solvents on PA6,6 T_g . On the basis of the results obtained with neat or modified polyamide 6,6 in presence of the different solvents, plasticization mechanisms will be proposed and discussed.

The interactions between PA6,6 and solvents mixtures are poorly described in the literature. This topic is yet of great importance from the applicative point of view, since biofuels in contact with polyamide fuel tanks can be modeled by mixtures of polar and non-polar solvents, namely ethanol, toluene and isooctane. In order to better understand the interactions between PA6,6 and such solvents mixtures, it is important to study the mixture thermodynamics. In this work, the chemical activities of the solvents in the mixture will be determined and the interaction between solvents will be discussed. At the end, the relative plasticization effect of the different components of the mixture will be discussed.

Finally, as the applicative context is the development of polyamide formulations exhibiting good barrier properties as well as good mechanical properties, it is relevant to wonder what will be the effect of solvents on PA6,6 mechanical behavior. On one hand, it has been shown that solvents like water can deeply affect polyamide amorphous phase molecular mobility. On the other hand, as PA6,6 possesses a relatively low crystalline ratio (ca. 40%_{wt}), the molecular mobility of the polymer's amorphous fraction is expected to play a prominent role in defining the mechanical behavior. In this work, it is then proposed to study in what extent the amorphous phase molecular mobility of PA6,6 influences its mechanical properties, the modification of the amorphous phase molecular mobility being provided by (1) a raise in

I. Review

temperature, (2) an addition of additives, (3) a modification of the chemical structure of the polymer, or (4) a conditioning in water at different hygrometry levels. In order to check if these modifications do not yield crystalline structure modifications that could themselves affect the mechanical properties, the crystallinity of PA6,6 will be accurately characterized.

This thesis is divided in three main parts. The first part deals with the presentation of the studied PA6,6 formulations as well as the description of the experimental techniques and setups that allowed us to characterize the molecular mobility, the sorption and permeability, and the mechanical properties of these formulations. The second part presents the study of the sorption of a series of pure solvents and that of a set of ternary mixtures in a neat PA6,6. The influence of the polarity, the size and the thermodynamics of these solvents on their sorption and plasticization effect is discussed. Finally the third part focuses on the effect of modifying a neat PA6,6 through additivation or chemical modification on the sorption and mechanical properties of this polymer. The molecular mobility of the obtained formulations is characterized and then the sorption, pervaporation, tensile strength, and impact strength properties of these formulations are studied and discussed.

II. Materials, samples and techniques

II.1. Polymer formulations

II.1.1. Neat PA66

In order to study and to better understand the interactions between polyamide and different solvents (polar, apolar, mixtures), we firstly studied a reference system which was a neat, non-filled, non-additivated PA6,6. A neat PA6,6 Rhodia-grade, called hereafter *NeatPA66*, was then chosen and it will be the formulation studied in chapter III devoted to the study of the effect of a wide range of solvents on polyamide. Table 2 shows the properties and characteristics of the *NeatPA66* formulation.

Table 2: Intrinsic properties of the *NeatPA66* formulation.

NeatPA66 formulation	
Glass transition temperature T_g (dry) – DSC	64°C
Melting temperature T_m – DSC	260°C
Crystalline fraction X_C – DSC	38%
Molecular weight M_W	25000 g/mol

Chapter IV is then devoted to the study of modified polyamide in presence of a selection of solvents. Another neat, non-filled, non-additivated PA6,6 Rhodia-grade reference was then chosen so as to keep the same molecular weight as the chemically-modified and additivated PA6,6 formulations,. Table 3 shows the intrinsic properties of this second neat PA6,6 reference denoted hereafter “REF”.

Table 3: Intrinsic properties of the *REF* formulation.

REF formulation	
Glass transition temperature T_g (dry) – DSC	71°C
Melting temperature T_m – DSC	264°C
Crystalline fraction X_C – DSC	34%
Molecular weight M_W	15000 g/mol

II.1.2. Modified PA66

Furthermore, after studying the effect of various solvents on neat PA6,6, we were interested in studying the effect of a selection of solvents in chemically modified or additivated polyamide 6,6. Two chemically-modified and two additivated PA6,6 were studied.

II.1.2.1. Chemically-modified PA66

Two chemically modified PA66 formulations were studied: PA66/6HIA and PA66/6AiSLi. These copolymers were obtained by polycondensation by mixing Nylon 6,6 salts (Figure 2,

II. Materials & Techniques

Chapter I) with 6HIA or 6AiSLi monomers. The chemical structures of the PA6HIA and PA6AISLI monomeric units are presented in Figure 46.

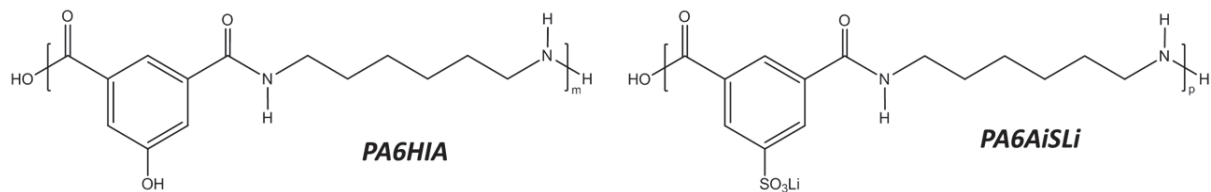


Figure 46: PA6HIA and PA6AISLi chemical structures.

These co-monomers were chosen because it was desired to obtain PA6,6 formulations having stronger intermolecular interactions (H bonds), the introduction of hydroxyl or alkylsulfonate functions in the aromatic rings providing stronger bonds with the PA6,6 amine groups than those formed between two “classic” amide groups. The molar composition of PA6,6/6HIA and PA6,6/6AiSLi both copolymers was 95/5_{mol}, this relatively low comonomer content being introduced in order to limit any decrease of the crystalline fraction. The PA6,6/6HIA and PA6,6/AiSLi copolymers denoted hereafter HIA and AiSLi were synthesized in a 200 L reactor by the Rhodia laboratory of Synthesis and Processing of Polymers (LSPP - Stéphane Jéol and Daniel Duchêne) in the Rhodia Research Center of Lyon (CRTL). The molecular mass of the obtained copolymer were around 15000 g/mol.

II.1.2.2. Additivated PA66

Furthermore, two resins were chosen as additives in order to modify PA6,6 formulations. These additives were the phenyl-laurylaldehyde (*LA*) and the phenyl-heptanaldehyde (*HA*) resins that belong to a family of phenolic resins developed by Rhodia (Caroll Vergelati, Olivier Andres) and synthesized in the KiloLab synthesis facility of the CRTL (Vincent Schanen). The molecular structure of the two additives is shown in Figure 47a, the main difference between the two additives being the length of the alkyl chain (R), laurylaldehyde containing 12 carbons segments, instead of 7 for heptanaldehyde.

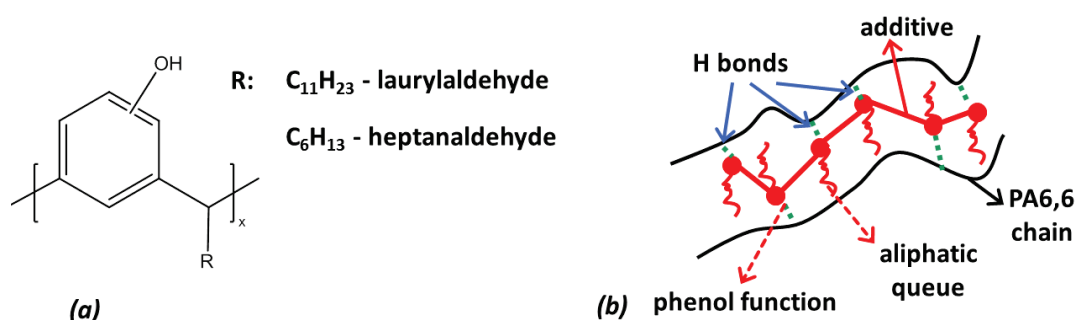


Figure 47: (a) Phenolic resin chemical structure. (b) Interactions between PA6,6 and the phenolic resins.

The molar masses of the heptanaldehyde (*HA*) and laurylaldehyde (*LA*) resins are $M_{HA}=190\text{g/mol}$ and $M_{LA}=260\text{g/mol}$ respectively. The polymerization degree X_n of these additives is of ca. 8-10, i.e. each additive chain is formed of between 8 and 10 monomeric units. These additives are supposed to be able to bond to PA6,6 amide groups via the phenolic function, the H-bonds formed between these phenolic functions and the amide groups of polyamide being stronger than those formed between amide groups. Moreover

II. Materials & Techniques

the presence of long alkyl chains might provoke an increase on the molecular mobility through steric effects, which would be beneficial for impact strength properties. A schematic representation of the interactions between the additives and PA6,6 is shown in Figure 47b. These additives were chosen because they modify polyamide intermolecular interactions, and they modify to different extents the local polarity of polyamide.

The phenol-additivated PA6,6 formulae were obtained by compounding 10%_{wt} of either laurylaldehyde or heptanaldehyde with the neat PA6,6 called REF, this neat PA6,6 grade being chosen because its molecular mass was similar to that of the copolymers. The obtained additivated formulations are called hereafter 10LA (REF + 10% laurylaldehyde) and 10HA (REF + 10% heptanaldehyde).

II.2. Polymer processing

II.2.1. Film-cast extrusion

Three formulations (*NeatPA66*, HIA, and AISLI) were film-casted thanks to a Leistritz extruder with a L/D ratio of 33 and a through put of 10 kg/hr, the film cast set-up being schematically shown in Figure 48. The principle of film-casting is the following: the polymer is introduced via a hopper in an extruder, in which the polymer melts. A dye is placed at the end of the extruder, which gives the molten polymer a planar form when it exits the extruder. Then the polymer is carried through a series of rolls that will cool it down (chill-rolls) and draw it to a given thickness.

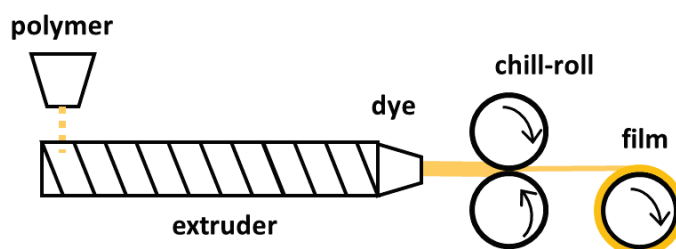


Figure 48: Film-cast setup

The processing of the different formulations was done at the Polymer Processing Facility of the CRTL (Vincent Curtil, Olivier Andrès, Thomas Jacquin, and Sandrine Rossi), Table 4 showing the processing conditions for the three formulations.

Table 4: PA6,6 formulae film-cast processing conditions.

Formula	Temperature [°C]		Film casting speed [m/min]	Draw ratio	Obtained thickness [μm]
	Extruder	Chill-roll			
<i>NeatPA66</i>	282	125	4.5	6	100
HIA	283	130	2	6.5	300
AISLI	278	135	2	7	300

The Chill-roll temperature corresponds to the temperature of the rolls that cool down the polymer after its exit through the dye. The film casting speed corresponds to the speed at which the films are stretched, giving the draw ratio between the polymer at the exit from

II. Materials & Techniques

the dye and the obtained film. The desired thickness is obtained by modulating the film cast speed and the draw ratio.

NeatPA66 100 μm -thick films were used to study PA6,6 / solvents interactions (see chapter III), whereas HIA and AiSLi 300 μm -thick films were used to study the interaction of modified PA6,6 with a selection of solvents (see chapter IV).

II.2.2. Compounding

The additivated formulae 10LA and 10HA were obtained by extruding *REF* with 10%_{wt} of either laurylaldehyde or heptanaldehyde phenolic resins. The extrusion setup used for compounding these formulations is shown in Figure 49.

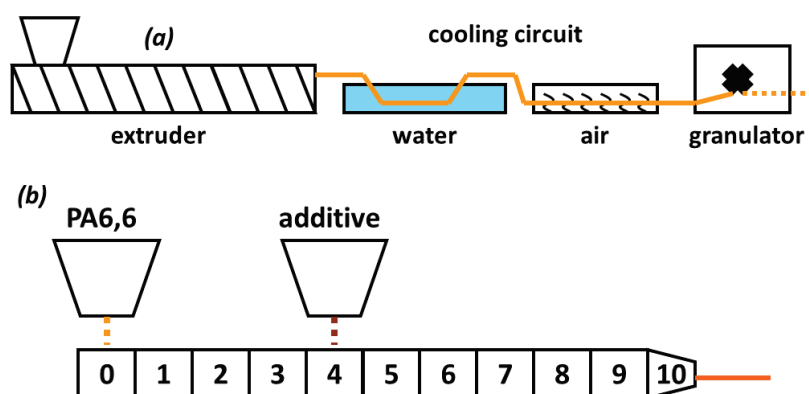


Figure 49: (a) Compounding setup and (b) extruder close-up with introduction zones.

PA6,6 *REF* pellets were introduced at the very rear of a Leistritz extruder (zone 0) thanks to a hopper, whereas the phenolic additives were added thanks to a dosing hopper, further at the middle of the extruder (zone 4) where the polymer is already in the molten state, the different introduction zones being schematically shown in Figure 49b.

The total through put of the Leistritz extruder was set at 10 kg/hr. The obtained compounded formulae were immediately cooled down and granulated after extruding as shown schematically in Figure 49a. The compounding of *REF*, 10LA and 10HA formulations was done at the Polymer Processing Facility (Vincent Curtil and Michel Sorin) of the CRTL. Table 5 shows the processing conditions for these formulations.

Table 5: Additivated formulae compounding processing conditions.

Formula	Average temperature in the screw [°C]	Screw speed [rpm]
REF	270	
10LA	269	200
10HA	270	

The obtained compounds were then injection molded in order to obtain sorption discs, tensile strength, and impact strength specimens.

II.2.3. Injection-molding

For obtaining impact strength, tensile, and sorption disc specimens, REF, 10LA, 10HA, HIA, and AISLI formulations were injection-molded. The principle of the injection-molding is the following: the polymer pellets are introduced in a hopper, and then a certain amount of the polymer gets into the screw, this amount being roughly the one needed to inject a set of specimens at a time. In the screw the polymer melts and it is carried to the mold. A motor coupled to the screw pushes the molten polymer into the mold and by applying a counter-pressure, the polymer is maintained in the mold. In the mold the polymer takes the form of the piece and it is cooled down into a solid part. The screw temperature, the dosing amount of polymer, the counter-pressure applied by the motor, the mold temperature and the piece retention time are the most important parameters that have to be optimized to get suitable specimens for testing. An injection-molding processing press is schematically represented in Figure 50.

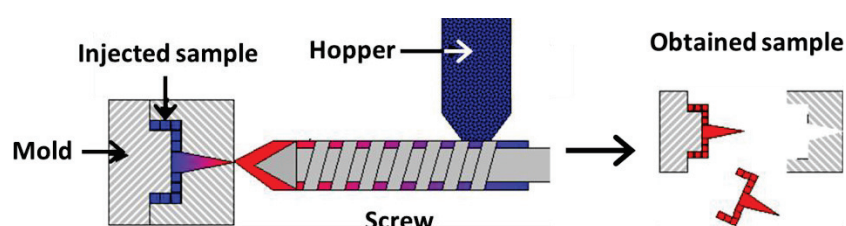


Figure 50: Injection-molding setup.

Before injection-molding, Karl-Fischer measurements were undertaken for all formulations in order to measure the water intake and to know if the pellets were sufficiently dry (less than 1200 ppm) for injection-molding. The presence of water in polyamides leads to a more fluid polymer that is relatively difficult to process and most importantly water reacts with PA6,6 through an hydrolysis reaction at high temperatures, provoking a drop on the molecular weight of PA6,6 because of chain scissions. If the pellets were not dry enough, they were dried overnight at 90°C under vacuum before processing. For obtaining impact strength, tensile, or sorption discs specimens, different specific molds were used. The samples were obtained using an Arburg press (closing pressure = 35 tons) at the Polymer Processing Facility (Vincent Curtil and Michel Sorin) of the CRTL. Table 6 shows the processing conditions for the REF, 10LA, 10HA, HIA, and AISLI formulations.

Table 6: Injection-molding conditions

Formula	Temperature [°C]		Molding cycle time [s]
	Screw	Mold	
REF	280	80	30.3 – 38.3
10LA	287	85	41.1
10HA	275	70	26.1 – 31.1
HIA	285	84	45.5 – 56.1
AISLI	285	84	56.7

The obtained specimens were ISO-527-1A standard tensile strength samples (150x10x4 mm³), impact strength samples (80x10x4 mm³), and sorption discs (diameter of 70mm and thickness of 3mm).

II.2.4. Review on the processed PA6,6 samples

In Chapter III only the *NeatPA6,6* formulation which was extruded into 100 μm -thick films is studied. On the other hand in Chapter IV modified PA6,6 samples that were either injected and/or film cast extruded are studied. As the polymer processing technique might influence the final properties of these samples a difference has to be made when comparing samples obtained by different processing techniques. A suffix was then added to the name of each formulation depending on how the samples were obtained: *I* for injection-molded and *F* for film cast-extruded as listed in Table 7.

Table 7: Listing of the different samples and specimens according to the processing technique for the modified PA6,6 formulations.

Formulation-Sample	Processing technique	Specimen(s)
REF-I		
10LA-I	Injection-molding	Tensile, impact, sorption discs
10HA-I		
HIA-I		
AISLI-I		
HIA-F	Film cast extrusion	300 μm -thick films
AISLI-F		

II.3. Experimental techniques

II.3.1. Structural characterization

II.3.1.1. Crystalline phase

II.3.1.1.1. Crystalline fraction

The Differential Scanning Calorimetry (DSC) technique was used to determine the melting and crystallization temperatures as well as the crystalline ratio. The principle of this technique is the following: a temperature ramp is applied on pans, one containing the polymer, and another one which is empty and acts as a reference. Then the difference of energy that has to be furnished to keep the reference pan and the pan containing the polymer at the same temperature is recorded. This difference of energy, called heat flow and the way it varies with the temperature give information on the polymer (glass transition, melting, crystallization...).

Melting or crystallization temperatures and the crystalline ratio were assessed with a TA Q2000 calorimeter in the standard mode. Samples (between 7 and 15mg) were put in non-hermetic aluminum pans and heated from 25°C to 300°C at a heating rate of 10°C/min, followed by an isotherm of 300°C during 5 minutes, and finally the samples were cooled down to 25°C at 10°C/min.

An example of a PA6,6 thermogram showing the melting and crystallization temperatures and heat capacities is shown in Figure 51:

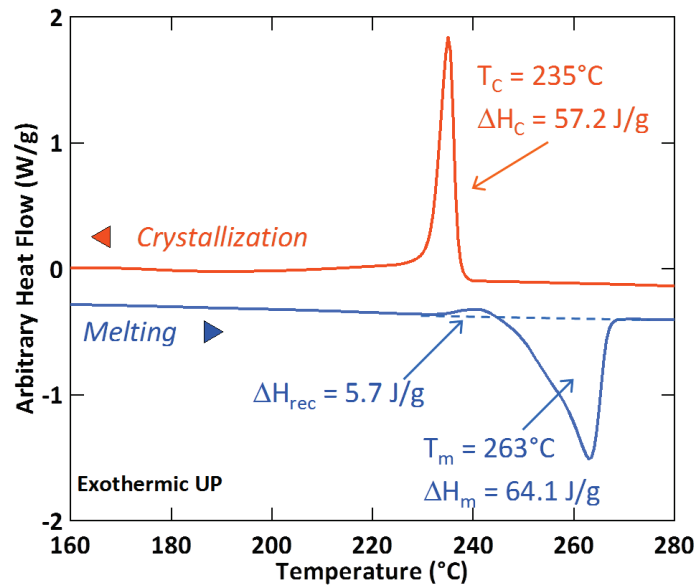


Figure 51: PA6,6 thermogram showing the melting and crystallization processes as obtained by DSC .

The crystalline ratio (in %_{wt}) was then determined from Equation 38:

$$X_c = \left(\frac{\Delta H_m - \Delta H_{rec}}{\Delta H_m^{100\%}} \right) * 100 \quad 38$$

where ΔH_m is the measured melting enthalpy, ΔH_{rec} is the enthalpy of recrystallization or rearrangement that occurs before the melting during the heating of the polymer in the DSC, and $\Delta H_m^{100\%}$ the reference melting enthalpy associated to a 100% crystalline PA6,6 ($\Delta H_m^{100\%} = 188.4 \text{ J/g}$ [62]).

II.3.1.1.2. Crystalline structure

The crystalline structure of the PA6,6 samples was analyzed and assessed by Wide Angle X-Ray Scattering (WAXS). This technique allows to identify the crystalline lattice of a polymer, and to be more specific X-ray scattering techniques allow to identify the crystallographic planes present in the crystalline lattice of the polymer's crystalline phase.

The X-Ray scattering techniques are based on the Bragg's Law of diffraction which describes the condition for a reflected X-Ray beam to constructively interfere with an incident beam:

$$\lambda = 2d \sin \theta \quad 39$$

where λ and θ are the wavelength and the angle of the incident X-Ray beam respectively, and d is the distance between the crystalline layers. The experimental setup of a X-Ray scattering technique is the following: an X-Ray beam is sent to the sample at a given incident angle, the beam penetrates in the sample and it is reflected. A detector placed behind the sample detects the reflected beams and their scattered intensity as shown schematically on Figure 52a.

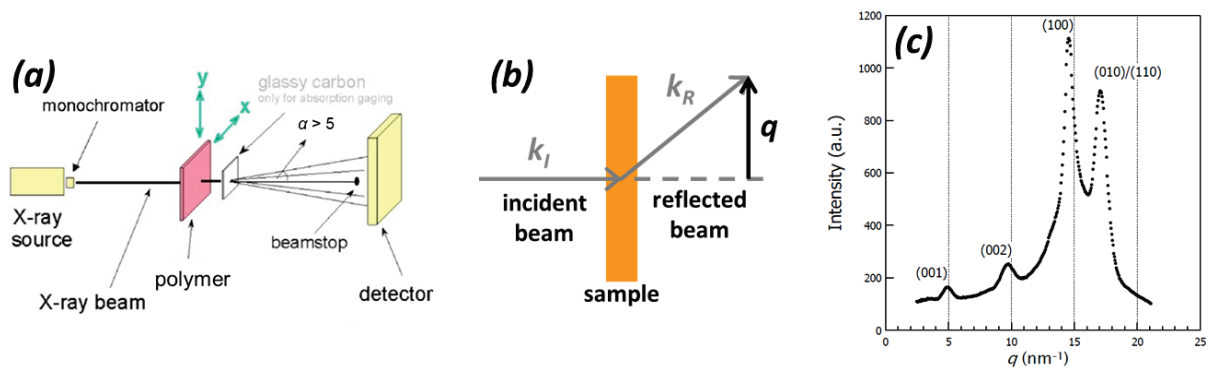


Figure 52: (a) experimental setup for a WAXS measurement, (b) schematic representation of the scattering vector, and (c) scattered intensity as a function of the scattering vector q showing the Bragg peaks for a PA6,6 sample [9].

In a WAXS measurement the detector is placed close to the sample so as to detect the scattered intensity at large angles (ca. larger than 5°). The Bragg diffraction peaks are obtained then as a function of the angle of the X-ray beams 2θ or as a function of the scattering vector q which is the difference between the reflected and the incident and reflected wave vectors (k_R and k_i respectively), as shown schematically in Figure 52b, and is equal to:

$$q = k_R - k_i = \frac{2\pi \sin 2\theta}{\lambda} \quad 40$$

Moreover, since a Bragg peak is representative of the distance between two crystallographic planes of a given orientation, the crystalline structure of a sample can be characterized. An example of a PA6,6 WAXS scattering spectrum is shown in Figure 52c, highlighting the various observed Bragg peaks, corresponding to the Miller lattice indexes of the crystalline structure of this polymer.

In this work, neat, chemically-modified, and additivated PA6,6 samples in the dry state or conditioned in water or ethanol were analyzed by WAXS. Before measurement, the samples that were conditioned in water or ethanol were let to desorb the solvent at room temperature. Samples were then analyzed at room temperature (23°C) and the X-Ray beam was filtered thanks to a $\text{CuK}\alpha$ filter. The WAXS experiments were carried out by Erwan Jeanneau at the “Henri Longchambon Diffraction Center”.

II.3.1.2. Molecular mobility

II.3.1.2.1. Calorimetry

The DSC was also used to obtain the samples T_g 's. It is relatively difficult to measure the polyamide T_g by classic DSC measurements since for this polymer, the heat capacity step ΔC_p (which is the signature of the glass transition) is wide, and its intensity is weak. In this work the Temperature-Modulated mode (MDSC) was used to determine the samples T_g 's. This mode applies a relatively fast temperature variation, enhancing the sample response to a thermal solicitation, thus increasing the heat flow signal. In this mode, the average

II. Materials & Techniques

temperature varies linearly but the actual temperature varies following a sinusoidal function as shown in Figure 53a.

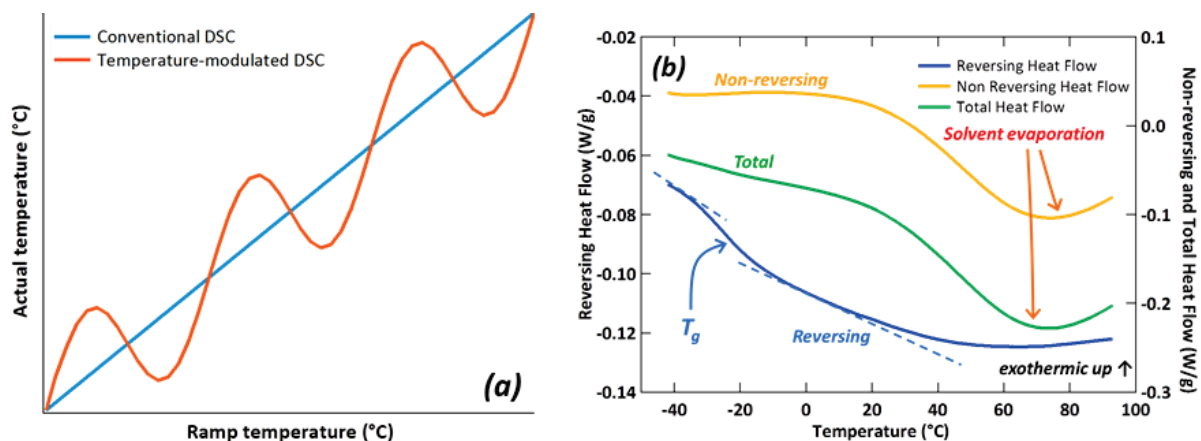


Figure 53: (a) Measured temperatures for Conventional and Temperature-Modulated DSC methods, and (b) Temperature-Modulated DSC thermogram for a water-saturated PA6,6 sample where the T_g and the solvent evaporation can be observed.

The Temperature-Modulated mode allows to distinguish the glass transition process from other kinetic processes like crystal melting and crystallization, chemical reactions, or the departure of species contained in the sample. The principle of the Temperature-Modulated DSC is the following: the DSC measures a total heat flow dH/dt which is the signal of all the thermic phenomena that a polymer may exhibit. The Temperature-Modulated DSC is able to separate this total heat flow into two components as defined in Equation 41: one that depends on the heat capacity C_p of the sample and the heating rate dT/dt named the Reversing component, and another term that depends on time (i.e. kinetic phenomena) at an absolute temperature ($f(T,t)$) named the Non-reversing component.

$$\frac{dH}{dt} = C_p \frac{dT}{dt} + f(T,t) \quad 41$$

The heat capacity C_p is the amount of heat needed to increase the temperature of 1 g of matter by 1°C. The heat capacity is measured by the DSC and corresponds to the measured sinusoidal heat flow that responds to the rate of temperature change dT/dt . By subtracting this Reversing component from the total heat flow, the Non-reversing component is obtained.

The glass transition as well as some melting processes can be observed on the reversing component. Kinetic phenomena, such as solvent evaporation, crystallization processes and decomposition are observed on the Non-Reversing component.

The use of modulated DSC is of great interest for studying solvent-saturated samples since the solvent evaporation phenomenon is separated from the polymer glass transition. As an example, a PA6,6 saturated in water is shown in Figure 53b: the glass transition is not observed in the Total Heat Flow, the transition being too weak and actually masked by the departure of water from the polymer, but thanks to the temperature-modulated mode, the glass transition is well observed in the Reversing Heat Flow while the water departure is seen in the Non-Reversing signal.

II. Materials & Techniques

The MDSC can also help us to identify or quantify the degree of heterogeneity of the amorphous phase. Indeed, only an amorphous phase fraction called MAF (Mobile Amorphous Fraction) contributes to the ΔC_p step observed at the glass transition temperature. By calculating the ratio of the measured heat capacity step at the T_g or ΔC_p for a given sample to the ΔC_p for a 100% amorphous polymer, the ratio of Mobile Amorphous Fraction (MAF) can be obtained according to Equation 42.

$$\%MAF = \left(\frac{\Delta C_{p-exp}}{\Delta C_{p-th}} \right) * 100 \quad 42$$

where ΔC_{p-exp} is the heat capacity step measured by MDSC for a given sample and ΔC_{p-th} is the heat capacity step for a 100% amorphous polymer ($\Delta C_{p-th}(PA6,6) = 0.51 \text{ J/gK}$ [153]). The ratio of Rigid Amorphous Fraction (RAF) can be then obtained according to in Equation 43.

$$\%RAF = 100 - X_c - \%MAF \quad 43$$

In order to assess the ΔC_{p-exp} , the procedure proposed by Pang et.al. [154] was used. This protocol consists in plotting the derivative with time of the Reversing Heat Capacity signal measured by MDSC as a function of the temperature. A peak representing the glass transition is obtained and by integrating this peak, the ΔC_{p-exp} is obtained as shown in Figure 54.

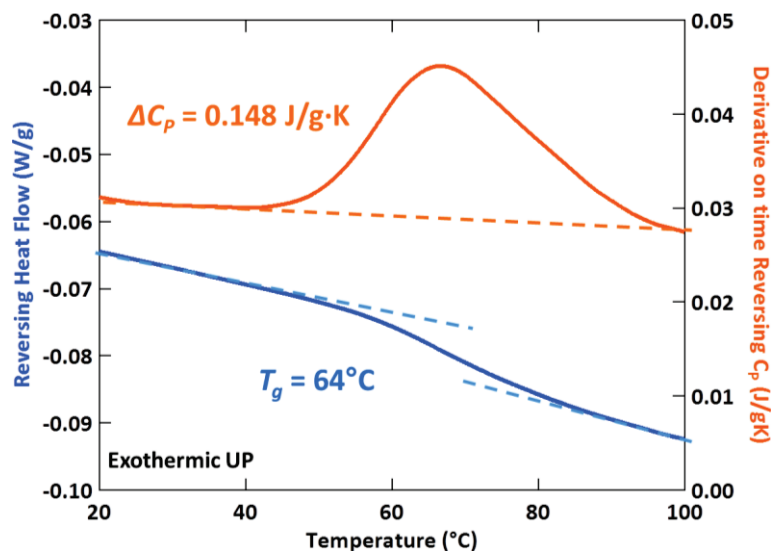


Figure 54: Thermogram obtained by MDSC highlighting the glass transition temperature T_g and the heat capacity step ΔC_p of a dry PA6,6 sample.

A TA Q2000 DSC was used to measure the samples' T_g 's. Dry samples (between 7 and 15mg) were introduced in non-hermetic aluminum pans, and a 110°C isotherm during 15 minutes was firstly carried out in order to be certain that the sample was dry. Then the temperature was dropped to 0°C, and finally the sample was heated up to 140°C at a heating rate of 3°C/min with a temperature modulation of $\pm 2^\circ\text{C}$ every 60 s. For PA6,6 samples swollen in solvent (also between 7 and 15mg), samples were rapidly prepared in order to avoid solvent evaporation, then cooled down quickly to -100°C and then heated up to 100°C with the same ramp and modulation parameters described above.

II. Materials & Techniques

Two cooling units and inert flow gases were used during the MDSC experiments: a RCS90 (Refrigerating Cooling System) with a ultra-dry Nitrogen flow (set at 50 ml/min) was used for the dry samples, whereas for the solvent-swollen samples a LNCS (Liquid Nitrogen Cooling System) with a Helium flow (set at 25 ml/min) was used. The LNCS was used because of its capability of cooling down to cryogenic temperatures (ca. -180°C vs. ca. -70°C for the RCS) and because its cooling rate was far larger (ca. twice or thrice) than that of the RCS90. By using the LNCS, a limitation of solvent desorption before T_g measurement was expected. And as shown in example in Figure 53b, the solvent evaporation for all our samples was observed well above the measured T_g .

II.3.1.2.2. Dynamic mechanical analyses

A Dynamic Mechanical Analyzer (DMA) applies a dynamic strain to the polymer $\gamma(t) = \gamma_0 \sin \omega t$ that leads to a dynamic stress. By applying a very small strain in the polymer (ca. 0.1%), the mechanical response of the sample will be found in the linear regime. The ratio between stress and strain is given by the dynamic modulus that can be decomposed into two parts, the storage modulus (E') and the loss modulus (E''), as described by Equation 44:

$$\sigma(t) = \gamma_0 [E' \sin \omega t + E'' \cos \omega t] \quad 44$$

A part of the applied energy will be elastically restored by the polymer; this energy is associated to the storage dynamic modulus E' . The polymer will also absorb a part of the applied energy which will be dissipated as heat; this energy is associated to the loss dynamic modulus E'' . The ratio between the loss and the storage moduli is called the loss angle or $\tan \delta = E''/E'$, which is the out-of-phasing angle between stress and strain, and which represents the energy proportion dissipated as heat by the polymer in a sample.

When a polymer relaxation temperature is reached, the storage dynamic modulus E' decreases. In the case of a secondary relaxation there is only a slight drop on E' , however when the main relaxation temperature is reached, E' drops significantly (by 1 or 2 orders of magnitude). The molecular relaxations also appear in the loss dynamic modulus E'' and $\tan \delta$ signals in the form of peaks. Figure 55 shows a common curve obtained by DMA highlighting the different PA6,6 molecular relaxations.

In this study injected samples of dimensions 4x10x80 mm³ were used to characterize the mechanical relaxations. A Q800 DMA was used to characterize these samples using the three-point bending method, in which the sample is put in between two supports and the mechanical stress is applied by a cantilever situated at the middle of the sample. The measurements are carried out in a closed furnace; the samples are cooled up to -150 °C and heated up to 200 °C at 2 °C/min. The frequency of the applied stress is fixed at 1 Hz in order to compare the measured α relaxation temperature T_α to the T_g obtained by DSC. The value of T_α is taken at the maximum of the peak corresponding to this relaxation of the dynamic loss modulus E'' .

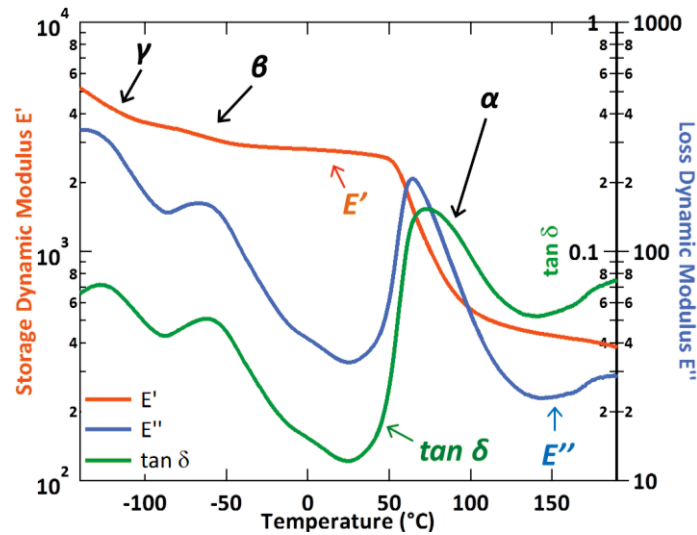


Figure 55: PA6,6 DMA curve showing the polymer's molecular relaxations.

II.3.1.2.3. Dielectric analyses

In order to characterize more accurately the different molecular relaxations of PA66 formulae, Broadband Dielectric Spectroscopy (BDS) was also used. In this technique a sinusoidal electric field, analogous to the periodic mechanical stress in DMA, is applied to the sample which is placed between two gold-plated electrodes which act as capacitors. When the electric field is applied, the dipoles attached to the polyamide chains align with the field as shown in Figure 56. By measuring the orientation of these dipoles, the relaxation processes of polymer chains and the temperatures at which they occur can be obtained.

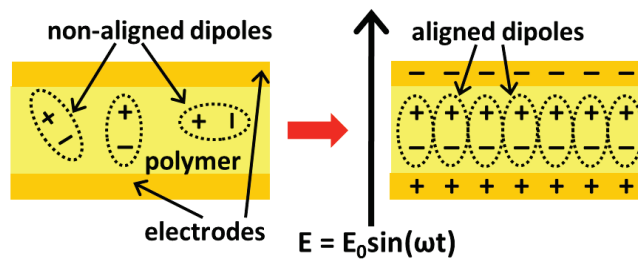


Figure 56: Schematic representation of a polymer being analyzed by Dielectric Spectroscopy

The advantage of BDS when compared to DMA is the range of frequencies that can be studied. In DMA the frequency range goes typically from 0.1 to 100 Hz whereas in BDS the frequency range goes from 0.01 to 1×10^7 Hz.

In this work, a Novocontrol Alpha Analyzer and a Quatro temperature control system were used. PA66 samples were cut into disks of diameter 2 cm and placed between gold-plated electrodes. Samples were then heated from -150 up to 200 °C with 4°C steps and scanned at frequencies varying from 0.01 to 1×10^7 Hz.

The BDS actually measures the polymer complex permittivity ϵ^* defined by:

$$\epsilon^* = \epsilon' - i\epsilon''$$

II. Materials & Techniques

where ϵ' and ϵ'' are respectively the real and imaginary parts of the permittivity. In order to characterize the relaxations of a given sample, we can either study the complex permittivity ϵ^* or its inverse function the complex modulus M^* , and to be more specific the loss permittivity ϵ'' and the loss modulus M'' which is then defined in Equation 46.

$$M'' = \frac{\epsilon''}{\epsilon'^2 + \epsilon''^2} \quad 46$$

Figure 57 shows the loss permittivity ϵ'' / loss modulus M'' – frequency – temperature 3D plots for a dry PA66, with the molecular relaxations being highlighted.

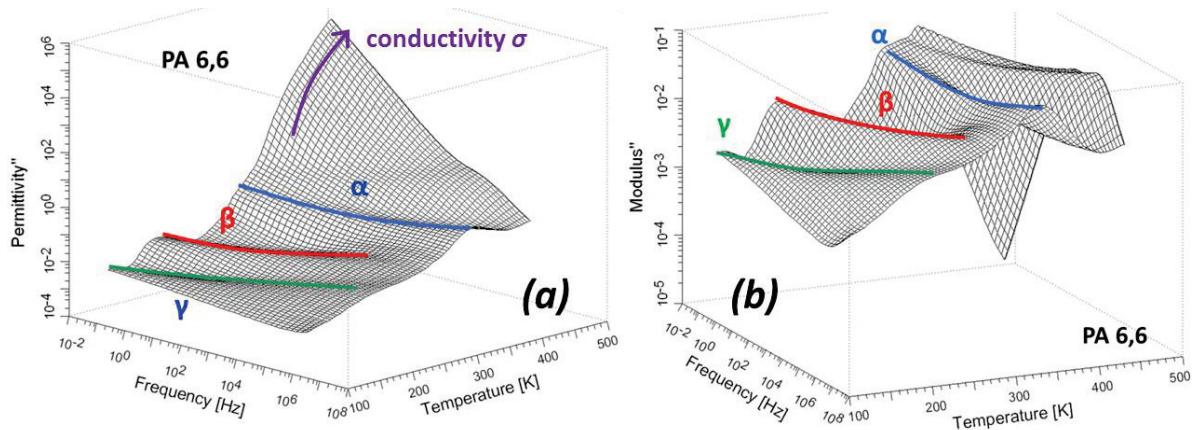


Figure 57: Dry-PA6,6 (a) loss permittivity ϵ'' and (b) loss modulus M'' spectra showing the polymer's molecular relaxations.

Figure 57a shows that at high temperatures (above the α relaxation process) and low frequencies, the loss permittivity ϵ'' signal increases by several orders of magnitude. Indeed, at high temperatures the sample is relaxed and the polymer chains are more mobile, the dipoles present in the chains not only respond to the applied electric field but also start conducting the electric current that is applied to the electrodes, especially at low frequencies because the dipoles have more time to align with the electric field. This increase in ϵ'' corresponds to the linear dependence of ϵ'' on the polymer electric conductivity if ϵ'' becomes much more larger than ϵ' , as shown in Equation 47.

$$\epsilon'' \approx \mu \frac{i \epsilon_{DC}}{\omega} \quad 47$$

By considering M'' the signature of the conductivity is reduced because M'' is roughly the inverse of ϵ'' , thus a large value becomes a small one when the inverse of this value is plotted. Figure 58 shows a comparison between ϵ'' and M'' at 1 Hz, it is observed that the temperature values of the maxima of the peaks associated to molecular relaxations, are relatively close.

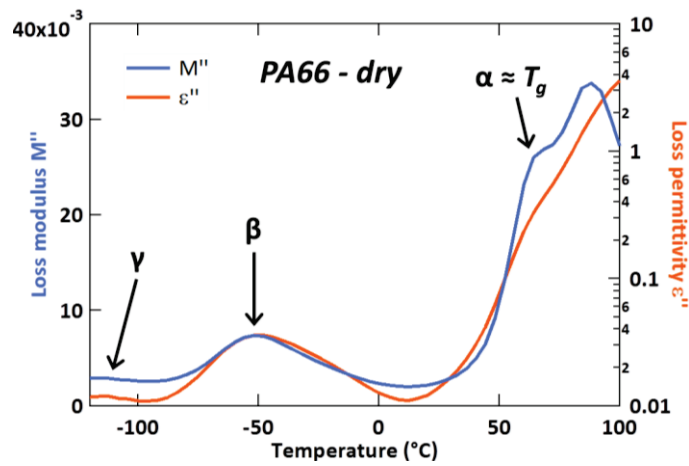


Figure 58: Comparison between the loss permittivity ϵ'' and the loss modulus M'' spectra at 1 Hz for dry PA6,6.

Two methods were then considered for analyzing the obtained results. The first method, was a graphic method in which the loss moduli M'' are plotted as a function of the temperature for a given frequency or set of frequencies. The maxima of the γ , β , and α relaxations peaks observed in the M'' – temperature plot are then considered to be the T_γ , T_β , and T_α relaxation temperatures respectively for a given frequency as shown in Figure 59. Moreover the T_α at 1 Hz was considered to be roughly equivalent to the T_g obtained by DSC.

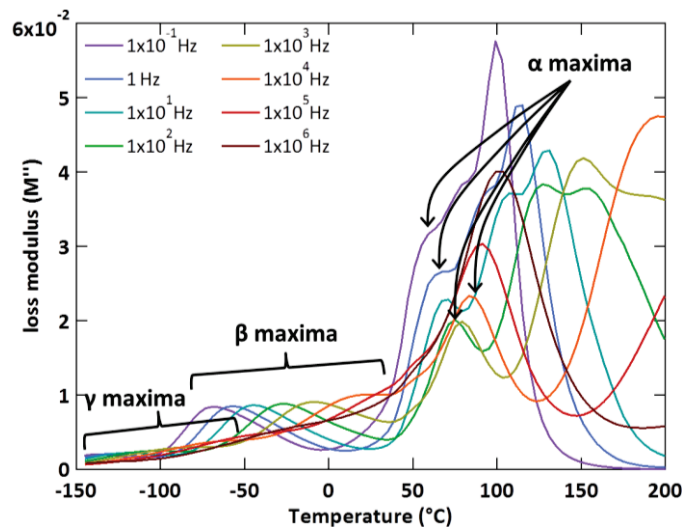


Figure 59: Graphic method for determining the relaxation temperatures from the loss moduli M'' spectra as a function of the temperature for a given frequency.

This method was efficient for PA66 films swollen in polar solvents. Indeed, the conductivity of these samples was very high because of the presence of the solvents, and thus the molecular relaxations were difficult to identify on the loss permittivity ϵ'' spectra. As conductivity does not greatly affect the loss modulus, and the molecular relaxations of PA6,6 swollen samples were more easily identified on the loss moduli M'' spectra.

In the second method, which is an analytical one, the loss permittivity ϵ'' maxima at given temperatures and frequencies are analyzed. In order to do so, different mathematical models are available so as to obtain the distribution of the relaxation times and the relaxations temperatures. Three main models are hereby considered: Debye, Cole – Cole, and Havriliak – Negami.

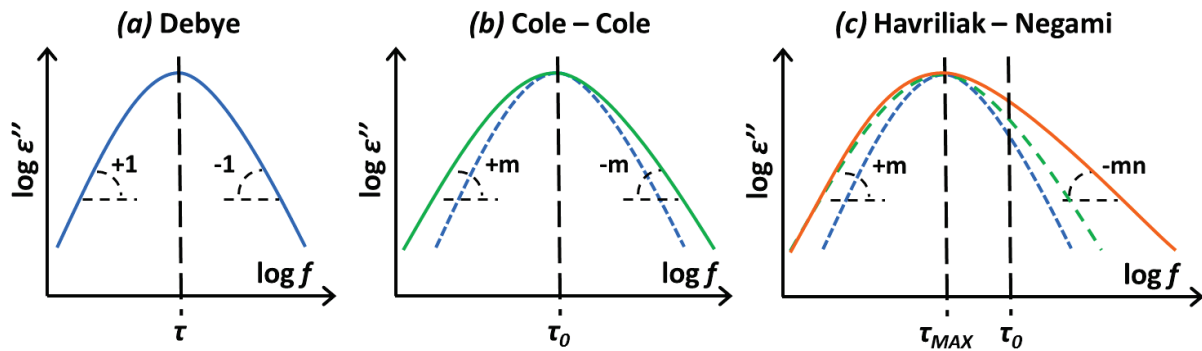


Figure 60: (a) Debye, (b) Cole – Cole, and (c) Havriliak – Negami distribution models [29,155,156].

The first and the simplest is the Debye model [155,156]. This model considers that the orientation of molecular dipoles is slower than the electronic and atomic polarization and that when an electric field is applied to the polymer a single response is observed. This single response means that all the dipoles align with the electric field at the same time, thus all the dipoles have a sole relaxation time. The complex dielectric permittivity of the polymer when a time-dependent electric field is applied is given by Equation 48:

$$\epsilon^* = \epsilon_\infty + \frac{\epsilon_s - \epsilon_\infty}{1 + i\omega\tau_D} \tag{48}$$

where ω is the frequency, t is the time, and τ_D is the relaxation time. The Debye model is described by a symmetrical peak having slopes of values +1 and -1, corresponding to the existence of only one relaxation time, as shown in Figure 60a.

The Debye distribution works well on dipoles diluted in non-polar liquids or gases, however the obtained dielectric response of a polymeric material rarely follows a Debye distribution, the response peak being broader than the one defined by this model. Several models describe in a heuristic manner the broadening of the relaxation peak, corresponding to a distribution of relaxation times. Herein, the Cole – Cole and the Havriliak – Negami empiric models are presented [29,155,156].

The Cole – Cole model [155,156] is an empiric development of the Debye model, in which the broadening of the characteristic relaxation times is symmetrical. This model defines then the complex permittivity as shown in Equation 49.

$$\epsilon^* = \epsilon_\infty + \frac{\epsilon_s - \epsilon_\infty}{1 + (i\omega\tau_0)^m} \tag{49}$$

where m ($0 < m < 1$) is the exponent describing the broadening of the molecular relaxation and the characteristic times as shown in Figure 60b. The Debye model becomes then a special case of that of the Cole – Cole model for $m=1$.

II. Materials & Techniques

The Havriliak – Negami model [29,156] is an empiric development of the Cole – Cole model in which an asymmetry, observed for certain molecular relaxations, is introduced. This model defines then the complex permittivity as shown in Equation 50.

$$\epsilon^* = \epsilon_{\infty} + \frac{\epsilon_s - \epsilon_{\infty}}{1 + (i\omega\tau)^m} \quad (50)$$

where n ($mn \leq 1$) is the exponent describing the asymmetry of the molecular relaxation as shown in Figure 60c. The Cole – Cole model becomes then a special case of that of the Havriliak – Negami model for $n=1$.

In order to characterize the molecular relaxations of our samples, the WinFit software was used. This software allows us to fit the loss permittivity ϵ'' spectra of a polymer sample following a Havriliak – Negami model and thus to obtain the characteristic relaxation times, the broadening and the asymmetry of the molecular relaxations and the relaxation temperatures as a function of the frequency. In order to obtain an accurate fit, two relaxations are fitted at a time.

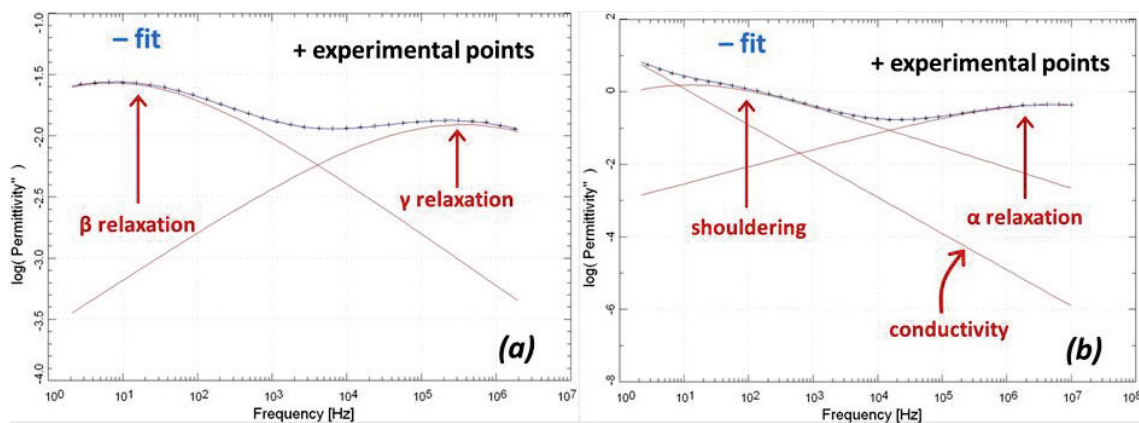


Figure 61: WinFit fit of the loss permittivity ϵ'' for (a) the γ and β relaxations and (b) the α relaxation, shouldering, and conductivity.

In our case for the PA6,6 samples, the fit departs from the lowest towards the higher temperatures, the γ and β relaxations being fitted first. These two relaxations, shown in Figure 61a, are symmetric so in the Havriliak – Negami model the exponent n is set as being equal to the unity. Afterwards, the relaxation and the shouldering are then fitted, considering both relaxations as asymmetrical, and since close to the T_g and beyond PA6,6 starts to conduct electricity a conductivity parameter is added to the fit program as shown in Figure 61b. The function used for fitting the real and imaginary parts of the permittivity (ϵ' and ϵ'' respectively) becomes:

$$\epsilon^* = \epsilon_{\infty} + \frac{\epsilon_s - \epsilon_{\infty}}{1 + (i\omega\tau)^m} + \frac{i\omega\tau_{DC}}{\omega} \quad (51)$$

II. Materials & Techniques

II.3.2. Sorption and diffusion

II.3.2.1. Pure solvents

III.3.2.1.1. Sorption of liquid solvents

The sorption of a series of polar and non-polar solvents was studied. The polar solvents were water, methanol, ethanol, ethylene-glycol, 1-propanol, 2-propanol, 2-butanol, and cyclopentanol. The studied non-polar solvents were 2,3-dimethylbutane, 3-methylpentane, n-hexane, isooctane, toluene, o-xylene, and p-xylene. Figure 62 shows the chemical structures of the studied solvents.

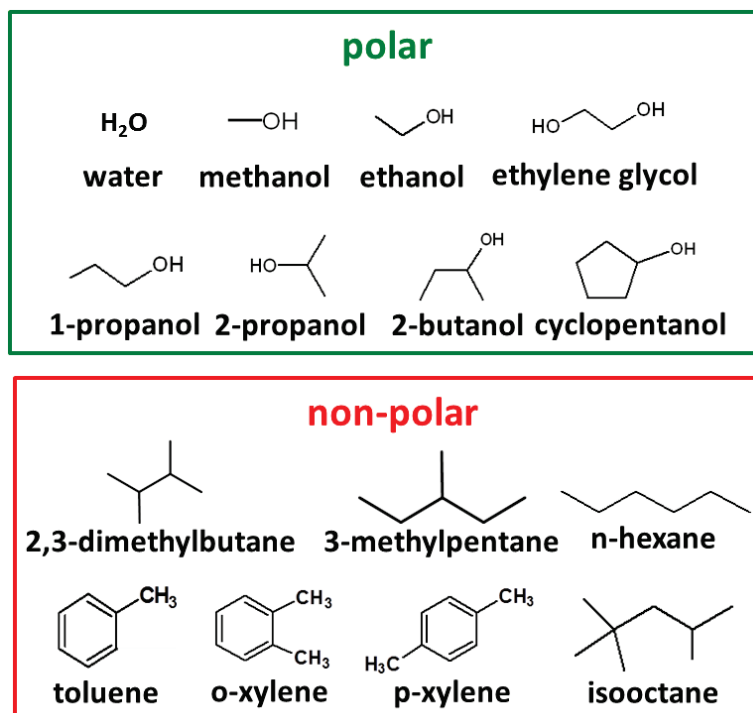


Figure 62: Chemical structure of the studied solvents.

Table 8 shows the density at room temperature (23°C) ρ and the boiling point T_B of each solvent.

Table 8: Density at 23°C ρ and boiling point T_B for the studied polar and non-polar solvents. All values were obtained from [157].

Solvent	ρ [g/cm ³]	T_B [°C]	Solvent	ρ [g/cm ³]	T_B [°C]
Water	1.000	100.0	Toluene	0.867	110.6
Methanol	0.792	64.7	o-xylene	0.870	144.4
Ethanol	0.789	78.4	p-xylene	0.870	138.4
Ethylene glycol	1.113	197.3	2,3-dimethylbutane	0.660	57.9
1-propanol	0.786	82.4	3-methylpentane	0.660	64.0
2-propanol	0.803	97.1	n-hexane	0.655	69.0
2-butanol	0.806	99.0	Isooctane	0.688	99.3
Cyclopentanol	0.949	139.0	-	-	-

II. Materials & Techniques

Deionized water and analytical-grade solvents were used. The alcohol solvents were carefully kept anhydrous with a desiccant. PA66 samples were dried overnight at 110°C under vacuum prior to solvent conditioning. PA66 films were then put in contact with each of these solvents as shown schematically in Figure 63a, and were regularly weighed (balance precision of $\pm 0.5\text{mg}$) during time until the sorption equilibrium was reached, that is when no more solvent is absorbed by the polymer as shown in Figure 63b.

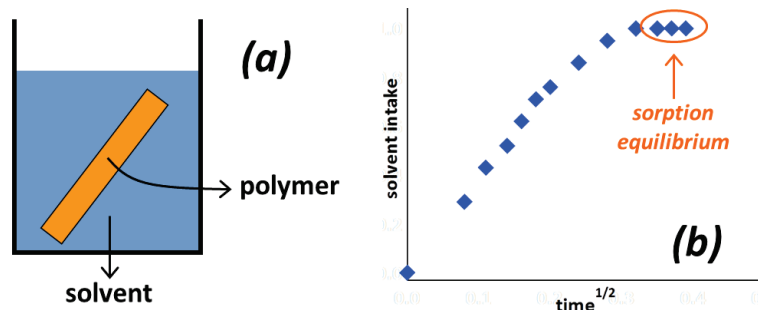


Figure 63: (a) schematized liquid sorption test in a polymer and (b) sorption kinetics of a solvent intake as a function of the square root of time.

Concerning the first part of this thesis (Chapter III) *NeatPA6,6* films of surface of $5 \times 5 \text{ cm}^2$ and thickness of $100 \mu\text{m}$ were studied. The sorption of all the mentioned solvents was carried out in at room temperature (23°C). Moreover the sorption at equilibrium of water, ethanol, and toluene were also measured at 23, 40, 50 and 60°C . Finally the sorption kinetics of these three solvents at 23°C were also assessed.

In the second part of the thesis (Chapter IV), the sorption kinetics and sorption equilibrium of water, ethanol, and toluene in the modified PA6,6 formulations presented above were assessed at 23°C . For REF, 10LA, and 10HA formulations, sorption discs of thickness 3mm were obtained by injection-molding. These discs were then machined in order to obtain plaques of surface of $5 \times 5 \text{ cm}^2$ and thickness of $300 \mu\text{m}$. Moreover, HIA and AISLI formulations were extruded into films of thickness of ca. $300 \mu\text{m}$ and then cut into samples having a surface of $5 \times 5 \text{ cm}^2$.

III.3.2.1.2. Sorption of vaporized solvents

The sorption of pure ethanol in the vapor state by *NeatPA6,6* $100 \mu\text{m}$ -thick films was also studied. This was done thanks to a Dynamic Vapor Sorption apparatus (DVS). In the DVS, a polymer sample is put in a chamber, and then a pump takes the liquid solvent, vaporizes it and pumps it to the chamber. The chemical activity (or partial pressure) as well as the temperature of the vaporized solvent are controlled by the DVS. The DVS measures then the solvent intake as a function of time. This set-up is schematically represented in Figure 64. The sorption of vaporized ethanol at chemical activities ranging from 0.6 to 0.9 was studied at room temperature (23°C). The tests were stopped automatically when the solvent intake variation was inferior to $0.005\%_{wt}$. At this point, the sorption equilibrium was considered to be reached.

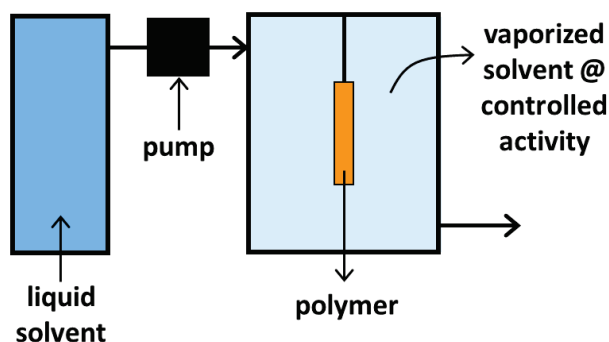


Figure 64: Schematic representation of a Dynamic Vapor Sorption (DVS) set-up.

II.3.2.2. Ternary mixtures

II.3.2.2.1. Measurement of the chemical activities of the ternary mixtures

The interactions between PA6,6 and a set of liquid ternary mixtures were also studied. These mixtures were composed by ethanol, toluene, and isooctane at different concentrations so as to model the commercially available biofuels, the composition of the mixtures being illustrated in Figure 65.

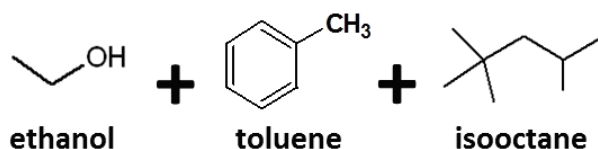


Figure 65: Chemical structures of the solvents composing the EX ternary mixtures.

These mixtures were named “EX”, X standing for the volumetric concentration of ethanol in each one of them. The composition of these mixtures is shown in Table 9.

Table 9: Volumetric composition in ethanol, toluene and isooctane of the studied EX mixtures.

Mixture	% _{vol} Ethanol	% _{vol} Toluene % _{vol} Isooctane	Mixture	% _{vol} Ethanol	% _{vol} Toluene % _{vol} Isooctane
<i>E0</i>	0.0	50.00	<i>E60</i>	60.0	20.00
<i>E2.5</i>	2.5	48.25	<i>E65</i>	65.0	17.50
<i>E5</i>	5.0	47.50	<i>E70</i>	70.0	15.00
<i>E7.5</i>	7.5	46.25	<i>E75</i>	75.0	12.50
<i>E10</i>	10.0	45.00	<i>E80</i>	80.0	10.00
<i>E22</i>	22.0	39.00	<i>E85</i>	85.0	7.50
<i>E40</i>	40.0	30.00	<i>E95</i>	95.0	2.50
<i>E50</i>	50.0	25.00	<i>E100</i>	100.0	0.00

In order to determine the chemical activities of ethanol, toluene, and isooctane in these mixtures, the vapor phases of these mixtures were analyzed by an Agilent G1530N Gas Chromatograph (GC) equipped with an FID detector. The GC was equipped with a Heliflex AT-1 non-polar column, a FID detector (Flame Ionization Detector), and an 8-entry 1:50 splitless injector (injection volume = 50 μl) with a fixed split ratio of 1:1 which allows us to connect multiple solvent mixtures to the GC-FID setup. The carrier gas from the sample to

II. Materials & Techniques

the injector was dry nitrogen with a flux set at 15 ml/min. Then from the injector to the chromatographic column, helium at a 20 ml/min flux was used as the carrier gas. Both the injector and the column were heated at 150°C. Hermetic stainless steel and aluminum boxes were used for housing the samples. The GC-FID setup is shown in Figure 66.

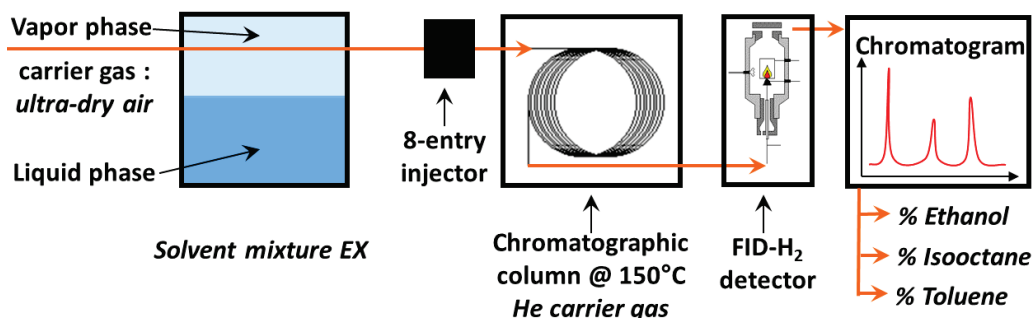


Figure 66: GC-FID setup for obtaining the chemical activities of the species composing the EX ternary mixtures.

In this setup, liquid mixtures are put in metallic boxes. Then ultra-dry air flows into the boxes so as to carry the vapor phase to the Gas Chromatograph. The vaporized solvents are then injected in the capillary column, separated and quantified by an FID detector. By obtaining the concentration of the solvents in the vapor phase, the chemical activities and the partial pressures of these species can be calculated. Four mixtures were studied at a time, with measurements being carried out every eight minutes (each mixture was analyzed every 40 minutes) with the temperature set at 25°C.

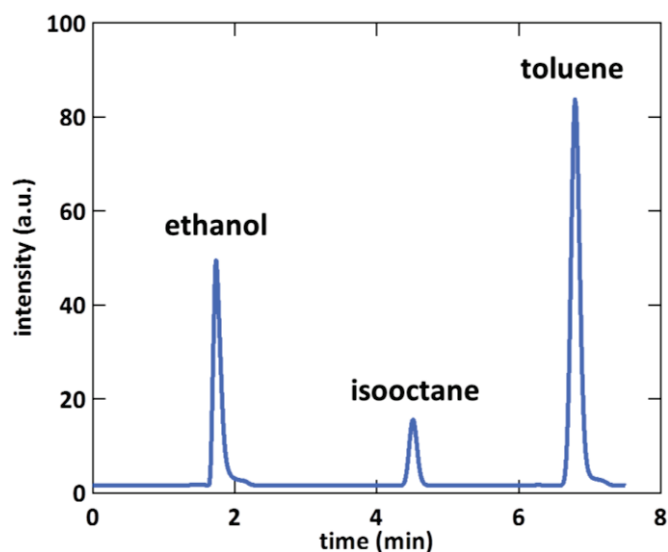


Figure 67: GC chromatograph obtained for an ethanol-toluene-isooctane mixture highlighting the response peaks for each of the species.

The molar concentrations of the species i in the vapor phase c_i were calculated from the area of the peaks S_i of the obtained chromatograms (an example is shown in Figure 67) according to Equation 52:

$$c_i = k_i S_i$$

52

where k_i is the concentration coefficient, which was calibrated for each solvent in the same proper conditions of temperature (25°C) and pressure (1 atm) by injecting well defined

II. Materials & Techniques

amounts of solvent. By knowing the absolute value of the molar concentration in the vapor phase c_i for each solvent i , the partial pressure p_i can be obtained from the ideal gas law for each species i as shown in Equation 53:

$$p_i = c_i RT \quad 53$$

where R is the ideal gas constant ($=8.314 \text{ J/mol}\cdot\text{K}$) and T the temperature at which the measurement was done ($25^\circ\text{C} = 298.15 \text{ K}$).

II.3.2.2.1. Measurement of the composition of the absorbed species by PA6,6

After having put *NeatPA6,6* 100 μm -thick films in contact with the mixtures indicated in bold in Table 9, it was desired to determine the composition of the absorbed species at sorption equilibrium. In order to do that, PA6,6 swollen samples were analyzed by Gas Chromatography. The setup for these measurements is the same as the one described in Figure 66, with Figure 68 showing a focus on the swollen PA66 sample.

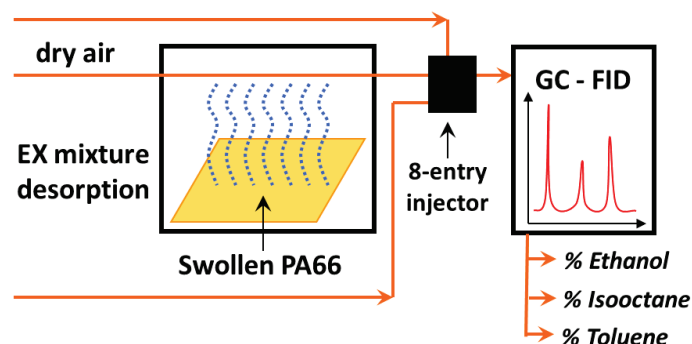


Figure 68: Simplified GC-FID setup for quantifying the absorbed species by PA6,6 films in contact with EX ternary mixtures.

PA6,6 samples swollen by the ternary mixtures were introduced in metallic boxes, ultra-dry air flowed into the boxes so as to carry the desorbed vapors to the Gas Chromatograph. These vapors were then analyzed and quantified. Four mixtures were studied at a time, with measurements being carried out every eight minutes (each mixture was analyzed every 40 minutes). The temperature was set at 40°C so as to accelerate solvent desorption.

II.3.3. Pervaporation

The pervaporation kinetics of ethanol in contact with the modified PA6,6 formulations (films or discs) were studied as well. The studied samples were either machined injection-molded discs (REF, 10LA, and 10HA) or extruded films (HIA and AISLI) of surface of $5 \times 5 \text{ cm}^2$ and thickness of ca. $300 \mu\text{m}$. The pervaporation tests were carried out at 40°C under an atmosphere controlled in hygrometry and set at 20% (RH20). In order to carry out these experiments, pervaporation cells were used. These cells are composed of a tank which contains the solvent and a holding plate having a hole in the middle with a diameter of 4cm. The PA66 film is put then in between the tank and the holding plate in a "sandwich" configuration as it is schematically shown in Figure 69a. A sealing joint is placed between the polymer and the tank in order to avoid solvent leaks. One of the sides of the polymer is then

II. Materials & Techniques

directly in contact with the solvent and the other side is in contact with the ambient air. A solvent concentration gradient is then created between both sides of the polymer which will provoke the diffusion and the pervaporation of the solvent through the polymer film.

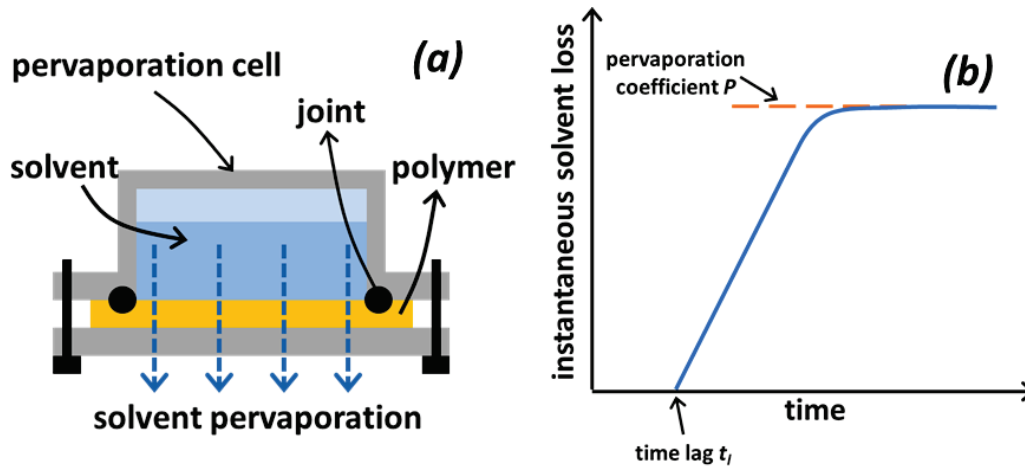


Figure 69: (a) schematized liquid pervaporation test in a polymer and (b) pervaporation kinetics of a solvent as a function of time with the graphical method for obtaining the permeability coefficient P and the time lag t_l highlighted.


The pervaporation cells are regularly weighed (balance precision of $\pm 0.5\text{mg}$) at intervals of several three days. The weighing of these cells is done until the permanent pervaporation regime is reached, that is when the instantaneous solvent loss (i.e. the derivative of the solvent loss with time) is constant with time as shown schematically in Figure 69b. From such a plot, the permeability coefficient P as well as the permeability time lag t_l can be calculated.

II.3.4. Mechanical properties

II.3.4.1. Tensile strength

In order to characterize the Young modulus E and the yield stress σ_y of studied samples tensile strength tests were carried out. The tests were done according to the ISO-527 Standard. Specimens were injection-molded with the dimensions defined in Table 10.

Table 10: ISO-527-1A Standard tensile specimen dimensions

Sample	Parameter	Dimensions [mm]
	Total length	150
	Reference length for extensometer	50
	Width	10
	Thickness	4
	Initial distance between jaws	117

All the samples were tested with a crosshead speed of 1 mm/min for the first 0.5% of deformation, so as to obtain the Young modulus E , then the crosshead speed for the rest of the experiment was set at 5 mm/min. Samples were dried at 90°C under vacuum for a weekend. These dry samples tested at four temperatures: 23, 45, 65, 90 and 140°C .

II. Materials & Techniques

Some of these dry specimens were then conditioned in a humid atmosphere: in order to obtain a 50% hygrometry level conditioning (RH50), samples were placed in a conditioning unit at 70°C and RH63 for 2 weeks and then put in a room with a controlled atmosphere at 23°C and RH50 until the sorption equilibrium was reached. In order to obtain a 100% hygrometry level conditioning (RH100), the polymer samples were immersed in water at 80°C and weighed periodically until the sorption equilibrium was reached (ca. 4 nights). RH50 and RH100 conditioned samples were only tested at 23°C.

Seven samples per temperature and conditioning state were tested. A Zwick/Roell Z020 machine equipped with a temperature chamber and a laser extensometer was used to carry out the tensile tests. The experimental setup is shown in Figure 70a.

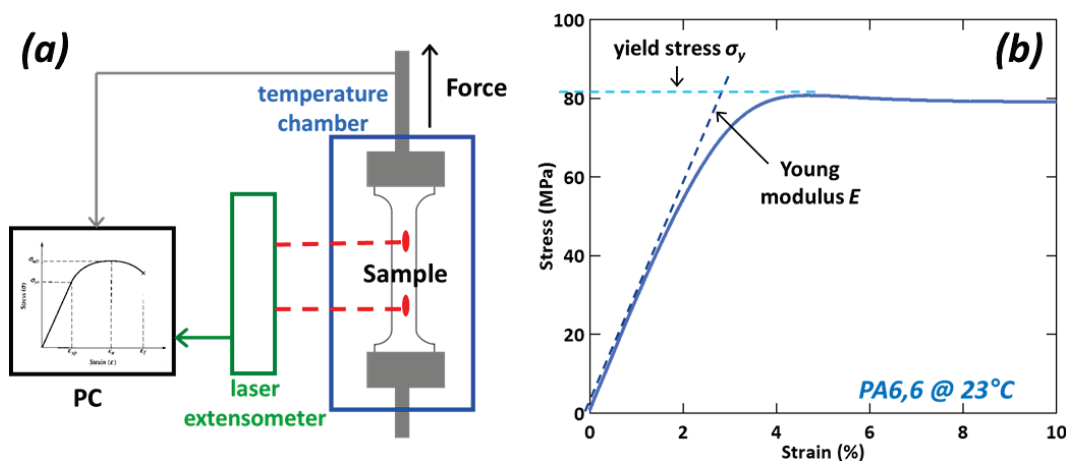


Figure 70: (a) tensile strength test setup and (b) PA6,6 stress-strain plot at 23°C.

From these measurements, a strain-stress curve is obtained. Figure 70b shows an example of such a curve for a neat PA6,6 at 23°C. The Young modulus E is calculated from the tangent line in the elastic domain and the yield stress σ_y is defined as the observed maximum stress.

II.3.4.2. Impact strength

A Charpy impact setup was used in order to obtain the resilience of the studied polymers as well as to characterize their brittle-tough transition temperature. This setup consists in a classic Charpy pendulum equipped with a 7.52 J-energy hammer to which a piezoelectric force captor is attached. The captor is linked to a PC as shown in Figure 71a.

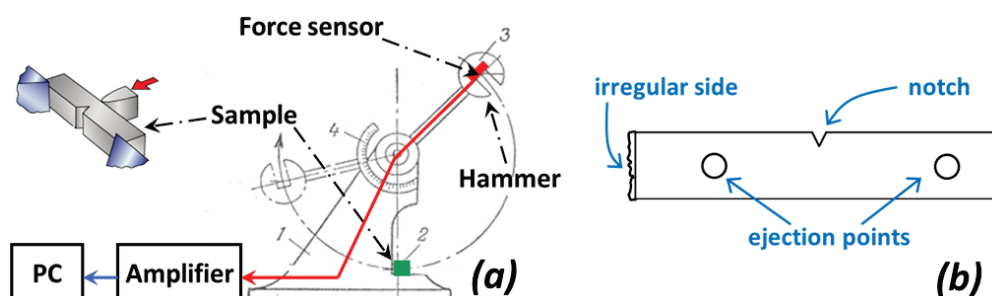


Figure 71: (a) instrumented Charpy Impact test setup and (b) sense in which the samples were notched.

II. Materials & Techniques

The polymer samples, having a dimension of 80x10x4 mm³ were notched with a notch radius of 0.1 mm and the notch depth was fixed at 2 mm. In order to limit the dispersion of results, notching was always done on the same side of the samples, identified by the ejection points, as shown in Figure 71b. Samples were hit with a speed of 1m/s, the deformation rates $\dot{\epsilon}$ being roughly 1x10⁴ Hz according to Equation 54.

$$\dot{\epsilon} \approx \frac{V_{impact}}{r_{notch}}$$

54

A Rhodia-developed software was used to record the load-time curve. As the signal is generally disturbed by the vibrations of the hammer during the impact test, silicon grease was put on the sample side facing the hammer. Figure 72 shows the obtained load-time curves for PA6,6 at 23°C with and without silicon grease. It is observed that silicon grease makes the interferences disappear without affecting the curve shape or the obtained load.

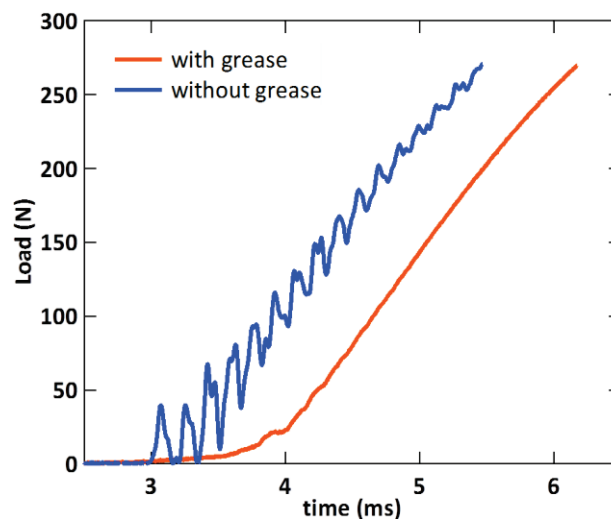


Figure 72: Load-time signal comparison between a PA66 with (orange) and without (blue) silicon grease obtained at 23°C

In order to obtain the brittle-tough transition temperature, shown schematically in Figure 73, impact strength tests were conducted at different temperatures.

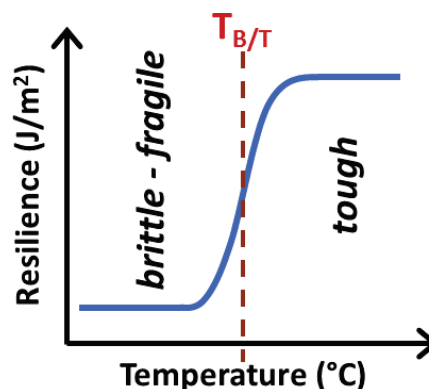


Figure 73: Schematic representation of the evolution of the resilience with temperature and the brittle-tough transition temperature TB/T.

A material is said to be “brittle” if it fails upon impact and the obtained load-time curve is similar to that shown in Figure 72. However, a material is said to be “ductile” if it does not

II. Materials & Techniques

fail completely upon impact and thus a bell-shaped curve is obtained. Figure 74 shows the brittle or tough behavior of a polymer when tested at different temperatures (25, 75 and 100 °C).

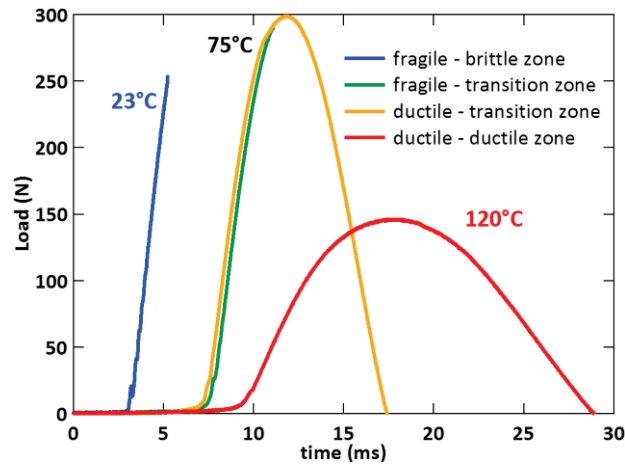


Figure 74: PA6,6 load-time curves showing the behavior at the brittle (23°C), transition (75°C) and ductile (100°C) regimes.

The polymer resilience can be deduced from the load-time curve. By knowing the impact speed v_i , one can determine the displacement l_p from Equation 55:

$$v_i = l_p \times t \quad 55$$

where t is the impact time shown in the load-time curve. Then the load-displacement curve is plotted, the area below this curve being the resilience. The curves were fitted by polynomial functions: the fragile curves were fitted by linear functions ($ax + b$) and the ductile curves by third-degree functions ($ax^3 + bx^2 + cx + d$). By integrating these functions one obtains the impact energy and when referring it to the impact surface one finally obtains the material resilience.

In order to study the relationship between molecular mobility and impact strength properties, the REF, 10LA, 10HA, HIA, and AISLI formulations impact specimens were also conditioned at dry, RH50 and RH100 states, as it was described above for the tensile strength specimens. Dry samples were tested at temperatures varying from 23 to 140°C, RH50-conditioned samples were tested at temperatures from -20 to 70 °C, and RH100-conditioned samples were tested at temperatures ranging from -60 to 23°C. The conditioning above 23°C was done in a Memert 100 Loading model oven, and below this temperature a Dycometal CV-65 refrigerator was used. Between five to seven samples per formula per temperature were tested. For temperatures above 23°C, samples were conditioned during 30 minutes at the test temperature whereas for temperatures below 23°C, the samples were conditioned during 1 hour at the desired temperature. The samples were notched at 0.1mm before temperature conditioning.

III. Sorption and plasticizing effect of pure polar or non-polar solvents and mixtures of solvents in neat PA66

III.1. Heterogeneity of the amorphous phase

As it was mentioned in Chapter 1, PA6,6 morphology could be considered as a two-phase system comprising a crystalline phase and an amorphous phase but several authors [29-32] have proposed the existence of a third intermediate phase named Rigid Amorphous Fraction (RAF). The RAF is expected to exhibit a reduced molecular mobility when compared to the Mobile Amorphous Fraction (MAF), as well as a possible reduced accessibility to solvents. In order to correctly interpret the solvent intakes, it is thus important to firstly study the heterogeneity of the amorphous phase of the studied samples.

The amorphous phase molecular mobility of neat PA6,6 samples as well as its heterogeneity were then assessed by DSC measurements in the Temperature Modulated mode as described in Chapter II, the determination of the glass transition temperature T_g and the heat capacity step ΔC_p being shown in Table 11.

Table 11: T_g and ΔC_p obtained by Modulated DSC for *NeatPA66* samples.

NeatPA66 Modulated DSC measured data	
T_g [°C]	64
ΔC_p [J/g·K]	0.15

The T_g measured for *NeatPA66* (64°C) corresponds well with the values cited in the literature for dry PA6,6 samples. By knowing the values of the ΔC_p of a fully amorphous PA6,6 (0.51 J/g.K [153]), the current value of the ΔC_p of the sample and that of the crystalline ratio X_c , which is of 38% as measured by DSC, the fractions of Mobile and Rigid Amorphous fractions (MAF and RAF respectively) of *NeatPA66* can be calculated (see Chapter II). Figure 75 shows the obtained values for X_c , %MAF and %RAF for *NeatPA66*.

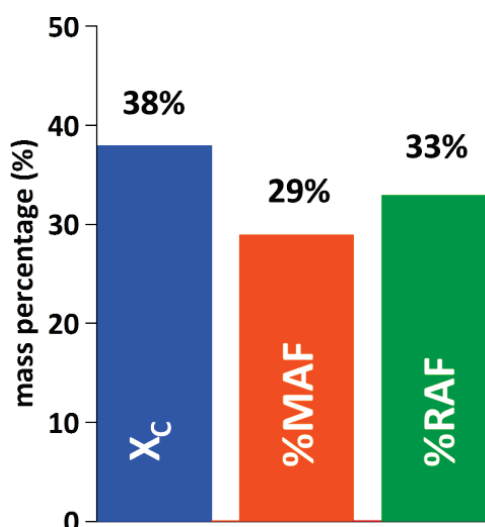


Figure 75: Crystalline, MAF, and RAF mass fractions obtained by DSC and Modulated DSC for *NeatPA66* samples.

III. Pure solvents in Neat PA6,6

Figure 75 shows that the amorphous phase of PA6,6 would be composed approximately half of RAF and half of MAF, in other words the suspected amount of RAF in the PA6,6 samples is relatively high. Cebe et.al. studied the thermal and dielectric properties of several semi-crystalline polymers, namely PEEK and NEW-TPI, a technical polyimide [158,159]. Concerning the dielectric properties of these polymers, a relaxation process which appeared at a higher temperature than that of the main α relaxation was observed for these polymers. Cebe et.al. attributed the observed relaxations to the molecular relaxation motions of the Rigid Amorphous Fraction (RAF).

However, this high-temperature relaxation might be the signature of the Maxwell-Wagner-Sillars interfacial polarization [160,161]. This polarization can occur at the interfaces between the crystalline and amorphous conductive domains, as shown schematically in Figure 76, and would be observed at temperatures higher than those of the α relaxation when the polymer chains have a relatively large mobility. Indeed, at high temperatures, the higher mobility of polymer chains allows charges that are trapped at the crystal / amorphous interfaces to follow the variation of the electric field. These motions could be interpreted as being a molecular relaxation.

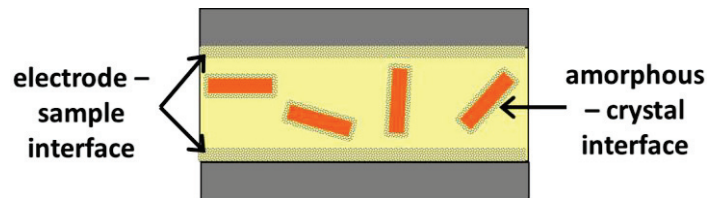


Figure 76: Schematic representation of the polarization in the polymer-electrode and the charges trapped at amorphous - crystal interfaces.

Xu et. al. [160] studied the dielectric properties of polyamide 6,10 (PA6,10). and the dispersion and loss permittivities of PA6,10 they obtained are shown in Figure 77.

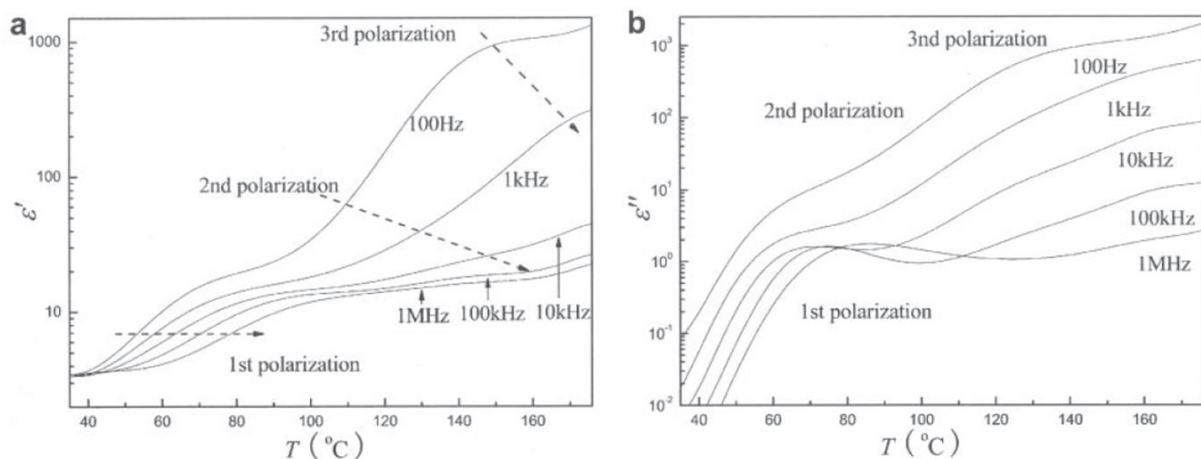


Figure 77: Dispersion (ϵ') and loss (ϵ'') permittivities for PA6,10 at five different frequencies obtained by Xu et.al. [160].

Xu et.al. observed various relaxation processes at high temperatures which they interpreted as being MWS polarization phenomena accompanied by a raise in the polymer electric conductivity. Indeed the values observed for the dispersion permittivity ϵ' shown in Figure 77 are relatively high (i.e. more than 10), and this suggests that these relaxation processes are

III. Pure solvents in Neat PA6,6

not molecular relaxations (value of ϵ' lower than 10) but rather electrical polarization processes at the amorphous – crystal or polymer – electrode interfaces.

Dielectric measurements were carried out in order to study the high-temperature relaxations of PA6,6. Figure 78 shows the dispersion ϵ' , and loss ϵ'' permittivities at several frequencies between 40°C and 200°C and Figure 79 shows the amplitude and the width of the two observed processes labeled α and α' as a function of the frequency. If the α process could be attributed without ambiguity to the main alpha relaxation of PA6,6, the α' process (shouldering) could be interpreted as being either the signature of the RAF or that of interfacial polarization. The origin of this process is now discussed.

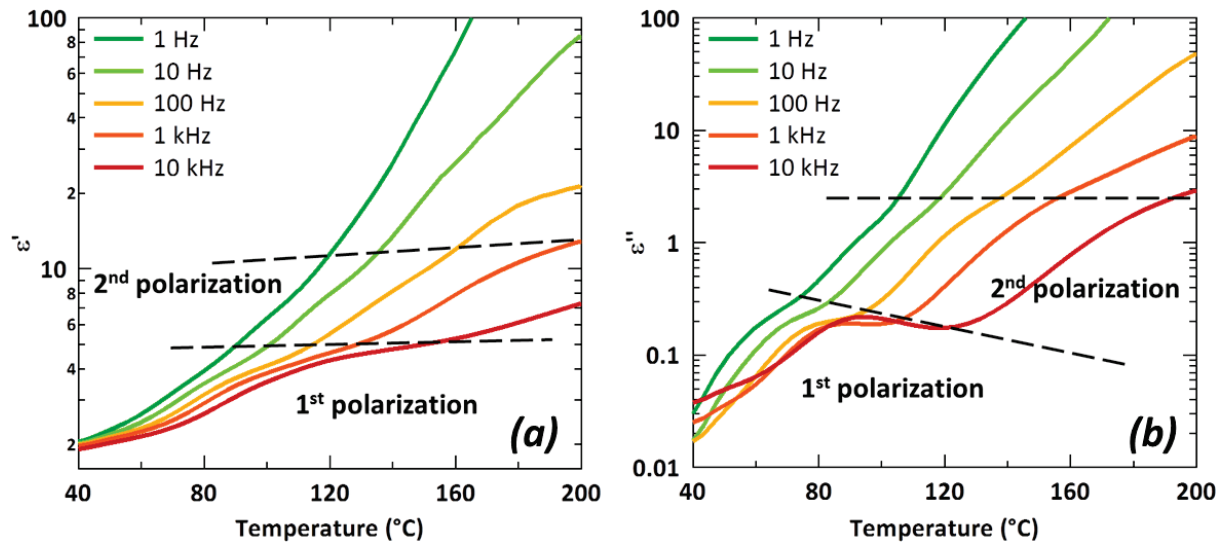


Figure 78: Measured (a) dispersion ϵ' , and (b) loss ϵ'' permittivities for dry PA6,6 samples at five different frequencies.

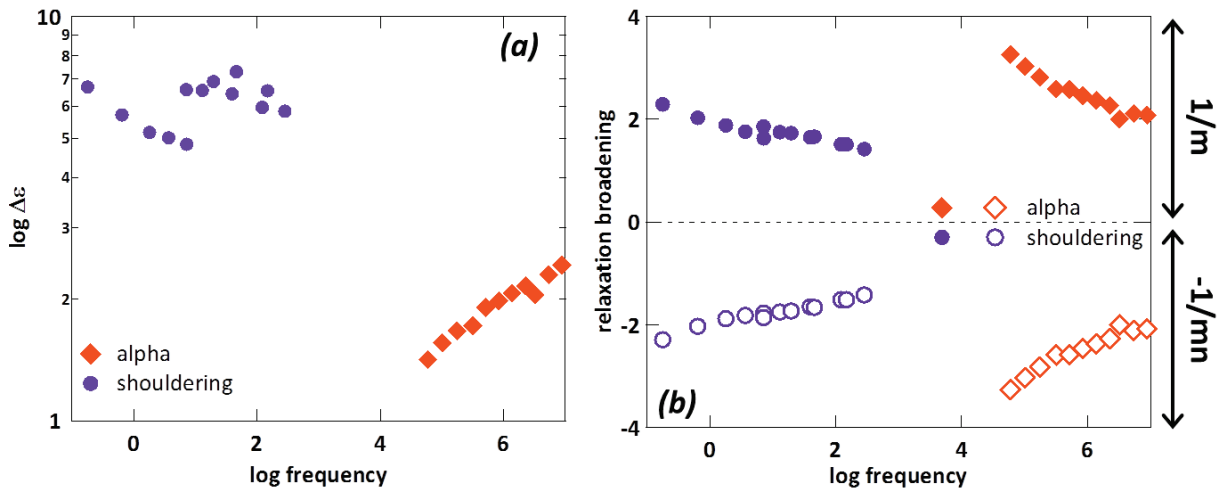


Figure 79: Main α and shouldering α' relaxations (a) intensities $\log \Delta\epsilon$ and (b) widths as a function of the frequency for dry PA6,6 samples.

Figure 79 shows that the amplitude of the shouldering is almost 10 times higher than that of the α alpha relaxation. This fact is a strong argument to suggest that the shouldering is not a molecular relaxation but an electrical polarization process.

It has been observed by DSC measurements that the studied PA6,6 samples might contain a certain percentage of RAF heterogeneity of the amorphous phase. This heterogeneity is of a

dynamic character, since it deals with the molecular motion of polymer chains. The sorption of solvents in polymers is driven by thermodynamic driving forces. So even if the amorphous phase exhibits an heterogeneous molecular mobility, this phase is *thermodynamically* homogeneous for solvent sorption since the driving forces leading to the sorption of such molecules are the same (homogeneous) in the whole amorphous phase. The molecular mobility of this phase will be characterized by the glass transition temperature T_g and its fraction will be simply determined by subtracting the crystalline fraction (calculated from the melting peak) from the total mass of the polymer sample.

III.2. Sorption of pure polar and non-polar solvents

III.2.1. Sorption at equilibrium

The sorption of a series of pure polar and non-polar solvents in polyamide was studied. *NeatPA6,6* 100 μ m-thick film samples were put in flasks containing each of the solvents listed in Chapter II at room temperature (25°C), and solvent intake was measured until the sorption equilibrium was reached as described in that same Chapter. Table 12 shows the mass (Δm) and molar (Δn) intakes at equilibrium for these solvents. The mass intake Δm is the raw percentage of absorbed solvent referred to the total mass of PA66, i.e. considering both the crystalline and the amorphous phases in the calculation of the overall mass:

$$\Delta m = \left(\frac{m_{eq} - m_0}{m_0} \right) \times 100\% \quad 56$$

where m_{eq} is the mass of the polymer swollen with solvent at the sorption equilibrium, and m_0 is the overall initial mass of the polymer. The molecular intake Δn is defined herein as the number of solvent molecules divided by the number of amide groups within the amorphous phase, in which solvent diffusion is supposed to exclusively occur. The molecular intake Δn is defined in Equation 57.

$$\Delta n = \Delta m \times \frac{M_{PA66}}{M_{solvent}} \times \frac{1}{1 - X_C} \left[\frac{in \quad eq_{solv}}{eq_{CONH}} \right] \quad 57$$

where $M_{solvent}$ is the molar mass of the diffusing molecule, X_C is the crystalline fraction measured by DSC ($X_C=38\%$ for NeatPA66), and $M_{PA66}=113$ g/mol is the molar mass of PA66 per amide group (this polymer has two amide groups per monomer as shown in Chapter I, Figure 2).

Table 12 shows that the mass intake Δm of water and polar alcohols in *NeatPA66* is very high (ca. 10 – 15%) and that this intake is larger for the polar alcohols than for water. Moreover, 2-butanol, cyclopentanol and toluene have very low mass intake values when compared to the polar solvents. Since PA66 is a highly polar polymer, polar solvents have an affinity with PA66 because these molecules can interact with the amide functions found in PA66 chains, and more specifically to the H bonds formed between these functions. Non-polar molecules do not have any preferential polar interactions with PA66, but these species should nevertheless be good solvents for the PA66 non-polar methylene backbone. The presence of H bonds formed between amide functions, which act as a physical crosslinks, may hinder

III. Pure solvents in Neat PA6,6

non-polar solvents from swelling PA66, thus limiting the absorbed amounts of non-polar solvents.

Table 12: Mass (Δm) and molar (Δn) intakes at sorption equilibrium, molar volume (V), dipolar moment (μ), and relative dielectric constant (ϵ_r) of the studied solvents at room temperature.

Solvent	$\Delta m[\%]$	$\Delta n[\text{eq}_{\text{solv}}/\text{eq}_{\text{CONH}}]$	$V[\text{cm}^3/\text{mol}]$	$\mu[\times 10^{30} \text{C}\cdot\text{m}][157]$	$\epsilon_r[157]$
Dry	-	-	-	-	-
Water	9.6	0.97	18.00	6.7	78.5
Methanol	13.2	0.64	40.40	5.5	32.6
Ethanol	11.9	0.47	58.30	5.7	24.3
Ethylene glycol	14.5	0.43	55.71	6.7	37.0
1-propanol	10.8	0.33	74.72	5.6	20.1
2-propanol	9.5	0.29	76.34	5.5	18.3
2-butanol	1.1	0.03	91.81	5.6	15.8
Cyclopentanol	1.0	0.02	90.62	-	-
Toluene	1.7	0.034	106.11	1.3	2.43
o-xylene	2.9	0.049	120.54	1.5	2.57
p-xylene	2.7	0.047	123.30	0.2	2.20
2,3-dimethylbutane	2.0	0.042	132.75	-	-
3-methylpentane	2.3	0.048	129.73	-	-
n-hexane	1.2	0.026	130.69	0.3	1.89
Isooctane	1.9	0.030	165.10	0.0	2.10

We considered that the true physically meaningful parameter describing the sorption of a solvent in PA6,6 was the molecular intake Δn . It is then this parameter which will be considered hereafter in the following figures. In order to better compare the different solvent intakes in *NeatPA66*, Δn was plotted as a function of the molecular size of each of the solvents. The parameter considered to define the molecular size of a given solvent is the molar volume V :

$$V = \frac{M}{\rho} \quad \left[\frac{\text{cm}^3}{\text{mol}} \right] \quad 58$$

where M is the solvent molar mass and ρ is the solvent density. The molecular intake Δn of the studied solvents was then plotted in Figure 80 as a function of the molecular volume V of each of these molecules.

III. Pure solvents in Neat PA6,6

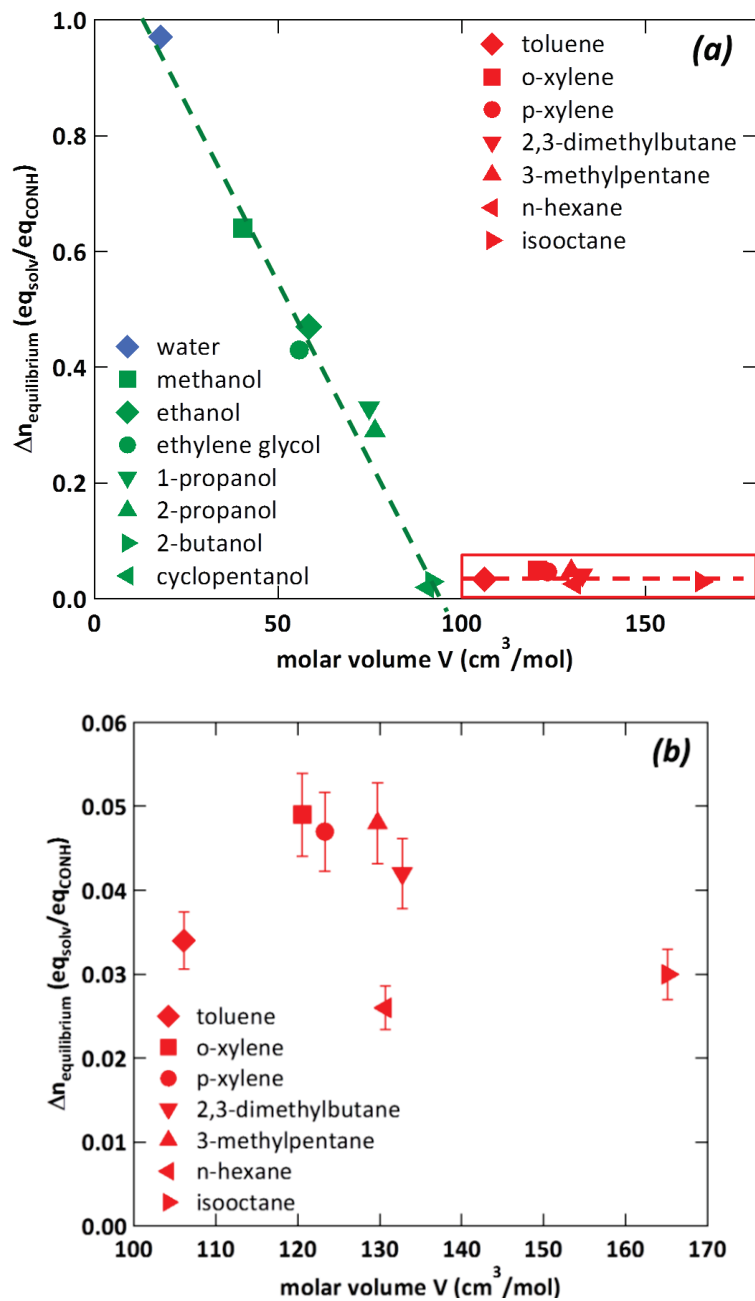


Figure 80: (a) Molar intake at equilibrium $\Delta n_{equilibrium}$ for the studied solvents as a function of their molar volume V and (b) zoom on the non-polar solvents. Dashed lines are guides for the eyes.

Figure 80 shows that the polar solvents seem to follow a linear relationship or a master curve: when the polar solvent molecular size increases, the molecular intake in PA6,6 decreases. Concerning non-polar solvents, it is observed that their intake in PA6,6 seems to not depend on their molar volume. An hypothesis to explain this constant intake could be that these solvents are absorbed in the cavities created during PA6,6 processing, but the volume fraction of these cavities has been estimated to be no more than 0.1% [162]. As these solvents are absorbed at ca. 2% in mass, the presence of cavities cannot alone explain the constant intake of these solvents. This suggests that molecular interactions between PA6,6 and these solvents are at the origin of the relatively large amount of non-polar solvent absorbed in PA6,6.

III. Pure solvents in Neat PA6,6

In order to take into account the polarity of the molecule, the molar intake of each solvent was plotted as a function of the relative dielectric constant ϵ_r (Figure 81a) or as a function of the dipole moment μ normalized by the molar volume V (Figure 81b). In this comparison only the polar solvents and toluene were considered, since the remaining non-polar solvents would yield a similar behavior to that of toluene. The ratio μ/V normalizes the value of the dipole moment of the hydroxyl function to the size of the solvent. The values of ϵ_r and μ are tabulated in Table 12.

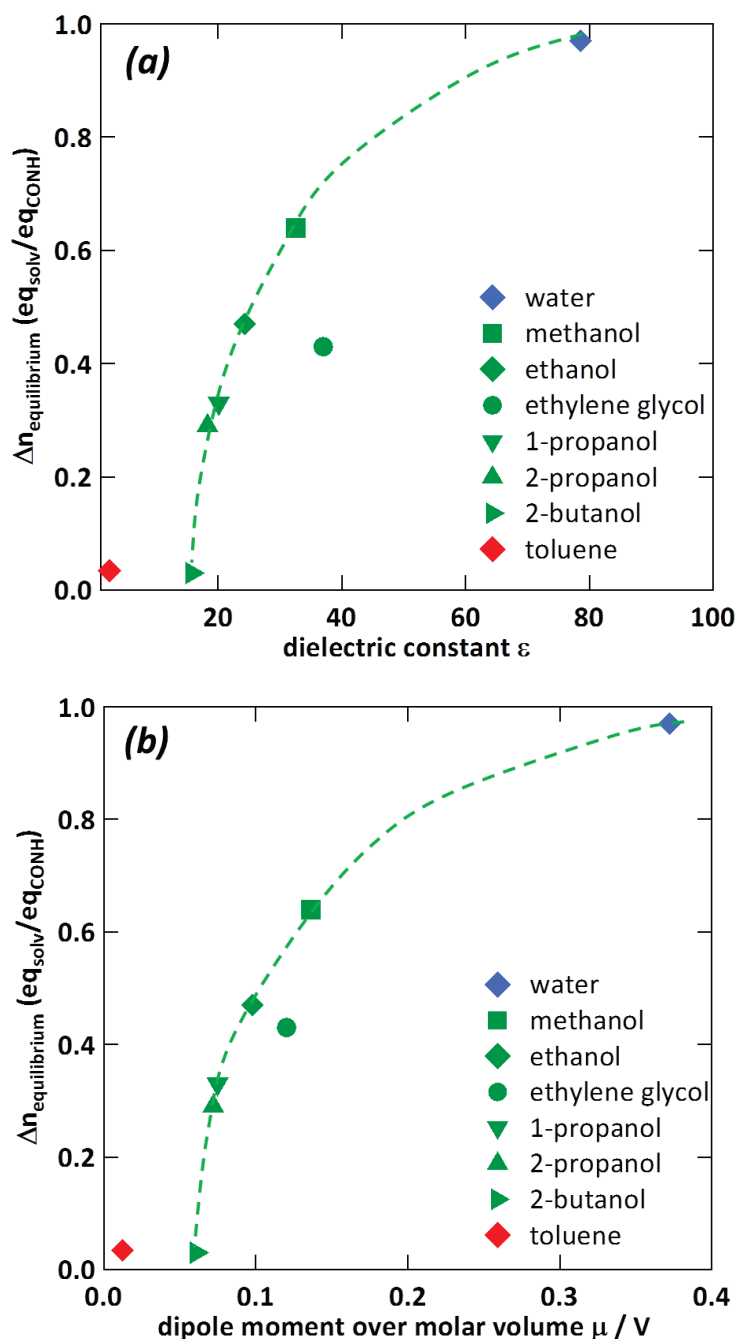


Figure 81: Molar intake at equilibrium $\Delta n_{\text{equilibrium}}$ for the studied solvents as a function of (a) their relative dielectric constant ϵ_r and (b) the ratio of their dipole moment μ over their molar volume V . Dashed curves are guides for the eyes.

It is observed in both figures that there seems to be a master curve or trend linking the polarity of a molecule to its intake in PA6,6. It is observed that when the dielectric constant or the μ/V ratio increases, meaning that the molecule is more polar, its intake in PA6,6

III. Pure solvents in Neat PA6,6

increases as well. It would appear that there seems to be a polarity threshold from which the molar sorption increases when the polarity does, as a large alcohol molecule such as 2-butanol is placed as the same level as toluene, a non-polar molecule. It is further observed that ethylene glycol is less absorbed than the other alcohols despite its polarity, which might mean that up to a certain limit, the size of the solvent could influence its intake in PA6,6.

From the results observed in Figure 80 and Figure 81, it can be concluded that the polarity of the solvent appears to be the main factor conditioning its intake in PA6,6: the more polar the solvent, the larger its intake in PA6,6. It has to be pointed out though that in this study, the size and the polarity of polar solvents cannot be easily decoupled from each other because the size increase of these solvents corresponds automatically to a decrease in the molecule's polarity, the considered solvents having increasing alkyl functions lengths in their structures.

The same approach is now considered for the non-polar solvents, shows the molar intake at equilibrium $\Delta n_{equilibrium}$ as a function of their dielectric permittivity ϵ_r .

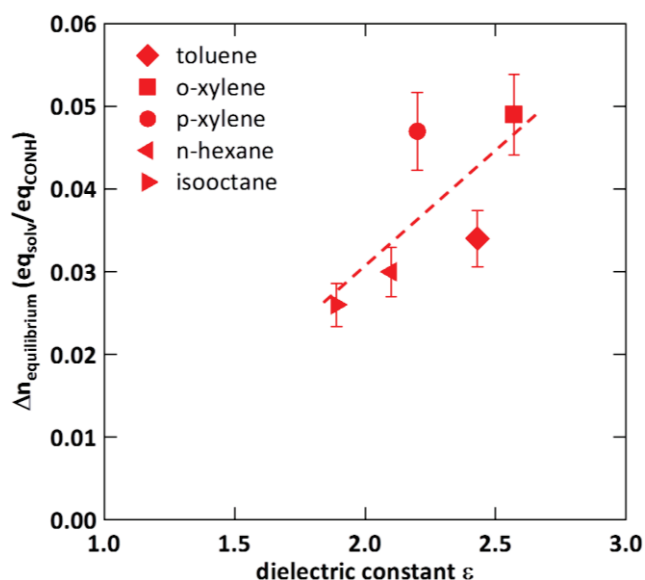


Figure 82: Molar intake at equilibrium $\Delta n_{equilibrium}$ for the studied non-polar solvents as a function of their relative dielectric constant ϵ_r .

Figure 82 shows that the molar intake of a non-polar molecule seems to decrease when its permittivity does. This does not mean that the weak polarity of such solvents determines their intake in PA6,6 but rather the weak interactions that these solvents may have with the polymer. Indeed, in the case of non-polar solvents, the value of the permittivity not only accounts for the weak polarity of the solvent but also it accounts for its ability to be polarized by light or an electric current, as well as the weak interactions between molecules (i.e. non-polar and van der Waals interactions). The sum of all these properties might then have an influence on the sorption of a non-polar solvent in PA6,6, since these weak interactions might determine the solubility of these solvents in the polymer.

III.2.2. Discussion of the results on solvent sorption in PA6,6

In the previous section, experimental results on solvents intakes were presented and the effect of solvent polarity and solvent size were highlighted. In this section, the physical mechanisms associated to solvent sorption in PA6,6 are discussed.

Equilibrium sorption isotherms of non-polar solvents in amorphous non-polar polymers are described by the Flory-Huggins approach [35-47], in which sorption equilibrium at a given activity is determined by a single interaction parameter χ , which effectively contains the balance of monomer-monomer, monomer-solvent and solvent-solvent pairwise molecular interactions (mostly van der Waals, in the case of non-polar systems), measured in units of $k_B T$ per molecule. The balance of interactions is always repulsive, that is, the Flory-Huggins parameter χ is *positive*. In systems with polar interactions able to form hydrogen bonds, i.e. with specific interaction sites, other sorption models have been proposed, based e.g. on modifications of the BET [163,164] or GAB [49,52] approaches. Combinations of different models have also been proposed in order to obtain heuristic fits of sorption isotherms [51,55,165].

Let us first consider the orders of magnitude of absorbed solvent amounts given by thermodynamic models. In the Flory-Huggins approach, the total free energy of a system of n_p polymer chains of length N with n_s solvent molecules absorbed is (in unit of $k_B T$):

$$F = n_s \ln \phi_s + n_p \ln(1 - \phi_s) + \chi n_s (1 - \phi_s) \quad 59$$

where $\phi_s = n_s / (n_s + Nn_p)$ is the solvent volume fraction and $1 - \phi_s = Nn_p / (n_s + Nn_p)$. The equilibrium solvent volume fraction ϕ_s is given by $\frac{\partial F}{\partial n_s} = \mu - \mu_0 = \ln a_s$ which gives the relationship between the activity and the solvent volume fraction (in the limit of long chains):

$$\ln a_s = \ln \phi_s + (1 - \phi_s) + \chi (1 - \phi_s)^2 \quad 60$$

The Flory-Huggins interaction parameters χ_{1p} , χ_{2p} , and χ_{12} can be estimated from the Hildebrand relationship:

$$\chi_{ij} = \frac{(\delta_i - \delta_j)^2}{RT} V \quad 61$$

where δ_i and δ_j are measured Hildebrand solubility parameters for species i and j [14,166-168], and V is the molar volume of the predominant species. The calculated values of PA6,6 –ethanol/toluene solubility parameters at 23°C are shown in Table 13.

According to the values of interaction parameters reported in Table 13, ethanol should be a very good solvent of PA6,6, toluene should be a bad solvent of this polymer, and water should not have any affinities with PA6,6. From Equation 60, the toluene volume fraction at equilibrium sorption should be of the order of 40% for $a_{toluene} = 1$. Ethanol is a good solvent, and thus should dissolve PA6,6 at $a_{ethanol} = 1$. Therefore, Flory parameters derived previously

III. Pure solvents in Neat PA6,6

are not appropriate at all to describe the observed volume (or molar) fractions at equilibrium (15% for ethanol and 2% for toluene). Note that a slightly different value of the solubility parameter for PA6 is tabulated in [14] $\delta = 21.5 \text{ MPa}^{1/2}$. Using this value, it would be found that both toluene and ethanol would be good solvents and would dissolve PA6,6, with $\chi_{1P} \cong 0.45$ and $\chi_{2P} \cong 0.4$.

Table 13: Hildebrand solubility parameters δ for ethanol, toluene, and PA6,6 [166-168] and deduced Flory-Huggins pair interaction parameters χ .

Species	$\delta [\text{cal}^{1/2}/\text{cm}^{3/2}]$	χ_{ij}
Ethanol (1)	12.7 [167]	$\chi_{2P} = 0.07$
Toluene (2)	8.9 [167]	$\chi_{3P} = 0.89$
PA6,6 (P)	13.6 [168]	-

The interaction parameters are mean field quantities appropriate for non-polar systems, in which the polymer-solvent mixture may be considered to be homogeneous (homogeneously swollen) down to the molecular scale or so. However, these interaction parameters are not appropriate for amphiphilic polymers with specific interaction sites like polyamides, which contain polar (amide) groups along the chains.

Let us first discuss the case of toluene. Let us first consider the orders of magnitude of absorbed solvent amounts given by thermodynamic models. In regards of the low solvent content at equilibrium ($\Delta n_{\text{toluene}} \cong 3.4 \%$), solvent sorption can be described to a good approximation with the Henry law (whatever the detailed mechanism, Langmuir or Flory-Huggins or any other composite model):

$$\varphi = a \exp \left[-\frac{E}{k_B T} \right] \quad 62$$

The value of the solvent content at equilibrium (for an activity $a = 1$) thus gives an estimate of the free enthalpy E (the sorption enthalpy, which mainly contains the extra energy to pay for absorbing one molecule of solvent in the material). Because φ is small even at activity $a = 1$, the free enthalpy cost E must be *positive*. For $a = 1$, φ is of the order 3 to 4 %_{mol}. This leads to $E \cong 3.2$ to $3.4 k_B T$ or $E \cong 13 \times 10^{-21} \text{ J}$ (per molecule).

The qualitative picture that can be proposed (*in the case of toluene*) is the following one. Polyamide chains are made of aliphatic segments ($-\text{CH}_2-$). Toluene is a good solvent for aliphatic (hydrophobic) parts. In the absence of amide groups, toluene should be able to dissolve the chains, according to the Flory-Huggins swelling mechanism. However, at room temperature, amide groups form hydrogen bonds [20-28,61,130]. Thus, the system has a large density of relatively strong interactions. These interactions form a tridimensional network which counterbalances the Flory swelling effect, in the same way as in crosslinked elastomers or gels [169-172]. By adding an elastic term E_{elast} associated to dilatation in the free energy, the classical Flory model (Equation 59) becomes:

$$F = n_s \ln \varphi_s + n_p \ln(1 - \varphi_s) + \varphi_s n_s \left(\frac{1 - \varphi_s}{\varphi_s} \right) + E_{\text{elast}} \quad 63$$

III. Pure solvents in Neat PA6,6

In Equation 63, F is the total free energy (in units of RT with R the ideal gas constant $R=k_B N_A$) of a swollen sample of volume V , χ is the Flory-Huggins solubility parameter for the given solvent-polymer system, and n_s is the number of solvent molecules.

However, in PA6,6, compared to usual elastomers or gels, the density of interactions (acting as effective ‘crosslink points’) is expected to be much larger, or equivalently the mesh size of this network is expected to be much smaller. This has several consequences. First, it may be expected that the associated effective dilatation modulus be much larger than the typical values 10^5 to 10^6 Pa observed in gels or elastomers. Then, the overall volume variation of the sample being relatively small, contrary to loosely crosslinked systems, it may be expected that this dilatation term can be modeled in the linear regime, that is, the elastic term may be written of the form:

$$E_{elast} = \frac{KV(V-V_{eq})^2}{2V_{eq}^2} \cong \frac{Kb^6}{2V} n_s^2 = \frac{KV}{2} \phi_s^2 \quad 64$$

in which K is an effective (osmotic) dilatation modulus, V_{eq} is the total equilibrium volume of the sample in the dry state, and V the actual total volume in the swollen state. K has the dimension of energy per unit volume (expressed here in units of RT). The volume change is simply the volume of absorbed solvent $V-V_{eq} = V\phi_s = n_s b^3$, where ϕ_s is the solvent volume fraction in the swollen material, n_s the total number of absorbed solvent molecules and b^3 the solvent molecular volume. Note that additivity of molecular volumes is implicitly assumed (which is known to be erroneous for some solvents, water being the most spectacular case). Equilibrium is given by $\left(\frac{\partial F}{\partial n_s}\right)_{n_p} = \mu_s - \mu_s^0 = \ln a_s$, in which a_s is the activity

of the solvent, and μ_s and μ_s^0 are respectively the chemical potential of the solvent in the polymer–solvent system and the chemical potential of the solvent in the reference state (activity $a_s = 1$). This leads to the following relationship for the solvent volume fraction as a function of the activity at equilibrium:

$$\ln a_s = \ln \phi_s + (1 - \phi_s) + \chi(1 - \phi_s)^2 + Kb^3 \phi_s \quad 65$$

In this relationship, the term depending on Kb^3 takes into account the elasticity due to effective ‘crosslinks’, whereas the other terms on the right hand side take into account the interactions and the entropy of mixing of the solvent-polymer system. The constant K should not be considered as characteristic of the polymer only, but rather of a polymer-solvent system, as this constant may also depend on the solvent nature, e.g. on its molecular size and/or polarity. Large K values should be considered to account for the small amounts of absorbed solvent. The values of the coefficient Kb^3 can be estimated by considering the pure solvent equilibrium sorption values at activity $a_i = 1$.

For toluene, taking a volume fraction $\phi_s = 0.02$ at activity $a = 1$, the value $Kb^3 \cong 150 k_B T$ is found. With a molecular volume of the order $b^3 \cong 0.15 \times 10^{-27} \text{ m}^3$, and with $k_B T = 4 \times 10^{-21} \text{ J}$, this corresponds to a modulus K of the order 4 GPa.

Let us now discuss this value of the effective modulus K . As already mentioned above, the situation described here is quite different from loosely crosslinked gels, because the density

III. Pure solvents in Neat PA6,6

of effective ‘crosslink’ points (H-bonds between amide groups) is comparatively very high. There is another important difference, which is that H-bonds are formed along effective ‘chains’ between successive rigid $-\text{CONH}-$ entities, as schematized in Figure 83.

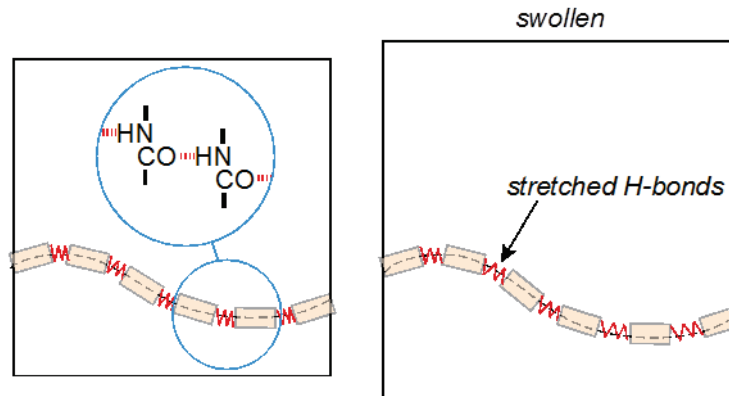


Figure 83: Stretching of the H-bond network upon the swelling action of a solvent.

Note indeed that a very large fraction of amide groups are bonded at room temperature [20]. As a consequence, in order to allow the swelling of the polymer, the H bonds between PA6,6 must stretch upon solvent sorption. Thus, we propose to estimate the bulk modulus associated to the stretching of H bonds upon swelling. H bonds may be represented by an interaction potential. The bulk modulus K is directly related to the stiffness of this potential and to the density ρ_H defined as the number of H bonds per monomeric unit volume of material. The dipole-dipole interaction potential E_d between two dipoles m_1 and m_2 separated by the vector r is:

$$E_d = \frac{1}{4\pi\epsilon_R\epsilon_0} \left[\frac{\vec{m}_1 \cdot \vec{m}_2}{r^3} - \frac{3}{r^5} \left(\vec{m}_1 \cdot \vec{r} \right) \left(\vec{m}_2 \cdot \vec{r} \right) \right] \quad 66$$

The energy E_d is minimized in the configuration in which dipoles are parallel to each other and aligned with the vector r . In this configuration, the interaction energy is defined as:

$$E_d = -\frac{m_1 m_2}{2\pi\epsilon_R\epsilon_0 r^3} \quad 67$$

The order of magnitude of this energy can be estimated. Tabulated H-bond energies (the difference in energy between the bonded state and the non-bonded state) are of ca. 25 to 30 kJ/mol as found in the literature [173], which corresponds to 4 to 5×10^{-20} J per H-bond. The value for the dipolar moments of an amide function is of $m = 12.3 \times 10^{-30}$ C·m (i.e. for acetamide or N-methylacetamide [157]). The value of E_d can be calculated from Equation 67 with the values $m_1 = m_2 = 10^{-29}$ C·m, $r = 0.2$ nm and $\epsilon_R = 4$ [2], giving an $E_d = 5.6 \times 10^{-20}$ J. This value is of the right order of magnitude.

In order to obtain the total potential, a short range repulsive contribution must be added. The total potential may be written as:

III. Pure solvents in Neat PA6,6

$$E_{tot} = -\frac{m_1 m_2}{2\pi\epsilon_R\epsilon_0 r^3} + \frac{J}{r^{12}} \quad 68$$

where the constant J is chosen to adjust the distance r_0 at the minimum. The stiffness or curvature C of the potential at the minimum is given by:

$$C = \left(\frac{d^2 E_{tot}}{dr^2} \right)_{r_0} = \frac{12m_1 m_2}{2\pi\epsilon_R\epsilon_0 r_0^5} + \frac{156J}{r_0^{14}} = \frac{27m_1 m_2}{2\pi\epsilon_R\epsilon_0 r_0^5} \quad 69$$

With the values $m_1 = m_2 = 10^{-29}$ C·m, $r_0 = 0.2$ nm and $\epsilon_R = 4$, the order of magnitude of the stiffness C is equal to 38 C/m². The value of the bond energy at the minimum of the potential is then defined as:

$$E_{min} = -\frac{3m_1 m_2}{8\pi\epsilon_R\epsilon_0 r_0^3} \quad 70$$

Figure 84 shows then the total potential describing an H bond (from Equation 68), expressed in kJ/mol.

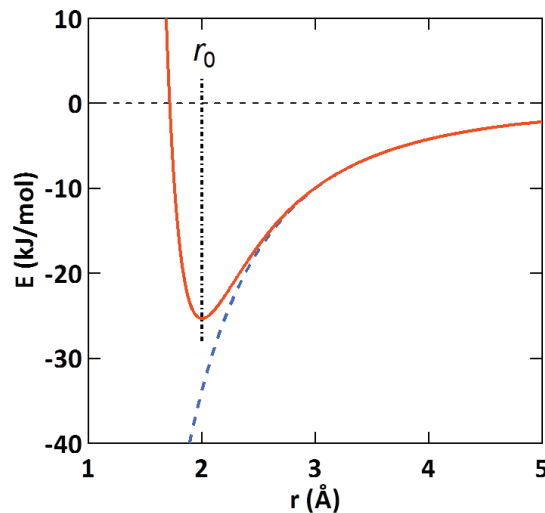


Figure 84: Energy potential for an H bond. Dashed blue curve dipole-dipole interaction (Equation 67) calculated with the parameter values specified in the text. Full orange curve is the total potential (Equation 68), adjusted to have the minimum at $r_0=0.2$ nm

So, with a relative variation $\Delta r/r_0 = 1/3$ $\Delta V/V_0$ associated to isotropic and homogeneous swelling of PA6,6 by a solvent, the variation of energy for one H bond is:

$$\Delta E = \frac{C}{2} (\Delta r)^2 \quad 71$$

where C is the curvature of the potential (Equation 69). The variation of energy per unit volume is given by:

$$\Delta E = \frac{C}{2} \rho_H (\Delta r)^2 \quad 72$$

where ρ_H is the number of H bonds per unit volume of material as defined above. By analogy

to Equation 64 ($\Delta E = \frac{K}{2} \left(\frac{\Delta V}{V_0} \right)^2$), the modulus K can be defined as:

$$K = \frac{\rho_H C r_c^2}{9}$$

73

where $r_c \approx 0.5$ nm is the radius of the monomeric unit $-(CH_2)_5CONH-$ which is defined as the cubic root of the molecular volume V_H of this unit ($r_c^3 = V_H = 1/\rho_H = 0.17 \times 10^{-27}$ m³). From Equation 73, the value of the modulus K is of the order of 5 GPa. This value is in *very good agreement* with the value deduced previously from the equilibrium sorption of toluene under activity $a = 1$. According to Equation 72, the energy change upon swelling (per H-bond) is of the order 3×10^{-22} J. That is, a relative variation $\Delta E/E$ of the order 6×10^{-3} (or at most let us say $\Delta E/E \approx 10^{-2}$).

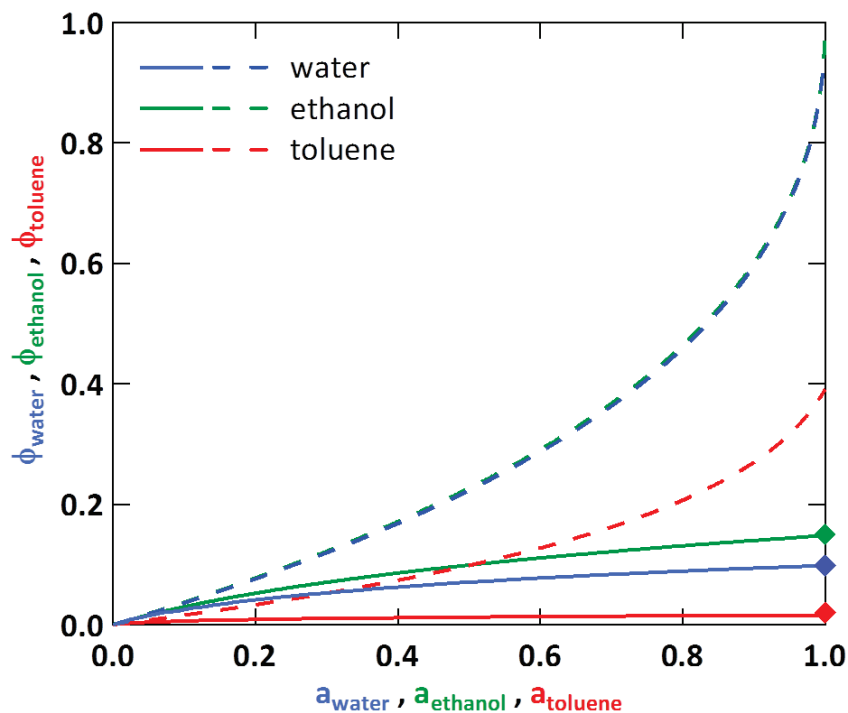


Figure 85: Solvent volume fraction as a function of the solvent activity (sorption isotherms) for ethanol and toluene, using interaction parameter values listed in Table 13: modeled with the standard Flory-Huggins model defined in Equation 60 (dashed curves); and modeled with Equation 65 with values of the modulus K chosen for each solvent to match the measured absorbed solvent amount at $a = 1$ (plain curves). Measured values are indicated by diamond symbols.

Let us now discuss the case of the other solvents such as water and ethanol. Using Equation 65 in the same way as for toluene, one finds a value $Kb^3 \cong 7$ for ethanol. This corresponds to an effective modulus K of the order 0.2 MPa. This value is much smaller than that for toluene, because it has to account for a much higher volume fraction of ethanol absorbed at equilibrium. This value might be explained by the fact that ethanol, having a polar group, can itself form H-bonds with amides (mostly $-CO|||HO-$ H-bonds), thus effectively breaking H-

III. Pure solvents in Neat PA6,6

bonds between amide groups, with then a strong impact on the modulus K . In the case of water, the molar sorption is even larger than that of ethanol. According to the above discussion, this qualitatively corresponds to the fact that water interacts with H-bonds and thus disrupts the amide-amide H-bond network even more than ethanol.

The effect of the dilatation elastic term Kb^3 (Equation 65) is illustrated in Figure 85 for the cases of toluene and ethanol. Figure 85 illustrates how the effect of the dilatation coefficient Kb^3 (plain curves) greatly limits the intake of solvents in PA6,6 when compared to the classical Flory-Huggins model (dashed curves). It is also noted that the effect of Kb^3 becomes quite large with respect to other terms for values of a_i higher than 0.5.

III.3. Effect of pure solvents on the molecular mobility of neat PA6,6

III.3.1. Effect of pure solvents on the main alpha relaxation (associated to the glass transition)

The effect of polar and non-polar solvents on PA6,6 molecular mobility was studied, and we firstly focused on the main alpha relaxation associated to the glass transition. After obtaining the sorption equilibrium at room temperature, *NeatPA6,6* 100 μ m-thick film samples were analyzed by both Modulated DSC in order to assess their T_g 's and by Broadband Dielectric Spectroscopy (BDS) to obtain the α relaxation temperatures T_α at 1Hz from the maxima of the loss moduli M'' spectra. Table 14 shows the obtained data.

Table 14: Molar (Δn) intakes at sorption equilibrium for the studied solvents obtained at room temperature, and glass transition (T_g) and α relaxation temperatures (T_α) of dry and solvent-saturated PA66 samples.

Solvent	Δn [eq _{solvent} /eq _{CONH}]	T_g [°C] - DSC	T_α @1 Hz [°C] - BDS
Dry	-	64	68
Water	0.97	-22	-24
Methanol	0.64	-53	-32
Ethanol	0.47	-35	-32
Ethylene glycol	0.29	-36	-34
1-propanol	0.33	-30	-22
2-propanol	0.29	-10	-10
2-butanol	0.03	50	61
Cyclopentanol	0.02	51	53
Toluene	0.034	20	23
o-xylene	0.049	13	16
p-xylene	0.047	12	20
2,3-dimethylbutane	0.042	25	28
3-methylpentane	0.048	23	24
n-hexane	0.026	40	38
Isooctane	0.030	35	34

It is observed in Table 14 that both Modulated DSC and Dielectric Spectroscopy yield results of the same order of magnitude except for methanol, for which we suspect that some of the solvent departed during the Dielectric measurements, leading to a reduced effect on T_α . We

III. Pure solvents in Neat PA6,6

will then only consider hereafter the data obtained by calorimetric experiments. Figure 86 plots the T_g obtained by DSC of the solvent-saturated samples as a function of their molar intake at equilibrium.

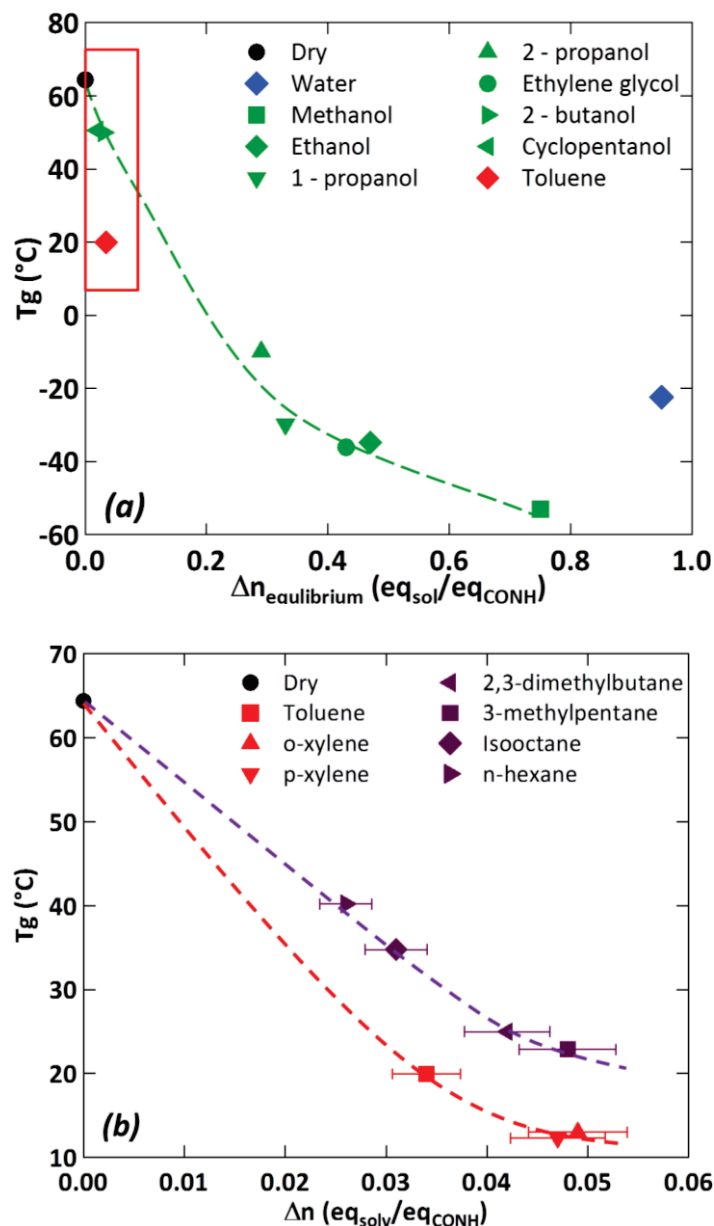


Figure 86: PA6,6 T_g measured by DSC as a function of the molar intake at equilibrium $\Delta n_{equilibrium}$ for (a) the polar solvents and toluene, and (b) for the non-polar solvents. Dashed curves are guides for the eyes.

Figure 86a shows that the alcohol series (green markers) seems to follow a master curve: as solvent molecular intake increases, the induced T_g drop increases as well, methanol being the most absorbed alcohol and the one that provokes the largest T_g drop in PA6,6. It is observed as well in Figure 86a that water and toluene do not seem to follow the master curve associated to the alcohol molecules.

Moreover Figure 86b shows that there might be two different plasticization trends for non-polar solvents. Although these solvents are absorbed in comparable amounts, the aromatic solvents (red markers) provoke a larger T_g drop than the aliphatic molecules (purple

III. Pure solvents in Neat PA6,6

markers). This difference might come from their structural nature. A hypothesis of the possible origin of these trends will be explained further in this Chapter, along with the hypotheses on the plasticization mechanisms of polar and non-polar solvents.

In order to better compare the different plasticization trends of polar and non-polar solvents, Modulated DSC measurements were carried out on *NeatPA6,6* 100 μm -thick film samples swollen with different molecular intakes of water, ethanol, and toluene. PA6,6 samples were immersed in these solvents during different periods always shorter than the time needed to reach the sorption equilibrium, and then the T_g of these partially swollen samples were analyzed straight ahead by Modulated DSC. As samples exhibit in that configuration an out-of-equilibrium swelling, it should be pointed out that solvent concentration in the sample may not be perfectly homogeneous. As a consequence, the measured T_g should be considered as an “average T_g ”, the local T_g in the sample depending on the local solvent concentration. Figure 87 shows then the measured T_g of the partially swollen samples as a function of the molecular intake for water, ethanol and toluene in comparison with the T_g values obtained at sorption equilibrium for water, toluene and the alcohol series.

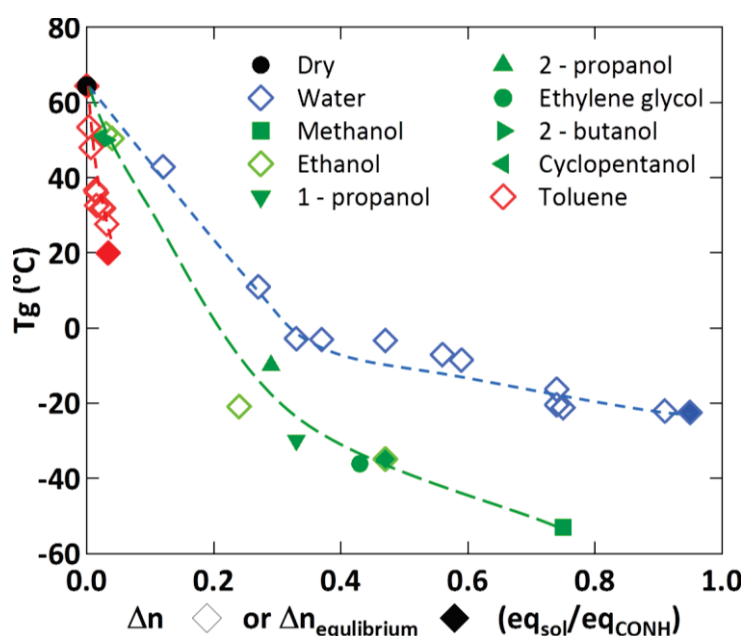


Figure 87: PA6,6 T_g measured by DSC as a function of the partial molar intake Δn (hollow markers) or the molar intake at equilibrium $\Delta n_{\text{equilibrium}}$ (plain markers). Dashed curves are guides for the eyes.

It is confirmed in Figure 87 that water and toluene do not follow the same plasticization trend as that of the alcohol series. For a given molecular intake, toluene exhibits the largest plasticization effect, i.e. the largest induced T_g drop, followed by the alcohol molecules and finally by water.

The measured variations of the glass transition temperature of PA6,6 in presence of solvents were then compared to several plasticization models that were presented in Chapter I. Figure 88 shows the measured T_g as a function of the molecular intake for water, ethanol, and toluene compared to the T_g drop expected in the presence of these solvents as calculated from the Fox, Couchman-Karasz, Lu-Weiss, Gordon-Taylor, and Kelley-Bueche models [131-141]. The input data used in these relationships is shown in Table 15.

III. Pure solvents in Neat PA6,6

Table 15: PA6,6, water, ethanol, and toluene data used as input for computing the T_g of a PA6,6 – solvent systems according to the plasticization models mentioned above.

	PA6,6	Water	Ethanol	Toluene
T_g (°C)	64	-137 [112]	-176 [174]	-156 [175]
M (g/mol)	113	18	46	92
ρ (g/cm ³)	1.14 [2]	1	0.789	0.867
ΔC_p (J/g·°C)	0.22	1.92 [112]	0.28 [174]	0.56 [175]
$\Delta\alpha$ (1/K)	4.8×10^{-4} [138]	2.04×10^{-4} [112]	1.09×10^{-3} [157]	1.08×10^{-3} [157]
$\chi_{PA66-solvent}$	-	0.70	0.07	0.89

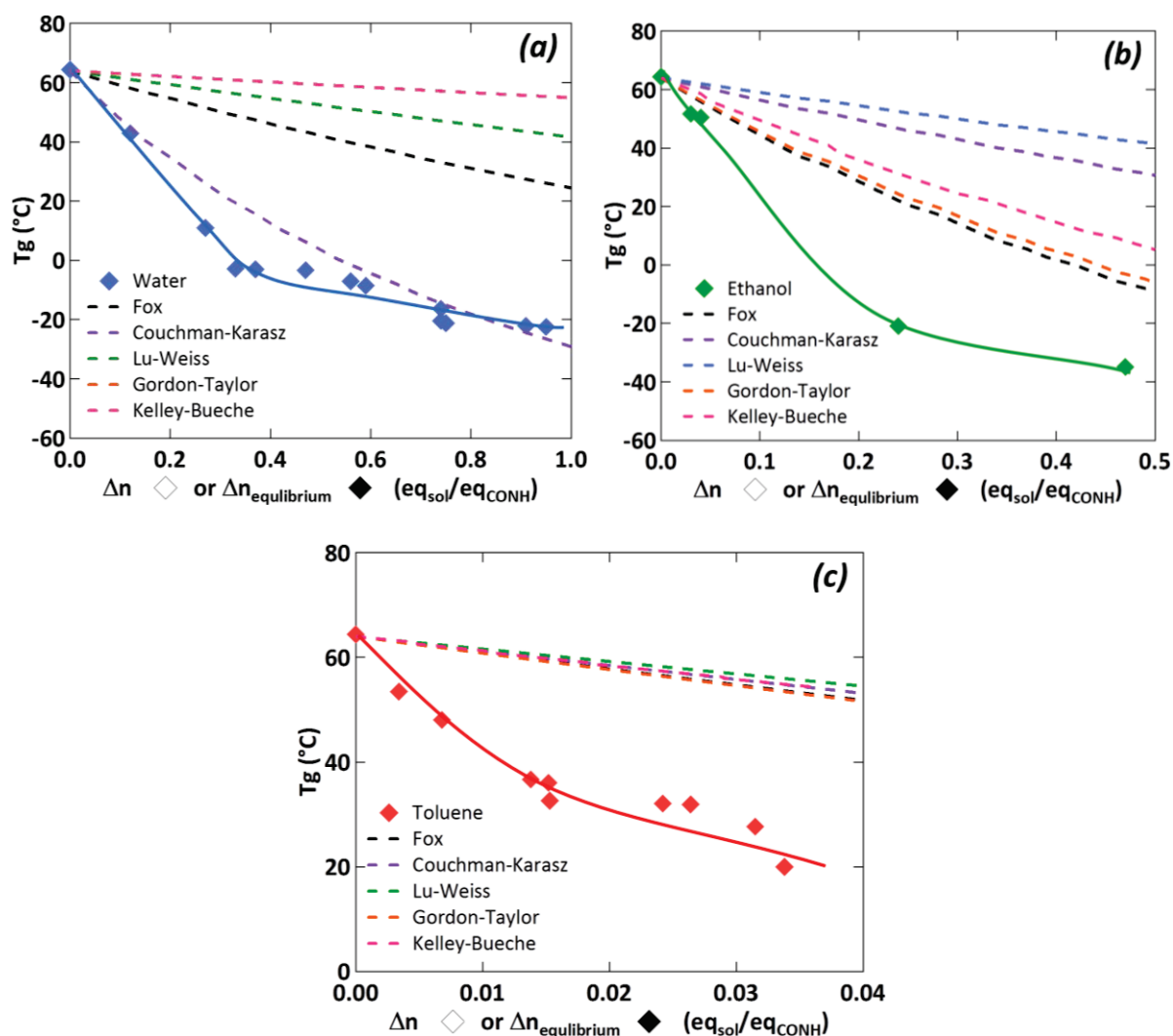


Figure 88: PA66 T_g drop measured by DSC in presence of (a) water, (b) ethanol, and (c) toluene compared to several plasticization models in mixtures presented in Chapter I [131-141]. Plain curves are guides for the eyes.

Figure 88 shows that none of the plasticization models describes well the plasticization trends of water, ethanol and toluene in PA6,6.

As mentioned in Chapter I, the plasticization models mentioned herein only consider some physico-chemical properties of these species such as their densities, thermal coefficients,

III. Pure solvents in Neat PA6,6

heat capacities, and the Flory-Huggins interaction parameters to estimate the T_g of a polymer/plasticizer blend. These models do not consider the nature of a polymer or a solvent (i.e. polar species or cross-linked polymers) and the eventual strong interactions that might be present between a polymer and a solvent such as H-bonding or even the disruption of a polymer structure by the introduction of a solvent. The significant T_g drop observed for the PA6,6-solvent systems when compared to the model predicted values could be then another signature of specific, relatively strong interactions between water, ethanol, or toluene with PA6,6. Moreover, the different plasticization trends observed for water, toluene and the alcohol series in Figure 87 suggest that these molecules provoke a PA6,6 T_g drop through different plasticization mechanisms. These mechanisms will be further discussed in paragraph “III.3.3. Discussion of plasticization mechanisms”.

The effect of water, ethanol, and toluene on PA6,6 main and secondary relaxations was more precisely studied by Dielectric Spectroscopy. Figure 89 shows the loss permittivity – frequency – temperature 3D plots for dry and solvent-swollen samples, highlighting the observed molecular relaxations.

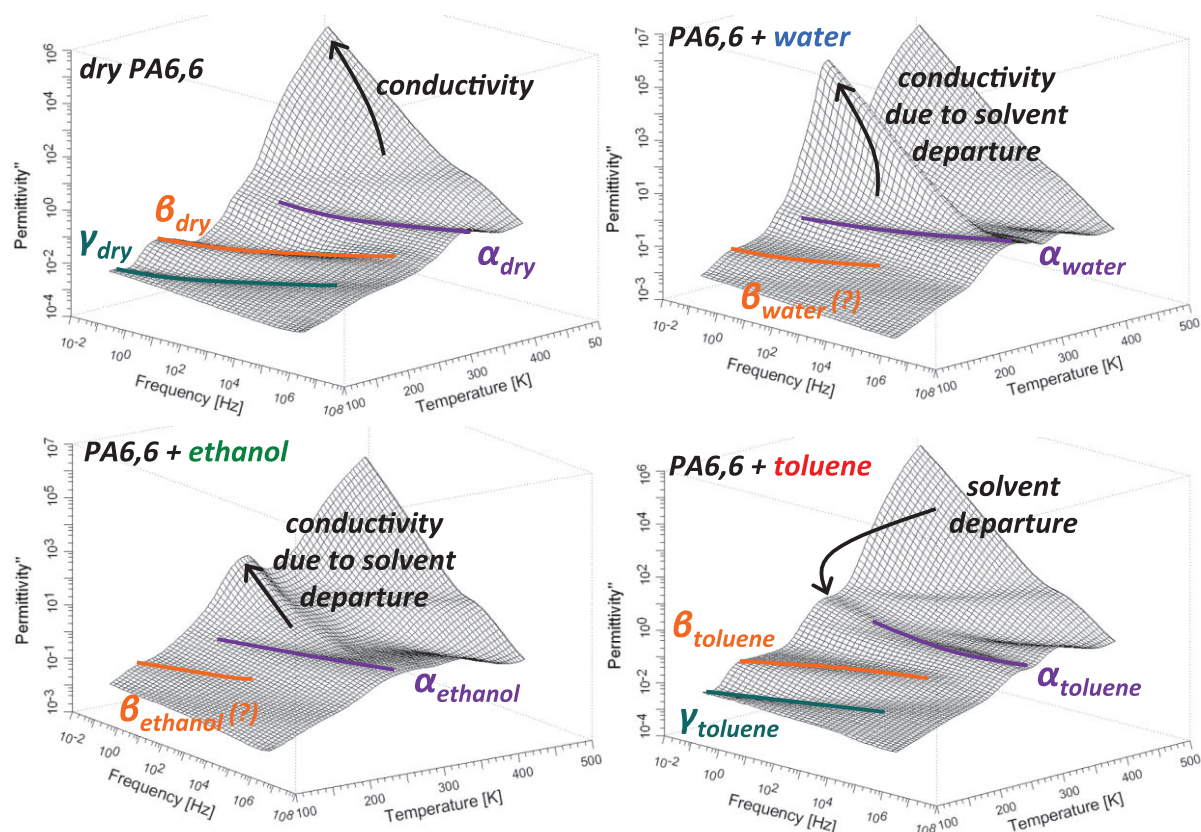


Figure 89: Loss permittivity – frequency – temperature 3D plots obtained by Dielectric Spectroscopy highlighting the observed molecular relaxations for dry and water-, ethanol-, and toluene-swollen PA6,6 samples.

Figure 90 shows then the α relaxation temperatures as a function of the frequency for dry and solvent-swollen PA6,6 samples obtained from the maxima of the dielectric modulus M'' as described in Chapter II.

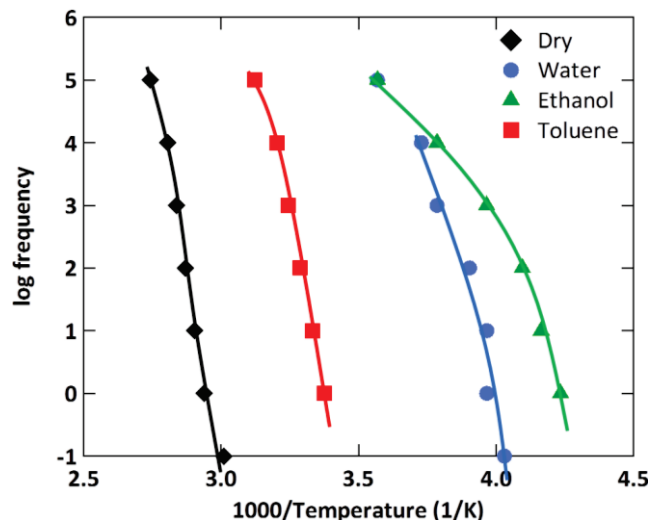


Figure 90: α relaxation temperatures as a function of the frequency for dry, water- ($\Delta n_{water}=0.97$), ethanol- ($\Delta n_{ethanol}=0.47$), and toluene- ($\Delta n_{toluene}=0.034$) swollen *NeatPA66* samples obtained from the maxima of the dielectric modulus M'' . Plain curves are guides for the eyes.

Figure 90 confirms on a wide frequency range the shift of the glass transition temperature in presence of the solvents already measured by DSC.

The loss permittivity of the samples was then fitted with a Havriliak-Negami fitting relationship, defined in Equation 74, so as to obtain the temperature, the intensity and the width of the α relaxation temperature as a function of the frequency.

$$\epsilon'' = \epsilon''_0 + \frac{\epsilon''_s}{(1 + (j\omega\tau)^m)^n} \quad 74$$

The values of the Havriliak – Negami exponents m and n were then obtained from fitting the α relaxation according to Equation 74. Figure 91 shows the α relaxation broadening as obtained from the Havriliak – Negami exponents m and n for the dry and solvent-swollen PA6,6 samples.

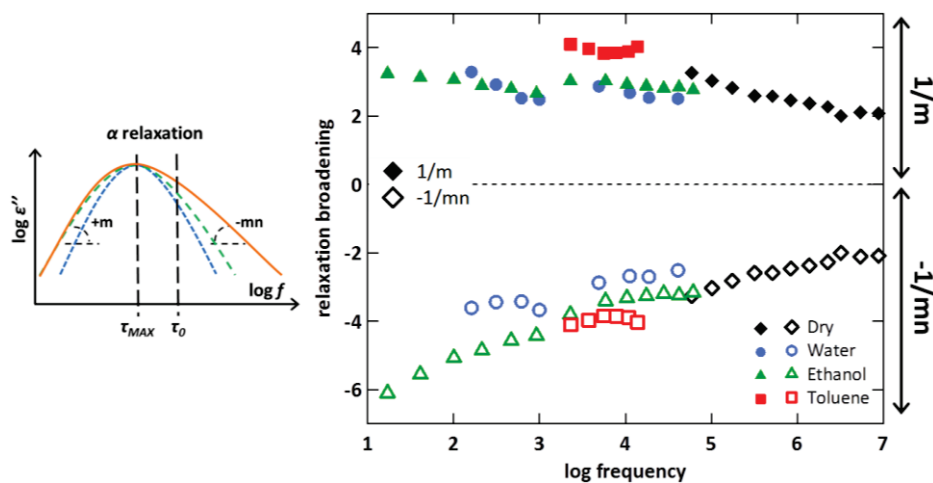


Figure 91: α relaxation width as a function of the frequency for dry, water- ($\Delta n_{water}=0.97$), ethanol- ($\Delta n_{ethanol}=0.47$), and toluene- ($\Delta n_{toluene}=0.034$) swollen *NeatPA66* samples.

III. Pure solvents in Neat PA6,6

Figure 91 shows that the presence of solvents does not seem to broaden the α relaxation of PA66. In other words the distribution of the relaxation times for the α molecular process appears to be not affected by PA66 solvents sorption. Moreover, thanks to the presence of solvents and the associated shift of the alpha process to lower frequencies, the Havriliak-Negami exponent values were determined on a wide frequency range. Figure 91 shows that the α relaxation is symmetric at high frequencies (dry and toluene-swollen PA66), but at low frequencies, the relaxation becomes asymmetric towards the long relaxation times (low frequencies). A hypothesis to explain the relaxation asymmetry could be that at high frequencies the applied dielectric field changes very fast, obliging the polymer chains to respond all together as a whole block with a given width of relaxation times. However at lower frequencies the change in the dielectric field is smoother and the polymer chains are able to respond individually with their own relaxation times because they can better follow the applied field. A widening or broadening of relaxation times can then be observed at low frequencies especially for relaxations that are not symmetrical, such as the main α relaxation.

Furthermore, the intensity $\Delta\epsilon = \frac{\epsilon_s - \epsilon_\infty}{5}$ of the α relaxation (Equation 74). The values of the intensity $\Delta\epsilon$ can also be obtained by fitting the experimental data with a Havriliak – Negami relationship as shown in Equation 74. Figure 92 shows the α relaxation intensity for dry and solvent-saturated NeatPA66.

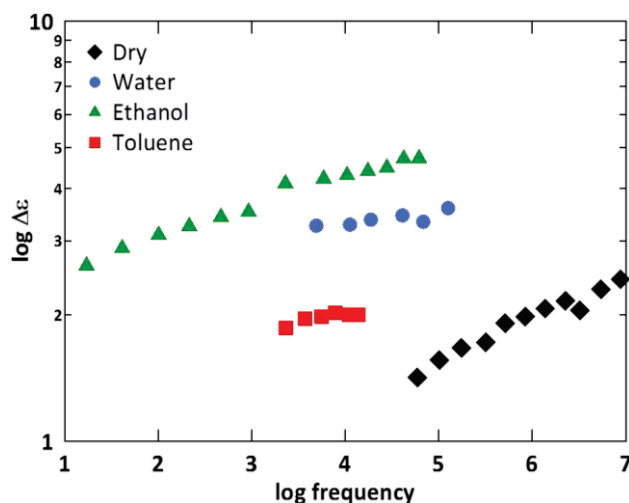


Figure 92: α relaxation intensities $\log \Delta\epsilon$ as a function of the frequency for dry, water- ($\Delta n_{water}=0.97$), ethanol- ($\Delta n_{ethanol}=0.47$), and toluene- ($\Delta n_{toluene}=0.034$) swollen NeatPA66 samples.

The α relaxation amplitude appears to increase when solvent is absorbed by PA66, especially in the case of water or ethanol-swollen samples. The amplitude of a relaxation is related to the concentration of dipoles within a material, although the quantitative value of the amplitude may not be simply proportional to the density of dipoles. Since water and ethanol possess dipoles within their structure (Table 12), the concentration of dipoles within the swollen polymer is expected to increase when compared to a dry sample, which could explain the raise in the amplitude of the α relaxation. For toluene the molecular dipole is much smaller (Table 12) and in fact it is comparable to that of PA6,6, thus the α relaxation amplitude should not change, as shown in Figure 92.

III.3.2. Effect of pure solvents on the secondary relaxations

We were then interested in studying the effect of solvent sorption on the β and γ secondary relaxations. As it was stated in Chapter I, the β relaxation corresponds to the rotation of the amide groups whereas the γ relaxation corresponds to the local motions of the methylene backbone of PA6,6. The effect of water on the secondary relaxations of PA6,6-based formulations, corresponding to the molecular motions of small segments of the polymer, was already studied at LPMA and the Materials Physics Center of the Basque Country University at San Sebastián by Marco Laurati et.al. [176]. He studied by BDS and by Neutron Scattering the dynamics of water in two PA6,6-based copolymers, PA6,6-6I 40/60_{mol} and PA6,6-6T 65/35_{mol}, whose chemical structures are shown in Figure 93.

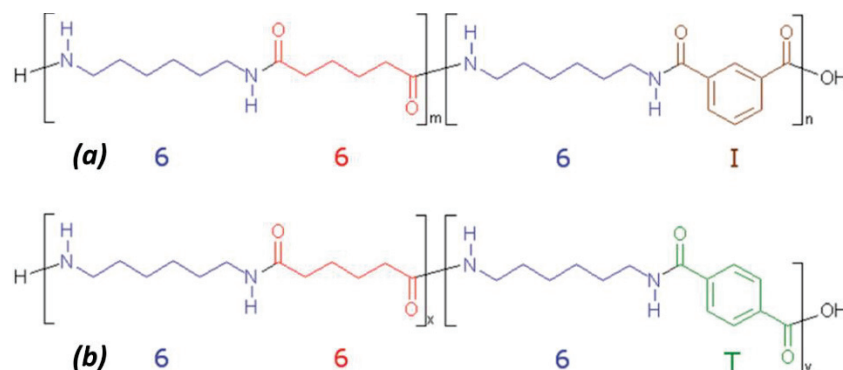


Figure 93: Chemical structure of the (a) PA6,6-6I and (b) PA6,6-6T copolymers studied by Laurati et.al. [176].

For the β relaxation we first recall in this section the results obtained by Laurati et.al. [176] on the copolymers in the presence of water. Concerning the Dielectric Spectroscopy, measurements were carried out in dry and water-swollen samples. Water had a molar intake in PA6,6-6I of $\Delta n_{water}=0.93$ whereas in PA6,6-6T it was $\Delta n_{water}=0.72$. It was observed that for the dry samples, the β and γ relaxations of these copolymers were well identified as shown in the graphs of loss permittivity ϵ'' as a function of frequency plotted in Figure 94a (PA6,6-6I) and Figure 94b (PA6,6-6T).

In the case of water-swollen samples a raise in the loss permittivity ϵ'' , attributed to the contribution of water to the conductivity of the polymer, is observed. Moreover three relaxation processes were identified as shown in Figure 94c (PA6,6-6I) and Figure 94c (PA6,6-6T). A relaxation process, named A, is observed in the temperature range of the γ relaxation for dry samples but its intensity is more pronounced, furthermore going towards lower frequencies two more relaxation processes B and C are observed. Process C is observed in the temperature range of the β relaxation for dry samples. Furthermore the width of the β , γ , A, B, and C relaxation processes were studied. A Cole-Cole relationship, given in Equation 75, was used to fit the β relaxation.

$$\epsilon^* = \epsilon_{\infty} + \frac{\epsilon_s - \epsilon_{\infty}}{1 + (i\omega\tau)^m} \tag{75}$$

III. Pure solvents in Neat PA6,6

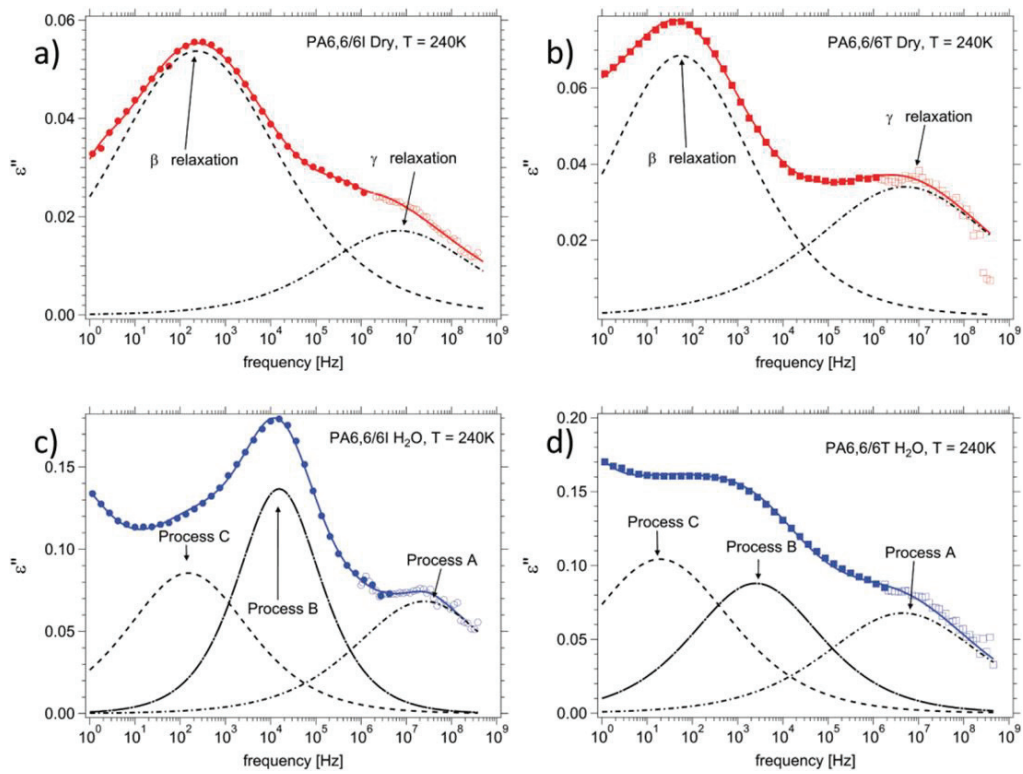


Figure 94: Loss permittivity ϵ'' as a function of frequency obtained at 240 K for dry (a) PA6,6-6I and (b) PA6,6-6T, and water-swollen (c) PA6,6-6I and (d) PA6,6-6T with the observed relaxation processes highlighted as observed in [176].

Figure 95 shows the amplitude $\Delta\epsilon$ of the relaxation processes for dry and water-swollen PA6,6-6I and PA6,6-6T samples.

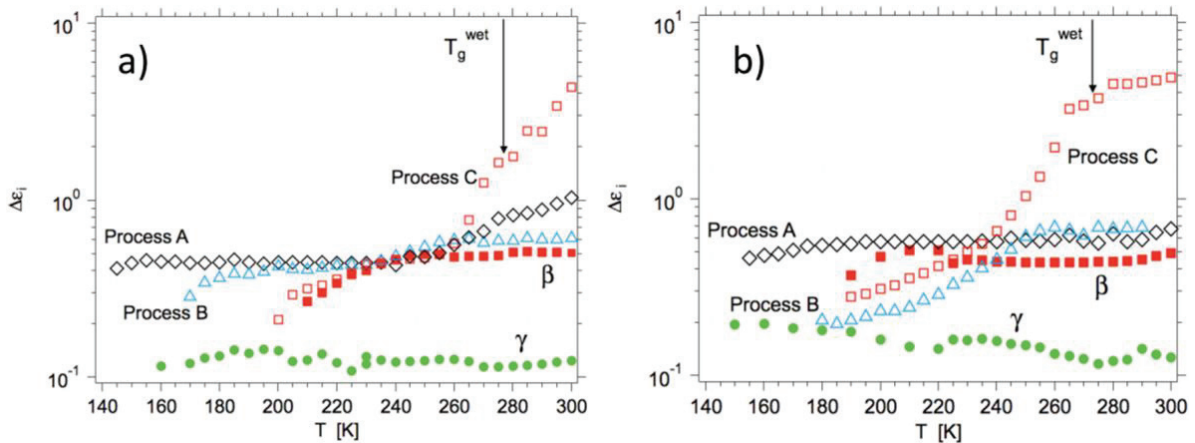


Figure 95: Amplitude $\Delta\epsilon$ of the observed relaxation processes for dry and water (a) PA6,6-6I and (b) PA6,6-6T samples as observed in [176].

It is observed in Figure 95 that the amplitudes of the β and γ relaxations of dry PA6,6-6I and PA6,6-6T samples do not depend on the temperature. Concerning water-swollen samples it is seen that the Process A does not depend on the temperature and has a larger amplitude than that of the γ relaxation, which would mean that this process rather corresponds to water motions and not to the γ relaxation itself, although this does not mean that the γ process is not present in water-swollen samples.

III. Pure solvents in Neat PA6,6

It is also seen for both copolymers that the amplitude of Process C is temperature-dependent and that it largely increases when reaching the samples' T_g 's. Concerning Process B, in the case of PA6,6-6I samples it is seen that its amplitude remains constant with temperature and that its value is close to that of the β relaxation. In the case of PA6,6-6T, the amplitude of Process B depends slightly on temperature and its value is lower than that of the β relaxation but when temperature increases, its value gets closer to that of the Process A.

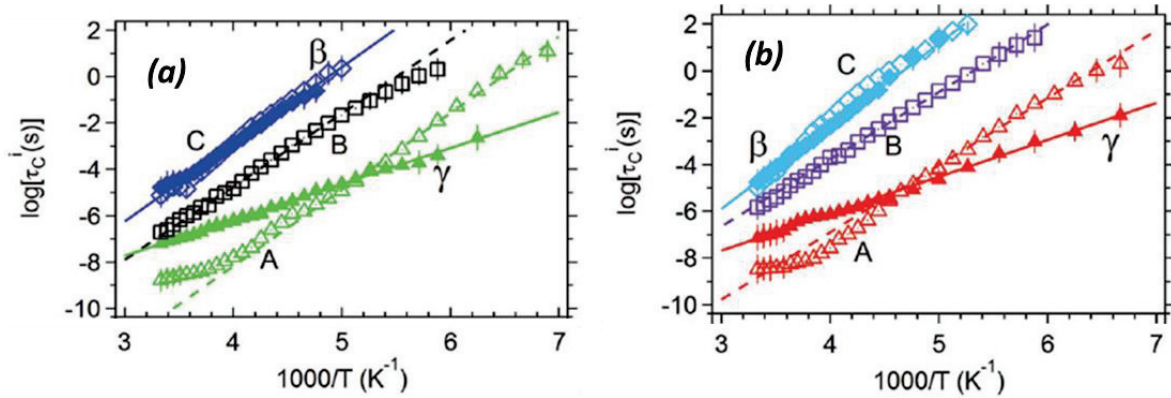


Figure 96: Arrhenius plots for the observed relaxation processes for dry and water (a) PA6,6-6I and (b) PA6,6-6T samples as observed in [176].

The observed relaxations were considered to be Arrhenius processes. Their activation energies were calculated according to Equation 76 from the plots shown in Figure 96 and their values are listed in Table 16.

$$\tau(T) = \tau_0 \exp\left(\frac{E}{RT}\right) = \frac{1}{2f_{\max}} \quad (76)$$

Table 16: Activation energies for the β and γ relaxations, and for the A, B, and C processes for dry and water-swollen PA6,6-6I and PA6,6-6T samples according to [176].

Process	Activation energy [kJ/mol]	
	PA6,6-6I	PA6,6-6T
β	64	65
γ	38	38
A	56	58
B	55	57
C	57	57

Laurati et.al. observed that the values of E_β and E_γ are in accordance to those found in the literature for polyamides [116,117]. In his work the values of E_A , E_B , and E_C , which correspond well to values found for confined water [177-179], as well as the Neutron scattering measurements not discussed herein lead him to conclude that process A corresponds to water loosely bound to amide groups. Process B would correspond to the motions of hydrated amide groups and Process C would correspond to the motion of amide groups not bonded to water.

III. Pure solvents in Neat PA6,6

In the case of ethanol, as in the case of water, there is an apparently very broad relaxation in the β region, which probably corresponds to several processes. These β processes were very difficult to fit quantitatively. Here, we only focus on the effect of toluene which was not considered by Laurati et.al. Figure 97 shows the frequency-temperature plot of the beta relaxation of dry or solvent-swollen PA66 samples, and the values of the β relaxation temperatures taken at 1Hz from the maxima of the loss moduli M'' spectra are tabulated in Table 17.

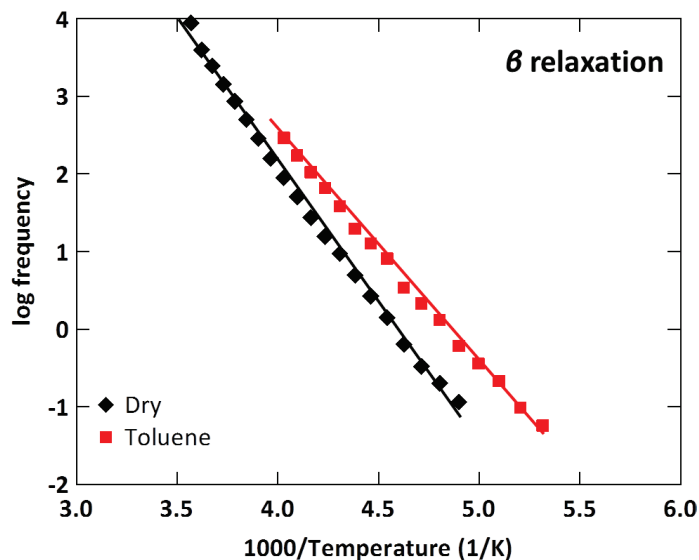


Figure 97: β relaxation temperatures as a function of the frequency for dry and toluene- ($\Delta n_{\text{toluene}}=0.034$) swollen *NeatPA66* samples.

Table 17: β relaxation temperatures (T_{β}) of dry and solvent-saturated *NeatPA66* samples obtained from the dielectric loss moduli M'' .

Solvent	T_{β} @1 Hz [°C] – BDS
Dry	-57
Toluene	-69

It is found that toluene provokes a drop on the β relaxation temperature. As it was mentioned in Chapter I, the β relaxation corresponds to the rotation of the amide functions and thus the shift of T_{β} in presence of toluene towards lower temperatures might suggest that this molecule modifies the molecular motions of the amide groups by disturbing them at a local scale. Moreover from Figure 97 the activation energies E_{β} of the relaxation process can be calculated from the Arrhenius relationship defined in Equation 76. Table 18 shows the obtained activation energies E_{β} for dry and solvent-swollen PA6,6 samples.

Table 18: Activation energies obtained for the β relaxation for dry, water-, ethanol-, and toluene-swollen *NeatPA66* samples.

Solvent	Activation energy E_{β} [kJ/mol]
Dry	70
Toluene	56

III. Pure solvents in Neat PA6,6

The values of the activation energies of the β relaxation process decrease in the presence of toluene. This suggests that toluene not only decreases the β relaxation temperature, but by disturbing the amide functions it is able to lower the energy needed for this relaxation process to occur. Furthermore the width of the β relaxation was studied. Figure 98 shows the broadening of the β relaxation times estimated by exponent m of the Cole-Cole relationship defined in Equation 75 for the dry and toluene-swollen PA6,6 samples.

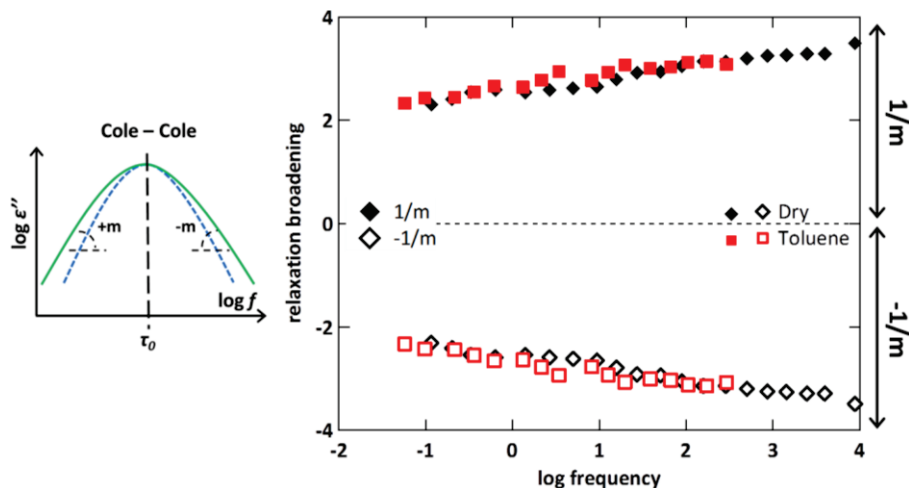


Figure 98: β relaxation width as a function of the frequency for dry, water- ($\Delta n_{water}=0.97$), ethanol- ($\Delta n_{ethanol}=0.47$), and toluene- ($\Delta n_{toluene}=0.034$) swollen NeatPA66 samples.

The width of the β relaxation process of toluene swollen sample appears to be similar to that of dry PA66. Figure 99 shows then the intensity of the β relaxation as a function of the frequency for dry or solvents swollen PA66 samples.

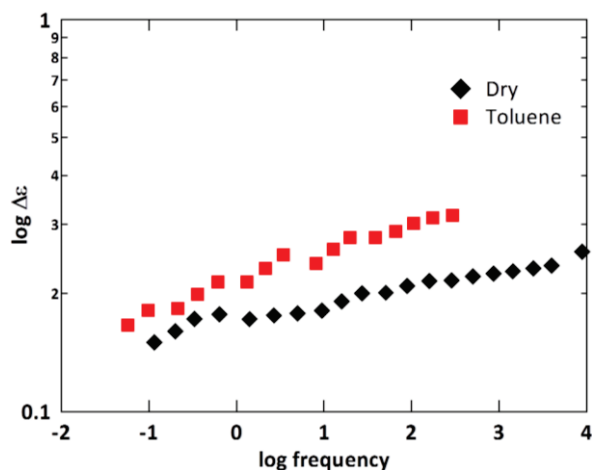


Figure 99: β relaxation intensities $\log \Delta \epsilon$ as a function of the frequency for dry and toluene- ($\Delta n_{toluene}=0.034$) swollen NeatPA66 samples.

Figure 99 shows that the intensity or amplitude of the β relaxation seems to be affected by the presence of toluene. It might be possible that since aromatic rings can be polarized, the presence of toluene in PA6,6 contributes to a raise in the relaxation amplitude. Finally we were interested in the effect of toluene on the γ relaxation, which corresponds to the motions of the methylene backbone of PA66. Table 19 shows the γ relaxation temperatures T_γ obtained by Dielectric Spectroscopy at 1Hz from the maxima of the loss moduli M'' spectra.

III. Pure solvents in Neat PA6,6

Table 19: γ relaxation temperatures (T_γ) of dry and solvent-saturated *NeatPA66* samples obtained from the dielectric loss moduli M'' .

Solvent	T_γ @1 Hz [°C] - BDS
Dry	-130
Toluene	-134

Figure 100 shows the temperature – frequency plot for the γ relaxation for dry and toluene-saturated PA66 samples. Toluene seems to slightly decrease the temperature of the gamma process but this difference in temperature might certainly come from the incertitude of the measurement and especially from the incertitude coming from the numerical fit of this relaxation.

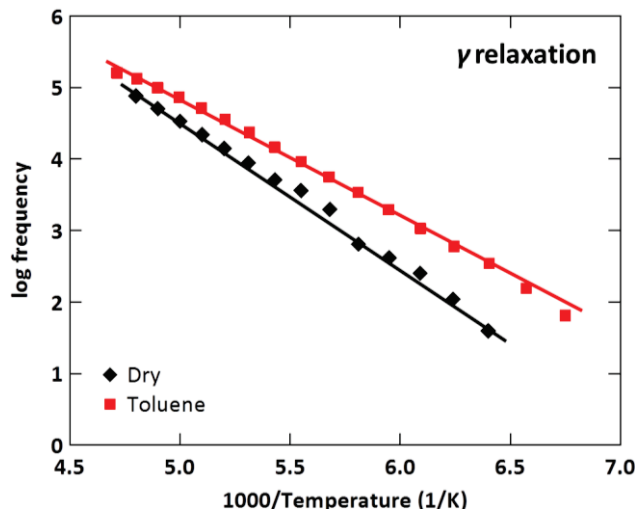


Figure 100: γ relaxation temperatures as a function of the frequency for dry and toluene- ($\Delta n_{toluene}=0.034$) swollen *NeatPA66* samples.

The width of the γ relaxation was also studied. Figure 101 shows the m exponent of the Cole-Cole relationship defined in Equation 75, obtained for dry and toluene-saturated *NeatPA66* samples.

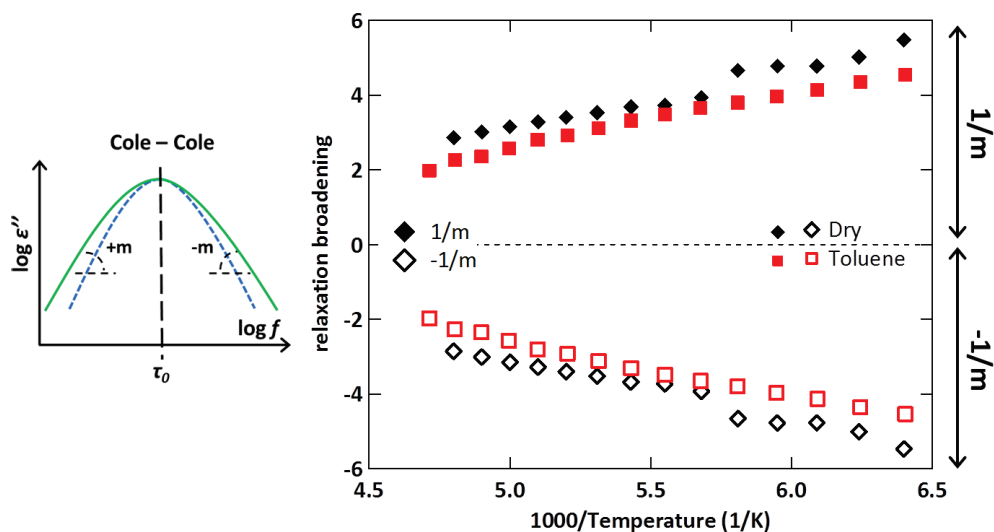


Figure 101: γ relaxation width as a function of the frequency for dry and toluene- ($\Delta n_{toluene}=0.034$) swollen *NeatPA66* samples.

It is observed in Figure 101 that toluene does not modify the width of the γ relaxation. Finally the intensity $\Delta\varepsilon$ of the γ relaxation was also studied, the obtained values being shown in Figure 102 for dry and toluene-swollen PA66 samples.

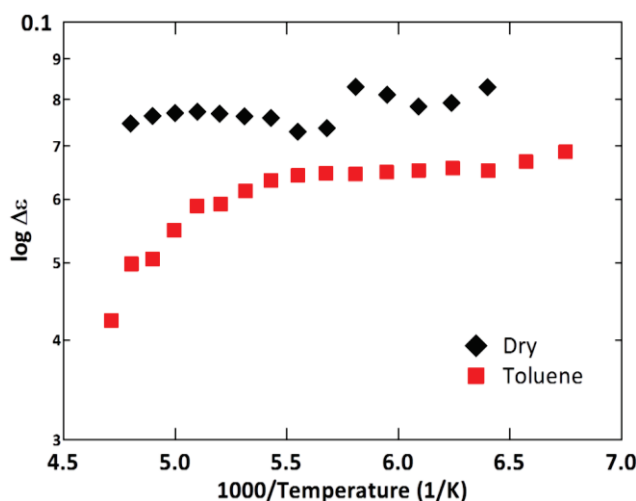


Figure 102: γ relaxation intensity $\log \Delta\varepsilon$ as a function of the frequency for dry and toluene-swollen ($\Delta n_{\text{toluene}}=0.034$) *NeatPA66* samples.

The intensity of the γ relaxation diminishes slightly in presence of toluene, but this slight difference may not be representative of a variation on the intensity of the relaxation provoked by the presence of toluene, but rather by the fact that this relaxation is weak and relatively difficult to fit. Although another hypothesis to explain the diminishing in the relaxation amplitude would be that toluene is a non-polar molecule that possesses a very weak or non-existent dipole, so it would be possible that when this molecule is absorbed by PA6,6, the overall concentration of strong dipoles slightly diminishes when compared to a dry polymer sample, decreasing the amplitude of the γ relaxation.

To summarize, the effect of a series of polar and non-polar solvents on the molecular mobility of PA6,6 has been studied. It was observed that water, the alcohol solvents, and toluene do have an effect on not only the glass transition temperature but also on the secondary relaxations of PA6,6. It was also found that none of the plasticization models found in the literature describes accurately the plasticization effect observed for these solvents. This might lead us to think that water, alcohols, and toluene might strongly interact with the polymer chains, specifically with the amide functions, and that these solvents are able to modify the dynamics of PA6,6 amorphous phase. Hypotheses on the plasticization mechanisms for each of the studied solvents are hereafter presented and discussed.

III.3.3. Discussion of plasticization mechanisms by solvents

From the results observed above on the effect of a series of solvents having different polarities and sizes, some hypotheses on how these solvents may plasticize PA6,6 are discussed herein. In this discussion, the plasticization phenomenon is defined as the change of glass transition temperature T_g induced by the presence of the solvent in the material, or equivalently by the change of the main relaxation time τ_α .

III.3.3.1. Case of toluene

Let us first discuss the case of toluene. As a non-polar solvent, toluene does not form H-bonds (i.e. strong bonds with large interaction energies) with the amide functions of PA66 chains, but it has some affinity with the non-polar methylene backbone of the polymer.

It is rather counter-intuitive that this solvent has the strongest plasticization effect relative to its volume or molar fraction in the material, since it is not supposed to interact with or disrupt the H-bond network of PA6,6. Here we propose to examine whether its plasticization effect can be related to its swelling effect described in section “III.2. Sorption of pure polar and non-polar solvents”. In this section we have discussed a model for the sorption in which toluene would swell the material (more precisely the amorphous phase of the material) homogeneously. As a consequence, H-bonds are stretched to some extent, which results in an effective elastic modulus. This modulus was estimated to be of order a few GPa, and it was shown that this order of magnitude is fairly coherent with the amount of solvent absorbed at equilibrium. This mechanism is schematically illustrated in Figure 103.

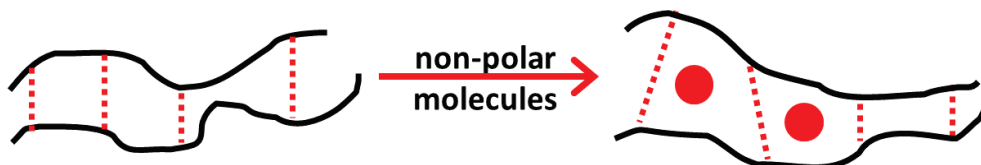


Figure 103: Schematic representation of the plasticization mechanism of a non-polar solvent in PA6,6.

Let us now examine the effect on the polymer dynamics. A first strong hypothesis is to consider that the principal (glassy) relaxation time is somehow related to the life-time of H-bonds. This hypothesis may be justified by the fact that polyethylene, and more generally non polar, aliphatic polymers, have a quite low glass transition temperature compared to PA6,6 (around -120°C for polyethylene), which could indicate that at the glass transition temperature of PA6,6, motions of the aliphatic parts of the chains are effectively very fast.

A consequence of the stretching of H-bonds is the reduction of their energy. Let us consider the potential modeling H-bonds as it has been schematized in Figure 104.

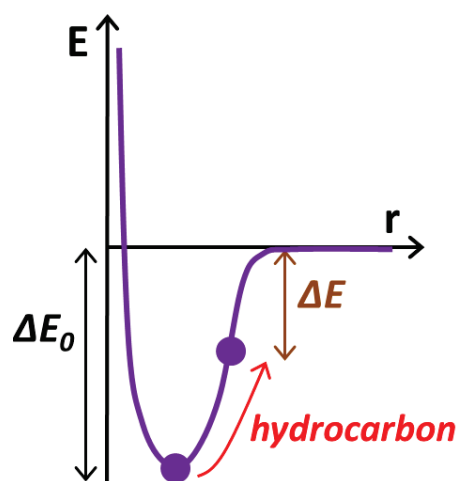


Figure 104: Schematic representation of a H-bond Lennard-Jones potential energy diagram in which the equilibrium is displaced by the spacer effect of toluene when absorbed by PA6,6.

Within this picture, the stretching of H-bond (increase of the distance from r_0 to $r_0 + \Delta r$) results in a decrease of the H-bond energy from E_0 to $E_0 - \Delta E$. By writing for the life-time:

$$\tau = \tau_0 \exp \left[\frac{E}{k_B T} \right] \quad 77$$

The decrease of the energy barrier will result in a decrease of the life-time of H-bonds. Or, equivalently, according to Equation 78, for a given value of the life-time (i.e. the value at T_g), the decrease of the energy barrier will induce a change in temperature given by:

$$\frac{\Delta T}{T} = \frac{\Delta E}{E} \quad 78$$

The relative change $\Delta E/E$ in H-bond energy associated to swelling was estimated to be less than 10^{-2} (see Equation 72). With $\Delta E/E \approx 10^{-2} \approx \Delta T/T$ this would result in a shift of T_g of the order 3 K. However, the shift of T_g experimentally observed at equilibrium swelling in toluene (2% in volume) is of order 40 K. Thus, the homogeneous swelling by toluene as it was described previously and the related change in H-bond energy is not sufficient to explain the comparatively very large (at least one order of magnitude larger) change of T_g which is observed experimentally.

It follows that plasticization mechanisms cannot be understood in a mean field (homogeneous) picture. A more detailed analysis of the effect of toluene on the dynamics of H-bonds at the molecular scale or at the scale of the PA6,6 monomer is needed. Indeed, the volume of a toluene molecule is about ($V_{toluene} = 0.15 \times 10^{-27} \text{ m}^3$). This is very close to the volume of one monomeric unit $-(CH_2)_5-CONH-$, containing one amide group ($V_H = 0.17 \times 10^{-27} \text{ m}^3$), which is, equivalently, the volume associated to one H-bond, that is $1/\rho$ with ρ the number of H-bonds per unit volume. This indicates that the penetration of a toluene molecule must strongly distort H-bonds in its surrounding, and may probably even break at least one H-bond in its surrounding.

On the other hand, breaking one H-bond per absorbed toluene molecule would cost 5×10^{-20} J per molecule. We have estimated previously that this cost (estimated from the amount of toluene absorbed at equilibrium) is of order 1.3×10^{-20} J. Thus, from this simple energetic balance, this would mean that about $1/4^{\text{th}}$ of absorbed toluene molecules would on average effectively break a H-bond.

As toluene is absorbed in very small amounts ($\Delta n=0.03$), its effect in PA6,6 must be very localized, nevertheless it is sufficiently strong to modify the molecular dynamics of the polymer chains and provoke a large T_g drop in PA6,6. In order to better understand the plasticization effect of toluene, a more developed model taking into account this suspected localized effect should be considered. However, at the moment, experimental results giving access to this detailed level are still lacking. Molecular dynamics simulation for example could perhaps give more detailed insight on the relaxation mechanisms at the molecular level, in the presence of various types of solvents (polar vs. non polar).

III. Pure solvents in Neat PA6,6

Note also the following important point. At the glass transition temperature, τ_α is by definition 100 s. Writing $\tau_\alpha = \tau_0 \exp[E/k_B T]$, with τ_0 of the order 10^{-13} s, then the effective energy barrier E to cross at T_g is of the order $30 k_B T$, that is 1.2×10^{-19} J. In comparison, the energy of one H-bond is of the order 4 to 5×10^{-20} J. Thus, one alpha relaxation motion close to T_g should correspond to the cooperative motion of about 2 to 3 H-bonds.

It was observed in the previous part in Figure 86b that there seemed to be two different plasticization trends provoked by the aromatic and the aliphatic non-polar solvents. It was observed that for a given molecular intake Δn , the aromatic solvents provoked a larger (ca. 10°C) T_g drop than the aliphatic molecules. This difference might come from the inherent molecular structure of these solvents, toluene and xylene isomers presenting aromaticity. This property of certain hydrocarbons is defined by the arrangement of the electronic orbitals in the space, and the presence of conjugated rings of unsaturated bonds allowing electron delocalization and resonance. The unsaturated bonds hinder the carbon-carbon bonds from rotating and thus influence the arrangement of the molecule in space. Because of their limited arrangement in space, aromatic solvents could be able to further stretch the PA6,6 H-bond network, in comparison with aliphatic solvents, which are totally saturated hydrocarbons and whose carbon-carbon bonds can rotate freely in space without conditioning the arrangement of these molecules in space.

III.3.3.2. Case of water

Concerning water, as it was mentioned in Chapter I, it is generally accepted in the literature that this solvent is able to plasticize polyamides by bonding itself to the amide groups and replacing the existing interchain H-bond network of these polymers. Water is able to bond to the amide groups of PA6,6 because creating this bond corresponds to a gain of energy in the system, i.e. the energy of an amide-amide bond is ca. 25 kJ/mol [173], whereas for a water-amide bond is ca. 30-35 kJ/mol as estimated by molecular modeling [180-182], and shown schematically in Figure 105.

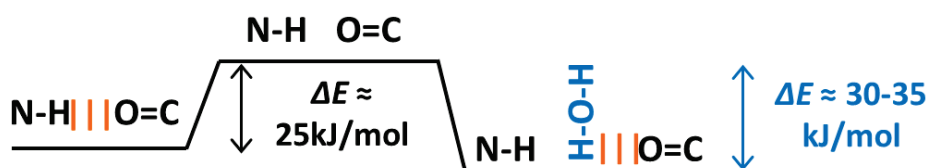


Figure 105: Schematic representation of water “breaking” an amine-carboxyl bond and bonding to a carboxyl group of PA6,6 representing a gain in the system energy.

Moreover it has been proposed that one molecule of water that is already bonded to an amide group can form another bond with yet another molecule of water or with another amide group [120-127], somehow forming bridges between polymer chains. It might be possible then that for high concentrations of water in PA6,6 (e.g. at molar fractions referred to amide groups close to one), polymer chains are “linked” together through water bridges as it is schematically shown in Figure 106.

The dynamics of the amide-amide and water-amide bonds have then to be taken into account to explain the plasticization effect of water. In particular, for comparable interaction energies, the lifetime of these ‘bridges’ may be reduced because they would be formed by several (typically two to three) water molecules. Another very important point is that amide-

III. Pure solvents in Neat PA6,6

water-amide bonds have more mobility than amide-amide, because intercalating water molecules introduce additional degrees of freedom in rotation.

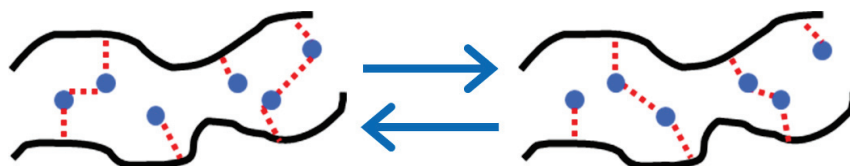


Figure 106: Schematic representation of the plasticization mechanism of water in PA6,6.

III.3.3.3. Case of ethanol

Finally concerning the alcohol series, being polar molecules, they might be able to directly interact with PA66 polymer chains by forming H-bonds between the hydroxyl functions of the alcohol molecules and the amide functions of PA66. The bonding between alcohols and the amide functions of PA6,6 is possible because this bond is stronger, ca. 30 kJ/mol for ethanol, than an amide-amide bond. This energy slightly drops when alkyl functions are added to the alcohol structure [183]. Since the studied alcohols have one hydroxyl function (except for ethylene glycol that possesses two hydroxyl functions), one might think that by forming an H-bond with an amide function they would effectively disrupt the bonding between two amide functions leading to a T_g drop of the polymer. A schematic representation of this hypothesis is shown in Figure 107.

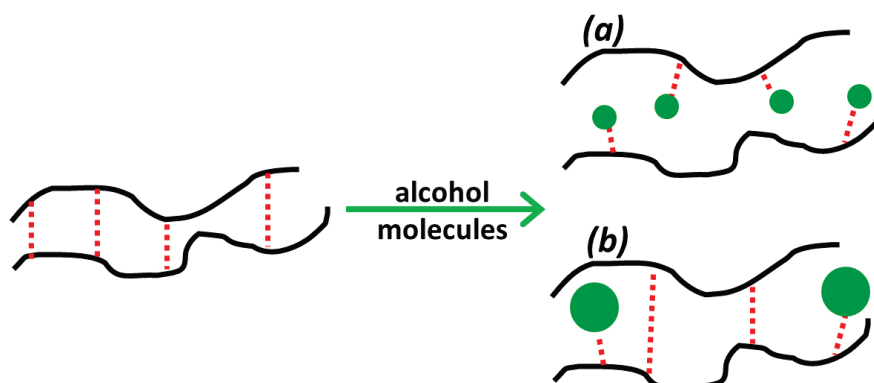


Figure 107: Schematic representation of the plasticization mechanism of (a) a small and (b) a large alcohol molecule in PA6,6.

Moreover the alkyl functions of these solvents might also have a local effect on H-bonds, as it was mentioned for toluene, thus increasing further the mobility and resulting in a subsequent T_g drop. It would be possible then that the alcohol molecules have a “double” effect by both directly interacting with the H bond network and also provoking a spacing of PA6,6 chains through steric effects as schematically represented in Figure 108.

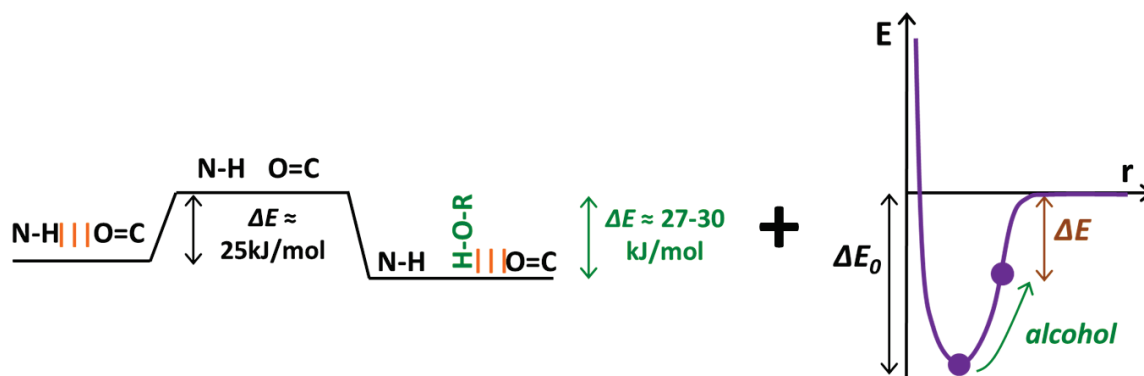


Figure 108: Schematic representation of a suspected “double effect” where ethanol “breaks” an amine-carboxyl bond and bonds to a carboxyl group and also is able to displace the energy equilibrium state of H bonds through steric effects.

The formulated hypotheses give us an idea on how the solvents might be able to plasticize the polymer. The important point is that for a solvent to induce a T_g drop in PA66, it does not have necessarily to be polar, i.e. to be able to directly interact with the interchain H-bond network of the polymer. Both polar and non-polar solvents studied herein are able to affect the lifetime of the H-bonds, either by substituting the original H-bond network or by stretching/disrupting them because of their size. To get deeper in the details on the plasticization mechanisms of these series of solvents, a physical modeling of PA66-solvent systems has to be carried on. However, at the moment, experimental results giving access to this detailed level are still lacking. Molecular dynamics simulation for example could perhaps give more detailed insight on the relaxation mechanisms at the molecular level, in the presence of various types of solvents (polar vs. non polar).

III.3.4. Relationship between solvent sorption and mesoscale simulations

III.3.4.1. Solvent sorption kinetics in PA6,6

The diffusion kinetics of water, ethanol, and toluene in PA6,6 were then studied. The sorption kinetics of these solvents might give an eyesight on the polymer-solvent interactions and their effect on the molecular mobility of PA6,6 during solvent sorption. The sorption of these solvents were carried out at 23°C as explained in Chapter II, *NeatPA6,6* 100 μm -thick film samples were put in contact with these solvents and were regularly weighed until the sorption equilibriums were reached. Figure 109 shows then the sorption kinetics for water, ethanol.

III. Pure solvents in Neat PA6,6

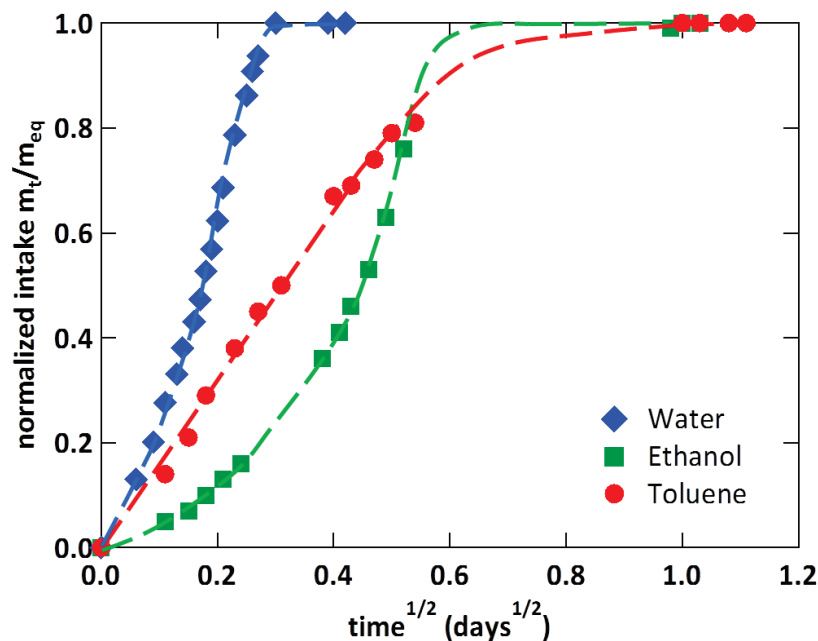


Figure 109: Sorption kinetics in *NeatPA66* (thickness 100 μm) obtained at 23°C for water, ethanol and toluene. Dashed curves are guides for the eyes.

Figure 109 shows clearly different dependences of the solvent intake with the square root of time. In the case of toluene, its intake depends linearly with the square root of time whereas for water and ethanol a change in slope is observed. As it was mentioned in Chapter I, during solvent sorption the diffusion will be governed by the interactions between the polymer and the solvent, the molecular mobility state of the polymer, and the size of the diffusing solvent. Two main sorption kinetic diffusions describing the intake of a solvent in a polymer are found in the literature: the Fickian and the Case II diffusions.

The Fickian diffusion corresponds to the case when the solvent sorption varies linearly with the square root of time, with the diffusion coefficient D being constant and not depending on the concentration of solvent throughout the whole solvent diffusion. Concerning Case II diffusion, the glass transition temperature T_g of the polymer diminishes during diffusion because of a plasticizing effect of the solvent. The diffusion is then accelerated and a change in sorption regime is observed during time.

The amount of water, ethanol, and toluene needed to provoke a T_g drop down to 23°C, the testing temperature, can be roughly estimated from the drop of T_g as a function of the molar sorption obtained for these solvents and shown in Figure 88. Table 20 shows then the estimated values of molar Δn and normalized mass m_t/m_{eq} sorption needed for water, ethanol and toluene to diminish PA6,6 T_g to 23°C.

Table 20: Necessary molar Δn and normalized mass m_t/m_{eq} intake for provoking a drop of PA6,6 T_g to 23°C for water, ethanol, and toluene.

Solvent	Δn for obtaining $T_g = 23^\circ\text{C}$	m_t/m_{eq} for obtaining $T_g = 23^\circ\text{C}$
Water	0.25	0.26
Ethanol	0.12	0.25
Toluene	0.034	1

III. Pure solvents in Neat PA6,6

From the values listed in Table 20 it is observed that toluene might not be able to plasticize the polymer during the sorption since the amount needed to bring down PA6,6 T_g corresponds the amount of absorbed solvent at equilibrium. Water and ethanol might be able to plasticize PA6,6 while diffusing according to the values listed in Table 20. These values correspond roughly to the values for which a change in sorption regime is observed for these solvents in Figure 109. In order to better understand the sorption of solvents and their effect on the molecular mobility of PA6,6, an analogy with mesoscale simulations of solvent diffusion is discussed hereafter.

III.3.4.2. Modeling of solvent diffusion

Theoretical simulations on the sorption of a solvent in a glassy polymer were done in our laboratory by Eric Lange [184]. The approach that was considered was a mesoscopic scale approach in which a non-linear diffusion equation as well as a set of thermodynamic driving forces are considered.

The thermodynamic model used to describe the sorption of a solvent in a polymer was that of Long and Lequeux [185] which is a further development of the Flory-Huggins model with an additional term representing the entropy of the void. From this model the chemical potential of the solvent μ_s was defined and considered as the driving force for the solvent sorption. Equation 79 is then the diffusion relationship that was to be solved by the simulations.

$$\partial_t \phi_s = -\text{div} \vec{j}_s = \text{div} \left[\phi_s \lambda \vec{\text{grad}}(\mu_s) \right] \quad 79$$

where ϕ_s is the fraction of solvent in the polymer-solvent system, j_s is the solvent flux and λ could be regarded as the diffusion coefficient. In the case that a polymer-solvent system in which the solvent diffuses with a non-constant diffusion coefficient is considered, λ was defined as a non-linear exponential function as shown in Equation 80.

$$\lambda = \lambda_0 \exp \left(\frac{\phi_p^0 - \phi_p}{\kappa} \right) \quad 80$$

where ϕ_p^0 is the fraction of polymer at the very beginning of the solvent diffusion, ϕ_p is the fraction of polymer at the end of the solvent diffusion, and κ would be the representation of RT product, that is the ideal gas constant R times the temperature T .

Moreover the swelling or the variation of volume $\partial N_n / \partial t$ of the system when the solvent diffuses in the polymer was defined as shown in Equation 81.

$$\frac{\partial N_n}{\partial t} = \alpha \pi \quad 81$$

where π is the osmotic pressure of the polymer-solvent system and α is the so-called swelling coefficient which is defined as shown in Equation 82.

$$\alpha = \alpha_0 \exp\left(\frac{\phi_p^0 - \phi_p}{\kappa}\right)$$

By modifying the φ_p , ϕ_p , λ , and α parameters in the simulation calculations, one can model the different sorption diffusion regimes that can be observed experimentally and thus one can discuss on the effect of these physical parameters in the diffusion of a solvent in a glassy polymer so as to better understand this phenomenon.

After the thermodynamic equations for a solvent diffusion have been established, simulations of the diffusion of solvents where the sorption equilibria are reached at the end of the calculations were carried on. The system considered for the simulations was a polymer in contact on both sides with a solvent tank having a higher solvent concentration than that of the polymer.

The evolution of three parameters will be mainly discussed herein: φ_s , π , and $\Sigma(t)$. φ_s is the fraction of the solvent in the polymer, π is the osmotic pressure of the polymer-solvent system, and $\Sigma(t)$ is the equivalent of the normalized mass intake m_t/m_{eq} defined for the experimental sorption tests.

Firstly, the simulation of the diffusion of a solvent in a very rigid polymer is carried out. The results of these calculations are shown in Figure 110.

By considering a very rigid polymer, the swelling provoked by the presence of a solvent is very small if not non-existent as shown in Figure 110b. The obtained solvent uptake will then be very limited as it is shown in the logarithmic scale of Figure 110a. Since the solvent is not able to swell or plasticize the polymer, it will diffuse following a Fickian regime as it is observed in Figure 110c.

The conditions set for this system describe the limited diffusion of a solvent in a crosslinked polymer. One can deduce that this system is able to describe the diffusion of toluene in PA66. Indeed, PA66 could be considered as a highly crosslinked polymer because of the presence of the H-bond network in this polymer. Toluene, being a bulky solvent, is not able to be absorbed in large quantities, which would prevent this solvent from plasticizing PA6,6 while diffusing. Toluene follows then a Fickian diffusion regime as observed in Figure 109. A diffusion coefficient can be then calculated, with a value of $D \approx 2 \times 10^{-13} \text{ m}^2/\text{s}$ for the sorption of toluene at 23°C.

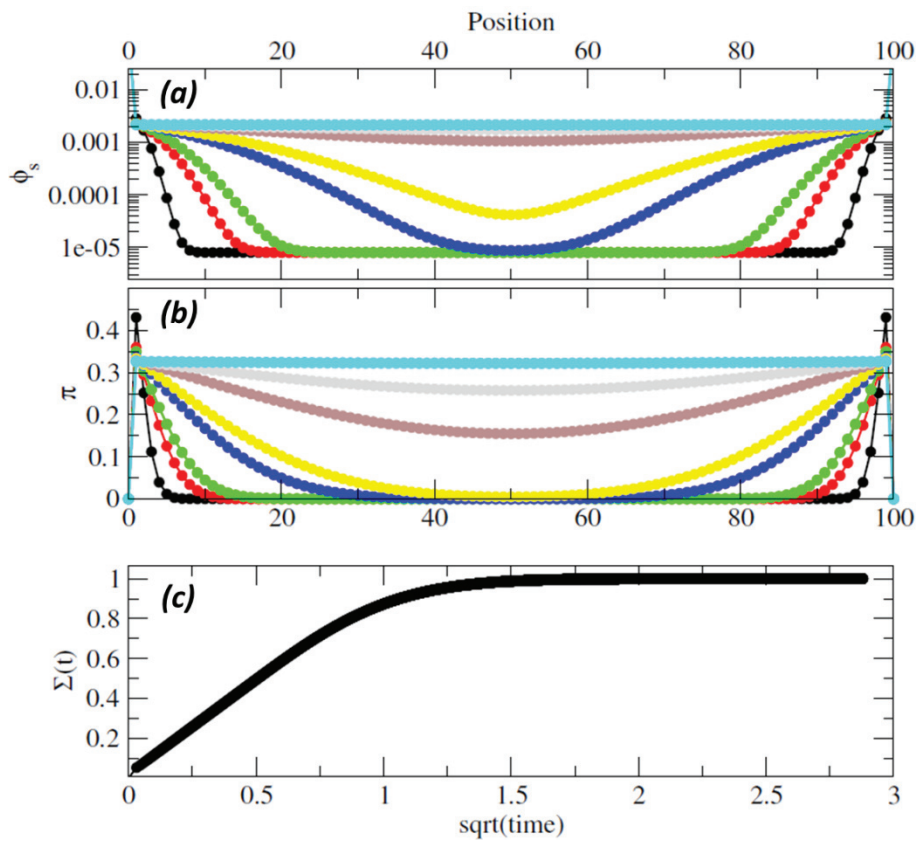


Figure 110: Simulation of a solvent diffusion (a – concentration of solvent in the polymer) where the polymer is not allowed to swell (b – the osmotic pressure π limits the solvent absorption). A pure Fickian diffusion regime is then obtained (c).

Furthermore, the simulation of a polymer-solvent system in which the solvent is absorbed with a constant diffusion coefficient λ and that it is allowed to swell the polymer according to a swelling coefficient α was carried out. The gradient of solvent fraction φ_s in the polymer is then shown in Figure 111.

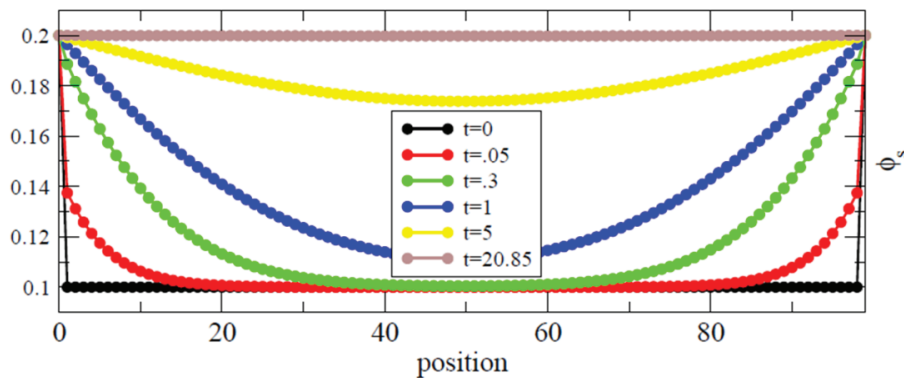


Figure 111: Simulation of a solvent sorption where the polymer swelling is allowed and the solvent is absorbed with a constant diffusion coefficient.

It is observed in that if a solvent is absorbed with a constant diffusion coefficient, even if this solvent is able to swell or plasticize the polymer, the gradient of solvent concentration evolves following a nearly Fickian diffusion regime. This system might be considered to be close to the water – PA66 system that was studied experimentally above. It might be possible that water is able to swell PA66 very quickly, leading to the diffusion of this solvent in a plasticized polymer following a pseudo-Fickian diffusion regime.

Finally, the simulation of a polymer-solvent system in which the solvent is absorbed with a non-constant diffusion coefficient (herein an exponential variation as defined in the paragraph above) and that it is allowed to swell the polymer was done. The gradient of solvent fraction ϕ_s in the polymer is then shown in Figure 112.

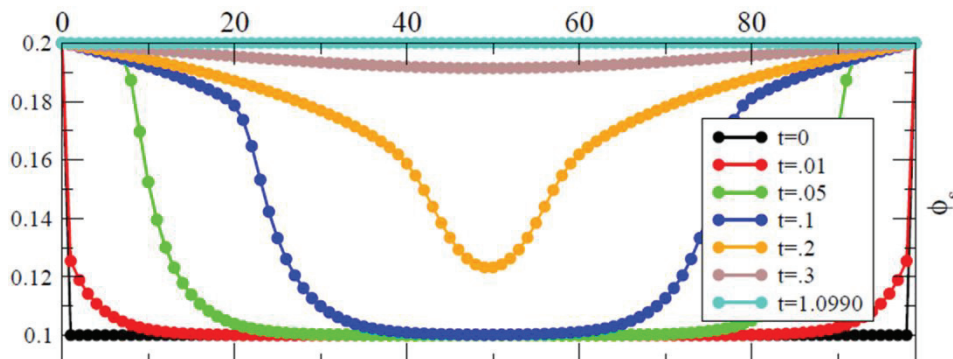


Figure 112: Simulation of a solvent sorption where the swelling is allowed and the solvent is absorbed with a non-linear diffusion coefficient.

It is observed in Figure 112 that at the beginning of the solvent diffusion, the gradient of concentration of the solvent is similar to that observed for a constant diffusion coefficient solvent absorption shown in Figure 111, which would correspond to a Fickian regime. As the solvent diffusion continues, the shape of the gradient of concentration changes and the appearance of a solvent front or wave is observed. This is because the swelling has an influence in the diffusion coefficient. Then, as the solvent sorption continues, the swelling of the polymer accelerates, the solvent diffusion coefficient increases, and the solvent intake becomes faster. This condition corresponds to a Case II diffusion and it may be similar to that observed for ethanol experimentally, for which the diffusion regime changes during solvent sorption. A diffusion coefficient can be calculated for ethanol in the Fickian regime, which is $D \approx 2 \times 10^{-14} \text{ m}^2/\text{s}$ which is lower than that obtained for toluene, maybe because ethanol forms H-bonds, which have a given lifetime and might limit or slow down ethanol diffusion when compared to toluene, which does not interact directly with the amide functions.

Moreover these simulations also allow predicting the shape of the sorption diffusion kinetics for solvents able to swell (i.e. plasticize) the polymer. As it was mentioned above the λ coefficient describes the speed of diffusion of a solvent whereas the α coefficient describes the speed with which the solvent is able to swell the polymer, with the simulations being characterized by these coefficients. Various shapes of solvent sorption kinetics can be obtained by modifying or modulating the values of λ and α coefficients and specifically the ratio λ/α as shown in Figure 113.

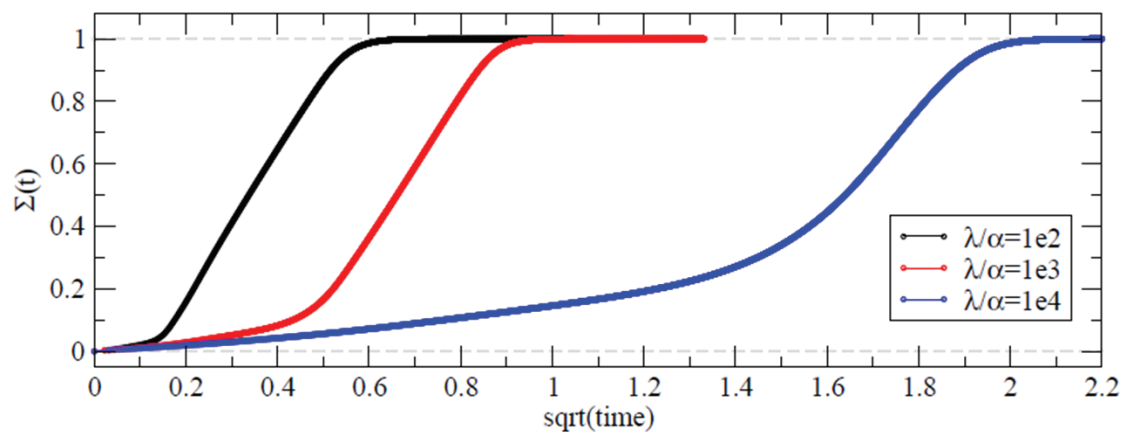


Figure 113: Sorption kinetics for a polymer-solvent system in which the parameters λ and α vary.

It is observed in Figure 113 that if the λ/α is large (i.e. α much smaller than λ) the swelling of the polymer occurs in a longer period of time and thus it provokes a very marked Case II diffusion with a large Fickian regime at the beginning of the sorption followed by a change in sorption regime when the solvent starts swelling the polymer. When the ratio λ/α decreases (i.e. α becomes of the same time scale of λ) the swelling of the polymer is faster, leading to a short Fickian regime and a quick change in solvent sorption regime.

The mesoscale simulations developed by Eric Lange in our laboratory allow to describe accurately, in a qualitative way, the diffusion of toluene (Fickian diffusion with no swelling), water (Case II diffusion with instant swelling) and ethanol (Case II diffusion with delayed swelling) in PA6,6.

III.4. Effect of pure solvents on the crystalline phase of neat PA6,6

The effect of solvent sorption on the crystalline phase of PA6,6 was also investigated. It is important to remind that the so-called kinetic crystalline phase α_{II} of PA6,6 generally evolves toward the presumably more thermodynamically stable form α_I [8], the kinetics of this transition depending on temperature and humidity of the environment.

The influence of water and ethanol on the crystalline structure of *NeatPA66* samples was investigated. Dry, water, and ethanol saturated *NeatPA66* films were analyzed by wide angle X-Ray diffraction (WAXS) experiments following the protocol mentioned in Chapter II: water and ethanol swollen samples were let to desorb before testing, whereas the dry sample was analyzed immediately after drying. Figure 114 shows the WAXS diffraction spectra for dry or solvent-saturated *NeatPA66* samples and Table 21 shows the values of the angular gap ($\Delta 2\theta$) between the (100) and the (010) crystallographic planes of PA6,6 obtained from Figure 114.

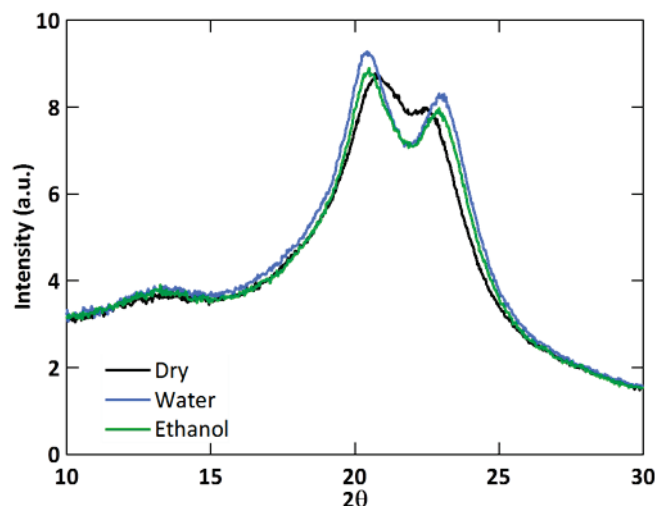


Figure 114: X-Ray Diffraction spectra of *NeatPA66* films at the dry state and after water or ethanol sorption.

Table 21: Scattering angular distance $\Delta 2\theta$ values between the (100) and the (010) crystallographic planes of PA6,6 at the dry state and after water or ethanol sorption.

Conditioning state	$\Delta 2\theta$ [°]
Dry	1.72
Water	2.56
Ethanol	2.42

Figure 114 and Table 21 show that the sorption of water or ethanol slightly modifies the crystalline structure of PA6,6. The scattering angular distance $\Delta 2\theta$ associated to the perfection degree of the PA6,6 α crystalline phase is smaller in the case of the dry sample than that in the case of samples swollen by water or ethanol.

As it was observed earlier, these solvents raise the molecular mobility of the chains in the amorphous phase, which would allow a rearrangement of the chains in the crystalline phase, suggesting that these solvents provoke an evolution of PA6,6 crystalline phase towards a perfect thermodynamically stable α_i form. These results would suggest that if a solvent has an effect on the molecular mobility of PA6,6 amorphous phase, it would also have an effect on the evolution from the α_{ii} crystalline phase towards the α_i form.

It would be of great interest to study the case of a dry sample heated up at a temperature that yields a molecular mobility state similar to that induced by the sorption of the studied solvents, in order to compare the crystalline phases in dry or swollen samples at a given T_g difference. It would be interesting then to acknowledge if this raise in temperature would have the same effect on the evolution of PA6,6 crystalline structure as that provoked by the presence of solvents, which would mean that the effect provoked on the molecular mobility of the polymer by introducing solvents in its structure would be the same as just increasing the temperature of a dry sample. Preliminary observations suggest that the effect of temperature in the dry state on polyamide crystallinity is not equivalent to the T_g drop provoked by the sorption of a solvent. However, this question needs further investigation.

III.5. Ternary solvent mixtures

III.5.1. Thermodynamics of ternary mixtures

After studying the sorption and plasticization effect of pure solvents in PA6,6, it was desired to study the sorption of a set of ternary mixtures and their effect on the molecular mobility of this same polymer. As mentioned in Chapter II, these ternary mixtures are composed of ethanol, toluene, and isooctane at different concentrations and are called herein “EX” mixtures, X standing for the volumetric concentration of ethanol in the mixtures. These EX mixtures were conceived to model the commercially available biofuels found in gas stations throughout the world. The study of the sorption of the EX mixtures is relevant for the applicative context of this work, since PA6,6-based automotive gasoline tanks will be in contact with biofuels containing ethanol. It is important then to understand the sorption of the EX mixtures and their effect on the molecular mobility of PA6,6.

A thermodynamic approach was considered to study the sorption of the EX mixtures in PA6,6. The situation considered in our experiments is schematized in Figure 115. It corresponds to a closed system with no mass exchange with the environment, at a given temperature $T = 25^\circ\text{C}$ and total pressure $P = 1 \text{ atm}$. The polymer material is put in a liquid phase formed by a mixture of ethanol, toluene and isooctane. The vapor phase is composed of ethanol, toluene, isooctane and dry air.

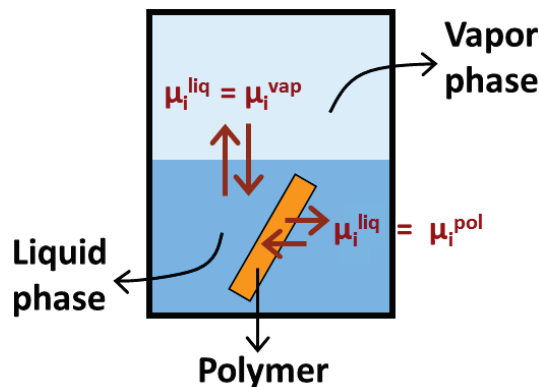


Figure 115: Schematic representation of the system considered in our experiments, with thermodynamic equilibrium between the liquid phase, the vapor phase and a swollen polymer.

Over time, equilibrium between the liquid and the vapor phases will be established. This equilibrium will depend on the temperature and the pressure of the environment, and it will be reached when the free enthalpy G of the system equals zero, that is, when the physicochemical matter exchanges between the different phases have been completed as shown in Equation 83 [34,35]:

$$dG(P, T, n_{liq}, n_{vap}) = \frac{\partial G}{\partial P} dP + \frac{\partial G}{\partial T} dT + \frac{\partial G}{\partial n_{liq}} dn_{liq} + \frac{\partial G}{\partial n_{vap}} dn_{vap} = 0 \quad 83$$

where P is the pressure, T the temperature, and finally n_{liq} and n_{vap} the molar concentrations of the solvent in the liquid and the vapor phases respectively. Moreover $n = n_{liq} + n_{vap}$. Since the pressure and the temperature remain constant and $dn_{liq} = -dn_{vap}$ we obtain:

$$dG = \frac{\partial G}{\partial n_{liq}} dn_{liq} - \frac{\partial G}{\partial n_{vap}} dn_{liq} = 0 \Rightarrow \frac{\partial G}{\partial n_{liq}} dn_{liq} = \frac{\partial G}{\partial n_{vap}} dn_{liq} \Rightarrow \frac{\partial G}{\partial n_{liq}} = \frac{\partial G}{\partial n_{vap}} \Rightarrow \mu^{liq} = \mu^{vap} \quad 84$$

where μ^{liq} and μ^{vap} are the chemical potentials of the solvent in the liquid and the vapor phases respectively and that can be regarded as the partial molar free enthalpy of each of the existing phases. At equilibrium, the chemical potential of each solvent must be uniform through the whole system [34], that is:

$$\mu_i^{liq} = \mu_i^{vap} = \mu_i^{polymer} \quad 85$$

where μ_i^{liq} , μ_i^{vap} , and $\mu_i^{polymer}$ are the chemical potentials of constituent i in the liquid phase, the vapor phase, and in the swollen polymer respectively. Note that this thermodynamic equilibrium depends on temperature and total pressure. Thus, sorption of solvent i in the polymer material is driven by the chemical potential μ_i of this solvent in the environment of the polymer sample, or equivalently by its thermodynamic activity a_i defined as:

$$\mu_i = \mu_i^0 + RT \ln a_i \quad 86$$

where μ_i^0 is the chemical potential in the reference state, defined here as the pure solvent in the liquid state at $T = 25^\circ\text{C}$, and total pressure $P = 1 \text{ atm}$.

Since the liquid EX ternary mixtures (and more generally ethanol/hydrocarbon mixtures) are non-ideal [99,100,103], the thermodynamic activities of the components are not equal to the molar fractions in the liquid phase. They must be determined in the vapor phase and are given by:

$$a_i = \frac{p_i}{p_i^{sat}} \quad 87$$

where p_i is the partial vapor pressure of species i and p_i^{sat} the vapor pressure of species i in the reference state, i.e. the saturating vapor pressure above the pure species i in the liquid state at $T = 25^\circ\text{C}$ and $P = 1 \text{ atm}$. Indeed, it may be safely assumed that the vapor phase behaves as an ideal gas mixture. The partial pressures p_i of each species can be calculated from Equation 85 from the concentrations in the vapor phase c_i measured by GC-FID as described in Chapter II.

Each EX mixture was firstly analyzed by GC-FID following the experimental setup shown in Figure 66, Chapter II. The molar fractions x_i in the liquid phase of each of the solvents forming the EX mixtures were calculated from $x_i = n_i / \sum_j n_j$, where $n_i = \rho_i v_i / M_i$ is the molar concentration in the liquid phase, with ρ_i the density, v_i the volume fraction and M_i the molar mass of solvent i . Likewise, the molar fractions y_i in the vapor phase for each solvent were calculated from $y_i = c_i / \sum_j c_j$ where c_i is the molar concentration in the vapor phase of solvent i measured by GC.

III. Pure solvents in Neat PA6,6

The molar fractions in the liquid x_i and in the vapor y_i phases respectively of the three solvents are shown in Table 22.

Table 22: Molar fractions in the liquid (x_i) and vapor (y_i) phases of solvent i measured by GC-FID analyses. All measurements fall within a standard deviation of ± 0.01 of the indicated value.

Mixture	$x_{ethanol}$	$y_{ethanol}$	$x_{toluene}$	$y_{toluene}$	$x_{isooctane}$	$y_{isooctane}$
E0	0.000	0.000	0.610	0.490	0.390	0.510
E2.5	0.054	0.605	0.577	0.195	0.369	0.202
E5	0.105	0.668	0.546	0.160	0.350	0.173
E7.5	0.152	0.694	0.517	0.162	0.331	0.144
E10	0.198	0.702	0.489	0.142	0.313	0.156
E22	0.385	0.736	0.375	0.120	0.240	0.145
E40	0.597	0.760	0.246	0.104	0.157	0.138
E50	0.689	0.781	0.189	0.092	0.121	0.127
E60	0.769	0.805	0.141	0.082	0.090	0.117
E65	0.805	0.816	0.119	0.074	0.076	0.109
E70	0.838	0.831	0.099	0.068	0.063	0.101
E75	0.869	0.850	0.080	0.059	0.051	0.091
E80	0.899	0.873	0.062	0.049	0.040	0.078
E85	0.926	0.904	0.045	0.063	0.029	0.040
E95	0.977	0.960	0.014	0.015	0.009	0.025
E100	1.000	1.000	0.000	0.000	0.000	0.000

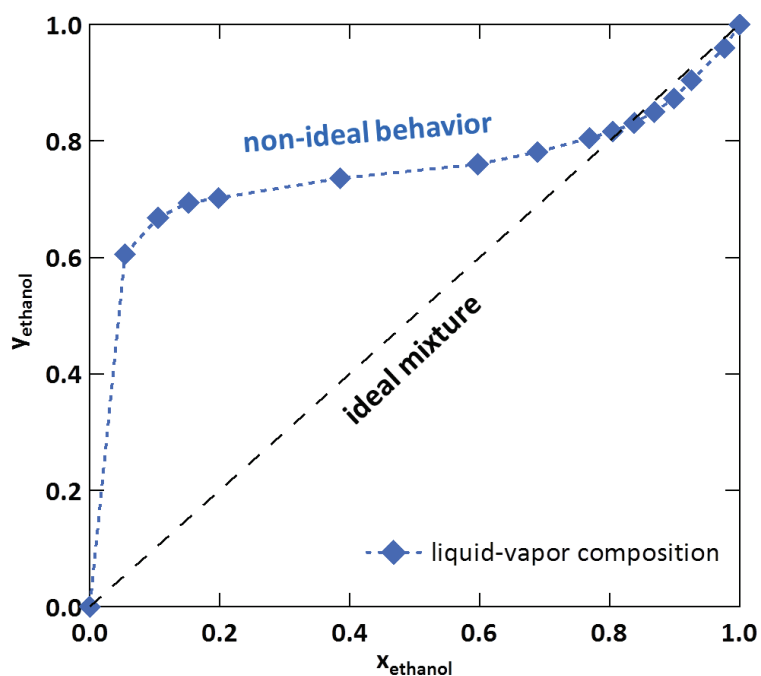


Figure 116: Ethanol molar fraction in the vapor phase $y_{ethanol}$ as a function of ethanol molar fraction in the liquid phase $x_{ethanol}$ for EX mixtures given by GC-FID measurements (markers). The behavior of an ideal mixture would correspond to the dashed line.

III. Pure solvents in Neat PA6,6

The molar fraction of ethanol in the vapor phase $y_{ethanol}$ is plotted as a function of the molar fraction of ethanol in the liquid phase $x_{ethanol}$ in Figure 116. This figure clearly shows that the liquid-vapor composition deviates strongly from the ideal behavior. Indeed, for example, at very low ethanol concentrations, ethanol is mostly surrounded by non-polar molecules, so the strong repulsive effects existing between these two kinds of solvents induce an increase in the ethanol content in the vapor, that is, an increase of the ethanol partial pressure $p_{ethanol}$, as compared to the ideal case.

The chemical activities a_i can then be calculated according to Equation 87. The values of the partial vapor pressures p_i and activities a_i for ethanol, toluene and isooctane in each mixture are shown in Table 23. The p_i^{sat} values obtained from [157] for pure ethanol, toluene and isooctane are also reported in Table 3 with the E100 mixture corresponding to pure ethanol.

Table 23: Ethanol, toluene and isooctane partial pressures p_i and chemical activities a_i measured by GC-FID analyses in EX mixtures obtained at room temperature. All reported data fall within a standard deviation of 10% of the printed value. Values for the pure toluene and the pure isooctane are also reported.

Mixture	$p_{ethanol}$ [mmHg]	$a_{ethanol}$	$p_{toluene}$ [mmHg]	$a_{toluene}$	$p_{isooctane}$ [mmHg]	$a_{isooctane}$
E0	0.00	0.000	11.13	0.426	27.87	0.577
E2.5	25.11	0.481	9.82	0.384	25.40	0.515
E5	32.01	0.613	9.26	0.362	24.14	0.490
E7.5	33.59	0.644	9.18	0.358	22.01	0.447
E10	35.74	0.685	8.35	0.326	23.85	0.484
E22	39.03	0.748	7.95	0.311	22.84	0.463
E40	42.85	0.821	7.33	0.286	23.22	0.471
E50	44.29	0.848	6.76	0.264	22.26	0.451
E60	46.57	0.892	5.94	0.232	20.42	0.414
E65	47.64	0.913	5.31	0.208	19.45	0.395
E70	48.46	0.928	4.89	0.191	18.72	0.380
E75	49.74	0.953	4.29	0.167	15.87	0.322
E80	49.81	0.954	3.52	0.138	13.16	0.267
E85	50.00	0.958	2.68	0.105	8.76	0.178
E95	51.81	0.993	0.99	0.039	3.87	0.079
E100	52.20 [157]	1.000	0.00	0.000	0.00	0.000
Toluene	-	-	25.60 [157]	1.000	-	-
isooctane	-	-	-	-	49.30 [157]	1.000

From the values reported in Table 23 for the partial pressure p_i and the molar fractions in the liquid (x_i) and vapor (y_i) phases for ethanol, toluene, and isooctane, the liquid-vapor equilibrium phase diagram for the studied ethanol-toluene-isooctane ternary mixtures can be plotted as shown in Figure 117.

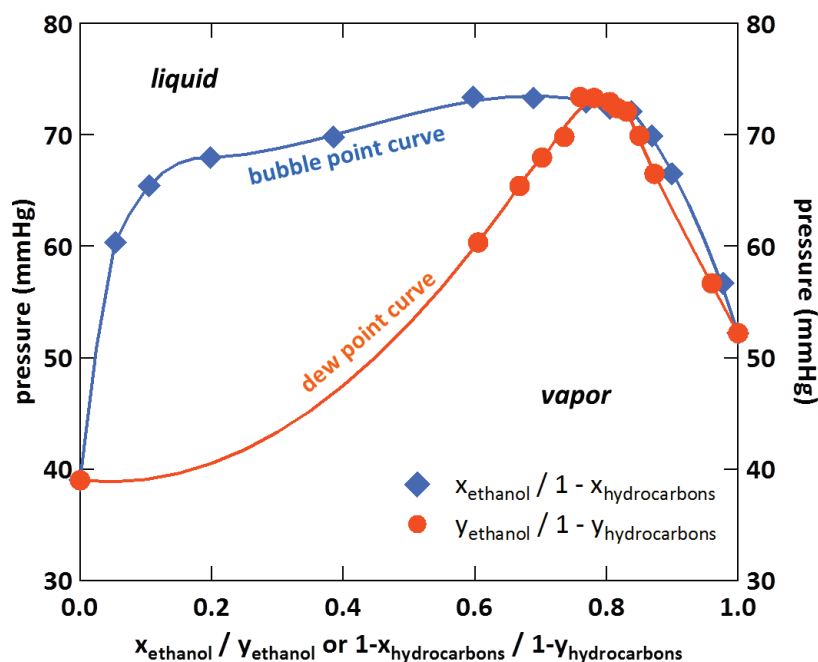
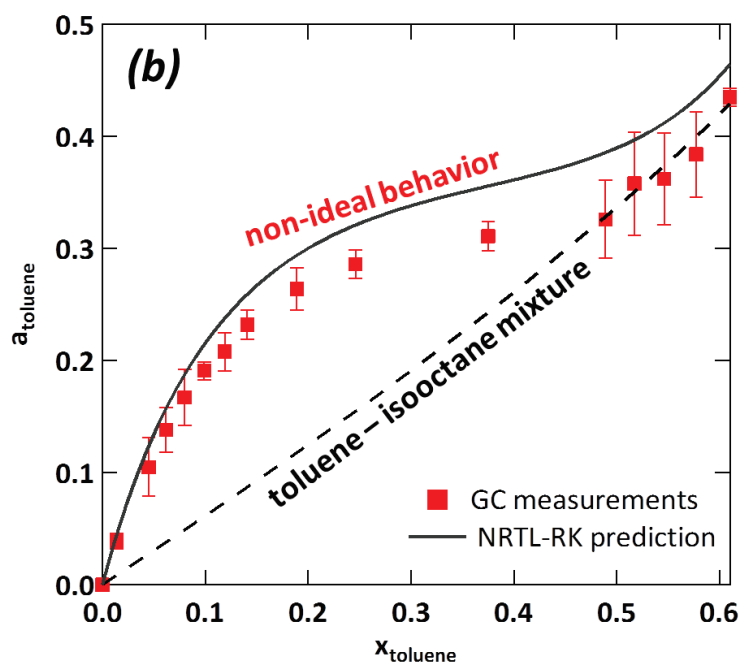
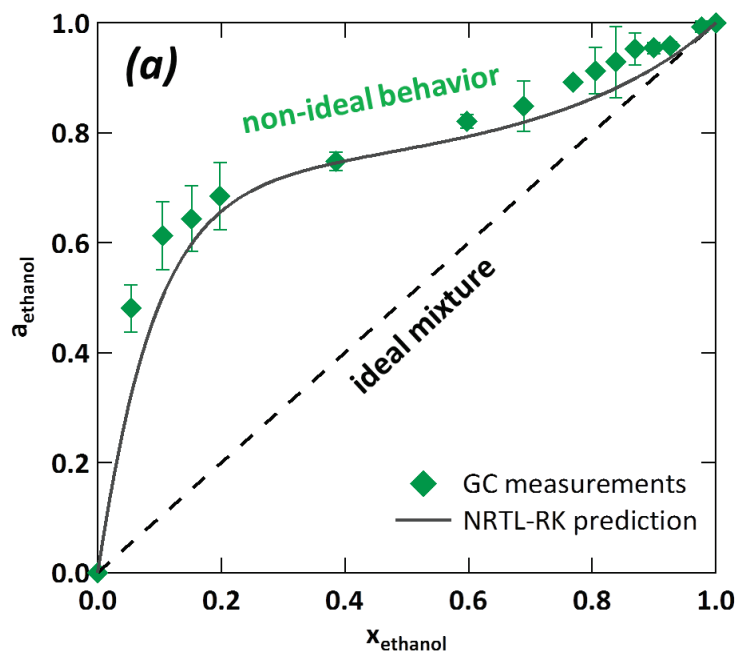


Figure 117: Liquid-vapor phase equilibrium diagram for ethanol in the EX mixtures obtained by GC measurements showing the existence of an azeotropic point and the large deviation between the bubble and the dew point curves. The plotted values of the total pressure are the sum of the partial pressures of ethanol, toluene, and isooctane for a given liquid composition x_i . Plain curves are guides for the eyes.

It is observed in Figure 117 that the bubble point (vapor phase) and the dew point (liquid phase) curves differ significantly one from each other and the mixtures possess a negative azeotropic point, which also confirm that the ternary mixtures are strongly non-ideal. As expected, this diagram is very close to the liquid-vapor equilibrium diagram for either an ethanol-toluene or an ethanol-isooctane binary mixture documented in the literature [99,100,103].

The experimentally determined chemical activities of ethanol, toluene, and isooctane a_i are plotted in Figure 118 as a function of their solvent molar fraction in the liquid phase x_i for all the studied EX mixtures. Again, the strong non ideality of the mixture appears clearly in Figure 118. This figure shows indeed that the activities of ethanol, toluene or isooctane a_i in the EX mixtures are relatively high, especially for those mixtures containing a low concentration in each of these species. As it was mentioned before, because of the repulsive effects between ethanol and non-polar solvents, an increase on the partial pressure of ethanol $p_{ethanol}$ (or equivalently of the ethanol chemical activity $a_{ethanol}$) as compared to the hypothetical ideal case, is observed.



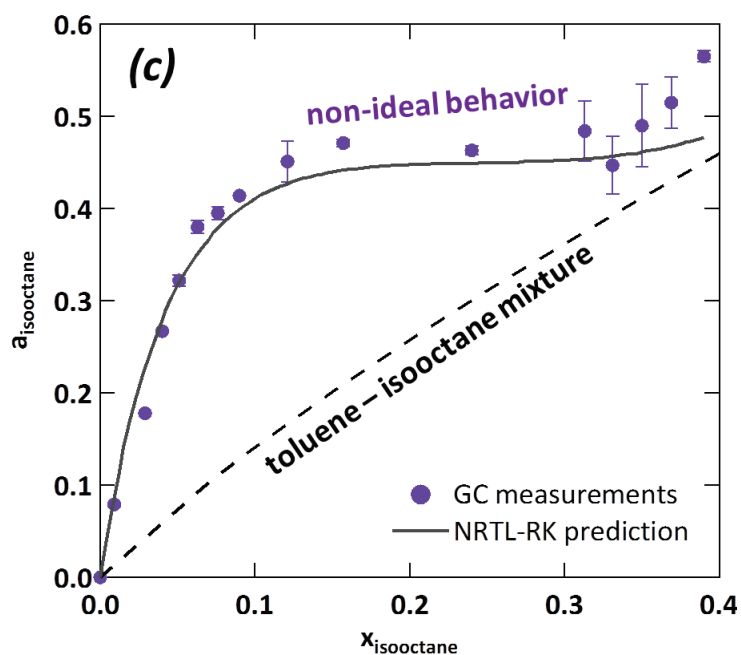


Figure 118: (a) ethanol, (b) toluene, and (c) isooctane chemical activities a_i , given by GC-FID measurements, as a function of their molar fraction in the liquid phase x_i for EX mixtures (markers), compared to the results obtained by NRTL-RK simulations (solid curves) and to the case of an ideal (dashed line in graph (a)) or a real toluene-isooctane mixture (dashed lines in graphs (b) and (c)).

The chemical activities a_i obtained experimentally for the three species are compared to the ideal case in Figure 118. For ethanol (Figure 118a), the dashed line would correspond to an ideal ethanol/hydrocarbon ideal mixture, with $a_{\text{ethanol}} = x_{\text{ethanol}}$. For toluene and isooctane, the chemical activities a_{toluene} and $a_{\text{isooctane}}$ were compared to a reference state considered to be a toluene-isooctane binary system (Figure 118b and Figure 118c respectively). This reference state was taken from the data obtained by Góral et.al. [186] for such a binary mixture, whose liquid-vapor equilibrium phase diagram is plotted in Figure 119. Then, the dashed lines in Figure 118b and Figure 118c would represent the toluene or isooctane activity in a binary toluene/isooctane mixture with the same molar concentration x_i in toluene or isooctane. It has to be noted that the toluene/isooctane binary mixture is not ideal either, even though the deviation from ideality is smaller than in ethanol/hydrocarbon mixtures.

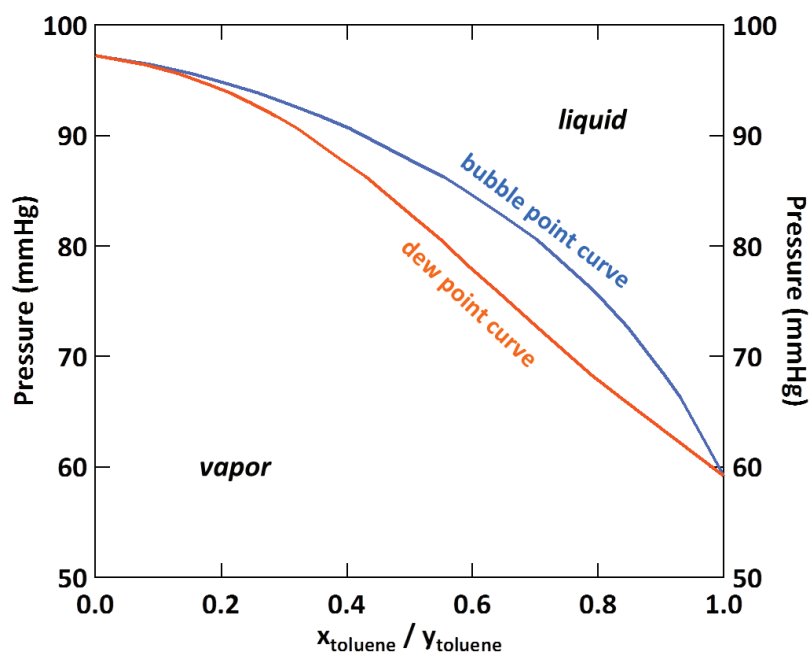


Figure 119: Liquid-vapor phase equilibrium diagram for a toluene – isooctane binary mixture as obtained by Góral et.al. [186].

It was found useful to compare the obtained experimental values of the chemical activities a_i with simulation data for a ternary solvent mixture obtained by the NRTL-RK (Non-Random Two-Liquid - Redlich-Kwong) thermodynamic equation of state [187,188]. This model is often used to predict the thermodynamic behavior of a ternary system at given temperature and pressure, from actual experimental data of binary mixtures. The results obtained by the NRTL-RK are plotted in Figure 118 (continuous curve). They compare favorably with our data obtained experimentally by GC measurements for ethanol, toluene, and isooctane. Deviations between model curves and data are inherent to the approximations used in the model.

III.5.2. Sorption of ethanol-toluene-isooctane mixtures in neat PA6,6

To study the sorption of the EX mixtures in PA66, seven ternary mixtures (E2.5, E5, E7.5, E10, E65, E75 and E85) were considered. The corresponding molar fractions x_i of ethanol, toluene, and isooctane are reported in Table 22 and the activities a_i (as obtained by GC-FID measurements) in Table 23. After reaching sorption equilibrium in the EX mixtures, the saturated *NeatPA6,6* 100 μ m-thick film samples were weighted and their desorption vapors were straight ahead analyzed and quantified by GC-FID according to the experimental setup schematized in Chapter II. Table 24 shows the overall relative mass intakes of the PA6,6 samples in the presence of the various EX mixtures, as well as the relative mass intakes of each component of the EX mixtures.

III. Pure solvents in Neat PA6,6

Table 24: Total relative mass intake (Δm) of PA66 samples saturated in the presence of EX mixtures and relative mass intake of ethanol, toluene, and isooctane, as measured by GC-FID. Equilibrium relative mass intakes for pure toluene and pure isooctane are also reported.

Mixture	Δm [%] - total	$\Delta m_{\text{ethanol}}$ [%]	$\Delta m_{\text{isooctane}}$ [%]	$\Delta m_{\text{toluene}}$ [%]
<i>E0</i>	2.1	-	0.4	1.7
<i>E2.5</i>	7.1	6.1	0.1	0.9
<i>E5</i>	9.7	8.3	0.2	1.2
<i>E7.5</i>	10.3	9.4	0.2	0.7
<i>E10</i>	10.2	9.8	traces	0.4
<i>E65</i>	10.7	10.1	0.1	0.5
<i>E75</i>	10.8	10.2	0.2	0.4
<i>E85</i>	10.8	10.4	traces	0.4
<i>E100</i>	11.9	11.9	-	-
<i>Toluene</i>	1.7	-	-	1.7
<i>Isooctane</i>	1.9	-	1.9	-

It is seen in Table 24 that the overall mass absorption of the EX mixtures is relatively high, and that, for all the studied EX mixtures, almost all the absorbed solvent is ethanol, followed by toluene and finally isooctane, which is absorbed only in trace quantities. As mentioned before, the mass intake of a solvent at sorption equilibrium depends on its activity in the environment. Indeed, it was seen above that the activity of ethanol a_{ethanol} in the EX mixtures is relatively high, even for those mixtures containing a small amount of this solvent, which would explain the observed large mass intakes, being mostly ethanol, for all studied EX mixtures.

Pure ethanol sorption in PA66 samples was measured at room temperature (25 °C) at for three different partial vapor pressures, i.e. three different ethanol activities: 0.6, 0.75, and 0.9, using a Dynamic Vapor Sorption (DVS) apparatus described in Chapter II. DVS analyses were complemented by pure ethanol sorption in PA66 in the liquid state, corresponding to an activity of 1. Relative molecular intakes were measured after reaching the ethanol sorption equilibrium. The obtained relative molecular intakes of pure ethanol as a function of the ethanol activity, obtained by DVS, are shown in Figure 120, together with the values of ethanol absorption in PA66 samples saturated in the presence of EX mixtures, obtained by GC-FID.

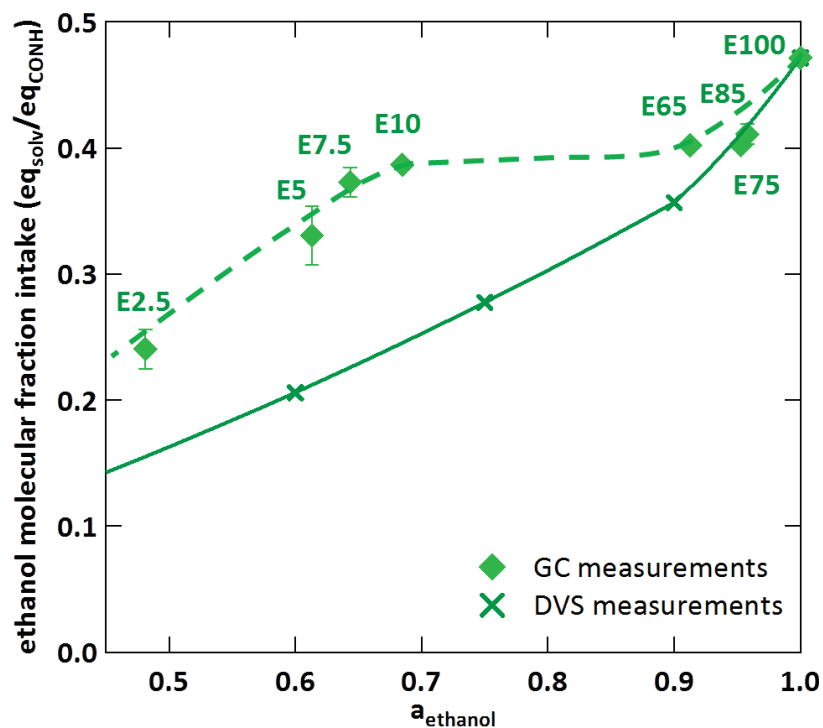


Figure 120: Comparison between the relative ethanol molecular intakes, obtained by DVS at various activities of pure ethanol and in pure ethanol in the liquid state (crosses and solid curve) and the relative ethanol molecular intakes in PA66 films saturated in the presence of EX mixtures, measured by GC-FID (diamonds), as a function of ethanol activity. Dashed curve is a guide for the eyes.

It is shown in Figure 120 that the observed ethanol molecular intakes are considerably larger (up to about 40%) than those expected from the sorption isotherm of the pure solvent at the same activity.

Toluene molecular sorption, obtained by GC measurements, is plotted in Figure 121 as a function of the ethanol chemical activity a_{ethanol} , in PA66 samples in contact with EX mixtures. It is observed in Figure 121 that the intake of toluene decreases only very slowly as the activity of ethanol a_{ethanol} increases. Note that, comparatively, isooctane is absorbed in very small (hardly detectable in most cases) amounts, whereas its equilibrium sorption in the pure state is comparable to that of toluene (see Table 24).

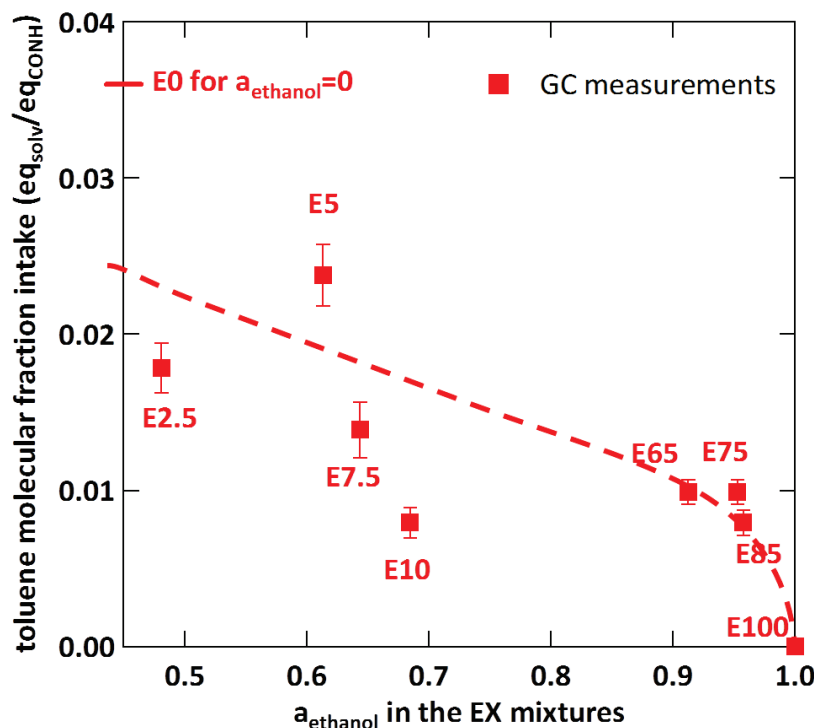


Figure 121: Relative toluene mass intakes in PA66 films saturated in the presence of EX mixtures, measured by GC-FID as a function of ethanol activity. Dashed curve is a guide for the eyes.

The objective of this study is to discuss the sorption in the presence of a mixture of solvents, and to focus on the differences observed in this case, as compared to pure solvents rather than discussing in details the shape of sorption isotherms and the most appropriate models to fit them. Specifically, the swelling mechanisms which may be responsible for the anomalous behavior illustrated in Figure 120 are discussed qualitatively.

The case of a binary (or ternary) mixture of solvents is considered in this section. In the presence of a mixture of solvents, the total amount of absorbed solvent of both species contributes to the volume increase and thus to the dilatation term, which is the predominant term at large activities, as we have seen above. Within the above picture, from Equation 65, in the presence of a mixture of two (or more) solvents, the presence of a non-zero volume fraction ϕ_2 of solvent 2 can only reduce the volume fraction ϕ_1 of solvent 1, at a given activity a_1 of solvent 1. This remains true insofar as the presence of solvent (or solvents) does not change the modulus K . This condition should be considered as reflecting the linear regime of swelling.

The effect observed in Figure 120 is opposite to that, in the sense that the presence of toluene results in an increase of ethanol content. Thus, the observed result indicates that the dynamics of the polymer are strongly affected by the fact that even a small amount of toluene decreases the modulus K of PA6,6 as it was observed in paragraph “III.2.2. Discussion of the results on solvent sorption in PA6,6”. Toluene thus has the effect of decreasing significantly the effective modulus, and by doing so, it might allow more ethanol to be absorbed by PA6,6.

III.5.3. Effect of ethanol-toluene-isooctane mixtures on PA66 molecular mobility

The variation of the glass transition temperature T_g as a function of the amount of absorbed solvent was measured for PA6,6 films swollen in EX mixtures by Modulated DSC as described in Chapter II. The T_g drop provoked by the sorption of EX mixtures was compared to that provoked by pure ethanol and pure toluene, obtained earlier in this Chapter. The results are shown in Figure 122.

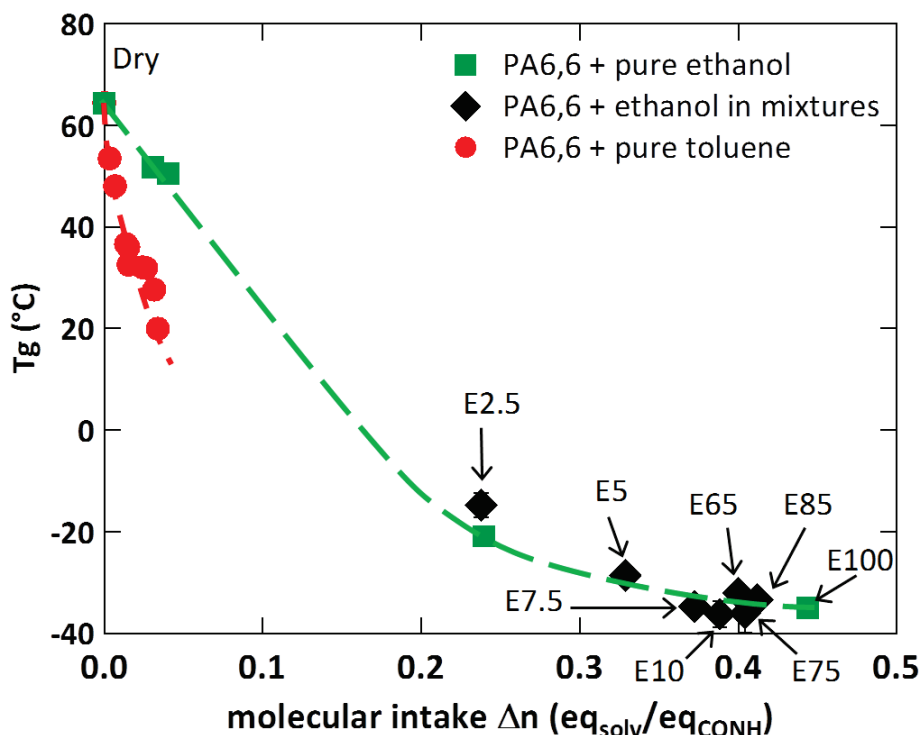


Figure 122: Drop of PA66 T_g as a function of the molecular intake Δn for pure ethanol (green squares), for EX mixtures (black diamonds), and for pure toluene (red circles). The long-dashed curves are guides for the eyes.

Figure 122 shows that despite the presence of toluene in the swollen samples, no further T_g drop provoked by this solvent is observed. The plasticization effects (T_g drops) of both solvents are not additive and the observed drop on PA66 T_g is mainly due to the presence of ethanol in the swollen polymer.

III.6. Conclusion

In this Chapter, the heterogeneity of the amorphous phase was briefly discussed. DSC measurements allowed us to estimate the percentage of Mobile and Rigid Amorphous Fractions (MAF and RAF respectively) in PA6,6 samples. The mobility of the MAF can be characterized by the T_g obtained by calorimetric, dielectric, or mechanical measurements, however the mobility of the RAF could not be characterized, so in this work the amorphous phase was considered to be homogeneously accessible to solvents, and its overall molecular mobility was characterized by the T_g .

Then sorption in PA6,6 of a series of pure polar and non-polar solvents and their effect on the crystalline and amorphous phases was studied. It was firstly observed that for the polar solvents their polarity is the main factor conditioning their intake in PA6,6. Concerning the series of non-polar solvents, it was observed that their intake remains constant and that it does not depend on their molecular size. As the molecular size does not influence the solvent sorption, we can conclude that the polarity of a solvent is the parameter of major importance that determines its sorption in PA6,6.

Furthermore the effect of temperature on solvent sorption at equilibrium was studied for water, toluene, and ethanol. It was observed that the intake of water and ethanol did not vary significantly with temperature, whereas for toluene it was observed that when the temperature increased, toluene intake in PA6,6 decreased significantly. The sorption of these solvents was qualitatively compared to the sorption described by the Langmuir and Flory sorption isotherm models. However more investigations are needed to fully understand the observed variation of solvent sorption with temperature.

The effect of the polymer nature on solvent sorption was also discussed. A classical Flory – Huggins equation was first considered for describing the sorption of water, ethanol, and toluene. However it was observed that this equation did not describe well the sorption of these solvents observed experimentally. An elastic term, describing a polymer system possessing a certain density of inter-chain H bonds that have a given rigidity and that act as physical crosslinks, was introduced to the Flory – Huggins equation. It was observed that this term greatly limits the intake of solvents in PA6,6 when compared to the classic Flory-Huggins model. It can be concluded from these observations that the H bond network of PA6,6 might act as crosslinks between chains and that their presence conditions or limits the intake of a solvent in this polymer.

Then the effect of solvent sorption on the molecular mobility of PA6,6 amorphous phase was discussed. Concerning the glass transition, characterized by the T_g , it was observed that for the alcohol solvents when their molecular intake increases, the induced T_g drop increases as well, and that water and toluene do not follow the same plasticization trend as that of the alcohols. To compare the different plasticization trends, the T_g of PA6,6 samples at different states of solvent sorption for water, ethanol, and toluene was measured. It was found that ethanol followed the same plasticization trend as that of the alcohol series, that water had a less marked effect than that of the alcohols when compared at the same molecular intake, and that toluene had the largest plasticization effect of all the studied solvents. These plasticization trends were compared to plasticization models available in the literature. It was observed that none of these models describes well the plasticization trends of water, ethanol, or toluene. This might be explained by the fact that the considered models do not take into account strong interactions between a polymer and a solvent. The significant T_g drop observed for the PA6,6-solvent could be then a signature of eventual strong interactions between water, ethanol, or toluene with PA6,6.

Moreover it was observed by Dielectric Spectroscopy that the presence of water, ethanol, and toluene do not provoke a broadening on the distribution of the relaxation times for the α molecular process, associated to the glass transition, nor they provoke a significant increase on the relaxation's amplitude. The results of the work of Marco Laurati et.al.[176] concerning the effect of water on the secondary relaxations were presented. Laurati

III. Pure solvents in Neat PA6,6

observed that for water-conditioned samples three molecular relaxations at low temperatures were observed. These molecular processes would correspond to the relaxations of water loosely bound to amide groups, to the motions of hydrated amide groups, and to the motion of amide groups not bonded to water. In this work we were interested on the effect of toluene on the secondary relaxations of PA6,6. It was observed that the β relaxation was shifted towards lower temperatures and that the associated activation energy was decreased in presence of this solvent. As the β relaxation corresponds to the rotation of the amide functions, the drop of T_β might suggest that toluene modifies the molecular motions of the amide groups by disrupting them at a local scale. It was also observed that the width and the amplitude of the β relaxation were not affected by toluene. Concerning the γ relaxation, it was observed that toluene had a slight effect on the T_γ but the accuracy of this result has to be considered, since the γ relaxation is relatively weak and difficult to fit. Toluene was also found to have little effect on the distribution of the relaxation times and on the amplitude of this relaxation.

A set of hypotheses on how water, alcohols, and toluene are able to plasticize PA6,6 were proposed. In the case of water, this solvent can directly interact with the amide functions of PA6,6, interacting with the interchain H-bond network of these polymers, diminishing their lifetime and thus provoking a drop on T_g . Moreover, since water is able to bond twice to form H-bonds it might be possible that for high concentrations of water, polymer chains are "linked" together through water bridges. Nevertheless, the lifetime of these bridges is smaller than that of the original H-bond network, leading to a raise in the molecular mobility of the polymer.

For toluene, this solvent does not have preferential interactions with the amide functions, but it does with the non-polar methylene backbone of the polymer. These interactions would allow the sorption of this solvent and because of its large molecular size, toluene might be able to stretch the interchain H-bond network, decreasing the energy of the H bonds and provoking a diminishing in the relaxation times of the H bonds, resulting in an increase of the PA66 amorphous phase molecular mobility, which is macroscopically observed as a T_g drop. In order to better understand the plasticization effect of toluene, the mean field argument developed for solvent sorption in this work was considered but it was observed that it was not sufficient to explain the very large plasticizing effect of toluene. As toluene and the H-bond network of PA6,6 have similar molecular volumes, it might be possible that for inserting one molecule of toluene in PA6,6, at least one H-bond must be broken. This effect would be localized but strong enough to provoke a large T_g drop. A more developed model taking into account this localized effect of toluene has to be developed so as to better understand the plasticization effect of this solvent in PA6,6.

Concerning the alcohol molecules, it might be possible that these solvents are able to plasticize PA6,6 through a double effect combining the effects of water and ethanol, i.e. the effect of directly perturbing the H bond network by interacting with the amide functions via their hydroxyl functions as well as a steric effect due to the presence of bulky alkyl groups borne by these solvents.

The sorption kinetics regimes of water, ethanol, and ethanol were also studied. It was observed that toluene diffused through a Fickian regime and water and ethanol diffused following a Case II regime. It was observed that the amount needed for toluene to plasticize PA6,6 was close to the total absorbed amount of this solvent, which means that toluene is

III. Pure solvents in Neat PA6,6

not able to plasticize PA6,6 while diffusing. In the case of water and ethanol, the amount of both solvents needed to plasticize the polymer is smaller than the total amount of absorbed solvent. This means that water and ethanol diffuse at the beginning following a Fickian regime and when the concentration of solvent needed to plasticize PA6,6 is reached, a change in sorption regime is observed, yielding a Case II diffusion. The differences between water and ethanol sorption regimes, especially at the Fickian part might come from the fact that water is able to diffuse faster since it is a smaller molecule than ethanol. Moreover it was observed that the diffusion of toluene was faster than that of ethanol in the Fickian regime, which might be explained by the fact that ethanol can form H-bonds with the amide functions of PA6,6. The mesoscale simulations founded on a thermodynamic approach developed by Eric Lange describe in an accurate, qualitatively way, the diffusion of solvents that are or not able to swell PA6,6 during solvent diffusion.

The effect of water and ethanol on the crystalline phase was studied. It was observed that the presence of both solvents in PA6,6 leads to an evolution of the polymer's crystalline phase towards the more stable α_i form. These solvents are able to raise the molecular mobility of the chains in the amorphous phase, which may allow a rearrangement of the chains in the crystalline phase. These results suggest that if a solvent has effect on the molecular mobility of PA6,6, it might have an effect on the evolution from the α_{II} crystalline phase towards the α_i form.

Moreover, the sorption of a series of ethanol-toluene-isooctane (EX) mixtures by PA66 was studied. These mixtures being strongly non-ideal, it was necessary to cautiously determine the chemical activity of each component of the solvent mixtures, since the activity is the driving force for sorption. Thus, a GC-FID setup was used to analyze quantitatively the vapor phase of each of the studied mixtures in order to obtain the molar fractions in the vapor phase. It was observed that the chemical activities of each of the species composing the ternary mixtures are relatively high, especially for those mixtures containing ethanol, toluene, or isooctane in low concentrations. This is because of repulsive effects between ethanol and hydrocarbon molecules in the mixtures. Then, the absorbed amounts of each component in PA6,6 were analyzed quantitatively by GC-FID. The sorption of ethanol in these samples was then compared to that of pure ethanol, obtained by DVS, at the same activities. It was found that the presence of toluene induces an increase on ethanol intake. This shows that toluene strongly affects PA6,6 even at relatively low content. This is also in accordance with the strong plasticization effect of toluene observed before. Finally it was observed that the drop of PA66 T_g when swollen in EX mixtures is mainly due to the presence of ethanol in the polymer and although toluene is also absorbed by the samples it does not induce a further plasticization effect.

At the end, it would be interesting to study if the effect of temperature on PA6,6 properties is comparable to the one provoked by the presence of solvents in the polymer. Indeed it would be of great interest to compare the properties of PA6,6 at a given amorphous phase molecular mobility state generated by either a temperature increase or the presence of solvents. In the next chapter, in order to further investigate this issue, some mechanical properties (tensile, impact strength) are assessed at various temperatures and various hygrometry levels, in the case of neat PA6,6 and modified PA6,6 in which intermolecular interactions are altered.

IV. Properties of additivated and chemically-modified PA66

After studying the solvents / polyamide interactions in the case of neat PA6,6, it was desired to modify PA6,6 structure in order to obtain a set of materials with different amorphous molecular mobility states and different affinities with solvents, the aim being to determine in what extent a good compromise between biofuel barrier properties and impact resistance could be found.

For this study, the five formulations presented in Chapter II were considered. By modifying the intermolecular interactions of PA6,6, it was expected to obtain polymers with different amorphous molecular mobility states and different affinities with solvents. These formulations are REF (Rhodia grade neat PA6,6), 10LA (PA6,6 + 10%wt laurylaldehyde), 10HA (PA6,6 + 10%wt heptanaldehyde), HIA (PA6,6/6HIA 95/5mol copolymer), and AISLI (PA6,6/6AiSLi 95/5mol copolymer).

In this part, the modifiers (additives and co-monomers) are considered to be expelled from PA6,6 crystalline phase, i.e. they do not co-crystallize with the polymer, and thus they would find themselves in the amorphous phase. The additive or co-monomer molar ratio in PA6,6 modified formulations amorphous phase is detailed in Table 25.

Table 25: Molar ratio of the additives or co-monomers present in PA6.6 modified formulations.

Modifier	molar ratio in the amorphous phase [%]
Laurylaldehyde	6.8
Heptanaldehyde	9.2
6HIA	7.4
6AiSLi	7.2

Firstly, the effect of the modification on PA6,6 crystalline and amorphous phases was studied. Then the barrier properties of such samples to water, ethanol, and toluene were characterized, and finally we were further interested in the modification influence on PA6,6 mechanical properties, namely the tensile strength and the impact strength properties.

IV.1. Effect of PA6,6 modification on its crystalline phase

IV.1.1. Effect of PA6,6 modification on crystallization and melting

Melting and crystallization DSC measurements were carried out as described in Chapter II in order to obtain the melting and crystallization temperatures as well as the crystalline fraction of the injection molded modified formulations. The thermograms obtained during the first heating scan and associated to melting process are shown in Figure 123. It is observed that the melting endotherms exhibit globally similar shapes, the peaks being slightly wider for the copolymers HIA and AISLI. Formulations containing additives (10LA and 10HA) exhibit a melting temperature T_m close to that of REF, whereas the T_m of HIA and AISLI copolymers are about 5°C lower than that of REF.

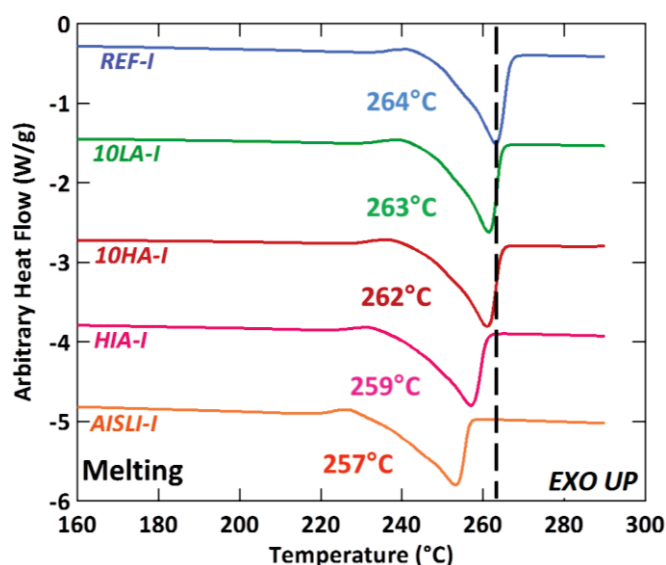


Figure 123: DSC Thermograms showing the melting behavior and the melting temperatures T_m of the injection-molded modified samples.

Crystalline ratios were determined by dividing the melting enthalpy of the sample by the reference enthalpy associated to a 100% crystalline PA6,6 as described in Chapter II. In the case of the additivated and chemically-modified formulations it was assumed that the additives and the polymer segments containing the aromatic functions were driven out into the amorphous phase since they cannot co-crystallize with the PA6,6 moieties. Thus, the crystalline ratio of the PA6,6 remaining phase was calculated by dividing the total crystalline ratio by the PA6,6 weight content. The obtained values are presented in Figure 124.

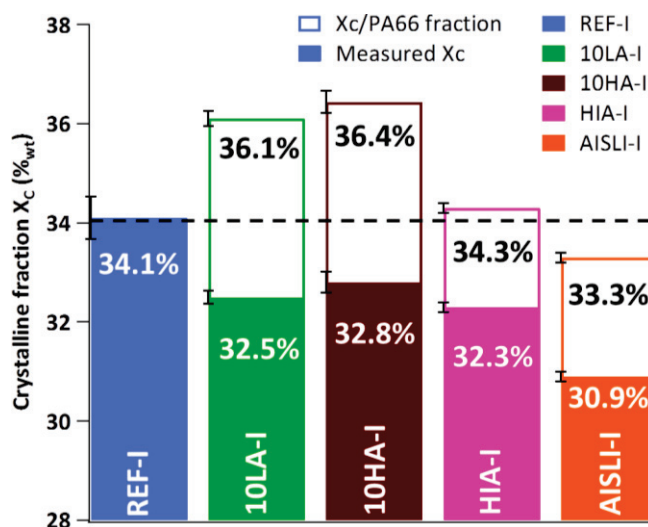


Figure 124: Measured total crystalline ratio X_c (filled) and PA66-mass corrected ratio X_{c-PA66} (empty) for the injection-molded modified samples as obtained from DSC.

It is observed that the overall crystalline ratios of the four modified polyamides are slightly lower than that of REF, this being due to the fact that the fraction of PA6,6 moieties is lower in the modified formulations, PA6,6 being the only component of the formulations able to crystallize. However the corrected crystalline ratios of the PA6,6 present in the copolymer samples (HIA, AISLI) are relatively similar to that of REF. This means that the introduction of 5%_{mol} aromatic co-monomers does not seem to affect the crystalline fraction of PA6,6 chains

IV. Modified PA6,6

segments. In the case of 10LA and 10HA, it seems that the presence of the additives slightly increases PA6,6 crystalline ratio.

The crystallization behavior was then characterized by DSC, thermograms obtained during cooling and associated to crystallization processes being shown in Figure 125. The shape and the position of the crystallization exotherms of 10HA and 10LA appear to be close to that of REF, whereas the crystallization exotherms of HIA and AISLI are much wider and shifted to lower temperatures by more than 10°C. This might mean that the presence of 6HIA and 6AiSLi co-monomers in PA6,6 hinders the crystallization process of this polymer.

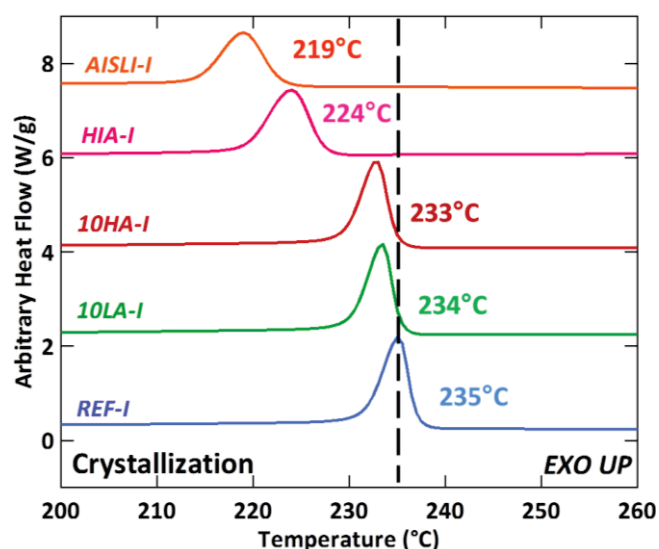


Figure 125: DSC Thermograms showing the crystallization process and the crystallization temperatures T_c for the injection-molded modified samples.

The melting and crystallization data show that despite similar crystalline ratios, the presence of co-monomers or additives seem to hinder the microstructural organization of PA6,6 segments to conform a crystalline phase, leading to a lower melting temperature and to apparent slower crystallization kinetics. Moreover the crystalline fraction is more affected by the presence of co-monomers than by the presence of additives. These results suggest that the resulting crystalline structure of the modified PA66 could differ from that of the neat PA6,6. The crystalline structure at the lattice scale was then characterized by X-Ray Scattering technique.

IV.1.2. Effect on the crystalline structure

WAXS measurements following the protocol mentioned in Chapter II were carried out on the modified formulations after drying the injection-molding or film-extrusion samples for one night at 110°C under vacuum. Figure 126 shows the obtained diffraction spectra for the samples in the dry state.

IV. Modified PA6,6

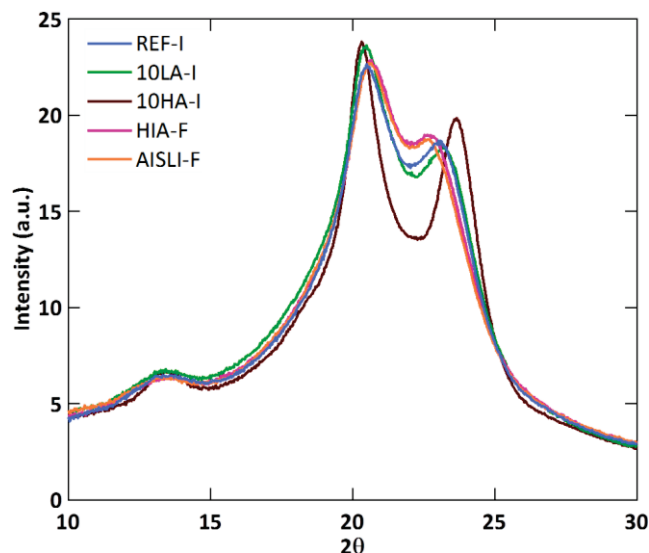


Figure 126: Wide Angle X-Ray Scattering spectra for REF-I, 10HA-I, 10LA-I, HIA-F, and AISLI-F samples at the dry state.

Table 26 shows then the values of the angular gap ($\Delta 2\theta$) between the (100) and the (010) crystallographic planes of the PA6,6 formulations obtained from Figure 126.

Table 26: Angular gap $\Delta 2\theta$ values between the (100) and the (010) crystallographic planes of the REF-I, 10HA-I, 10LA-I, HIA-F, and AISLI-F formulations at the dry state.

Formulation	$\Delta 2\theta$ [°]
REF-I	2.63
10LA-I	2.81
10HA-I	3.30
HIA-F	2.01
AISLI-F	2.15

From the values of the angular gap $\Delta 2\theta$ shown in Table 26, it is observed that in the case of HIA and AISLI, the gap between the Bragg diffraction peaks of the PA6,6 α crystalline phase is smaller for these two samples when compared to that of REF. This suggests that the presence of 6HIA and 6AiSLi co-monomers in PA6,6 molecular structure induce a less perfect PA6,6 α crystalline phase. But it has to be mentioned that the samples analyzed by WAXS were obtained through different processing techniques: REF, 10LA, and 10HA samples were obtained from an injection-molding process whereas HIA and AISLI films were obtained from an extrusion process. So the difference in crystalline structure between REF (injection molded) and the copolymers (film cast extruded) might come also from the influence of the materials processing. However, the suggested disordering effect of the co-monomer on PA6,6 crystalline structure is consistent with DSC measurements performed exclusively on injection-molded samples, which evidenced a decrease of the melting temperature in the case of the copolymers.

In the case of the additivated formulations, it is observed in that the Bragg diffraction peaks of 10LA and 10HA samples are narrower and are relatively well separated one from each other when compared to those of REF, especially for the 10HA formulation, whose Bragg diffraction peaks are well separated. The presence of laurylaldehyde and especially

IV. Modified PA6,6

heptanaldehyde in the molten polymer appear thus to allow PA6,6 to crystallize into a more stable form.

To summarize, the crystalline phase of the additivated and chemically-modified PA66 formulations was characterized by DSC and WAXS. The introduction of additives in the PA6,6 matrix appeared to little affect the melting and crystallization phenomena of PA6,6, but it appeared to induce a modification of the crystalline structure, leading to a more perfect lattice in additivated formulations. Concerning the copolymers, it was observed that the presence of co-monomers significantly affects the melting and crystallization phenomena, i.e. the melting and crystallization temperatures are diminished in presence of PA6HIA and PA6AiSLi moieties. In addition, the presence of the co-monomers could induce a less perfect crystalline structure when compared to neat PA6,6.

IV.2. Effect of PA6,6 modification on the amorphous phase molecular mobility

IV.2.1. Heterogeneity of the amorphous phase.

The heterogeneity of the modified PA6,6 amorphous phase, defined by the relative proportion of rigid and mobile fractions, was assessed by Modulated DSC measurements as defined in Chapter II from the values of the heat capacity step ΔC_p and the crystalline ratios X_{C-PA66} corrected to the fraction of PA6,6 in each formulation. Figure 127 shows the obtained values of the corrected X_{C-PA66} , %MAF and %RAF for the modified formulations.

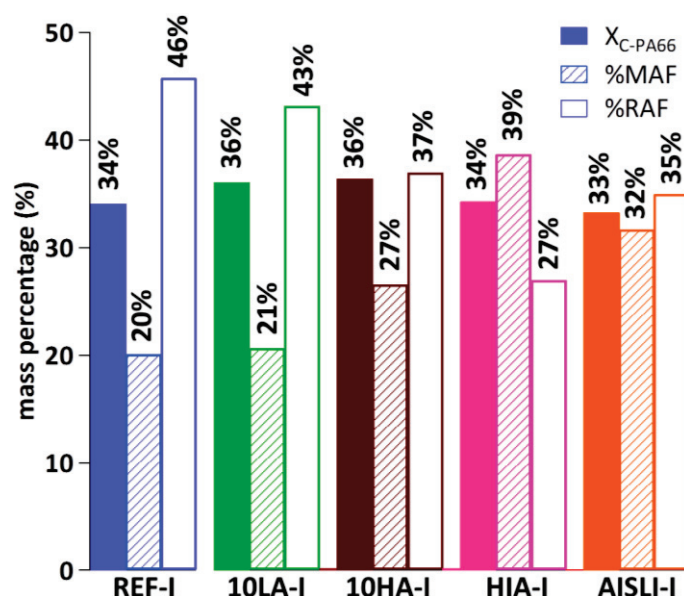


Figure 127: Corrected crystalline X_{C-PA66} , MAF, and RAF mass fractions obtained by DSC and Modulated DSC for the injection-molded modified samples.

It is observed in Figure 127 that the fraction of RAF for REF and 10LA is similar, whereas for 10HA, HIA, and AISLI this fraction is lower than that of REF. This difference could be interpreted as an intrinsic effect of the modification on RAF/MAF ratio in polyamide, but it should be pointed out that the MAF and RAF ratios were calculated using the ΔC_p value of a 100% amorphous neat PA6,6. The additives and co-monomers also contribute to the heat capacity step observed by DSC (i.e. signature of the T_g), and thus the ΔC_p values for 100%

IV. Modified PA6,6

amorphous neat additives and co-monomers should be taken into account to calculate the MAF and RAF ratios of these formulations. These ratios would perhaps be different from the ones shown herein. Consequently, it is not possible to assess without ambiguity the RAF in the modified formulations. In the following, similarly to Chapter III, the amorphous phase of the different formulations will be considered as homogeneously accessible to solvents, and its global molecular mobility will be characterized by the glass transition temperature T_g (or T_α).

IV.2.2. Effect of PA6,6 modification on the glass transition.

The molecular mobility of the modified PA6,6 in the dry state was characterized by DMA, DSC, and BDS. The methods for obtaining the values of T_g and T_α obtained by DSC and BDS have been described before. Figure 128 shows the elastic and loss dynamic moduli (E' and E'' respectively) obtained for the dry injection-molded samples obtained by DMA measurements, with T_α being taken at the maximum of the peak observed on E'' as described in Chapter II.

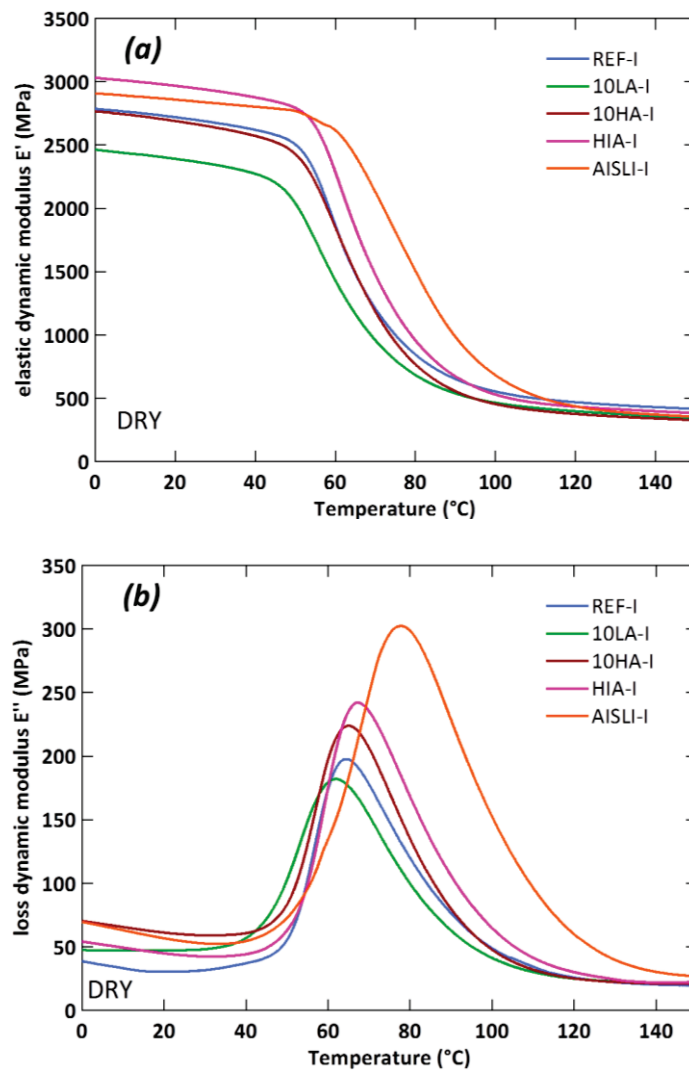


Figure 128: Dynamic (a) elastic moduli E' and (b) loss moduli E'' obtained by DMA at 1Hz for the injection-molded modified samples at the dry state.

IV. Modified PA6,6

The T_g and T_α values obtained by DSC, DMA, and BDS are shown in Figure 129. DSC and DMA measurements were done on injection-molded samples only, whereas the BDS measurements were carried out on injection-molded (REF-I, 10LA-I, and 10HA-I) and extruded (HIA-F, and AISLI-F) samples.

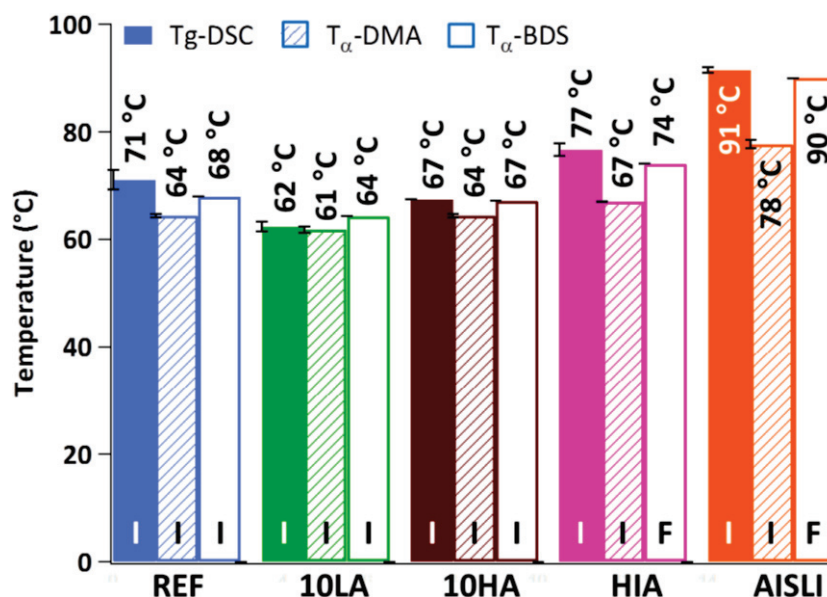


Figure 129: T_g and T_α (1 Hz) measured by DSC, DMA, or BDS for the dry REF, 10HA, 10LA, HIA, and AISLI samples.

The DSC, BDS, and DMA techniques yield comparable results and similar rankings for the modified formulations, as shown in Figure 129. It is observed that in comparison with REF, the T_g of 10LA is slightly decreased by about 5°C, the T_g of 10HA appears little affected, the T_g of HIA is increased by about 6°C, and the T_g of AISLI is increased by about 20°C. The origin of these differences in the formulations' T_g is now explained:

In the copolymers, the sole presence of aromatic rings is supposed to make the copolymers chains more rigid, thus increasing their T_g when compared to aliphatic PA6,6. Moreover, the interchain bonds are reinforced by the presence of co-monomers: PA6HIA phenyl functions form interchain H-bonds with amide groups that are stronger than those between amide functions (the energy of an amide-amide bond is ca. 27 kJ/mol whereas the one for an amide-phenol bond is ca. 40 kJ/mol). Concerning PA6AiSLi, lithium atoms present in the co-monomer are able to form chemical complexes of high energy values (ca. 40 – 50 kJ/mol) with either the carboxylic groups or the terminal amine functions found in other chains as shown in Figure 130.

The case of polyamide containing the additives (10LA and 10 HA) is now discussed. As mentioned in the previous part, laurylaldehyde and heptanaldehyde bond to PA6,6 amide groups via their phenolic functions, these new interactions being stronger than the amide-amide interactions (40 kJ/mol compared to 27 kJ/mol). As explained for the PA6,6/6HIA copolymer, these stronger interactions could lead to an increase of PA6,6 T_g , but in the case of laurylaldehyde and heptanaldehyde, the presence of the aliphatic chains could act as polymer chain spacers that could promote molecular mobility. At the end the overall molecular mobility of PA66 containing these additives should result in a competition between the increase of the molecular interactions that should raise the T_g and the presence of chain spacers that should lower the T_g . In the end, it seems that the plasticizing effect due

IV. Modified PA6,6

to the 12 carbons aliphatic chain predominates in the case of 10LA, whereas a balance is obtained in the case of 10HA which contains only 7 carbons aliphatic chains.

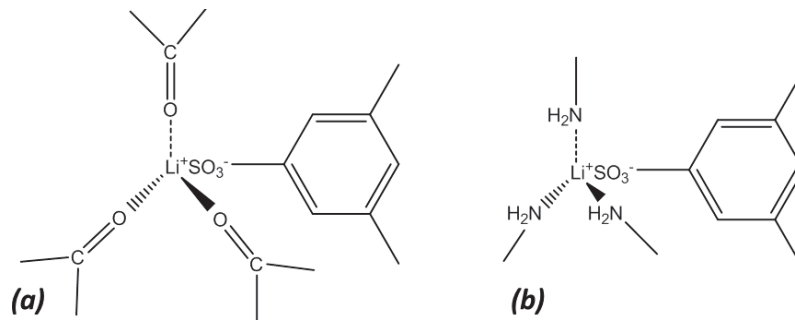


Figure 130: Coordination bonds between lithium sulfide Li^+SO_3^- and (a) Carboxylic groups within PA6,6 chains or (b) terminal Amine groups.

BDS experiments allow to investigate the effect of additives and co-monomers on PA6,6 relaxation processes on a wide frequency range. Figure 131 presents the frequency-temperature plot of the α relaxation of the modified formulations obtained from the loss modulus M'' measured by BDS.

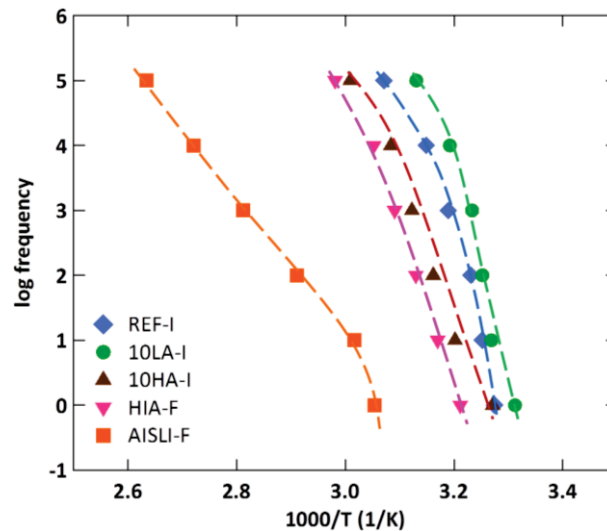


Figure 131: α relaxation temperatures as a function of the frequency for the modified PA6,6 samples (obtained from the loss modulus M'' measured by BDS). Dashed curves are guides for the eyes.

The widening or broadening of the α relaxation in presence of additives and co-monomers was then studied through the values of the Havriliak-Negami m and n exponents. These values were obtained by fitting the α relaxation with the following Equation that was defined in Chapter II:

$$\epsilon^* = \epsilon_{\infty} + \frac{\epsilon_s - \epsilon_{\infty}}{(1 + (i\omega\tau)^m)^n}$$

88

The m and n exponents give an idea on the width or amplitude of a molecular relaxation, if it is symmetrical or not, and to be more precise, on the broadening of the distribution times of the molecular relaxation. The Havriliak-Negami fit results for AISLI are not presented since this relaxation was weak, very difficult to fit, and also easily mistaken with the interfacial

IV. Modified PA6,6

polarization. Figure 132 shows the α relaxation broadening as obtained from the Havriliak – Negami exponents m and n for REF, 10HA, 10LA, and HIA formulations.

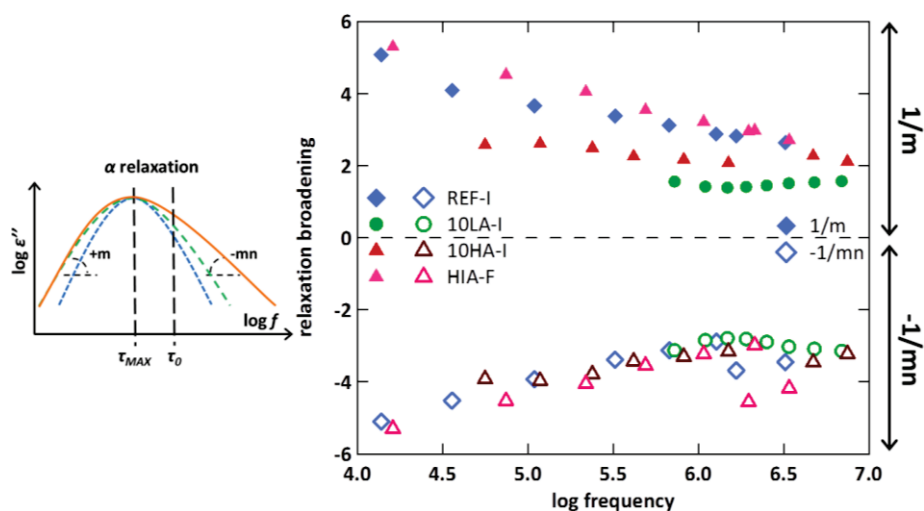


Figure 132: α relaxation width as a function of the frequency for the modified PA6,6 samples.

It is observed in Figure 132 that the presence of 6HIA co-monomers (HIA samples), lauryl- and heptanaldehyde additives (10LA and 10HA formulations) does not have an influence on the α relaxation width. To further discuss the width of the alpha process, the evolution of the loss modulus E'' with temperature measured by DMA can be considered. Table 27 shows the width at half-height ΔT for each formulation obtained from Figure 128b.

Table 27: Width at half-height ΔT for each modified formulation from the loss dynamic modulus E'' plotted in Figure 128b.

Formulation	ΔT [°C]
REF-I	25
10LA-I	26
10HA-I	24
HIA-I	26
AISLI-I	32

Table 27 shows that the width at half-height of the peak of the loss dynamic moduli E'' is similar for all formulations except for AISLI. The DMA results for REF, 10LA, 10HA and HIA are thus consistent with the BDS results shown in Figure 133. Concerning the widening of the E'' peak of AISLI associated to the α relaxation process, it could be the signature of a relatively important variation of the intermolecular interactions within PA6,6 chains provoked by the presence of PA6AiSLi co-monomers in the neat polymer.

IV.2.3. Effect of PA6,6 modification on the secondary relaxations.

The effect of additives and co-monomers on the secondary relaxations of modified PA6,6 was also studied. The secondary relaxations correspond to the molecular motions of small segments of the polymer. As it was mentioned before, concerning PA6,6, two secondary relaxations have been identified: the β relaxation corresponds to the motion of chain

IV. Modified PA6,6

segments containing amide groups, and the γ relaxation corresponds to the motions of the methylene backbone of the polymer.

IV.2.3.1. Beta relaxation

The β relaxation process is firstly discussed, the values of the β relaxation temperatures taken at 1Hz from the maxima of the loss moduli M'' spectra being tabulated in Table 28.

Table 28: β relaxation temperatures (T_β) of dry for the modified PA6,6 samples obtained from the dielectric loss moduli M'' .

Formulation	T_β @1 Hz [°C] - BDS
REF-I	-41
10LA-I	-46
10HA-I	-49
HIA-F	-43
AISLI-F	-44

The β relaxation temperature appears to be little affected in the case of HIA and AISLI formulations, however this relaxation is slightly shifted towards lower temperatures in the case of 10LA and 10HA formulations. Figure 133 shows the frequency-temperature plot of the β relaxation of these samples.

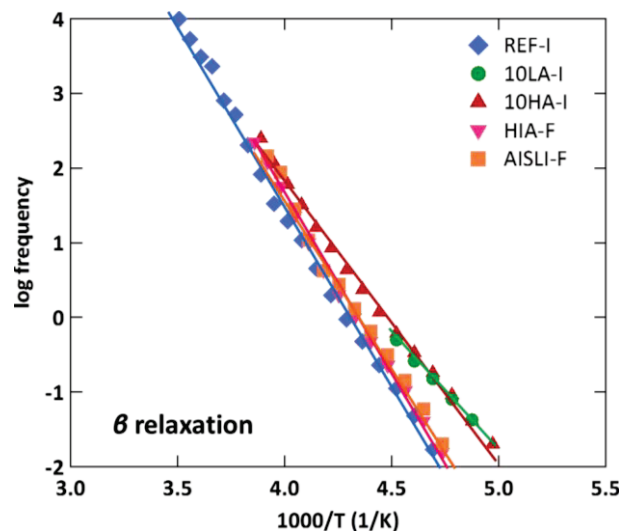


Figure 133: β relaxation temperatures as a function of the frequency for the modified formulations.

From Figure 133 the activation energies E_β of the β relaxation process can be calculated from an Arrhenius relationship:

$$\tau(T) = \tau_0 \exp\left(\frac{E_\beta}{RT}\right) = \frac{1}{2\pi f_{\max}}$$

IV. Modified PA6,6

Where $\tau(T)$ and f_{max} are the relaxation time and the frequency as a function of T the temperature, and R is the ideal gas constant ($R=8.314$ kJ/mol·K). Table 29 shows then the obtained activation energies E_β for the modified formulations.

Table 29: Activation energies obtained for the β relaxation for the modified formulations.

Formulation	Activation energy E_β [kJ/mol]
REF-I	94
10LA-I	58
10HA-I	71
HIA-F	90
AISLI-F	88

It is observed that the values of the activation energies of the β relaxation for HIA and AISLI formulations are comparable to those of REF and that for 10LA and 10HA formulations the activation energies diminish when compared to REF. This might mean that the lauryl- and heptanaldehyde additives not only diminish the β relaxation temperature but they are also able to lower the energy needed for this relaxation process to occur, whereas the co-monomers do not have a significant effect on this relaxation.

An effect on the β process would be expected for HIA and AISLI formulations since the co-monomer moieties bearing either phenol or lithium functions are able to interact with amide functions. It was observed that 6AiSLi moieties provoked a widening of the α relaxation, but this does not mean that if these co-monomers modify the α relaxation they shall also modify the β process.

In the case of 10LA and 10HA samples, the lauryl- and heptanaldehyde were conceived so as to interact with the amide groups of PA6,6. The phenol functions interact with the amide functions by disrupting bonds between PA6,6 chains. Even if the energy of an amide-phenol bond is stronger than an amide-amide one, the amide functions bonded to the additive are able to move more freely than those still bonded between each other. By increasing locally the molecular mobility of PA6,6 chains, the additives may provoke a modification of the dynamics of amide functions, which is then observed by a drop the β relaxation temperature and the associated activation energy.

Furthermore the width of the β relaxation was also studied, and as it was assumed that secondary relaxations possess mostly symmetrical relaxation times, a Cole-Cole relationship was used instead of a Havriliak-Negami one, to fit the β relaxation. This relationship is given in Equation 90:

$$\epsilon'' = \epsilon''_0 + \frac{\epsilon''_s - \epsilon''_0}{1 + (i\omega\tau)^m} \quad 90$$

where m ($0 < m < 1$) is the exponent describing the broadening of the molecular relaxation and the characteristic times. Figure 134 shows the width or the broadening of the β relaxation times estimated by exponent m of the Cole-Cole equation for the PA6,6 modified formulations.

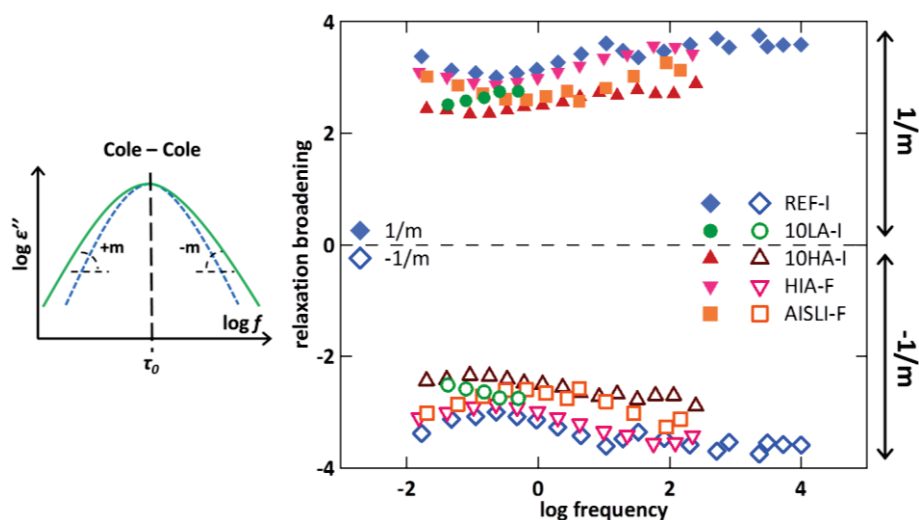


Figure 134: β relaxation width as a function of the frequency for the modified PA6,6 samples.

The width of the β relaxation process seems to be little affected by the presence of additives or co-monomers. The minor observed differences might come from the fit uncertainty rather than from an effect of these species on the relaxation itself.

IV.2.3.2. Gamma relaxation

Finally we were interested in the effect of additivation or chemical modification on the γ relaxation, which corresponds to the motions of the $-CH_2-$ functions of PA66. Table 30 shows the γ relaxation temperatures T_γ obtained by Dielectric Spectroscopy at 1Hz from the maxima of the loss moduli M'' spectra for the modified PA6,6 formulations.

Table 30: γ relaxation temperatures (T_γ) of the modified PA6,6 samples obtained from the dielectric loss moduli M'' .

Formulation	T_γ @1 Hz [°C] - BDS
REF-I	-126
10LA-I	-130
10HA-I	-133
HIA-F	-126
AISLI-F	-124

It is observed that the γ relaxation temperatures of HIA and AISLI samples are similar to that of REF, and that the presence of lauryl- and heptanaldehyde in the 10LA and 10HA formulations seems to slightly decrease the temperature of the γ process when compared to REF. These results might mean that the additives might be able to disrupt the molecular motions linked to the γ process but since this relaxation is quite difficult to analyze, the difference on the results may also come from the uncertainty of the numerical fit of this relaxation. Figure 135 shows the temperature – frequency plot for the γ relaxation the PA6,6 modified samples.

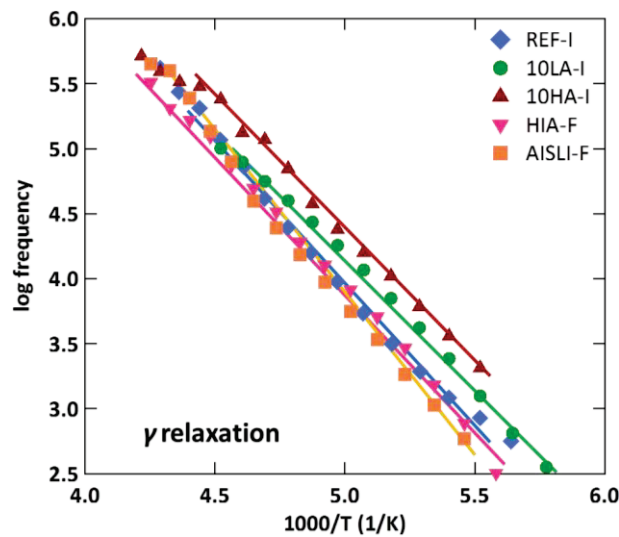


Figure 135: γ relaxation temperatures as a function of the frequency for the modified PA6,6 samples.

From Figure 135 the activation energies E_γ of the γ relaxation process can be calculated from Equation 89. Table 31 shows the obtained activation energies E_γ for the modified formulations.

Table 31: Activation energies obtained for the γ relaxation for the modified formulations.

Formulation	Activation energy E_γ [kJ/mol]
REF-I	42
10LA-I	42
10HA-I	39
HIA-F	42
AISLI-F	43

It is observed that the values of the activation energies of the γ relaxation are close for all formulations, which would mean that the additives or co-monomers do not have an effect on the variation of the relaxation times of the γ molecular process with temperature. The width of the γ relaxation was also studied, Figure 136 shows then the m exponent of the Cole-Cole relationship showed in Equation 90, obtained for the PA6,6 modified samples.

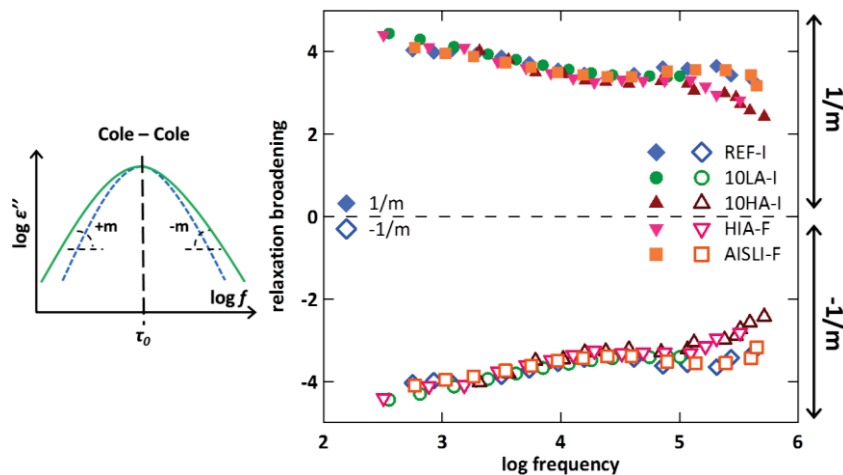


Figure 136: γ relaxation width as a function of the frequency for the modified formulations.

It is observed in Figure 136 that the introduced additives and co-monomers do not modify the width of the γ relaxation.

IV.3. Effect of PA6,6 modification on the barrier properties and molecular mobility

IV.3.1. Effect of PA6,6 modification on the solvent sorption at equilibrium

The solvent intake of water, ethanol, and toluene on the additivated and chemically-modified PA6,6 formulations was then studied. Solvent sorption was carried out on either extruded films (HIA-F and AISLI-F) or thinned-out injection-molded discs (REF-I, 10LA-I, and 10HA-I) with all samples having an average thickness of 300 μm and a surface of 5x5 cm^2 . Samples were immersed in water, ethanol, or toluene and weighed regularly until the sorption equilibrium was reached.

Similarly to the case of *NeatPA66* samples presented in the previous part, the mass (Δm) and molar intakes (Δn) at sorption equilibrium were calculated. In the case of REF, being a neat PA6,6 formulation, the molar intake Δn of the absorbed solvents was calculated from the relationship defined in Equation 91.

$$\Delta n = \Delta m \times \frac{M_{PA66}}{M_{solvent}} \times \frac{1}{1 - X_c} \quad 91$$

Concerning the additivated and chemically-modified formulations, some considerations have to be taken into account for obtaining the accurate molar intakes of water, ethanol and toluene in these formulations. In the case of 10LA and 10HA formulations, hydroxyl groups present in the lauryl- and heptanaldehyde additives are expected to interact with the amide functions borne by PA6,6 chains, but no particular interaction with the solvents is expected. So these additives can be considered as impermeable entities present in the polymer, just like the crystalline phase is considered, as it is schematically represented in Figure 137a. In that case the solvent molar intake Δn is calculated as follows:

$$\Delta n = \Delta m \times \frac{M_{PA66}}{M_{solvent}} \times \frac{1}{1 - X_c - \phi_{additive}} \quad 92$$

where $\phi_{additive}$ is the mass fraction of additive (referred to the total material) present in the 10LA and 10HA formulations.

Concerning the HIA and AISLI formulations, it is considered that PA6HIA and PA6AiSLi co-monomers do not co-crystallize with PA6,6, so the co-monomers are considered to be part only of the amorphous phase as it is schematically represented in Figure 137b. PA6HIA and PA6AiSLi also bear amide groups that might also interact with solvents, thus the fraction of amide functions borne by the co-monomer moieties should be taken into account when calculating the solvent molar intake. For HIA and AISLI formulations, the solvent molar intake Δn is calculated as follows:

$$\Delta n = \Delta m \times \frac{1}{M_{\text{solvent}}} \times \left[\frac{1}{\frac{1}{M_{PA66}} + \varphi_{CM} \frac{1}{M_{CM}}} - \frac{X_C}{M_{PA66}} \right]$$

where φ_{CM} is the molar fraction of co-monomers present in the formulation and M_{CM} is the molar mass of the co-monomer (i.e. $M_{PA6HIA}=131$ g/mol and $M_{PA6AISLI} = 166$ g/mol).

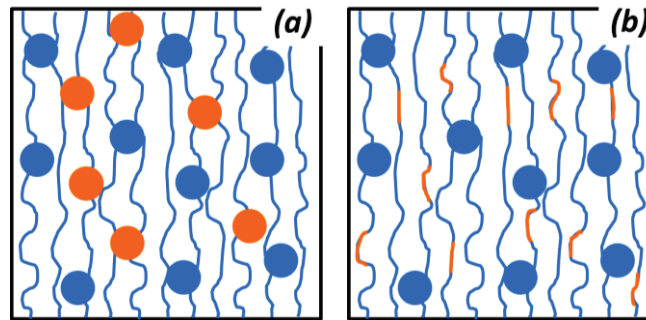


Figure 137: Schematic representation of a PA6,6 formulation highlighting the amorphous phase (irregular blue chains), the crystalline phase (blue dots) and (a) the phenolic additives (orange dots) or (b) the aromatic co-monomers (irregular orange segments).

IV.3.1.1. Case of water

The mass Δm and molecular Δn intakes obtained for water in the five studied formulations are shown in Figure 138.

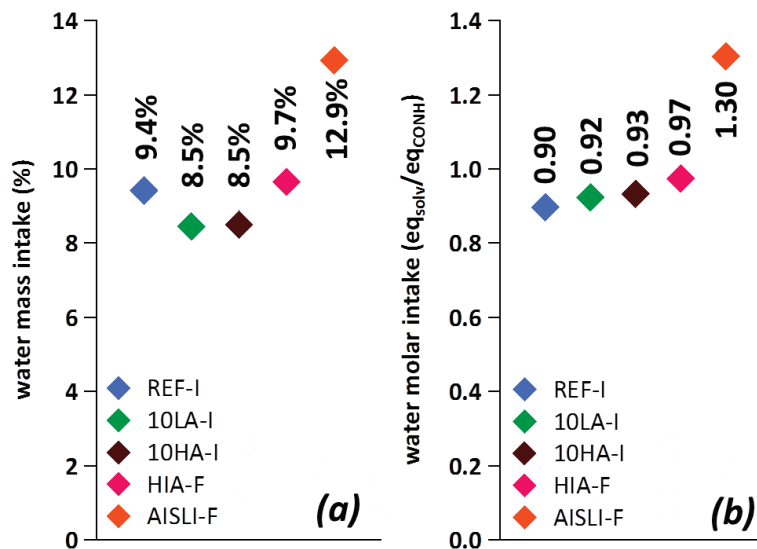


Figure 138: Water (a) mass Δm and (b) molar Δn intakes at sorption equilibrium for the modified PA6,6 samples. Δm values are measured results whereas Δn values are calculated from Equations 91, 92 and 93.

Concerning the additivated formulations 10LA and 10HA it is observed that the overall water mass intake is lower (ca. 10%) than that of REF. However when comparing the water molecular intake, it is seen that the molar intake for 10LA and 10HA is very close to that of REF. The apparent water inhibition effect observed on the overall mass water uptake

IV. Modified PA6,6

appears to come from the sole presence of impermeable additives in the formulation that reduces mathematically the actual amount of PA6,6 moieties that might be able to interact with water.

In the case of the copolymer formulations, it is seen that HIA and especially AISLI are more hygroscopic than REF. In the case of HIA, the presence of bulky aromatic moieties might induce a spacer effect between chains, maybe making some amide functions more accessible for water molecules, as the molar intake approaches one molecule of water per amide function in the amorphous phase. For all formulations, except for AISLI, it might be possible that 10% of the amide groups in the amorphous phase are not accessible to water, or that water forms small molecular clusters (2-3 molecules) as it has been suggested [53,61-63,120,121]. Concerning AISLI, the presence of lithium in its structure highly favors water absorption, since both water and lithium can ionize and/or form complexes, creating stronger interactions than the ones created by the coordination of lithium and the carboxylic functions of PA6,6, as it was observed by Kirsh et.al. for water sorption in alkaline sulfonate-bearing polyamides [189].

IV.3.1.2. Case of ethanol

The mass Δm and molecular Δn intakes obtained for ethanol in the five studied formulations are shown in Figure 139.

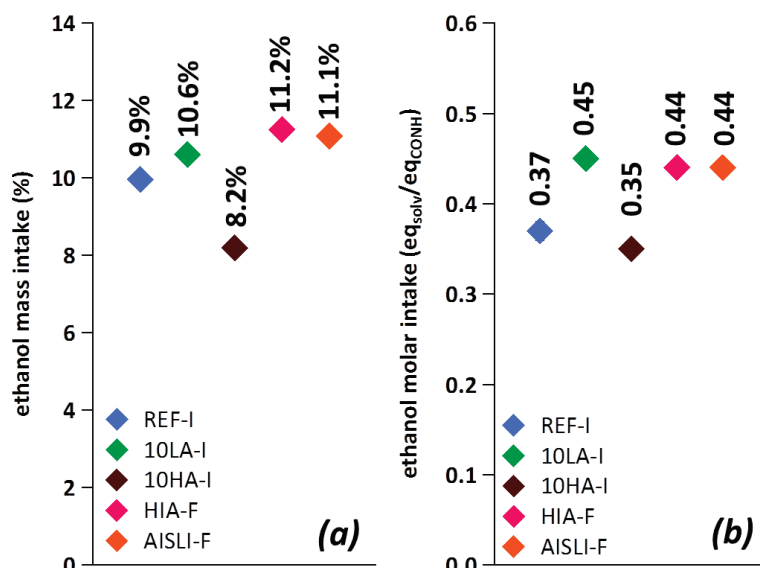


Figure 139: Ethanol (a) mass Δm and (b) molar Δn intakes at sorption equilibrium for the modified PA6,6 samples. Δm values are measured results whereas Δn values are calculated from Equations 91, 92 and 93.

It is observed that for 10LA, HIA, and AISLI, the molar intake is slightly higher than that of REF, whereas for 10HA the value is slightly smaller than that of REF. Thus, the presence of laurylaldehyde, 6HIA, or 6AiSLI in PA6,6 seems to induce a higher ethanol intake. It might be possible that the laurylaldehyde additive and the 6HIA and 6AiSLI co-monomers are able to modify the arrangement in space of PA6,6 chains. Since these modifiers are relatively bulky, they might be able to effectively act as chain spacers, increasing up to some extent the accessibility of some amide functions in PA6,6, and thus allowing more ethanol to be

IV. Modified PA6,6

absorbed by the polymer. The raise of accessibility affects more the ethanol sorption than that of water, as water is already absorbed in larger amounts. This hypothesis is analogous to the effect observed in Chapter III for the mixtures of solvents in which the presence of toluene enhances the intake of ethanol in PA6,6 films in contact with ethanol-toluene-isooctane mixtures. Moreover, Kirsh et.al. studied the sorption of ethanol in alkaline sulfonate-bearing polyamides [189], they stated that ethanol interacted with the amide functions of these polyamides rather than with the alkaline sulfonate moieties, which is in accordance with our hypothesis. Concerning heptanaldehyde, the intake of ethanol is even slightly inhibited, maybe because the additive effectively blocks some H bonds and also maybe because this additive might not be bulky enough to have a spacer effect on PA6,6 chains.

IV.3.1.3. Case of toluene

Finally, the mass Δm and molecular Δn intakes obtained for toluene in the five studied formulations are shown in Figure 140.

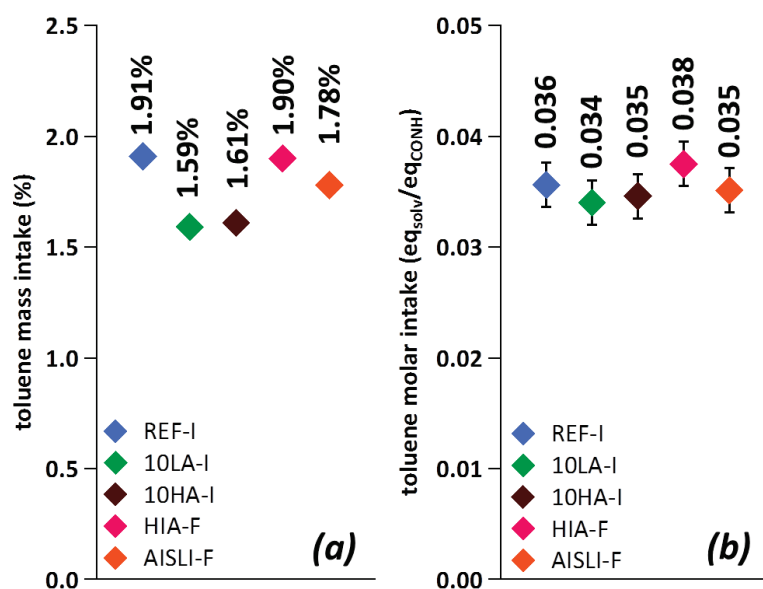


Figure 140: Toluene (a) mass Δm and (b) molar Δn intakes at sorption equilibrium for the modified PA6,6 samples. Δm values are measured results whereas Δn values are calculated from Equations 91, 92 and 93.

It can be observed that the overall mass intakes of toluene in the 10LA, 10HA, and AISLI formulations are lower than those for REF and HIA, but when comparing the toluene molecular intake, it is seen that all the formulations have very close molecular intakes. Even if the additives or co-monomers are suspected to act as chain spacers, the fact that toluene is absorbed in the same amounts by all formulations might mean that the space liberated by the modifiers is not large enough to let more toluene be absorbed.

IV.3.2. Plasticization effect of absorbed solvents in modified PA66 formulations

After conditioning and obtaining the solvent intake equilibrium, the effect of water, ethanol, and toluene on the amorphous phase molecular mobility of the modified PA6,6 formulations was assessed by Dielectric Spectroscopy. Measurements were also carried out by Modulated DSC but the T_g signature was very difficult to measure, if non-existent, especially for 10LA and 10HA ethanol-swollen samples. Table 32 shows the α relaxation temperatures (T_α) of these five formulations in presence of water, ethanol, and toluene. These temperatures were obtained from the maxima of the loss moduli M'' peaks corresponding to the α relaxation process measured at 1Hz for each of the solvent-conditioned samples. These values are also plotted in Figure 141.

Table 32: T_α values obtained by BDS for the modified formulations at the dry state and conditioned in water, ethanol, or toluene.

Formulation	T_α -dry (°C)	T_α -water (°C)	T_α -ethanol (°C)	T_α -toluene (°C)
REF-I	68	-26	-32	31
10LA-I	64	-32	-36	34
10HA-I	67	-20	-36	34
HIA-F	74	-22	-30	36
AISLI-F	90	-38	-24	28

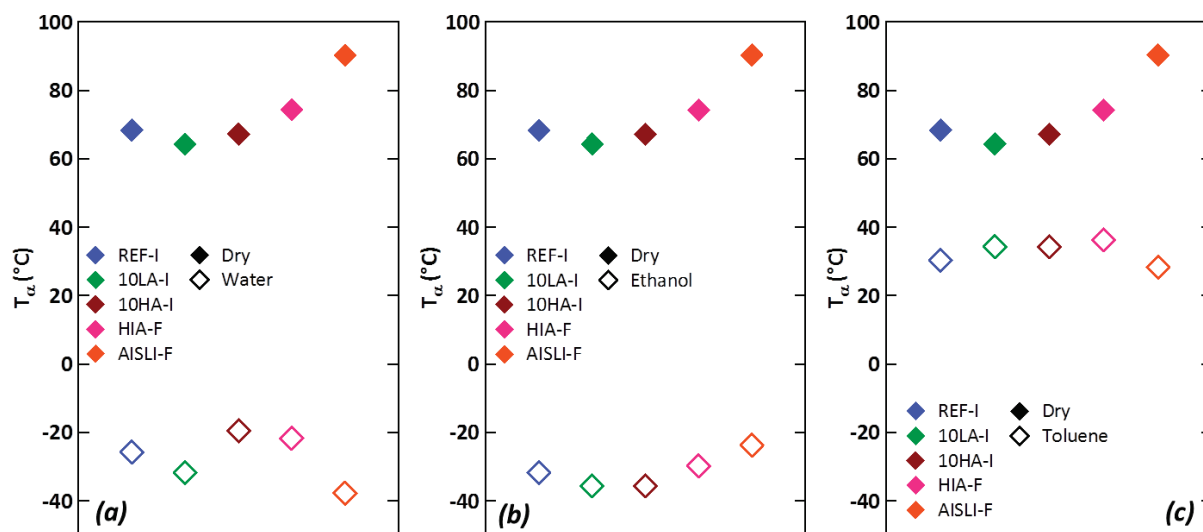


Figure 141: T_α (1 Hz) measured by BDS for the modified formulations at the dry state and conditioned in (a) water, (b) ethanol, and (c) toluene.

Figure 141 shows the measured values of T_α (1Hz) for dry and solvent-swollen samples. These results show that the T_α difference between dry and swollen states depends on both solvent nature and PA6,6 formulation. In order to better compare the effect of these solvents on the molecular mobility of the modified PA6,6 formulations, the T_α drop ($= T_{\alpha\text{-solvent}} - T_{\alpha\text{-dry}}$) provoked by these solvents was normalized by their molecular intake Δn in each formulation. The results are plotted in Figure 142.

IV. Modified PA6,6

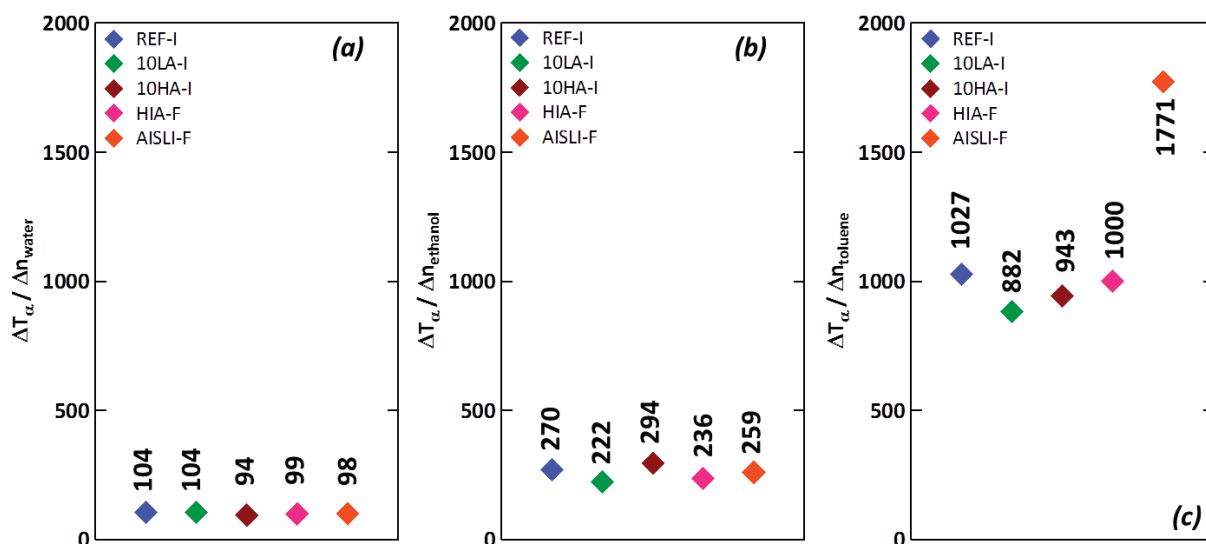


Figure 142: T_{α} drop (ΔT_{α}) normalized by the molecular intake Δn of (a) water, (b) ethanol, and (c) toluene for the modified formulations.

Figure 142a shows that water and ethanol seems to have roughly the same plasticization effect on all the formulations (i.e. close T_{α} drop/ Δn ratios for a given solvent). This suggests that solvents only interact with the amide groups of the formulations, and do not alter the initial additive/amide or co-monomer/amide interactions. However this is quite surprising in the case of AISLI because it is known that lithium sulfonate functions can interact with until 3 molecules of water [189], yielding a high water molar intake. A disruption of amide/sulfonate interactions and an associated important T_{α} drop could then be expected. But on Figure 142, T_{α} drop is normalized by the number of water molecules. If we consider that only one water molecule is enough to disturb the lithium sulfonate – amide bonds, the effective T_{α} drop would be higher than that of REF. In other words, in the case of AISLI, the water molecules may not all contribute to the plasticization effect.

Concerning toluene, Figure 142c shows that this solvent has the same plasticization effect for all formulations (T_{α} drop/ Δn ratios of ca. 1000) except for AISLI (T_{α} drop/ Δn ratio of ca. 1800). This suggests that toluene disrupts similarly the amide/amide interactions of REF, 10LA, 10HA, and HIA. In the case of AISLI, toluene appears able to disrupt the amide-sulfonate bond, yielding an important T_{α} drop.

IV.3.3. Effect of PA6,6 modification on the solvent sorption kinetics

The sorption kinetics of water, ethanol, and toluene in the modified PA6,6 formulations were then studied. 300 μm -thick injection-molded or extruded films were immersed in each solvent at room temperature (23°C) and weighed regularly so as to assess the sorption kinetics of each solvent, until the sorption equilibrium was reached. The sorption during time of each solvent was normalized to its sorption at equilibrium, which allows us to compare the sorption kinetics of different materials. Moreover, the normalized values are plotted as a function of the square root of time, which allows us to determine if the sorption kinetics correspond to a Fickian or to a Case II regime.

IV.3.3.1. Case of water

The sorption kinetics of water obtained for the five studied formulations are shown in Figure 143.

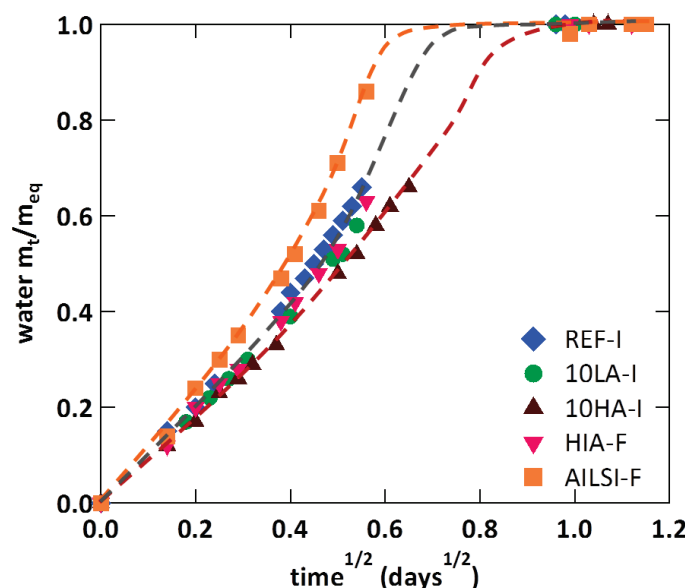


Figure 143: Water sorption kinetics at 23°C for the modified PA6,6 formulations (300 μm -thick samples). Dashed curves are guides for the eyes.

Figure 143 shows that water follows a Case II diffusion regime. Moreover it is seen that there are little differences in the sorption kinetics of water in the different formulations, except for AISLI for which the diffusion seems to be slightly faster. In the case of AISLI, this is consistent with the fact that AISLI samples are more hygroscopic than the other studied formulations, i.e. water can form strong interactions with the lithium atoms present in AISLI structure, prompting a quick sorption of this molecule in the sample.

IV.3.3.2. Case of ethanol

Ethanol sorption kinetics obtained for the five studied formulations are shown in Figure 144. It shows that ethanol follows clearly a Case II sorption regime in the samples. Also, the sorption kinetic plots show three different trends depending on the formulation. It is globally seen that the sorption of ethanol in 10LA is the fastest one, followed by REF, 10HA, and HIA that exhibit very close behaviors, and finally by AISLI, in which ethanol exhibits the slowest sorption. The observed difference might come from the fact that the formulations have different initial molecular mobilities. It is then seen that the diffusion kinetics of ethanol are conditioned by the T_g at the dry state. The dry T_g of 10LA (62°C) is lower than those of REF (71°C), 10HA (67°C), and HIA (77°C). Ethanol might then diffuse faster in 10LA than in the other three formulations at the beginning of the sorption process. It is the contrary for AISLI which has a higher dry T_g (91°C), and thus the sorption of ethanol is slower for the first part of the diffusion. Then, at some point of the sorption process, the absorbed ethanol is able to plasticize the polymer. It is observed in the plasticized regime, that ethanol exhibits roughly the same sorption kinetics in all formulations.

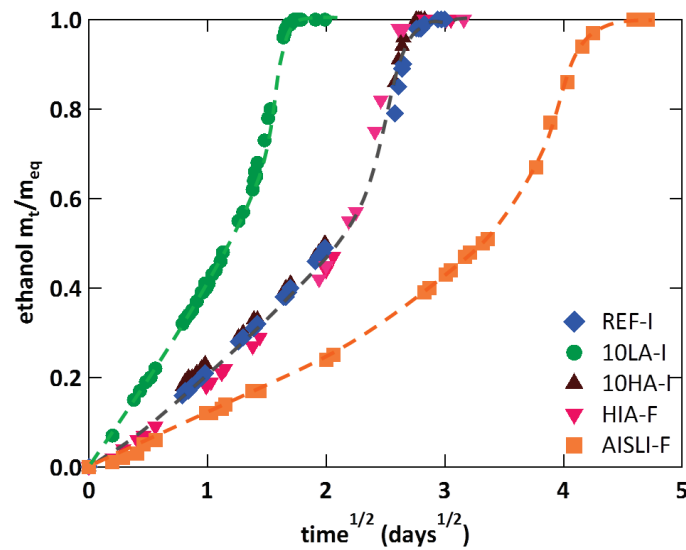


Figure 144: Ethanol sorption kinetics at 23°C for the modified PA6,6 formulations (300 μm -thick samples). Dashed curves are guides for the eyes.

IV.3.3.3. Case of toluene

Finally, the sorption kinetics assessed for toluene in the five studied formulations are shown in Figure 145.

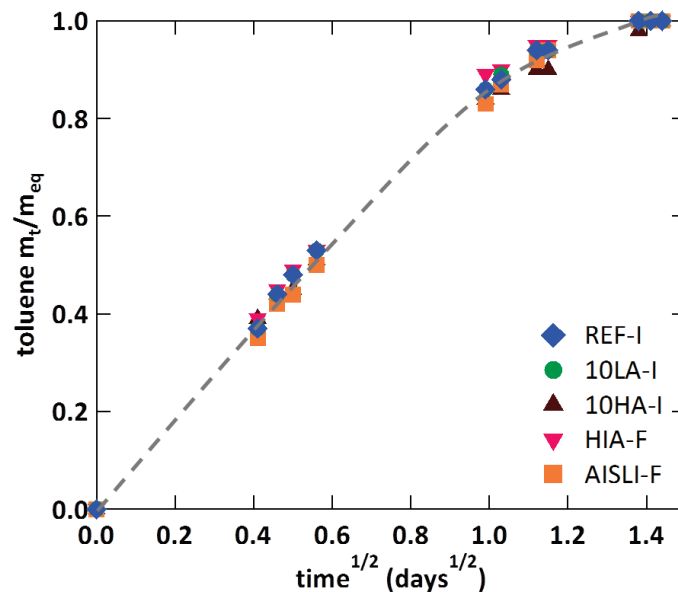


Figure 145: Toluene sorption kinetics at 23°C for the modified PA6,6 formulations (300 μm -thick samples). Dashed curve is a guide for the eyes.

Figure 145 shows firstly that toluene follows a Fickian diffusion regime in all the samples. It also seems that the toluene would diffuse through the modified formulations with very close sorption kinetics. This is an unexpected result since we would expect that similarly to the case of ethanol, the sorption kinetics of toluene would be driven by the molecular mobility of the modified formulations at the dry state. At this moment we are not able to explain or understand this phenomenon.

IV.3.4. Effect of PA6,6 modification on the solvent pervaporation kinetics

Ethanol pervaporation experiments were carried out at 40°C and RH20 on either extruded films (HIA and AISLI) or thinned injection-molded discs (REF, 10LA, and 10HA) with all samples having an average thickness of 300 μm and a surface of 5x5 cm^2 . The experimental setup used for these measurements is described in Chapter II, with the samples being weighed regularly until the steady pervaporation regime was reached. The instantaneous permeability coefficient, being the derivative of the pervaporation kinetics, is plotted in Figure 146 as a function of the thickness-normalized time.

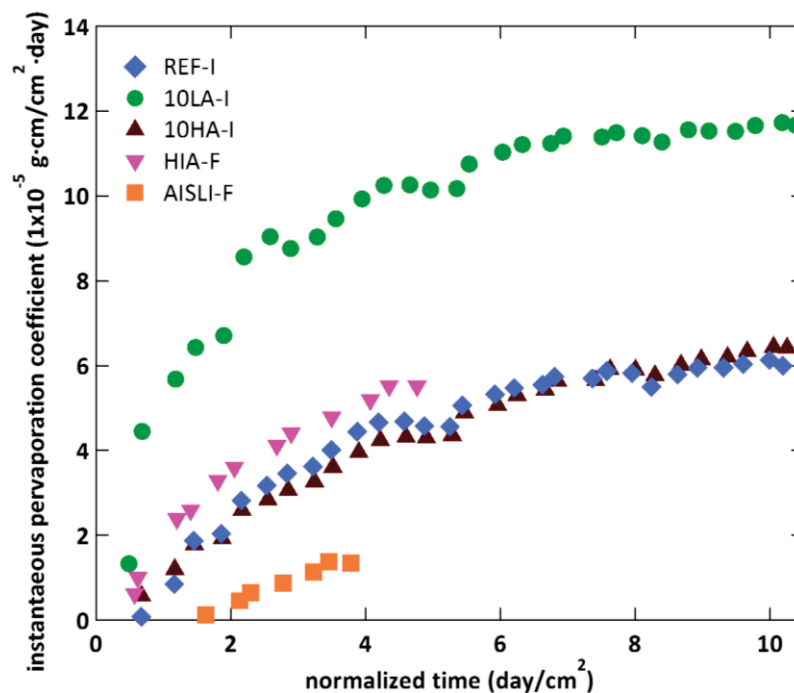


Figure 146: Ethanol instantaneous pervaporation coefficient as a function of the normalized-to-thickness time obtained at 40°C for the modified PA6,6 formulations.

The ethanol pervaporation kinetic plots shown in Figure 146 show three different trends. It is seen that the pervaporation of ethanol in 10LA is not only the fastest one (i.e. the time lag is the smallest one) but also the highest one. In the case of REF, 10HA, and HIA, these formulations have similar permeability properties to ethanol, and finally AISLI exhibits the highest time lag and the lowest permeability. The pervaporation kinetics of ethanol are in good agreement with the sorption kinetics of this solvent presented before. Figure 147 shows the pervaporation coefficient values for ethanol at 40 °C and RH20 for each studied formulation.

Figure 147 shows that 10LA exhibits a permeability coefficient to ethanol twice as large as that of REF, meaning that that 10LA samples tend to let ethanol permeate easily compared to the neat polymer. It is also observed in that HIA and 10HA have the same ethanol pervaporation coefficient than that of REF, and finally that the ethanol pervaporation coefficient of AISLI is ca. half of that of the REF, which would mean that the presence of PA6AiSLi co-monomer motifs limit the pervaporation of ethanol in PA6,6.

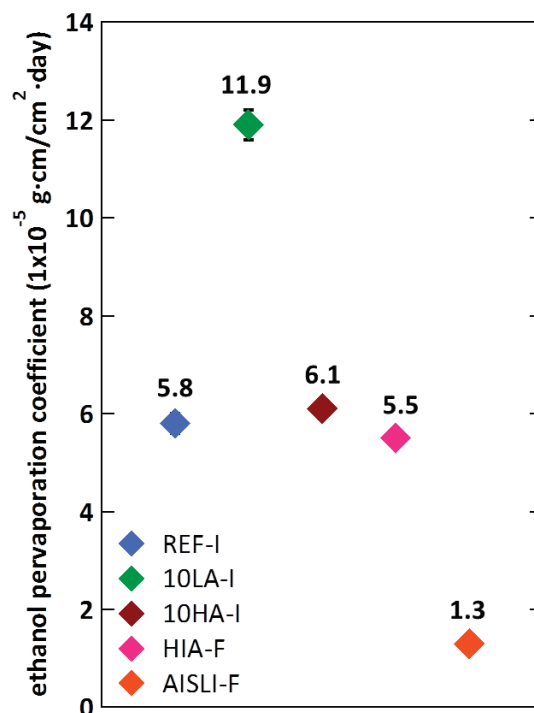


Figure 147: Ethanol pervaporation coefficients at steady pervaporation regime obtained at 40°C for the modified PA6,6 formulations.

The difference observed in the ethanol pervaporation in these samples can be discussed in regards of the sorption kinetics and the sorption at equilibrium for each of these formulations. The sorption of ethanol in PA6,6 follows a Case II regime, which means that the equality $P = D \times S$ obtained for a Fickian diffusion cannot be considered in our case (D cannot be calculated on Case II type sorption curves). Nevertheless, the pervaporation still depends on the sorption kinetics (diffusion coefficient D) and on the sorption at equilibrium (solubility S). It can be possible then to qualitatively compare the results observed for the permeability tests with those obtained by sorption experiments.

Concerning 10LA, ethanol solubility in this formulation is higher than that of REF ($\Delta n_{REF}=0.37$ v.s. $\Delta n_{10LA}=0.45$) and sorption kinetics is faster than that of REF. This might explain why the permeability coefficient of 10LA to ethanol is larger than that of REF.

In the case of AISLI, ethanol solubility in this formulation is slightly higher than that of REF ($\Delta n_{REF}=0.37$ v.s. $\Delta n_{AISLI}=0.44$) but the sorption kinetics of this solvent is much slower. The very low diffusion kinetics of ethanol in AiSLi could explain the lowest permeability coefficient for AISLI in comparison with REF.

Finally, for 10LA and HIA, the sorption kinetics and the sorption at equilibrium of ethanol are similar to that observed for REF, which could explain the similar permeability coefficient shown in Figure 147.

IV.4. Effect of PA6,6 amorphous phase molecular mobility on its mechanical properties

We were then interested in the effect of the molecular mobility of PA6,6 amorphous phase on its mechanical properties, namely the Young's modulus, the yield stress, the brittle-tough transition and the resilience on the brittle plateau. In order to vary the amorphous phase molecular mobility state, mechanical properties were assessed at different temperatures, modified PA6,6 formulations presenting different T_g 's were studied, and samples were conditioned at different hygrometry levels (RH50 and RH100) so as to obtain a wider range of molecular mobility states. The obtained results are presented and discussed hereafter.

IV.4.1. Effect of PA66 molecular mobility on its tensile strength properties

The Young's moduli E and the yield stress σ_Y of the modified PA6,6 formulations at the dry state were assessed at different temperatures (23, 45, 65, 90 and 140°C). These tensile properties were measured by the stress-strain tests described in Chapter II. Tests at different temperatures below 23°C were planned for the RH50- and the RH100-conditioned samples, but during the tests, it turned out that water condensation was formed on the samples and the extensometer could not precisely measure the strain of the samples. The values of E and σ_Y were thus not measured for the water-conditioned samples.

IV.4.1.1. Case of the Young's (tensile) modulus

Table 33 shows Young's moduli E measured for the modified formulations at different temperatures. The values of E at 140°C could not be obtained for REF, 10LA, 10HA, and HIA since at this temperature these samples were relatively viscous and the measurements were very difficult if not impossible to be carried out under such conditions.

Table 33: Young's (tensile) moduli E for the studied modified formulations at different test temperatures at the dry state. Values are given in MPa.

Formula	23°C	45°C	65°C	90°C	140°C
REF-I	3038	2700	1157	643	-
10LA-I	2608	1806	764	488	-
10HA-I	3194	2512	901	565	-
HIA-I	2988	2668	1034	550	-
AISLI-I	3117	2748	1664	670	294

It is observed in Table 33 that the Young's modulus decreases when the test temperature increases. This expected decrease can be attributed to the visco-elastic behavior of polyamide. The evolution of the Young's moduli E and the dynamic elastic moduli E' obtained at 1Hz by DMA are plotted in Figure 148 as a function of the temperature.

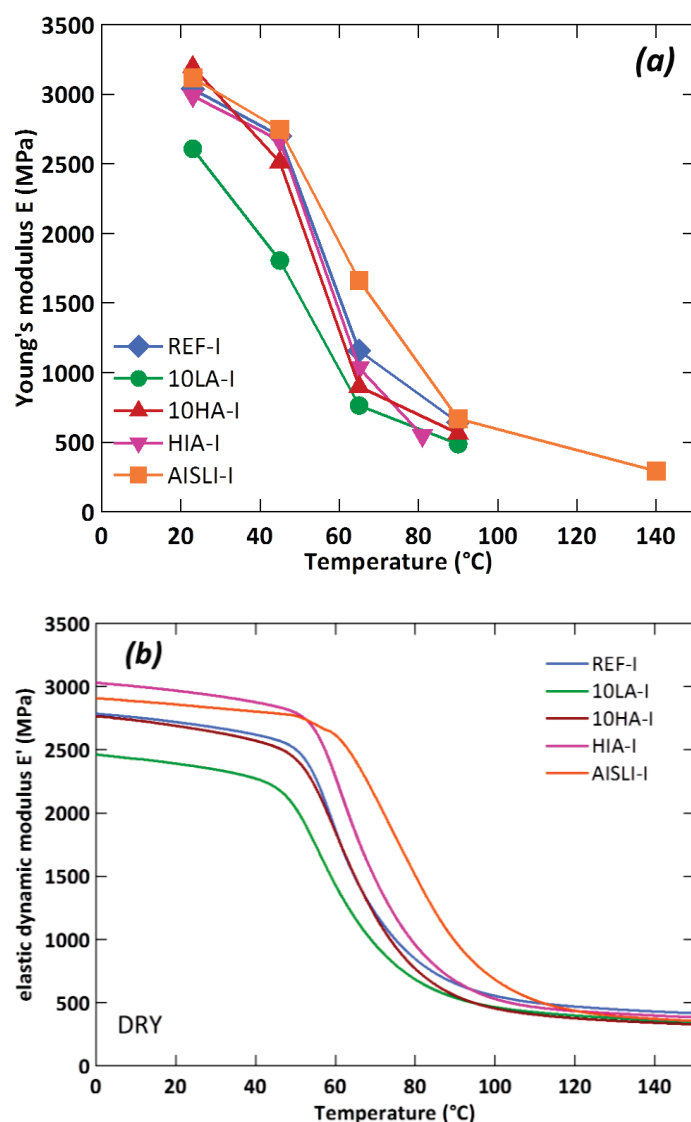


Figure 148: (a) Young's E and (b) dynamic elastic moduli E' moduli at 1Hz plotted as a function of the temperature for the injection-molded modified formulations.

Figure 148 shows that both the Young's E and the elastic E' moduli of the studied samples on the rubbery plateau are similar, probably because all the formulations have similar crystalline fractions. However the values of both E and E' on the glassy plateau differ from one formulation to the other. It is observed on DMA measurements that in comparison with REF, HIA and AISLI exhibit a higher E' , 10LA exhibits a lower E' , and 10HA exhibit an E' value close to that of REF. The value of E' at the glassy plateau depends on the crystalline ratio and the crystalline structure as well as on the molecular interactions in the amorphous phase. It might be possible that these interactions would be the responsible of the difference of values of E and E' at the glassy plateau: HIA and AISLI have aromatic functions in their chains and form strong intermolecular interactions that might make the polymer stiffer, leading to a higher elastic modulus. Concerning 10LA and 10HA, the difference in the E' values for these formulations might come from a competition between the phenyl-amide interactions and the length of the alkyl side-chains: heptanaldehyde has shorter alkyl functions and yields a higher E' value than that provoked by laurylaldehyde, whose alkyl segments are longer.

IV. Modified PA6,6

IV.4.1.2. Case of the Yield Stress

Table 34 shows the yield stress σ_Y values obtained for the five studied formulae by stress-strain tests at various temperatures (23, 45, 65°C, and 90°C). The values of σ_Y at 90°C could not be obtained for REF, 10LA, 10HA, and HIA since no yield stress was observed for these samples at such temperature.

Table 34: Yield stress σ_Y for the studied modified formulations at different test temperatures at the dry state. Values are given in MPa.

Formula	23°C	45°C	65°C	90°C
REF	85	59	56	-
10LA	63	53	44	-
10HA	-	59	48	-
HIA	87	62	50	-
AISLI	98	75	54	39

Table 34 shows that yield stress σ_Y decreases when the temperature increases, this expected trend being attributed to the visco-elastic behavior of polymers. Figure 149 shows then the yield stress σ_Y of each formula as a function of $T-T_g$, that could be, at the same state of molecular mobility. Only the σ_Y 's measured at temperatures below T_g were herein considered since beyond this temperature the polymer starts to respond as a nearly pure viscous material, the σ_Y being impossible to measure beyond a certain temperature (ca. 90°C for most samples)

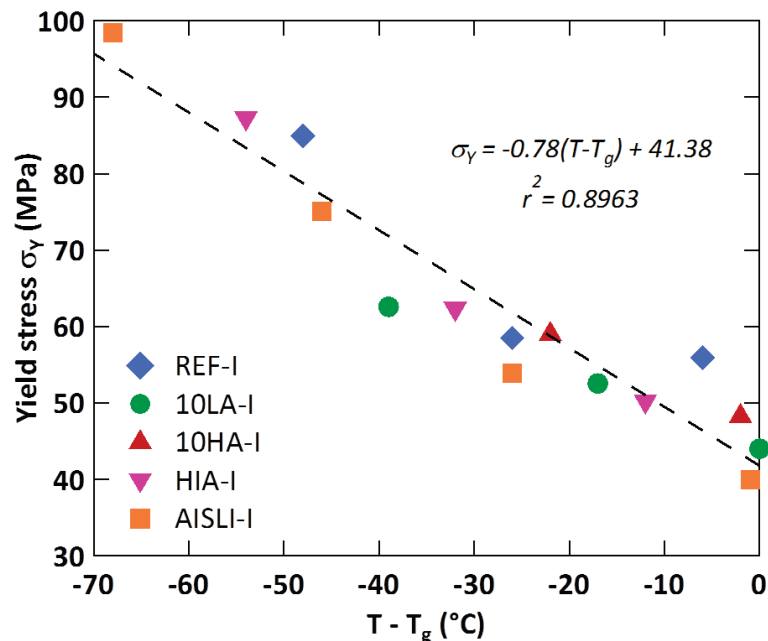


Figure 149: Yield stress σ_Y above T_g of the dry samples plotted as a function of $T-T_g$.

It can be observed in Figure 149 that the values of σ_Y for all the samples seem to follow a linear master curve. This suggests that there could be a direct linear relationship between the σ_Y and the amorphous phase molecular mobility of the studied PA6,6 formulations over a wide range of molecular mobility states. Despite some differences between the crystalline structures of the different formulations, which might lead to a modification of the

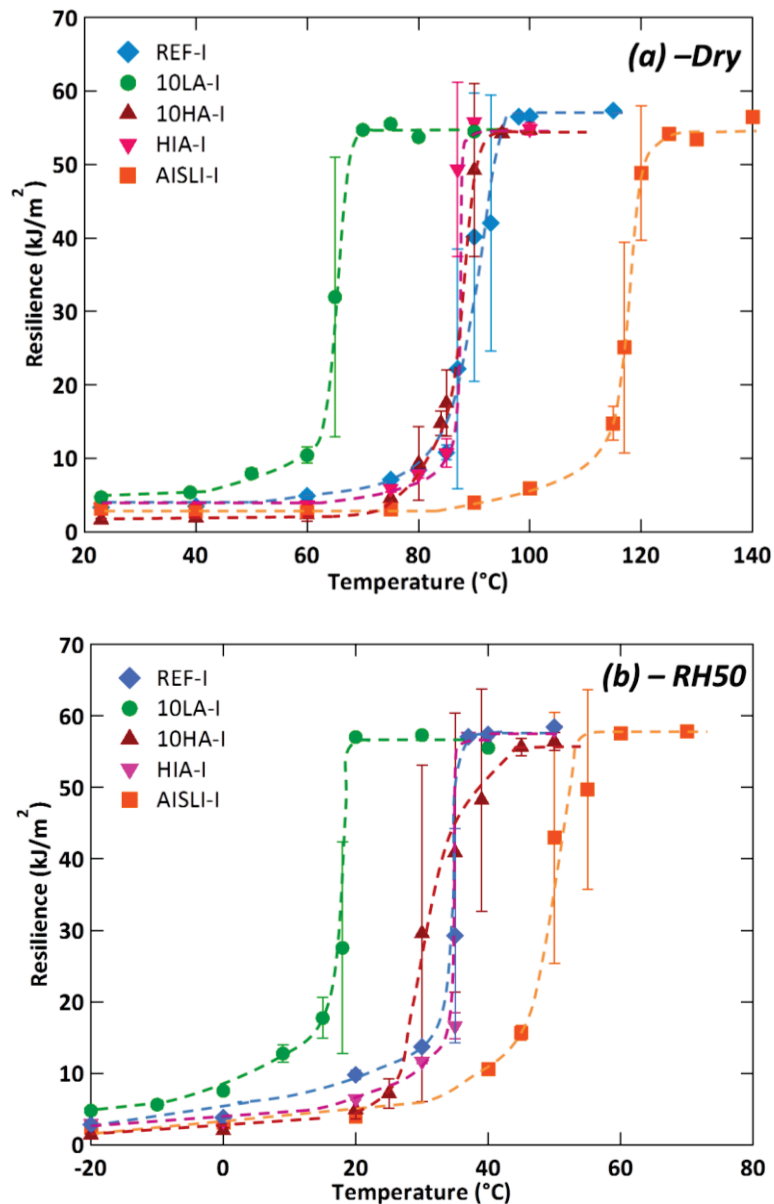
IV. Modified PA6,6

mechanical properties of polyamides as suggested for PA6 in Chapter I [145], a linear dependence of yield stress with $T-T_g$ is obtained, which suggests that yield stress seems to be mainly governed by the molecular mobility of the amorphous phase.

IV.4.2. Effect of PA66 molecular mobility on its impact strength properties

IV.4.2.1. Case of the brittle-tough transition temperature

Impact strength tests were conducted on the different formulations at different temperatures in order to assess the brittle-tough transition temperature ($T_{B/T}$). As mentioned in the experimental section, all samples were notched with a notch radius of 0.1 mm and an impact speed of 1 m/s. The formulations were evaluated in three different hygrometry degrees: dry, RH50 and RH100. Figure 150 shows respectively the brittle-tough transition curves for the five studied formulae at the (a) dry, (b) RH50, and (c) RH100-conditioning state.



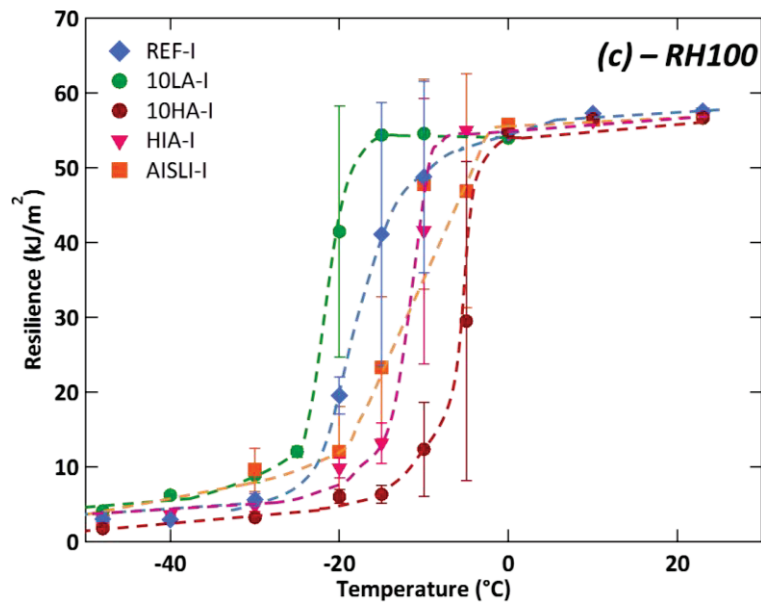


Figure 150: Brittle-tough transition curves of the modified PA6,6 formulations at (a) the dry state, (b) RH50-conditioning, and (c) RH100-conditioning. Dashed curves are guides for the eyes.

From the brittle-tough transition plots shown in Figure 150, the $T_{B/T}$'s of the five samples at dry, RH50 and RH100-conditioning states can be obtained. These values are shown in Table 37.

Table 35: $T_{B/T}$ transition temperatures obtained at the dry state, RH50-, and RH100-conditioning for the injection-molded studied formulations.

Formulation	$T_{B/T}$ –dry (°C)	$T_{B/T}$ –RH50 (°C)	$T_{B/T}$ –RH100 (°C)
REF-I	88	36	-17
10LA-I	65	18	-22
10HA-I	87	32	-5
HIA-I	86	36	-12
AISLI-I	118	47	-12

These $T_{B/T}$'s values are also plotted in Figure 151. It can be noticed that the maximum difference between the formulations decreases as hygrometry degree increases.

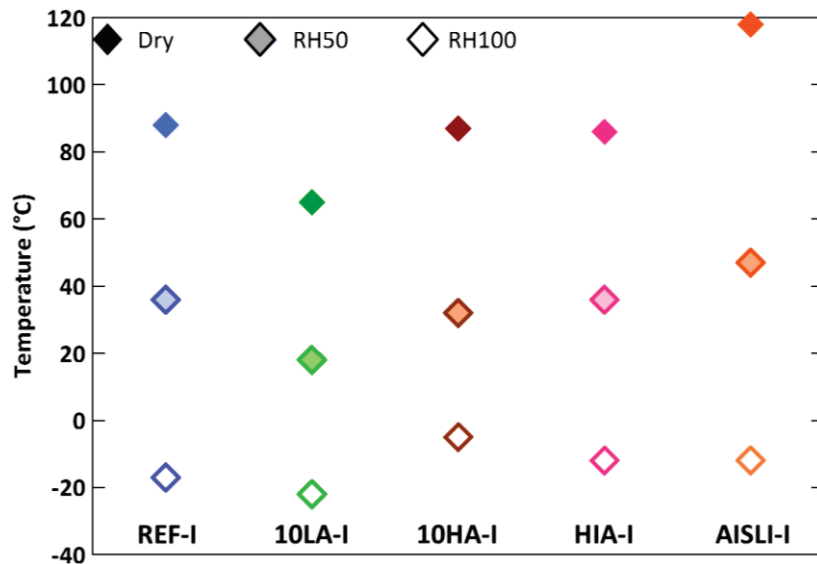


Figure 151: $T_{B/T}$ transition obtained at the dry state, RH50-, and RH100-conditioning for the injection-molded studied formulations.

The relationship between the brittle-tough transition and the glass transition was then investigated, Figure 152 showing the $T_{B/T}$ as a function of T_g for all the studied samples.

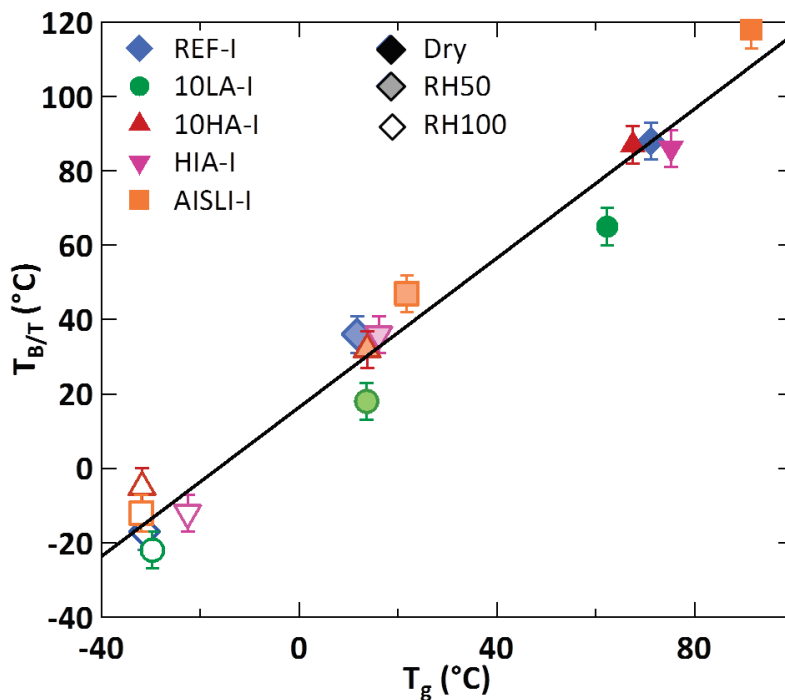


Figure 152: Brittle-tough transition temperature $T_{B/T}$ plotted as a function of the T_g for of the modified PA6,6 samples at 3 conditioning states: dry, RH50 and RH100.

It is firstly observed in Figure 152 that the $T_{B/T}$'s of all the samples seem to follow a linear relation as a function of each of the polymers T_g 's, which would mean that for a given polyamide formulation its brittle-tough transition depends directly on its molecular mobility state.

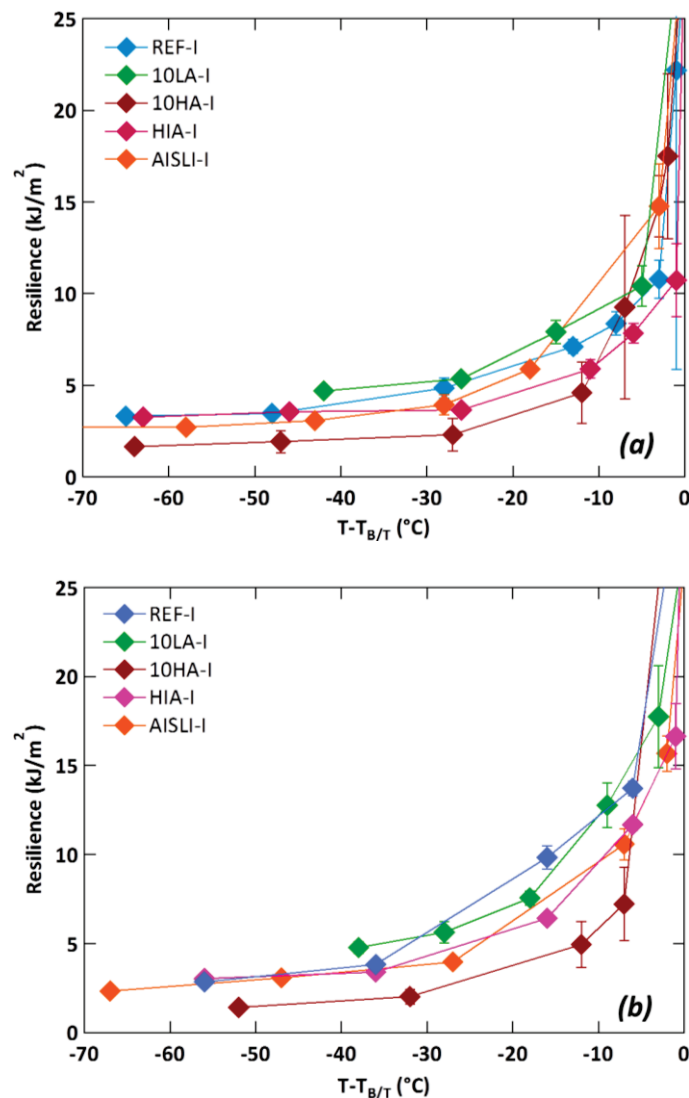
It is also observed that the $T_{B/T}$ values of the 10LA formulation are found slightly below the linear trend seen for the rest of the formulations. This means that for a given amorphous phase molecular mobility state, 10LA is closer to its brittle-tough transition than the rest of

IV. Modified PA6,6

the formulations. Internal experiments carried out at Rhodia showed that this additive macroscopically segregated from the polymer when it was introduced at 15%_{wt} or more. In this work the concentration of laurylaldehyde is of 10%_{wt} which is close to the segregation concentration. An hypothesis to explain these results would be that the laurylaldehyde might form small micelles in PA6,6. These micelles might act as stress concentrators, modifying the distribution of the stress upon impact, and decreasing the $T_{B/T}$ as do impact modifiers.

IV.4.2.2. Effect of the molecular mobility on the resilience

The values of resilience at the plateau for the modified formulations were then compared at $T-T_{B/T}$ which can be considered to be the same state of molecular mobility as $T_{B/T}$ is directly related to T_g . The values for dry, RH50-, and RH100-conditioned samples are shown in Figure 153.



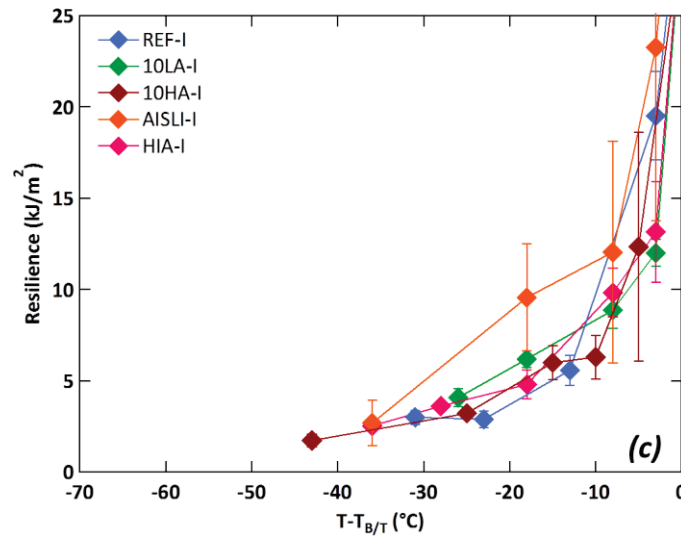


Figure 153: Resilience at the brittle plateau for the modified formulations compared at $T-T_{B/T}$ for (a) dry, (b) RH50-, and (c) RH100-conditioned samples

To better compare the modified formulations, Figure 154 shows then the resilience values at $T-T_{B/T} = -30^{\circ}\text{C}$ for the dry, RH50-, and RH100-conditioned injection-molded samples.

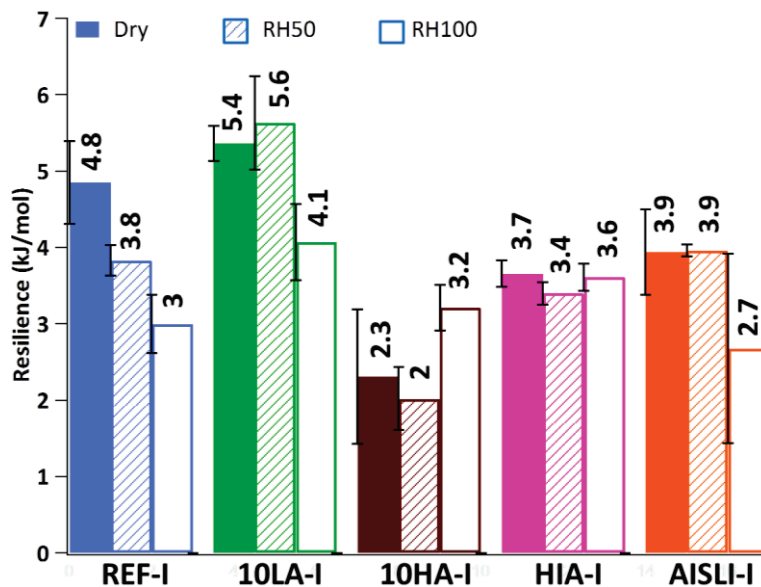


Figure 154: Resilience values of the injection-molded modified formulations compared at the same $T-T_{B/T}$ obtained at the dry state and at RH50- and RH100-conditioning.

Figure 154 shows firstly that globally the resilience of the modified formulations remains fairly constant or diminishes when water is absorbed by the samples. The drop on the resilience in presence of water may be related to the fact that when water is absorbed by polyamides, the mechanical modulus on the glassy plateau increases [2]. Water actually seems to rigidify polyamides, which means that these polymers become more brittle, and thus less energy will be needed to break polyamide samples upon impact.

It is then observed for 10HA samples that they exhibit a lower resilience value compared to REF, which might be explained by the fact that heptanaldehyde might have degraded during the formulation processing. Indeed, dark dots were observed in the 10HA formula pellets and injection-molded samples. Heptanaldehyde was introduced in the zone 4 of the extruder

IV. Modified PA6,6

(cf. Chapter II) whose temperature is around 280°C, so it might be possible that the additive was not able to stand that temperature. Thus the samples might have carbonized particles within their volume that might act charge concentrators, which would degrade the impact properties. These defects seem to not modify the other mechanical properties showed above (Young's and dynamic elastic moduli and the yields stress).

We then compared the resilience of the REF-I, 10LA-I, HIA-I, and AISLI-I dry formulations to their dynamic elastic moduli E' at the glassy plateau, as shown in Figure 155.

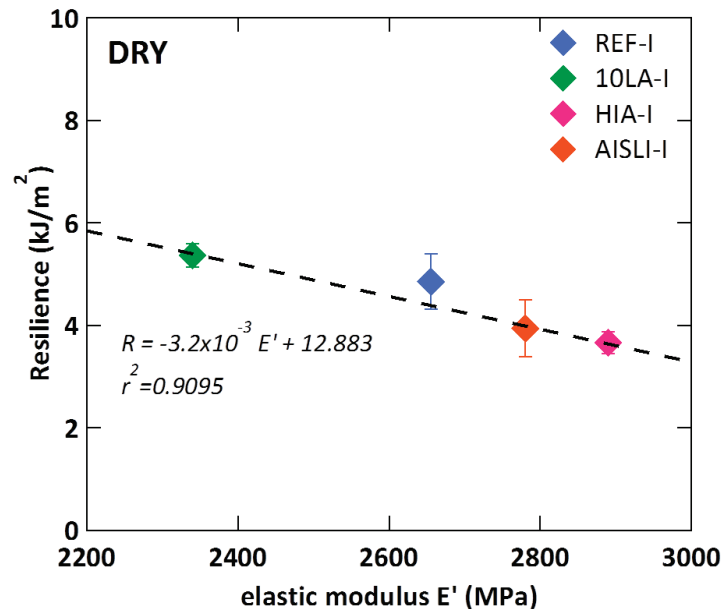


Figure 155: Resilience as a function of the elastic dynamic modulus E' at the glassy plateau for REF-I, 10LA-I, HIA-I, and AISLI-I dry formulations.

Figure 155 shows that the resilience of the studied dry formulations seem to follow a linear relation as a function of their dynamic elastic moduli E' at the glassy plateau. It is observed that for these formulations the lower their modulus, the higher their resilience. This would mean that the resilience at the brittle plateau of a given dry polyamide formulation could be linked to the value of the mechanical modulus at the glassy state.

IV.5. Compromise between impact strength and pervaporation properties

As presented in the introduction, the modified formulations were developed in order to obtain a good compromise between the impact strength and solvent pervaporation properties for the developing of suitable PA6,6-based automobile biofuel tanks.

Figure 156 shows a comparison between the resilience at the brittle plateau and the ethanol pervaporation properties of the reference formulation REF and those of the modified PA6,6 formulations. 10HA was not considered herein as it is suspected that the impact properties were affected by the degrading of the additive during the formulation processing.

IV. Modified PA6,6

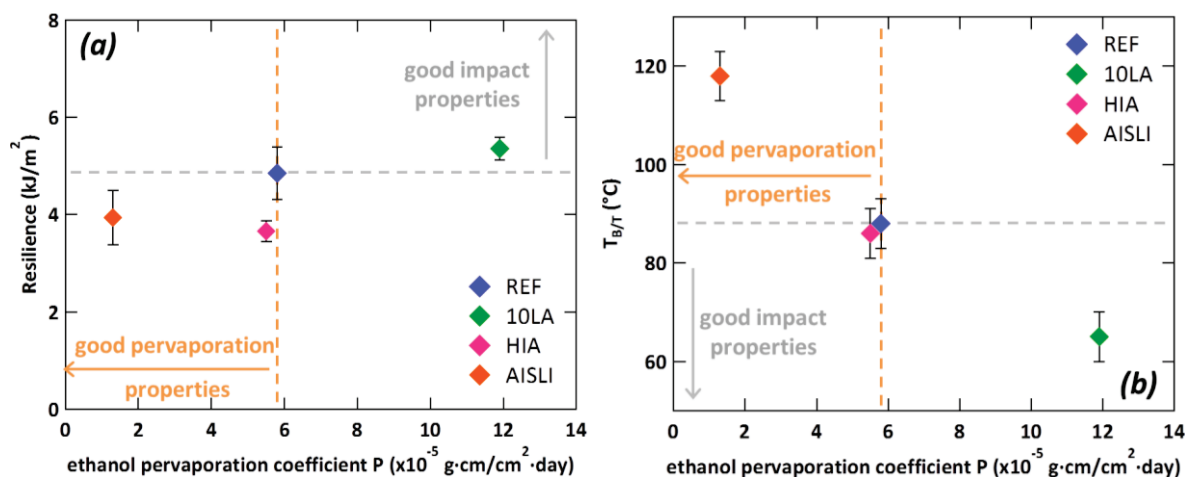


Figure 156: (a) Resilience at the brittle plateau and (b) $T_{B/T}$ of dry samples as a function of the ethanol pervaporation coefficient for REF-I, 10LA-I, HIA-I, and AISLI-I formulations.

Figure 156 shows that HIA has similar pervaporation properties as REF but the impact properties, namely the resilience is lower. Moreover, AISLI shows better pervaporation properties than REF but both the resilience and the $T_{B/T}$ are degraded for this formulation. Finally it is observed that 10LA shows an improved impact strength behavior and $T_{B/T}$ but the pervaporation properties of this formulation are degraded, which was unexpected as laurylaldehyde was designed to interact with amide functions and block them for preventing polar solvents to interact with these functions. To sum up, a good compromise between the impact strength and pervaporation properties by modifying PA6,6 was not obtained.

IV.6. Conclusion

In this chapter the effect of PA6,6 modification on barrier and mechanical properties was studied. Two additivated formulations: PA6,6 + 10%_{wt} laurylaldehyde (10LA) and PA6,6 + 10%_{wt} heptanaldehyde (10HA), two copolymers: PA6,6/6HIA 95/5_{mol} (HIA) and PA6,6/6AiSLi 95/5_{mol} (AISLI), and a neat PA6,6 (REF) were studied.

The effect of polyamide modification on the crystalline phase was firstly studied. It was observed that the introduction of modifiers in PA6,6 diminishes the overall crystalline ratio X_C of PA6,6. The presence of modifiers provokes a drop of the melting T_m and crystallization T_c temperatures, and also induces a widening on these processes' kinetics, the effect being more pronounced for co-monomers than for additives. Finally it was observed that the additives and co-monomers induced a variation on the crystalline structure of PA6,6, although the variation on the crystalline structure could also result from the processing technique (injection-molding or film cast extrusion) used to obtain the samples.

Then, the effect of additives or co-monomers on the molecular mobility of PA6,6 amorphous phase studied. The laurylaldehyde additive was found to induce a drop on PA6,6 T_g , as this additive is bulky and might act as a chain spacers, even if it is able to interact strongly with the amide groups of PA6,6. The heptanaldehyde additive was found to yield a similar molecular mobility state, probably because there is equilibrium between the anti-plasticizing effect of creating strong phenol-amide bonds and the plasticizing effect of the alkyl chains of the additive that might act as chain spacers. These additives also decrease the temperature and the activation energy of the β relaxation as well, which might mean that

IV. Modified PA6,6

they are able to disturb locally the amide functions of PA6,6. It was observed that PA6AiSLi and PA6HIA co-monomers induced a raise in T_g because of the presence of aromatic moieties in their structures and also because these co-monomers can form strong H bonds with the amide groups through the phenyl (HIA) or lithium sulfonate (AISLI) functions borne by these co-monomers. Moreover PA6AiSLi was observed to provoke a widening on the loss dynamic modulus E'' peak associated to the α relaxation which might be the signature of an important variation of intermolecular interactions within PA6,6 chains provoked by the presence of this co-monomer. It was observed also that the co-monomers did not modify the β relaxation.

The barrier properties of the modified formulations were studied. The sorption properties of these modified formulations to water, ethanol, and toluene were firstly assessed. Concerning water intake, it was observed that the intake of this solvent in AISLI was larger than in the other formulations, since water and the lithium sulfonate groups of AISLI can interact strongly with amides, forming complexation bonds. In the case of ethanol, it was observed that 10LA, HIA, and AISLI absorbed this solvent in larger amounts than REF or 10HA, probably because the additives (10LA) or aromatic moieties (HIA, AISLI) act as chain spacers, increasing the accessibility of amide functions. 10HA might also act as a chain spacer but an increase in ethanol intake was not observed for this formulation. Finally it was observed that the presence of modifiers had no effect on the sorption of toluene, maybe because the space created by the presence additives or co-monomers is not large enough to allow this solvent to be further absorbed by the polymer.

Then, the plasticization effect of water, ethanol, and toluene on the modified formulations was assessed by Dielectric Spectroscopy. In the case of REF, 10LA, 10HA and HIA, similar T_{α} drop were observed in presence of the three solvents, suggesting that solvents do not disturb the additive/amide or co-monomer/amide interactions. In the case of AISLI the plasticization effect of toluene is twice as large as that of the other formulations, suggesting that toluene disturbs the amide/sulfonate interactions that are partially responsible for the high T_g of this formulation. The signature of the amide/sulfonate disruption was not observed in the case of water or ethanol, but in the case of water, the high amount of water molecules could underestimate the observed plasticization effect.

The sorption kinetics of water, ethanol, and toluene in the modified polymers were also studied. It was observed that water diffused through a Case II regime, and that no differences of sorption kinetics were observed from one formulation to another, except for AISLI, in which the sorption was slightly quicker since AISLI is highly hygroscopic. Concerning ethanol, it was observed that this solvent was also able to plasticize the studied formulations and diffused with a Case II regime. However it was observed that the diffusion at the Fickian regime of ethanol, i.e. before plasticization, depended on the initial molecular mobility state of the polymer: the higher the T_g at the dry state, the faster the diffusion in the initial Fickian regime. Finally, in the case of toluene, Fickian behaviors were observed, suggesting as already observed in Chapter III that this solvent was not able to plasticize the modified formulations during sorption. Surprisingly, toluene exhibits similar sorption kinetics in all the formulations, and these sorption kinetics do not seem to be driven by the initial (dry) molecular mobility state of the formulation.

The permeability properties of these formulations were studied solely for ethanol. It was observed that 10LA had the largest permeability coefficient, AISLI the smallest one, and that

IV. Modified PA6,6

REF, 10HA, and HIA showed similar coefficients. These results are correlated to the results obtained from the solvent sorption and solvent kinetics experiments. In the case of large solvent uptake and fast kinetics, permeability is high (i.e.10LA). On the contrary, very slow sorption kinetics induces a low value of permeability (i.e. AISLI).

We then studied the mechanical properties at the dry state of the modified formulations, namely the Young's modulus E , the dynamic elastic modulus E' , and the yield stress σ_y . It was firstly observed that the values of the Young's and dynamic elastic moduli at the glassy regime depended on the interactions between PA6,6 and the added modifiers. HIA and AISLI rigidify PA6,6 because of the presence of aromatic functions in their structure and because of the strong intermolecular interactions formed between these co-monomers and PA6,6. 10LA and 10HA provoke a drop on the modulus because the added additives raise the mobility of the polymer through steric effects, even if these additives are able to strongly interact with the amide groups of PA6,6. Furthermore, concerning the yield stress σ_y , it was observed that at $T-T_g$ the values of σ_y for all the samples seem to follow a master curve at same state of mobility, which would mean that despite some differences in the crystalline structure, the yield stress σ_y for any of the studied samples is similar at the same state of molecular mobility.

The impact strength properties of the modified polymers were also studied. Dry samples as well as formulations conditioned at RH50 and RH100 were considered so as to obtain three different molecular mobility states. The brittle-tough transition temperatures $T_{B/T}$ were obtained for these formulations by conducting Charpy impact tests. The measured $T_{B/T}$'s were then compared to the T_g 's obtained by DSC for these formulations. It was observed that for a given formulation there was a linear dependence of $T_{B/T}$ with T_g , which would mean that for a given polyamide, its brittle-tough transition depends directly on its molecular mobility state. It was also observed that 10LA had lower $T_{B/T}$ values when compared to the other formulations, which fell within the same trend or master curve linking $T_{B/T}$ with T_g . This might be because laurylaldehyde might form micelles that might act as stress concentrators which would modify the distribution of the stress during an impact and thus decrease its $T_{B/T}$.

Finally the impact resilience at $T-T_{B/T}$ in the brittle plateau of dry and water-conditioned samples was also studied. It was observed that when water was absorbed by the modified formulations the resilience diminished, probably because water rigidifies PA6,6 at the glassy regime provoking the formulations to become more brittle. It was also found that for the dry formulations, their resilience at the brittle plateau seem to follow a linear relation as a function of their dynamic elastic moduli E' at the glassy plateau which would mean that the resilience of a given dry polyamide might be linked to the mechanical modulus at the glassy state.

As it was of great interest for the applicative context of this thesis, the compromise between barrier and impact properties of the modified formulations was also treated. At the end of this Chapter, a comparison between the impact and barrier properties of the modified polymers was done. It was found that none of the studied formulations exhibits a satisfying compromise between these two properties. It was observed that AISLI which had good barrier properties to ethanol had a bad impact strength behavior and 10LA which exhibited good impact properties had bad pervaporation properties to ethanol. The other

IV. Modified PA6,6

formulations had similar permeability and impact strength properties to those of the reference.

General conclusion

This PhD thesis was performed within an applicative context dealing with the development of Polyamide 6,6 (PA6,6) formulations suitable for manufacturing automotive gasoline tanks. These formulations should have good barrier properties to biofuels, composed of hydrocarbons and ethanol, while keeping a high impact resistance. Within this general context, one of the main scientific objectives of this work was the better understanding of the molecular interactions of PA6,6 with polar or non-polar solvents, or mixtures of solvents modeling biofuels. We were then interested in the effect of these solvents and mixtures on PA6,6 amorphous phase molecular dynamics, especially on the glass transition temperature T_g . Finally, we were interested in the influence of this change of molecular mobility on the mechanical properties of PA6,6. In this work, neat PA6,6 was studied as well as modified PA6,6 materials in which intermolecular interactions were modified by chemical functionalization of the PA6,6 chain or by additivation.

In the first part of this work, the sorption of a series of pure polar and non-polar solvents in neat PA6,6 was studied. Small polar molecules are the most absorbed ones. The polar solvent solubility decreases with the size and the associated decrease of polarity of the molecule. The solubility decreases down to a low solvent sorption value similar to that obtained for the non-polar solvents, for which the solubility does not seem to depend on the molecular volume (within the range of molecular volumes studied). These results suggest that the polarity of the molecule is in the case of PA6,6, the main driver of solvent solubility.

The sorption results have been discussed in relation to the presence of a H bond network between the amide functions acting as “physical crosslinks” which limit solvent equilibrium sorption.

The effect of pure polar and non-polar solvents on the glass transition temperature T_g of PA6,6 was then studied. It is observed that water, the alcohol series, and toluene have different plasticization abilities in PA6,6 and that, somehow surprisingly, *toluene has the strongest plasticization effect when referred to its absorbed molar amount per amide function*.

The plasticization effects of the studied solvents, that is their effect on PA6,6 molecular mobility, have been discussed. Water and ethanol, and more generally polar solvents, would be able to disrupt amide-amide H bonds and form H bonds with amide groups, accelerating molecular mobility by disturbing the H-bond network and decreasing the H bonds lifetime. Toluene, and more generally non-polar solvents, are also able to locally disrupt H bonds and modify the dynamics because their molecular volume is comparable to that of PA6,6 monomeric unit. Further molecular simulations have to be undertaken in order to better understand the plasticizing effect of toluene. Thus, in this part, the strong plasticization effect of non-polar solvents in PA6,6 has been observed and discussed for the first time.

The sorption kinetics of water, ethanol, and toluene in PA6,6 were then studied. It is observed that toluene follows a Fickian regime, that water exhibits a pseudo-Fickian regime, and that ethanol follows a Case II sorption kinetics. Moreover it was observed that the diffusion of toluene was faster than that of ethanol in the Fickian regime.

These various regimes were discussed in terms of combined diffusion and plasticization phenomena in the polymer. At the studied temperature, toluene does not plasticize PA6,6 while diffusing. Water and ethanol plasticize the polymer with different kinetics though. A theoretical/numerical model is being developed in our laboratory to model these different regimes. It includes the solvent diffusion dynamics (which depend on solvent concentration) and the plasticization kinetics of the polymer matrix.

The sorption of a series of ethanol-toluene-isooctane (EX) mixtures by PA66 was then studied. The chemical activities of each of the species composing these mixtures were measured for all compositions. They are found to be relatively high, due to the fact that these mixtures are *strongly non-ideal*. This non-ideality is a consequence of repulsive effects between ethanol and hydrocarbon molecules within the mixtures. Then, PA6,6 samples were put in contact with these mixtures and the absorbed amounts of each component in PA6,6 were quantified. The sorption of ethanol in these samples was compared to that of pure ethanol obtained at a given ethanol activity. It is found that the presence of toluene in PA6,6 samples in contact with solvent mixtures induced an increase of ethanol intake, which shows that toluene strongly affects PA6,6 molecular dynamics through steric effects (i.e. relatively bulky molecule) even at relatively low content as described above. Concerning the effect of ethanol-toluene-isooctane mixtures on PA6,6 T_g , it is observed that the drop of PA66 T_g swollen in EX mixtures is mainly due to the presence of ethanol in the polymer despite the presence of toluene in the samples.

In the second part of this thesis, the effects of additivating or chemically modifying PA6,6 on the molecular mobility, the solvent sorption, and the mechanical properties were studied. Five materials comprising two additivated PA6,6 (10LA, 10HA), two copolymers (HIA, AISLI), and a neat polymer (REF) were considered.

It is observed that the additives or co-monomers have an effect on PA6,6 molecular mobility and the relaxation processes, namely the T_g and the β relaxation, by modifying the chemical structure of the polymer and/or by interacting with the amide functions borne by PA6,6 chains. PA6AiSLi and PA6HIA co-monomers (AISLI and HIA) induce a raise in T_g both by introducing rigid aromatic moieties and by forming stronger H bonds with the amide groups. However these co-monomers do not modify the β relaxation. The peak in the loss dynamic modulus E'' associated to the α relaxation widens for AISLI when compared to the other materials. This might be the signature of an increased heterogeneity of intermolecular interactions within PA6,6 chains provoked by the presence of this co-monomer. The lauryl- and heptanaldehyde additives (10LA and 10HA) are found to provoke a drop on PA6,6 T_g as well as provoking a decrease on the temperature and the activation energy of the β relaxation. These additives interact with the amide functions and they are bulky and might act as chain spacers, modifying the molecular mobility of the polymer.

The sorption of water, ethanol and toluene was studied in the modified PA6,6 materials. It is observed that the intake of water in ASLI was larger than in the other formulations since water and the lithium sulfonate groups of AISLI can interact strongly forming complexation bonds. Concerning ethanol, it is observed that 10LA, HIA, and AISLI absorb this solvent in larger amounts than REF or 10HA, maybe because the presence of additives (10LA) or an aromatic backbone (HIA, AISLI) acting as chain spacers, increasing the accessibility of amide

Conclusion

groups in PA6,6 chains. Finally it is observed that the presence of modifiers has little or no effect on toluene sorption.

The plasticization effect of water, ethanol, and toluene on the modified materials was also studied. Similar T_g drops are observed for REF, 10LA, 10HA and HIA in presence of these solvents. This suggests that these solvents do not disturb the modifier/amide interactions. However, AISLI absorbs a much large amount of water than the other materials, but nevertheless the absolute plasticization effect does not increase in proportion. Moreover, the plasticization effect of toluene in AISLI is twice as large as that observed on the other formulations, suggesting that toluene might disturb the amide/sulfonate interactions responsible for the high T_g of this formulation.

The effect of the amorphous phase molecular mobility on PA6,6 mechanical properties was then characterized in the modified PA6,6 formulations, at different temperatures and different hygrometry levels. The yield stress σ_Y of these formulations at the dry state were compared at $T-T_g$ which was considered to be a parameter representative of a given state of molecular mobility. It is observed that the yield stress σ_Y depends linearly on $T-T_g$ for all formulations, which would mean that, despite some differences in the crystalline structure, the σ_Y for any of these formulations is similar at the same state of molecular mobility. *Concerning impact strength, a linear dependence of the brittle-tough transition temperature $T_{B/T}$ with T_g is observed for each formulation. This would mean that for a given polyamide formulation, its brittle-tough transition is directly related to the amorphous phase molecular mobility.* All the formulations but one (10LA) are aligned in a single master curve. The $T_{B/T}$'s measured for the 10LA formulation are found to be under this curve. This might be explained by the possibility that the additive might not be fully miscible and form clusters in the polymer that would act as stress concentrators, enhancing the impact properties behavior of this formulation. Moreover a decreasing linear relation between the resilience at the brittle plateau and the dynamic elastic moduli E' in the glassy state of all dry formulations is observed.

The pervaporation kinetics of PA6,6 modified formulations were studied for ethanol. It was observed that the results obtained from these experiments are well correlated to the results obtained from the solvent sorption and solvent kinetics experiments: it is observed that if ethanol is absorbed in large amounts and with fast kinetics, the permeability of this solvent is high (10LA). Conversely if the sorption kinetics of ethanol are slow, the permeability of ethanol in this formulation is reduced (AISLI).

Furthermore, as it is of a great interest for the applicative context of this thesis, the compromise between barrier and impact properties of the modified formulations was also discussed. Unfortunately, no satisfying compromise was obtained: the formulation exhibiting the best barrier properties turned out to exhibit a bad impact strength behavior (AISLI), the formulation exhibiting the best impact properties turned out to exhibit bad pervaporation properties (10LA). Indeed, both properties require antagonistic properties, as regards the molecular mobility state.

This thesis has been the first one in our laboratory devoted to this axis. It is clear that the full understanding of the observed properties will require further investigations both experimentally (e.g. influence of temperature on solvent sorption) and theoretically/numerically (e.g. molecular dynamic simulations to get a precise description at

Conclusion

the molecular scale). Nevertheless, the studies carried out and the results and conclusions observed in this thesis concerning the effect of solvents and modifiers on the molecular mobility, the barrier, and the mechanical properties of PA6,6, might be useful for designing more efficient structural modifications of PA6,6 in order to obtain a good compromise between barrier and mechanical properties for biofuel automotive tank applications.

References

1. *Plastics – The Facts 2010*, http://www.plasticseurope.org/documents/document/20101006091310-final_plasticsthefacts_28092010_lr.pdf, last consulted on June 19th, 2012.
2. M.L. Kohan, *Nylon Plastics Handbook*, Carl Hanser Verlag, Munich (1995).
3. V. Miri, S. Elkoun, E. Peurton, C. Vanmansart, J.-M. Lefebvre, P. Krawczak, and R. Séguela, Crystallization Kinetics and Crystal Structure of Nylon6-Clay Nanocomposites: Combined Effects of Thermomechanical History, Clay Content, and Cooling Conditions, *Macromolecules*, **41**, 9234 (2008).
4. V. Miri, O. Persyn, R. Séguela, and J.-M. Lefebvre, On the deformation induced order-disorder transitions in the crystalline phase of polyamide 6, *Eur. Polym J.*, **47**, 88 (2011).
5. C.W. Bunn and E.V. Garner, The Crystal Structures of Two Polyamides ('Nylons'), *Proc. R. Soc. Lond. A*, **189**, 39 (1947).
6. A. Ziabicki, Über die mesomorphe β -Form von Polycapronamid und ihre Umwandlung in die kristalline Form α , *Kolloid Z.*, **167**, 132 (1959).
7. L.A. Fillot, *Literature review on polyamide amorphous phase molecular mobility*, Rhodia Internal Report #090166348011def4 (2008).
8. C. Vergelati, *Modélisation du rôle de l'eau dans l'évolution structurale du polyamide 6,6*, Rhodia Internal Report #43400 (1990).
9. F.L. Beyer and C. Ziegler, *Wide-Angle X-Ray Scattering Characterization of the Morphology of Nylon 6 6 Obturator Materials*, U.S. Army Research Laboratory Report, August 2004.
10. E.S. Clark, C.A. Garber, Effect of Industrial Processing on the Morphology of Crystalline Polymers, *Int. J. Polym. Mater.*, **1**, 31 (1971).
11. A. Owen, R. Bonart, Cooperative relaxation processes in polymers, *Polymer*, **26**, 1034 (1985).
12. H.M. Le Huy and J. Rault, Remarks on the α and β transitions in swollen polyamides, *Polymer*, **35**, 136 (1994).
13. R. Diaz-Calleja, E. Riande, Comparative study of mechanical and dielectric relaxations in polymers, *Materials Science and Engineering A*, **370**, 21 (2004).
14. J. Brandrup and E.H. Immergut, *Polymer Handbook Third Edition*, John Wiley & Sons, New York (1989).
15. K.J. Laidler, A Glossary of Therms Used in Chemical Kinetics, Including Reaction Dynamics, *Pure & Appl. Chem.*, **68**(1), 149 (1996).
16. H. Vogel, Das temperaturabhängigkeit gesetz der viskosität von flüssigkeiten, *Phys. Z.*, **22**, 645 (1921).
17. G.S. Fulcher, Analysis of Recent Measurements of the Viscosity of Glasses, *J. Am. Ceram. Soc.*, **8**, 339 (1925).
18. G. Tammann and W. Hesse, Die Abhängigkeit der Viskosität von der Temperatur bei unterkühlten Flüssigkeiten, *Z. Anorg. Allg. Chem.*, **156**, 245 (1926).

References

19. M.L. Williams, R.F. Landel, and J.D. Ferry, The Temperature Dependence of Relaxation Mechanisms in Amorphous Polymers and Other Glass-forming Liquids, *J. Am. Chem. Soc.*, **77**, 3701 (1955).
20. D. Garcia and H.W. Starkweather, Hydrogen Bonding in Nylon 66 and Model Compounds, *J. Polym. Sci. Part B: Polym. Phys.*, **23**, 537 (1985).
21. E. Bessler and G. Bier, Über Wasserstoffbrücken in Polyamiden, *Makromol. Chemie*, **122(1)**, 30 (1969).
22. L.R. Schroeder and S.L. Cooper, Hydrogen bonding in polyamides, *J. Appl. Phys.*, **47(10)**, 4310 (1976).
23. D.J. Skrovanek, S.E. Howe, P.C. Painter, and M.M. Coleman, On the validity of a Commonly Employed Infrared Procedure Used to Determine Thermodynamic Parameters Associated with Hydrogen Bonding in Polymers, *Macromolecules*, **18**, 299 (1985).
24. D.J. Skrovanek, S.E. Howe, P.C. Painter, and M.M. Coleman, Hydrogen Bonding on Polymers: Infrared Temperature Studies of an Amorphous Polyamide, *Macromolecules*, **18**, 1676 (1985).
25. N.E. Triggs, R.T. Bonn, and J.J. Valentini, Do All Solid Amides Hydrogen Bond? Raman Evidence to the Contrary, *J. Phys. Chem.*, **97**, 5535 (1993).
26. J. Hirschinger, H. Miura, K.H. Gardner, and A.D. English, Segmental Dynamics in the Crystalline Phase of Nylon 66: Solid-State ^2H NMR, *Macromolecules*, **23**, 2153 (1990).
27. H. Miura, J. Hirschinger, and A.D. English, Segmental Dynamics in the amorphous phase of Nylon 66: Solid-State ^2H NMR, *Macromolecules*, **23**, 2169 (1990).
28. A. Xenopoulos and B. Wunderlich, Thermodynamic Properties of Liquid and Semicrystalline Linear Aliphatic Polymides, *J. Polym. Sci. Part B: Polym. Phys.*, **28**, 2271 (1990).
29. S. Havriliak and S. Negami, A Complex Plane Representation of Dielectric and Mechanical Relaxation Processes in Some Polymers, *Polymer*, **8**, 161 (1967).
30. B. Wunderlich, Reversible Crystallization and the Rigid-Amorphous Phase in Semicrystalline Macromolecules, *Prog. Polym. Sci.*, **28**, 383 (2003).
31. M. Takayanagi, K. Hoashi, S. Minami, and H. Yasuda, Some Features of Viscoelastic Behavior and Crystalline Texture of Poly- α -olefins, *Rept. Prog. Polym. Phys.*, **6**, 121 (1963).
32. G. Rotter and H. Ishida, Dynamic Mechanical Analysis of the Glass Transition: Curve Resolving Applied to Polymers, *Macromolecules*, **25**, 2170 (1992).
33. P. Pengtao and P. Cebe, ^{13}C N.M.R. Study of Phase Heterogeneity in Poly(phenyl sulphide), *Polymer*, **33(23)**, 4913 (1992).
34. L. D. Landau and E. M. Lifchitz, *Statistical Physics Vol. V Theoretical Physics*, Mir Editions, Moscow (1967).
35. P.J. Flory, *Principles of Polymer Chemistry*, Cornell University Press, Ithaca (1953).
36. P.G. Nilsson and B. Lindman, Water Self-Diffusion in Nonionic Surfactant Solutions, Hydration and Obstruction Effects, *J. Phys. Chem.*, **87**, 4756 (1983).
37. I. Mills, T. Cvitas, K. Homann, N. Kallay, and K. Kuchitsu, *IUPAC Quantities, Units and Symbols in Physical Chemistry 2nd Edition*, Blackwell Science, Oxford (1993).

References

38. I. Langmuir, The constitution and fundamental properties of solids and liquids. Part I. Solids, *J. Am. Chem. Soc.*, **38(11)**, 2221 (1916).
39. R. S. Hanson and R. P. Craig, The Adsorption of Aliphatic Alcohols and Acids from Aqueous Solutions by Non-Porous Carbons, *J. Phys. Chem.*, **58**, 211 (1954).
40. B.L. Dunicz, Surface Area of Activated Charcoal by Langmuir Adsorption Isotherm, *J. Chem. Ed.*, **38**, 357 (1961).
41. M.L. Huggins, Solutions of Long Chain Compounds, *J. Chem. Phys.*, **9(5)**, 440 (1941).
42. P.J. Flory, Thermodynamics of High Polymer Solutions, *J. Chem. Phys.*, **10(1)**, 51 (1942).
43. P.J. Flory, R.A. Orwoll, and A. Vrij, Statistical Thermodynamics of Chain Molecule Liquids. I. An Equation of State for Normal Paraffin Hydrocarbons, *J. Am. Chem. Soc.*, **86(5)**, 3507 (1964).
44. P.J. Flory, R.A. Orwoll, and A. Vrij, Statistical Thermodynamics of Chain Molecule Liquids. II. Liquid Mixtures of Normal Paraffin Hydrocarbons, *J. Am. Chem. Soc.*, **86(5)**, 3515 (1964).
45. P.J. Flory and A. Abe, Thermodynamic Properties of Nonpolar Mixtures of Small Molecules, *J. Am. Chem. Soc.*, **86(5)**, 3563 (1964).
46. P.J. Flory, Statistical Thermodynamics of Liquid Mixtures, *J. Am. Chem. Soc.*, **87(9)**, 1833 (1965).
47. P.J. Flory and A. Abe, The Thermodynamic Properties of Mixtures of Small, Nonpolar Molecules, *J. Am. Chem. Soc.*, **87(9)**, 1838 (1965).
48. L Perrin, Q.T. Nguyen, D. Sacco, and P. Lochon, Experimental Studies and Modelling of Sorption and Diffusion of Water and Alcohols in Cellulose Acetate, *Polym. Int.*, **42**, 9 (1997).
49. S. Basu, U.S. Shivhare, and A.S. Mujumdar, Models for Sorption Isotherms for Foods: A Review, *Drying Technology*, **24**, 917 (2006).
50. S.N. Dhoot, B.D. Freeman, M.E. Stewart, and A.J. Hill, Sorption and Transport of Linear Alkane Hydrocarbons in Biaxially Oriented Polyethylene Terephthalate, *J. Polym. Sci. Part B: Polym. Phys.*, **39**, 1160 (2001).
51. H. Feng, Modeling of vapor sorption in glassy polymers using a new dual mode sorption model based on multilayer sorption theory, *Polymer*, **48**, 2988 (2007).
52. N. Dolmaire, E. Espuche, F. Méchin, and J.-P. Pascault, Water Transport Properties of Thermoplastic Polyurethane Films, *J. Polym. Sci. Part B: Polym. Phys.*, **42**, 473 (2004).
53. E. Picard, J.-F. Gérard, and E. Espuche, Water transport properties of polyamide 6 based nanocomposites prepared by melting blending: On the importance of the clay dispersion state on the water transport properties at high water activity, *J. Membr. Sci.*, **313**, 284 (2008).
54. F. Sabzi, F. Ayatollahi, and A. Boushehri, Sorption Mechanism in Organic Solutions of Uncharged Polymers, *J. Appl. Polym. Sci.*, **117**, 1867 (2010).
55. E. Favre, Q.T. Nguyen, R. Clément, and J. Néel, The engaged species induced clustering (ENSIC) model: a unified mechanistic approach of sorption phenomena in polymers, *J. Membr. Sci.*, **117**, 227 (1996).
56. A. Jonquières, L. Perrin, A. Durand, S. Arnold, and P. Lochon, Modelling of vapour sorption in polar materials: Comparison of Flory-Huggins and related models with the ENSIC mechanism approach, *J. Membr. Sci.*, **147**, 59 (1998).

References

57. A. Elberaïchi, A. Daro, and C. David, Water vapour transport in polyethylene oxide/polymethyl methacrylate blends, *Eur. Polym. J.*, **35**, 1217 (1999).
58. F. Haidong, Prediction of Infinite Dilution Solvent Activity Coefficient in Rubbery Polymer Solutions Using Engaged Species Induced Clustering (ENSIC) Model, *J. Polym. Sci. Part B: Polym. Phys.*, **44**, 1668 (2006).
59. D. G. Hunt, Prediction of sorption and diffusion of water vapour by nylon-6,6, *Polymer*, **21**, 495 (1980).
60. H.W. Starkweather, The sorption of water by nylons, *J. Appl. Polym. Sci.*, **2(5)**, 129 (1959).
61. H.W. Starkweather, Some Aspects of Water Clusters in Polymers, *Macromolecules*, **8(4)**, 476 (1975).
62. L.T. Lim, I.J. Britt, and M. A. Tung, Sorption and Transport of Water Vapor in Nylon 6,6 Film, *J. Appl. Polym. Sci.*, **71**, 197 (1999).
63. M. Sabard, Effet des conditions de procédé et des nanocharges sur la morphologie et les propriétés de sorption à l'eau et à l'éthanol. Doctoral dissertation, Université de Lyon (2011).
64. J. Crank, *The Mathematics of Diffusion*, Oxford University Press, Oxford (2004).
65. A. Fick, Über Diffusion, *Ann. Phys. Lpz.*, **170(1)**, 59 (1855).
66. N. Follain, J-M Valleton, L. Lebrun, B. Alexandre, P. Schaetzel, M. Metayer, and S. Marais, Simulation of kinetic curves in mass transfer phenomena for a concentration-dependent diffusion coefficient in polymer membranes, *J. Membr. Sci.*, **349**, 195 (2010).
67. K-M. Krüger and G. Sadowski, Fickian and Non-Fickian Sorption Kinetics of Toluene in Glassy Polystyrene, *Macromolecules*, **38**, 8408 (2005).
68. P. Chandra and W.J. Koros, Sorption and transport of methanol in poly(ethylene terephthalate), *Polymer*, **50**, 236 (2009).
69. A.R. Berens and H.B. Hopfenberg, Diffusion and relaxation in glassy polymer powders: 2. Separation of diffusion and relaxation parameters, *Polymer*, **19**, 489 (1978).
70. C.-Y. Hui, K.-C. Wu, R.C. Lasky, and E.J. Kramer, Case-II diffusion in polymers. I. Transient swelling, *J. Appl. Phys.*, **61**, 5129 (1987).
71. C.-Y. Hui, K.-C. Wu, R.C. Lasky, and E.J. Kramer, Case-II diffusion in polymers. II. Steady-state front motion, *J. Appl. Phys.*, **61**, 5137 (1987).
72. E. Bagley and F. A. Long, Two-stage Sorption and Desorption of Organic Vapors in Cellulose Acetate, *J. Am. Chem. Soc.*, **77**, 2172 (1955).
73. F.A. Long and D. Richman, Concentration Gradients for Diffusion of Vapors in Glassy Polymers and their Relation to Time Dependent Diffusion Phenomena *J. Am. Chem. Soc.*, **82**, 513 (1960).
74. R. Ramani and C. Ranganathaiah, Free-volume microprobe study of iodine diffusion in polymers, *Polym. Int.*, **50**, 237 (2001).
75. C.C. McDowell, B.D. Freeman, and G.W. McNeely, Acetone sorption and uptake kinetic in poly(ethylene terephthalate), *Polymer*, **40**, 3487 (1999).
76. B. Alexandre, D. Langevin, P. Médéric, T. Aubry, H. Couderc, Q.T. Nguyen, A. Saiter, and S. Marais, Water barrier properties of polyamide 12/montmorillonite nanocomposite membranes: Structure and volume fraction effects, *J. Memb. Sci.*, **328**, 186 (2009).

References

77. P. Mansfield, R. Botwell, and S. Blackband, Ingress of Water into Solid Nylon 6,6, *J. Magnetic Res.*, **99**, 507 (1992).
78. J-T. Yeh, S-S. Chang, H-T. Yao, K-N. Chen, and W-S. Jou, The permeation resistance of polyethylene, polyethylene/polyamide, and polyethylene/modified polyamide blown tubes against unleaded gasoline, *J. Mat. Sci.*, **35**, 1321 (2000).
79. I. Auerbach and M.L. Carnicom, Sorption of Water by Nylon 66 and Kevlar 29. Equilibria and Kinetics, *J. Appl. Polym. Sci.*, **42**, 2417 (1991).
80. D. Jarus, A. Hiltner, and E. Baer, Barrier properties of polypropylene/polyamide blends produced by microlayer coextrusion, *Polymer*, **43**, 2401 (2002).
81. V. M. Litvinov, O. Persyn, V. Miri, and J.M. Lefebvre, Morphology, Phase Composition and Molecular Mobility in Polyamide Films in Relation to Oxygen Permeability, *Macromolecules*, **43**, 7668 (2010).
82. M.R. Kamal and I.A. Jinnah, Permeability of Oxygen and Water Vapor Through Polyethylene/Polyamide films, *Polym. Eng. Sci.*, **24(17)**, 1337 (1984).
83. B. Alexandre, L. Colasse, D. Langevin, P. Médéric, T. Aubry, C. Chappey, and S. Marais, Transport Mechanisms of Small Molecules through Polyamide 12/Montmorillonite Nanocomposites, *J. Phys. Chem. B*, **114**, 8827 (2010).
84. S. Eceolaza, M. Iriarte, C. Uriarte and A. Etxeberría, Barrier Property Enhancement of Polyamide 6 by Blending with a Polyhydroxyamino-Ether Resin, *J. Polym. Sci. Part B: Polym. Phys.*, **47**, 1625 (2009).
85. H.Y. Low, T.X. Liu, and W.W. Loh, Moisture sorption and permeation in polyamide 6/clay nanocomposite films, *Polym. Int.*, **53**, 1973 (2004).
86. T. Jiang, Y-H. Wang, J-T. Yeh, and Z-Q. Fan, Study on solvent permeation resistance properties of nylon6/clay nanocomposite, *Eur. Polym. J.*, **41**, 459 (2005).
87. R.M. Balabin, R.Z. Syunyaev, and S.A. Karpov, Molar Enthalpy of Vaporization of Ethanol-Gasoline Mixtures and Their Colloid State, *Fuel*, **86**, 323 (2007).
88. M.B. Gramajo de Doz, C.M. Bonatti, N. Barnes, and H.N. Sólamo, (Liquid + Liquid) Equilibria of Ternary and Quaternary Systems Including 2,2,4-trimethylpentane, Benzene, Methanol, and Water at T=303.15 K, *J. Chem. Thermodyn*, **33**, 1663 (2001).
89. M.B. Gramajo de Doz, C.M. Bonatti, and H.N. Sólamo, (Liquid + Liquid) Equilibria of Ternary and Quaternary Systems With Two Hydrocarbons, an Alcohol, and Water at T=303.15 K. Systems Containing Cyclohexane, Benzene, Methanol, and Water, *J. Chem. Thermodyn.*, **35**, 825 (2003).
90. M.B. Gramajo de Doz, C.M. Bonatti, and H.N. Sólamo, (Liquid + Liquid) Equilibria of Ternary and Quaternary Systems With Two Hydrocarbons, an Alcohol, and Water at T=303.15 K. Systems containing 2,2,4-trimethylpentane, Toluene, Methanol, and Water, or 2,2,4-trimethylpentane, Toluene, Ethanol, and Water, *Fluid Phase Equilib*, **205**, 53 (2003).
91. M.B. Gramajo de Doz, C.M. Bonatti, and H.N. Sólamo, Water Tolerance and Ethanol Concentration in Ethanol-Gasoline Fuels at Three Temperatures, *Energy & Fuels*, **18**, 334 (2004).
92. N. Peschke and S.I. Sandler, Liquid-Liquid Equilibria of Fuel Oxygenate + Water + Hydrocarbon Mixtures. 1, *J. Chem. Eng. Data*, **40**, 315 (1995).

References

93. S. Hellinger and S.I. Sandler, Liquid-Liquid Equilibria of Fuel Oxygenate + Water + Hydrocarbon Mixtures. 2, *J. Chem. Eng. Data*, **40**, 321 (1995).
94. A. Arce, M. Blanco, and A. Soto, Determination and Correlation of Liquid-Liquid Equilibrium Data for the Quaternary System 1-octanol + 2-methoxy-2-methylbutane + Water + Methanol at 25°C, *Fluid Phase Equilib.*, **158-160**, 949 (1999).
95. J. Chen, L-P. Duan, J-G. Mi, W-Y. Fei, and Z-C. Li, Liquid-Liquid Equilibria of Multi-component Systems Including n-hexane, n-octane, Benzene, Toluene, Xylene and Sulfolane at 298.15 K and Atmospheric Pressure, *Fluid Phase Equilib.*, **173**, 109 (2000).
96. B.E. García-Flores, G. Galicia-Aguilar, R. Eustaquio-Rincón, and A. Trejo, Liquid-Liquid Phase Diagrams of Ternary Systems as a Function of Temperature: Isooctane + Aromatic + Methanol With and Without Water, *Fluid Phase Equilib.*, **185**, 275 (2001).
97. J.A. Alkandary, A.S. Aljimaz, M.S. Fandary, and M.A. Fahim, Liquid-Liquid Equilibria of Water + MTBE + Reformate, *Fluid Phase Equilib.*, **187-188**, 131 (2001).
98. F. Aiouache and S. Goto, Liquid-Liquid Equilibria of Ternary 2M1B/2M2B-2M1BOH-H₂O and Quaternary 2M1B-2M2B-2M1BOH-H₂O Mixtures, *Fluid Phase Equilib.*, **187-188**, 415 (2001).
99. C.B. Kretschmer, J. Nowakowska, and R. Wiebe, Densities and Liquid-Vapor Equilibria of the System Ethanol-Isooctane (2,2,4-trimethylpentane) Between 0 and 50°, *J. Am. Chem. Soc.*, **70(2)**, 1785 (1948).
100. C.B. Kretschmer and R. Wiebe, Liquid-Vapor Equilibrium of Ethanol-Toluene Solutions, *J. Am. Chem. Soc.*, **71(5)**, 1793 (1949).
101. P. Oracz and G. Kolasinska, Vapour-Liquid Equilibria-III. Total Vapor Pressure Measurements for Binary Mixtures of Methanol, Ethanol, 1-propanol, and 1-butanol With Benzene, Toluene, and p-xylene at 313.15 K, *Fluid Phase Equilib.*, **35**, 253 (1987).
102. E.C. Bromiley and D. Quiggle, Vapor-Liquid Equilibria of Hydrocarbon Mixtures, *Ind. Eng. Chem.*, **25(10)**, 1136 (1933).
103. R. French and P. Malone, Phase Equilibria of Ethanol Fuel Blends, *Fluid Phase Equilib.*, **228-229**, 27 (2005).
104. R.Y.M. Huang, M. Balakrishnan, and J-W. Rhimh, Pervaporation separation of pentane-alcohol mixtures using nylon 6-polyacrylic acid (PAA) ionically crosslinked membranes. II. Experimental data and theoretical interpretation, *J. Appl. Polym. Sci.*, **46(1)**, 109 (1992).
105. R.Y.M. Huang and J.J. Shieh, Pervaporation Separation of Ethanol-Water Mixtures Using Crosslinked Blend Membranes, *Separation Science and Technology*, **32(17)**, 2765 (1997).
106. M. Yoshikawa, S. Takeuchi, and T. Kitao, Specialty polymeric membranes, 7. Pervaporation separation of benzene/cyclohexane mixtures with Nylon-6-graft-poly(oxyethylene) membranes, *Ang. Makro. Chem.*, **245**, 193 (1997).
107. J.P. García Villaluenga and A. Tabe-Mohammadi, A review on the separation of benzene/cyclohexane mixtures by pervaporation processes, *J. Memb. Sci.*, **169**, 159 (2000).
108. M. Yoshikawa, H. Shimada, K. Tsubouchi, and Y. Kondo, Speciality polymeric membranes: 12. Pervaporation of benzene-cyclohexane mixtures through carbon graphite-nylon 6 composite, *J. Memb. Sci.*, **177(1-2)**, 49 (2000).

References

109. B. Smitha, G. Dhanuja, S. Sridhar, Dehydration of 1,4-dioxane by pervaporation using modified blend membranes of chitosan and nylon 66, *Carbohydrate Polymers*, **66**, 463 (2006).
110. R.J. Hernández, J.R. Giacín, and E.A. Grulke, The Sorption of Water Vapor by an Amorphous Polyamide, *J. Memb. Sci.*, **65**, 187 (1992).
111. L.P. Razumovskii, V.S. Markin, and G. Ye. Zaikov, Sorption of Water by Aliphatic Polyamides. Review, *Polym. Sci. U.S.S.R.*, **27(4)**, 751 (1985).
112. Y. Park, J. Ko, T-K. Ahn, and S. Choe, Moisture Effects on the Glass Transition and the Low Temperature Relaxations in Semiaromatic Polyamides, *J. Polym. Sci. Part B: Polym. Phys.*, **35**, 807 (1997).
113. K-H. Illiers, Der Einfluß von Wasser auf die molekularen Beweglichkeiten von Polyamiden, *Makromol. Chemie*, **38(1)**, 168 (1960).
114. K-H. Illiers and H. Jacobs, Der Einfluß von Quellundsmitteln auf die Wasserstoffbrücken-Bindung und das elastische Verhalten von Polyamiden und Polyurethanen, *Makromol. Chemie*, **39(1)**, 234 (1960).
115. Y. S. Papir, S. Kapur, Effect of Orientation, Anisotropy, and Water on the Relaxation Behavior of Nylon 6 from 4.2 to 300°K, C.E. Rogers, and E. Baer, *J. Polym. Sci. Part A-2*, **10**, 1305 (1972).
116. E. Laredo, M.C. Hernández, Moisture Effect on the Low- and High-Temperature Dielectric Relaxations in Nylon-6, *J. Polym. Sci. Part B: Polym. Phys.*, **35**, 2879 (1997).
117. E. Laredo, M. Grimau, F. Sánchez, and A. Bello, Water Absorption Effect on the Dynamic Properties of Nylon-6 by Dielectric Spectroscopy, *Macromolecules*, **36**, 9840 (2003).
118. K. Pathmanathan, J.-Y. Cavaillé, and G.P. Johari, The Dielectric Properties of Dry and Water-Saturated Nylon-12, *J. Polym. Sci. Part B: Polym. Phys.*, **30**, 341 (1992).
119. H.M. Le Huy and J. Rault, Remarks on the α and β Transitions in Swollen Polyamides, *Polymer*, **35(1)**, 136 (1994).
120. R. Puffr and J. Sebenda, On the Structure and Properties of Polyamides.XXVII. The Mechanism of Water Sorption in Polyamides, *J. Polym. Sci. Part C.*, **16**, 79 (1967).
121. N.S. Murthy, Hydrogen Bonding, Mobility, and Structural Transitions in Aliphatic Polyamides, *J. Polym. Sci. Part B: Polym. Phys.*, **44**, 1763 (2006).
122. D.A. Dixon, J.J. Valentini, and K.D. Dobbs, Amide-Water and Amide-Amide Hydrogen Bond Strengths, *J. Phys. Chem.*, **98(51)**, 13435 (1994).
123. E.S. Eberhardt and R.T. Raines, Amide-Amide and Amide-Water Hydrogen Bonds: Implications for Protein Folding and Stability, *J. Am. Chem. Soc.*, **116**, 2149 (1994).
124. N.S. Murthy, M. Stamm, J.P. Sibilía, and S. Krimm, Structural Changes Accompanying Hydration in Nylon 6, *Macromolecules*, **22**, 1261 (1989).
125. R. Iwamoto and H. Murase, Infrared Spectroscopic Study of the Interactions of Nylon-6 with Water, *J. Polym. Sci. Part B: Polym. Phys.*, **41**, 1722 (2003).
126. S. Rastogi, A.E. Terry, and E. Vinken, Dissolution of Hydrogen-Bonded Polymers in Water: A Study of Nylon-4,6, *Macromolecules*, **37**, 8825 (2004).
127. E. Vinken, A.E. Terry, O. van Asselen, A.B. Spoelstra, R. Graf, and S. Rastogi, *Langmuir*, **24**, 6313 (2008).

References

128. N.S. Murthy, M.K. Akkapeddi, and W.J. Orts, Analysis of Lamellar Structure in Semicrystalline Polymers by Studying the Absorption of Water and Ethylene Glycol in Nylons Using Small-Angle Neutron Scattering, *Macromolecules*, **31**, 142 (1998).
129. T.A. Kotel'nikova, M.V. Lukyanova, E.P. Ageev, *Moscow Univ. Chem. Bull.*, **52(3)**, 23 (1997).
130. H.W. Starkweather and J.R. Barkley, The Effect of Water on the Secondary Dielectric Relaxations in Nylon 66, *J. Polym. Sci. Part B: Polym. Phys.*, **19**, 1211 (1981).
131. T.G. Fox and P.J. Flory, Second-Order Transition Temperatures and Related Properties of Polystyrene. I. Influence of Molecular Weight, *J. Appl. Phys.*, **21**, 581 (1950).
132. T.G. Fox and S. Loshaek, Influence of Molecular Weight and Degree of Crosslinking on the Specific Volume and Glass Temperature of Polymers, *J. Polym. Sci.*, **15**, 371 (1955).
133. T.G. Fox, Influence of Diluent and of Copolymer Composition on the Glass Temperature of a Polymer System, *Bull. Am. Phys. Soc.*, **1**, 123 (1956).
134. J.M. Gordon and J.S. Taylor, Ideal Copolymers and the Second-Order Transitions of Synthetic Rubbers. I. Non-crystalline Copolymers, *J. Appl. Chem.*, **2**, 493 (1952).
135. J.M. Gordon, G.B. Rouse, J.H. Gibbs, and W.M. Riesen, The Composition Dependence of Glass Transition Properties, *J. Chem. Phys.*, **66(11)**, 4971 (1977).
136. E. Penzel, J. Riger, and H.A. Schneider, The Glass Transition Temperature of Random Copolymers: 1. Experimental Data and the Gordon-Taylor Equation, *Polymer*, **38(2)**, 325 (1997).
137. E. Jenckel and R. Heusch, Die ernidrigung der einfriertemperatur organischer glaser durch losungsmittel, *Kolloid Z.*, **130**, 89 (1953).
138. F.N. Kelley and F. Bueche, Viscosity and Glass Temperature Relations for Polymer-Diluent Systems, *J. Polym. Sci.*, **50**, 549 (1961).
139. P.R. Couchman and F.E. Karasz, A Classical Thermodynamic Discussion of the Effect of Composition on Glass-Transition Temperatures, *Macromolecules*, **11(1)**, 117 (1978).
140. G. ten Brinke, F.E. Karasz, and T.S. Ellis, Depression of Glass Transition Temperatures of Polymer Networks by Diluents, *Macromolecules*, **16(2)**, 244 (1983).
141. X. Lu and R.A. Weiss, Relationship Between the Glass Transition Temperature and the Interaction Parameter of Miscible Binary Polymer Blends, *Macromolecules*, **25(12)**, 3242 (1992).
142. H.W. Starkweather, G.E. Moore, J.E. Hansen, T.M. Roder, and R.E. Brooks, Effect of Crystallinity on the Properties of Nylons, *J. Polym. Sci.*, **21**, 189 (1956).
143. M.N. Bureau, J. Denault, K.C. Cole, and G.D. Enright, The Role of Crystallinity and Reinforcement in the Mechanical Behavior of Polyamide-6/Clay Nanocomposites, *Polym. Eng. Sci.*, **42(9)**, 1897 (2002).
144. H.W. Starkweather and R.E. Brooks, Effect of Spherulites on the Mechanical Properties of Nylon 66, *J. Appl. Polym. Sci.*, **1(2)**, 236 (1959).
145. V. Miri, O. Persyn, J.-M. Lefebvre, and R. Séguela, Effect of Water Absorption on the Plastic Deformation Behavior of Nylon 6, *Eur. Polym. J.*, **45**, 757 (2009).

References

146. G. Shan, W. Yang, M. Yang, B. Xie, J. Feng, and Q. Fung, Effect of temperature and strain rate on the tensile deformation of polyamide 6, *Polymer*, **48**, 2958 (2007).
147. A.A. Collyer, *Rubber Toughened Engineering Plastics*, Chapman & Hall, London (1994).
148. N. Takeda, D.Y. Song, and K. Nakata, Effects of temperature and water content on impact properties of injection-molded glass nylon-6 composites, *Adv. Composite Mater.*, **5(3)**, 201 (1996).
149. K. Inoue and S. Hoshino, Swelling of nylon 6 film due to water sorption, *J. Polym. Sci. Polym. Phys.*, **14**, 1513 (1976).
150. H.K. Reimschuessel, Relationship on the Effect of Water on Glass Transition Temperature and Young's Modulus of Nylon 6, *J. Polym. Sci. Polym. Chem.*, **16**, 1229 (1978).
151. R.J. Gaymans, R.J.M. Borggreve, A.B. Spoelstra, Ductile Transition in Nylon-Rubber Blends: Influence of Water, *J. Appl. Polym. Sci.*, **37**, 479 (1989).
152. A. Fabre-Argoud, *Control and stabilization of morphologies in reactively compatibilized Polyamide 6/High Density Polyethylene blends*, Doctoral Dissertation, Université de Lyon (2011).
153. *The Advanced Thermal Analysis System*, <http://athas.prz.edu.pl/>, last consulted on October 4th, 2012.
154. Y.X. Pang, D.M. Jia, H.J. Hu, D.J. Hourston, and M. Song, A Quantitative Estimation of the Extent of Compatibilization in Heterogeneous Polymer Blends Using Their Heat Capacity Increment at the Glass Transition, *J. Appl. Polym. Sci.*, **74**, 2868 (1999).
155. N.G. McCrum, B.E. Read, and G. Williams, *Anelastic and Dielectric Effects in Polymer Solids*, Dover, New York (1991).
156. *3rd Laboratory Course on Dielectric Spectroscopy*, Material Physics Center of the Basque Country University, San Sebastián, Spain, May 21st-25th, 2012.
157. C.D. Hodgman, *CRC Handbook of Chemistry and Physics 44th Edition*, CRC Press, Cleveland (1962).
158. P. Cebe and P.P. Huo, Dielectric Relaxation as a Probe of Interphase Structure, *Thermochimica Acta*, **238**, 229 (1994).
159. S.X. Lu and P. Cebe, Effects of Annealing on the Disappearance and Creation of Constrained Amorphous Phase, *Polymer*, **37(21)**, 4857 (1996).
160. P. Xu and X. Zhang, Investigation of MWS Polarization and DC Conductivity in Polyamide 610 Using Dielectric Relaxation Spectroscopy, *Eur. Polym. J.*, **47**, 1031 (2011).
161. H. Lu, X. Zhang, and H. Zhang, Influence of the Relaxation of Maxwell-Wagner-Sillars Polarization and DC Conductivity on the Dielectric Behaviors of Nylon 1010, *J. Appl. Phys.*, **100**, 054104 (2006).
162. E. Mourglia-Seignobos, Compréhension des mécanismes physiques de fatigue dans le polyamide vierge et renforcé de fibres de verre. Doctoral dissertation, Institut National des Sciences Appliquées de Lyon (2009).
163. S. Brunauer, P.H. Emmett, and E. Teller, Adsorption of Gases in Multimolecular Layers, *J. Am. Chem. Soc.*, **60**, 309 (1938).

References

164. R.B. Anderson, Modifications of the Brunauer, Emmett and Teller Equation, *J. Am. Chem. Soc.*, **68**, 686 (1946).
165. E. Favre, R. Clement, Q.T. Nguyen, P. Schaetzel, and J. Neel, Sorption of organic solvents into dense silicone membranes. Part 2.—Development of a new approach based on a clustering hypothesis for associated solvents, *J. Chem. Soc. Faraday Trans.*, **89(24)**, 4347 (1993).
166. C.M. Hansen, The Three Dimensional Solubility Parameter – Key to Paint Component Affinities, *J. Paint Tech.*, **39(505)**, 104 (1967).
167. L.J. Hughes and G.E. Britt, Compatibility studies on polyacrylate and polymethacrylate systems, *J. Appl. Polym. Sci.*, **5(15)**, 337 (1961).
168. R.L. Patrick, *Treatise on Adhesion and Adhesives Vol. 1*, Marcel Dekker, New York (1967).
169. J. Bastide, C. Picot, and S. Candau, Small angle neutron scattering and light spectroscopy investigation of polystyrene gels under osmotic deswelling, *Macromolecules*, **17(1)**, 83 (1984).
170. B. Erman and P.J. Flory, Relationships between stress, strain, and molecular constitution of polymer networks. Comparison of theory with experiments, *Macromolecules*, **15(3)**, 806 (1982).
171. P.J. Flory and J. Rehner, Effect of Deformation on the Swelling Capacity of Rubber, *J. Chem. Phys.*, **12**, 412 (1942).
172. B. Erman and J.E. Mark, *Structures and Properties of Rubberlike Networks*, Oxford University Press, New York (1997).
173. I.M. Klotz and J.S. Franzen, Hydrogen Bonds between Model Peptide Groups in Solution, *J. Am. Chem. Soc.*, **84(18)**, 3461 (1962).
174. O. Haida, H. Suga, and S. Seki, Realization of Glassy Liquid and Glassy Crystal of Ethanol, *Proc. Japan Acad.*, **48**, 683 (1972).
175. E. León-Gutierrez, G. Garcia, M.T. Clavaguera-Mora, and J. Rodríguez-Viejo, Glass transition in vapor deposited thin films of toluene, *Thermochimica Acta*, **492**, 51 (2009).
176. M. Laurati, P. Sotta, D.R. Long, L.A. Fillot, A. Arbe, A. Alegría, J.P. Embs, T. Unruh, G.J. Schneider, and J. Colmenero, Dynamics of Water Absorbed in Polyamides, *Macromolecules*, **45(3)**, 1676 (2012).
177. S. Cervený, J. Colmenero, and A. Alegría, Dielectric Investigation of the Low-Temperature Water Dynamics in the Poly(vinyl methyl ether)/H₂O System, *Macromolecules*, **38(16)**, 7056 (2005).
178. S. Cervený, A. Alegría, and J. Colmenero, Universal features of water dynamics in solutions of hydrophilic polymers, biopolymers, and small glass-forming materials, *J. Phys. Rev. E*, **77**, 031803 (2008).
179. S. Cervený, A. Alegría, and J. Colmenero, Broadband dielectric investigation on poly(vinyl pyrrolidone) and its water mixtures, *J. Chem. Phys.*, **128**, 044901 (2008).
180. S.J. Gill and L. Noll, Calorimetric Study of Association of Diketopiperazine in Water, *J. Phys. Chem.*, **76(21)**, 3065 (1972).

References

181. R.F.W. Hopmann, Chemical Relaxation as a Mechanistic Probe of Hydrogen Bonding. Thermodynamics and Kinetics of Lactam Isoassociation in Nonpolar Solvents, *J. Phys. Chem.*, **78(23)**, 2341 (1974).
182. W.L. Jorgensen and C.J. Swenson, Optimized Intermolecular Potential Functions for Amides and Peptides. Hydration of Amides, *J. Am. Chem. Soc.*, **107(6)**, 1489 (1985).
183. M. Nagaraju and G. Narahari Sastry, Effect of alkyl substitution on H-bond strength of substituted amide-alcohol complexes, *J. Mo. Model*, **17**, 1801 (2011).
184. E. Lange, E. Masnada, A. Rios de Anda, L.A. Fillot, P. Sotta, and D. Long, Solvent Diffusion in Glassy Polymers – A Macroscopic Approach, *Paper to be submitted* (2012).
185. D. Long and F. Lequeux, Heterogeneous dynamics at the glass transition in van der Waals liquids, in the bulk and in thin films, *Eur. Phys. J. E*, **4(3)**, 371 (2001).
186. M. Góral and N. Asmanova, Vapour-liquid equilibria in nonpolar mixtures: Part I. 2,2,4-trimethylpentane with benzene, toluene, o-xylene, pxylene, ethylbenzene and propylbenzene at 313.15 K, *Fluid Phase Equilibria*, **86**, 201 (1993).
187. H. Renon and J.M. Prausnitz, Local Compositions in Thermodynamic Excess Functions for Liquid Mixtures, *AIChE Journal*, **14(1)**, 135 (1968).
188. O. Redlich and J.N.S. Kwong, On the Thermodynamics of Solutions V. An Equation of State. Fugacities of Gaseous Solutions, *Chem. Rev.*, **44**, 223 (1979).
189. Yu. E. Kirsch, Yu. A. Fedotov, S.I. Smenova, P.A. Vdovin, V.V. Valuev. O. Yu. Zemlianova, and S.F. Timashev, Sulfonate containing aromatic polyamides as materials of pervaporation membranes for dehydration of organic solvents: hydration, sorption, diffusion and functioning, *J. Memb. Sci.*, **103**, 95 (1995).

Résumé en français

Introduction

Ce travail de thèse s'inscrit dans un cadre applicatif mené par Rhodia-Solvay dont le but est le développement des réservoirs essence pour automobiles faits à partir des formulations base Polyamide 6,6 (PA6,6). Le PA6,6 est un bon candidat pour des applications techniques car il possède des bonnes propriétés thermomécaniques rapportés à son poids. Ces formulations doivent montrer des bonnes propriétés barrière aux essences classiques, aux biofuels qui sont des essences contenant un certain pourcentage d'éthanol, et aussi à l'eau qui est présente dans l'atmosphère, tout en ayant des bonnes propriétés mécaniques, notamment une bonne tenue aux impacts.

Les enjeux scientifiques de ce travail sont premièrement la meilleure compréhension des interactions entre le PA6,6 et une série de solvants purs de polarités et tailles différentes mais aussi des mélanges ternaires composés d'éthanol, toluène et isooctane à différentes concentrations et qui modélisent les biofuels disponibles commercialement en Europe. On veut aussi étudier l'effet de ces solvants ou mélanges de solvants sur la température de transition vitreuse T_g qui est la signature de la mobilité moléculaire de la phase amorphe de ce polymère. Ensuite, l'effet de l'additivation ou de l'ajout des co-monomères dans du PA6,6 pur sur les propriétés barrière et mécaniques, notamment les propriétés choc, a été étudié.

Chapitre I. Etude bibliographique

Le premier chapitre de ce manuscrit présente une étude bibliographique qui traite l'état de l'art sur la structure du PA6,6 et ses propriétés barrière et mécaniques. Les polyamides possèdent un réseau de liaisons H formés entre des groupements amide de différentes chaînes polymère. Ce réseau est présent dans la phase cristalline ce qui favorise la cristallisation du polymère, et il est aussi présent dans la phase amorphe.

La mobilité de la phase amorphe est gouvernée par des mouvements moléculaires à différentes échelles du temps. Dans le cas du PA6,6, trois processus de relaxation distincts ont été décrits : la relaxation principale α qui fait intervenir le mouvement des segments de chaîne assez longs (15 monomères) et deux relaxations secondaires β et γ qui correspondent à la rotation des groupements amides et aux vibrations des chaînes méthylène respectivement. Même s'il y a plusieurs facteurs qui ont une influence sur la mobilité moléculaire du PA6,6, la présence du réseau de liaisons H interchaînes pilote ou détermine d'une manière importante cette mobilité.

Ensuite, la sorption des solvants dans le PA6,6 ainsi que l'influence de la température et du taux de cristallinité sur ce processus sont décrits. Les différents modèles qui décrivent les isothermes de sorption sont aussi décrits.

La prise en eau et son effet plastifiant dans le PA6,6 sont bien connus dans la littérature. L'eau étant une molécule polaire est absorbée par le PA6,6 du fait que les groupements amide peuvent créer de fortes interactions avec ce solvant. Dans la littérature il est admis

que l'eau peut plastifier le PA6,6 du fait que ce solvant interagit et perturbe le réseau de liaisons H interchaînes. Il serait intéressant d'étudier la sorption à l'équilibre d'une série de solvants de différentes tailles et polarités pour mieux comprendre comment la nature et/ou la taille d'une molécule conditionne ses interactions avec le PA6,6 et donc sa prise par ce polymère. Dans ce travail il est envisagé d'étudier quel est l'effet des différents solvants étudiés sur la T_g du PA6,6 ainsi que sur les relaxations secondaires. Des mécanismes de plastification propres à chaque famille de solvants (polaires et apolaires) seront proposés.

Concernant la sorption des mélanges de solvants modélisant des biofuels commerciaux en lien direct avec l'application industrielle de ce travail qui est le développement des formulations PA6,6 pour des réservoirs à essence, peu d'informations sont disponibles dans la littérature, nous allons donc étudier la sorption et leur effet sur la mobilité moléculaire du PA6,6 des mélanges ternaires qui modélisent les biofuels et qui sont composés d'éthanol, toluène, et iso-octane à différentes concentrations.

Tout d'abord nous allons étudier l'équilibre liquide – vapeur de ces mélanges, ce qui nous permettra de mieux comprendre la thermodynamique de ces mélanges ainsi que d'estimer les interactions que ces solvants pourront avoir avec le PA6,6. La présence de ces mélanges dans le PA6,6 peut entraîner une modification des propriétés de ce polymère, il est donc important d'étudier la sorption de ces solvants et de comprendre les phénomènes thermodynamiques liés à ces sorptions. Finalement, nous étudierons l'effet de ces mélanges sur la mobilité moléculaire du PA6,6.

Finalement, et toujours en lien avec le contexte applicatif de cette thèse, nous nous sommes intéressés aux propriétés mécaniques du PA6,6. L'effet de la phase cristalline sur les propriétés mécaniques des polyamides a été déjà étudié dans la littérature. Il a été montré premièrement que quand le taux de cristallinité augmente, les performances mécaniques des polyamides augmentent aussi. La taille des sphérolites a une influence aussi sur ces propriétés : quand leur taille diminue, le module de Young augmente. Finalement la structure cristalline a aussi une influence sur les propriétés mécaniques : plus cette structure est stable et dense, plus les propriétés mécaniques seront bonnes.

Cependant le PA6,6 possède un taux de cristallinité relativement bas (40%_{wt}) ce qui pourrait signifier que la mobilité de la phase amorphe joue un rôle dans les propriétés du polymère. L'effet de l'eau sur les propriétés en traction et en choc du PA6,6 a été aussi étudié dans la littérature, dans cet étude nous nous servirons de l'eau comme un modifiant de l'état de la mobilité moléculaire du PA6,6. De plus cette mobilité peut être modifiée en ajoutant au PA6,6 des additifs ou des co-monomères ou en augmentant la température des échantillons. Les propriétés mécaniques qui seront étudiés sont la contrainte au seuil σ_Y , et le module de Young E , la température de transition fragile $T_{F/D}$ et la résilience au choc. L'influence de la mobilité moléculaire sur ces propriétés sera étudiée et discutée.

Chapitre II. Matériaux et techniques

Pour étudier la sorption d'une série de solvants purs et des mélanges de solvants, ainsi que leur effet sur la mobilité moléculaire de la phase amorphe et sur la structure cristalline, un PA6,6 standard non-additivé et non-chargé a été considéré. Ce PA6,6 de grade Rhodia nommé dans ce travail *Neat PA6,6*, a été extrudé sous forme de films de 100 μ m d'épaisseur.

Ensuite pour étudier l'effet de la modification de la matrice sur les propriétés barrière et mécaniques du PA6,6, une série de matériaux modifiés a été conçue. Cette série comprend deux formulations additivées PA6,6 + 10%_{wt} lauryldéhyde (10LA) et PA6,6 + 10%_{wt} heptanaldéhyde (10HA), deux copolymères PA6,6/6HIA 95/5_{mol} et PA6,6/6AiSLi 95/5_{mol}, et un PA6,6 pur de grade Rhodia (REF). Les structures chimiques des co-monomères et additifs sont montrées sur la Fig. I.

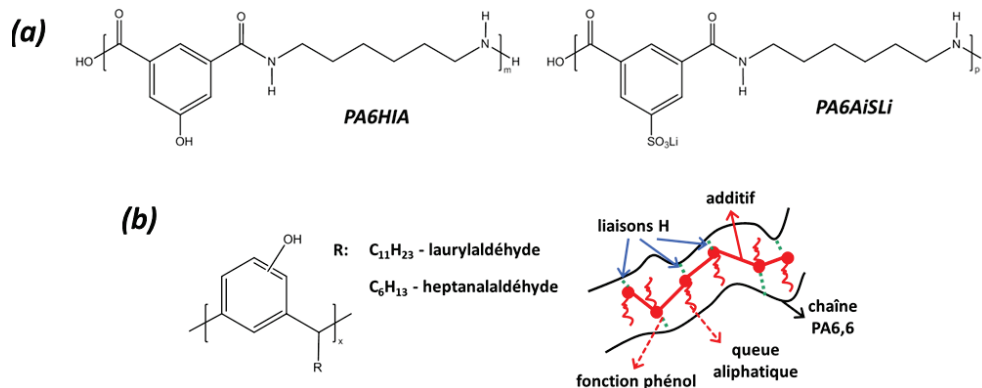


Fig. I: Structures chimiques (a) des co-monomères PA6HIA and PA6AiSLi et (b) des additifs phénoliques avec une représentation schématique des interactions avec le PA6,6.

Les formulations additivées 10LA et 10HA ainsi que REF ont été obtenues par extrusion puis injectées en disques et en barreaux choc et traction. Les copolymères HIA et AISLI, après avoir été synthétisés, ont aussi été injectés en barreaux et extrudés pour obtenir des films de 300µm d'épaisseur.

Pour caractériser la phase cristalline des échantillons on a utilisé la DSC et la diffraction des Rayons X. La DSC nous a permis d'obtenir les températures de fusion et de cristallisation ainsi que les degrés de cristallinité, tandis que la diffraction des Rayons X nous a permis de caractériser les structures cristallines. La DSC modulée (MDSC), la Spectroscopie Diélectrique (BDS) et l'Analyse Dynamique Mécanique (DMA) nous ont permis de caractériser la mobilité moléculaire de la phase amorphe des échantillons étudiés soit à l'état sec (MDSC, BDS et DMA) soit conditionnés en solvant (MDSC et BDS).

La sorption par le PA6,6 d'une série de solvants polaires et apolaires purs de taille et polarité différentes ainsi que leur effet sur la mobilité moléculaire du polymère ont été étudiés. Les solvants polaires sont: l'eau, méthanol, éthanol, l'éthylène glycol, 1-propanol, 2-propanol, 2-butanol et cyclopentanol. Les solvants apolaires sont : le toluène, o-xylène, p-xylène, 2,3-diméthylbutane, 3-méthylpentane, n-hexane et isooctane. La sorption de ces solvants s'est faite à température ambiante (23°C), les films PA6,6 ont été mis en contact avec chaque solvant et pesés régulièrement jusqu'à l'obtention de l'équilibre de sorption, qui est le moment où le polymère n'absorbe plus de solvant.

La sorption et l'effet plastifiant sur le PA6,6, d'une série de mélanges ternaires composés d'éthanol, toluène et isooctane (nommés EX) à différentes concentrations ont aussi été étudiés. Tout d'abord on s'est intéressé au calcul des activités chimiques de ces solvants dans chacun de ces mélanges, pour cela nous avons quantifié par chromatographie en phase gazeuse (GC-FID) la concentration des espèces dans les phases vapeurs de ces mélanges, et donc de calculer leurs activités chimiques.

Ensuite ces mélanges ont été mis en contact avec des films PA6,6 jusqu'à l'obtention de l'équilibre de sorption. La GC-FID nous a permis de quantifier les concentrations d'éthanol, de toluène et d'isooctane absorbés par les films, en quantifiant les vapeurs de désorption des échantillons. La sorption des mélanges par le PA6,6 a été comparée à celle de l'éthanol pur aux mêmes activités chimiques. Pour cela une DVS a été utilisée. Cet appareil permet d'avoir une atmosphère d'éthanol à une activité contrôlée. Des films ont été introduits dans la DVS, leur prise en solvant mesurée en continu jusqu'à l'obtention de l'équilibre de sorption.

Des essais de perméation à l'éthanol ont été effectués. Pour ce faire des cellules de perméation en montage type sandwich ont été réalisés : des films ou des plaques amincies ont été mis en contact d'un côté avec un réservoir contenant ce solvant et de l'autre à une atmosphère contrôlée en humidité (RH20). Les essais ont été faits à 40°C et les cellules ont été pesées régulièrement jusqu'à l'obtention du régime permanent de perméation, c'est-à-dire quand la perte instantanée de solvant est constante avec le temps.

Enfin, concernant la caractérisation des propriétés mécaniques, des essais de traction ont été effectués pour obtenir la contrainte au seuil σ_y et le module de Young E . Ces essais ont été conduits pour des échantillons à l'état sec à plusieurs températures : 23, 45, 65, 90 et 120°C. Des échantillons conditionnés à RH50 et RH100 ont été seulement étudiés à 23°C. Concernant les propriétés à l'impact, les résiliences des échantillons à différentes températures et leurs températures de transition fragile-ductile $T_{F/D}$ ont été obtenues par des essais choc Charpy instrumentés. Ces essais permettent d'obtenir des courbes force-temps et force-déplacement et à partir de ces courbes la résilience est calculée. Des échantillons secs et conditionnés à RH50 et RH100 ont été caractérisés à des températures allant de -60 à 140°C.

Chapitre III. Sorption et effet plastifiant de solvants polaires et apolaires purs et des mélanges de solvants sur du PA6,6 pur

Dans ce Chapitre on étudie la sorption d'une série de solvants polaires et apolaires purs et leur effet sur les phases cristalline et amorphe du PA6,6. La prise en solvant dans le PA6,6 pour la série de molécules citée précédemment a été tout d'abord considérée. Pour les solvants apolaires on observe que leur prise par le PA6,6 ne varie pas en fonction de leur taille comme montré dans la Fig. IIa. Dans le cas des solvants polaires, leur prise en masse diminue quand leur taille augmente (Fig. IIa) mais quand la taille des solvants polaires augmente, la polarité de ces molécules diminue. On observe donc, comme montré sur la Fig. IIb. que quand la polarité d'une molécule diminue, sa prise dans le PA6,6 diminue aussi. Ceci nous laisse penser que c'est bien la polarité d'une molécule qui va conditionner sa prise dans le PA6,6. Dans le cas des solvants apolaires, leur prise ne serait pas conditionnée forcément par leur taille mais par les faibles interactions (i.e. van der Waals) de ces solvants avec le PA6,6.

Résumé en français

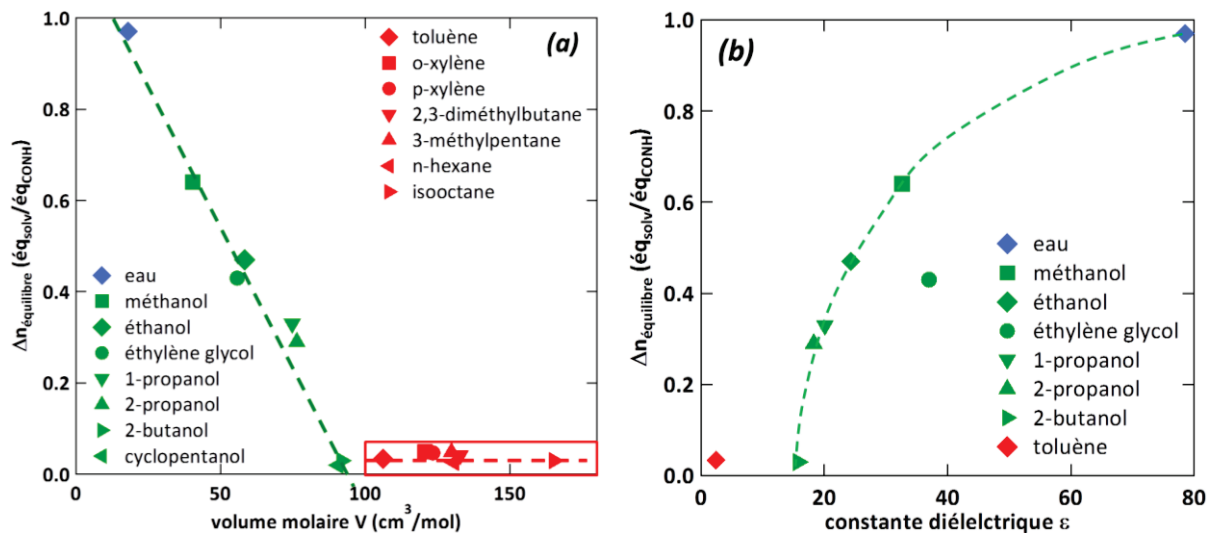


Fig. II: (a) Fraction molaire à l'équilibre $\Delta n_{\text{équilibre}}$ pour les solvants étudiés en fonction (a) de leur volume molaire V et (b) de leur constante diélectrique relative ϵ_r .

Ensuite l'effet de la matrice polymère sur la sorption de solvants a été étudié. Une approche thermodynamique a été proposée. L'équation de Flory – Huggins qui décrit la sorption en termes des interactions entre le solvant et le polymère a été tout d'abord considérée. Selon les résultats donnés par cette équation l'éthanol devrait solubiliser le PA6,6, la sorption du toluène devrait être d'environ 40%_{vol} pour une activité $a_{\text{toluène}} = 1$. Donc cette équation et notamment le paramètre d'interaction χ ne peut à lui seul décrire la sorption observée pour ces solvants (env. 15%_{vol} pour l'éthanol et 2%_{vol} pour le toluène).

Alors, un terme élastique qui décrit un polymère possédant des liaisons interchaînes qui agissent comme des points de réticulation physiques a été ajouté à l'équation de Flory – Huggins pour décrire la sorption des solvants dans du PA6,6. Ce terme élastique prend en compte la densité des liaisons H et un module de pression osmotique qui caractérise la raideur des liaisons H . On observe sur la Fig. III que l'effet de ce terme élastique limite d'une manière assez importante la prise des solvants dans le PA6,6 comparé au modèle de Flory – Huggins classique. Comme montré dans la littérature, d'autres modèles permettent par exemple de décrire la sorption de l'eau dans du polyamide, cependant ces modèles ne tiennent pas en compte l'élasticité de la matrice PA6,6. L'effet de ce terme élastique sur la prise en solvant montrerait que les liaisons H présentes dans la phase amorphe du polymère agissent comme des points de réticulation et limitent la reprise en solvant.

Ensuite nous nous sommes intéressés à l'effet des solvants sur la mobilité moléculaire du PA6,6, caractérisée par la T_g . Une tendance a été observée pour la série d'alcools comme montré sur la Fig. IV: quand leur prise molaire dans le PA6,6 augmente, leur effet plastifiant augmente aussi. On observe aussi que ni l'eau ni le toluène ne suivent la même tendance que les alcools. Pour comparer ces différentes tendances, la T_g du PA6,6 pour différents teneurs en eau, en toluène et en éthanol a été mesurée. On observe que l'éthanol suit la tendance de la série d'alcools, que l'eau a un effet plastifiant moins important que ces solvants pour la même prise molaire et que le toluène a l'effet plastifiant le plus important de tous les solvants comme montré sur la Fig. IV.

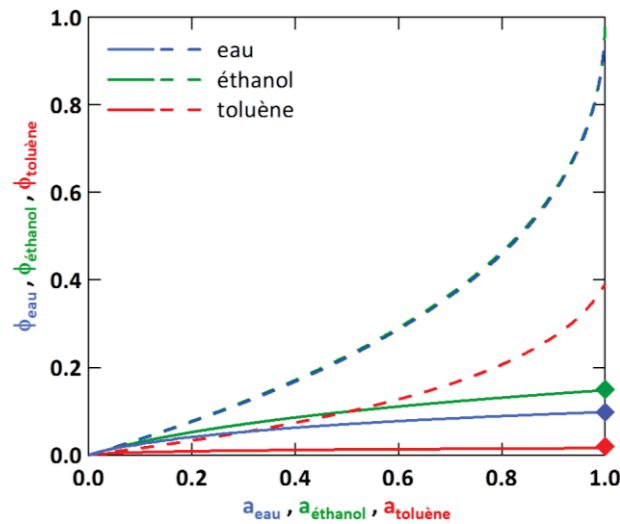


Fig. III: Fraction volumique en solvant en fonction de l'activité du solvant pour l'éthanol, l'eau, et le toluène obtenues avec un modèle de Flory – Huggins "classique" (courbes pointillées) et obtenues avec le modèle présenté dans ce travail (courbes plaines). Les valeurs mesurées à l'équilibre sont indiquées par des losanges.

Deux tendances différentes de plastification pour la série de solvants apolaires ont aussi été observées. Il semble que les solvants aromatiques provoquent une chute de T_g plus importante (env. 10°C) que les solvants aliphatiques pour la même prise molaire. Cet effet sera discuté plus loin lors de la description des hypothèses de mécanismes de plastification des solvants.

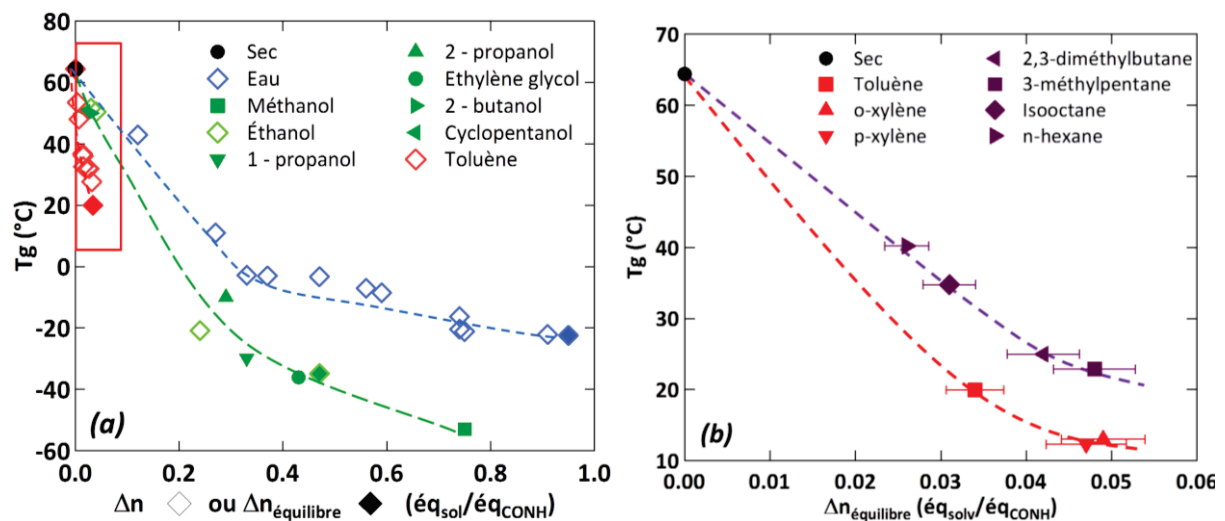


Fig. IV: PA6,6 T_g du PA6,6 obtenue par DSC en fonction de (a) la fraction molaire Δn pour les solvants polaires et le toluène et (b) de la fraction molaire à l'équilibre $\Delta n_{equilibrium}$ pour les solvants apolaires.

La chute de T_g provoquée par ces solvants a été comparée à des modèles de plastification de la littérature et il a été observé qu'aucun de ces modèles ne décrit bien les tendances de plastification de ces trois solvants. Ceci s'explique par le fait que ces modèles ne tiennent pas compte des interactions fortes qui peuvent exister entre un plastifiant/solvant et le polymère.

L'effet de l'eau, de l'éthanol et du toluène sur la relaxation principale α ainsi que l'effet du toluène sur les relaxations secondaires β et γ ont été étudiés par Spectroscopie Diélectrique.

Pour la relaxation α on observe que les solvants étudiés n'ont pas d'effet sur la largeur ni sur l'amplitude de cette relaxation. Concernant la relaxation β on observe que le toluène provoque une chute de la température de cette relaxation ainsi qu'une légère diminution de l'énergie d'activation associée à ce processus moléculaire. Ces résultats indiqueraient que le toluène serait capable de modifier localement les mouvements des groupements amide, associées à la relaxation β . De plus aucun effet du toluène sur la largeur ni sur l'amplitude de cette relaxation n'a été observé. Finalement on observe que le toluène n'a pas d'effet notable sur la relaxation γ .

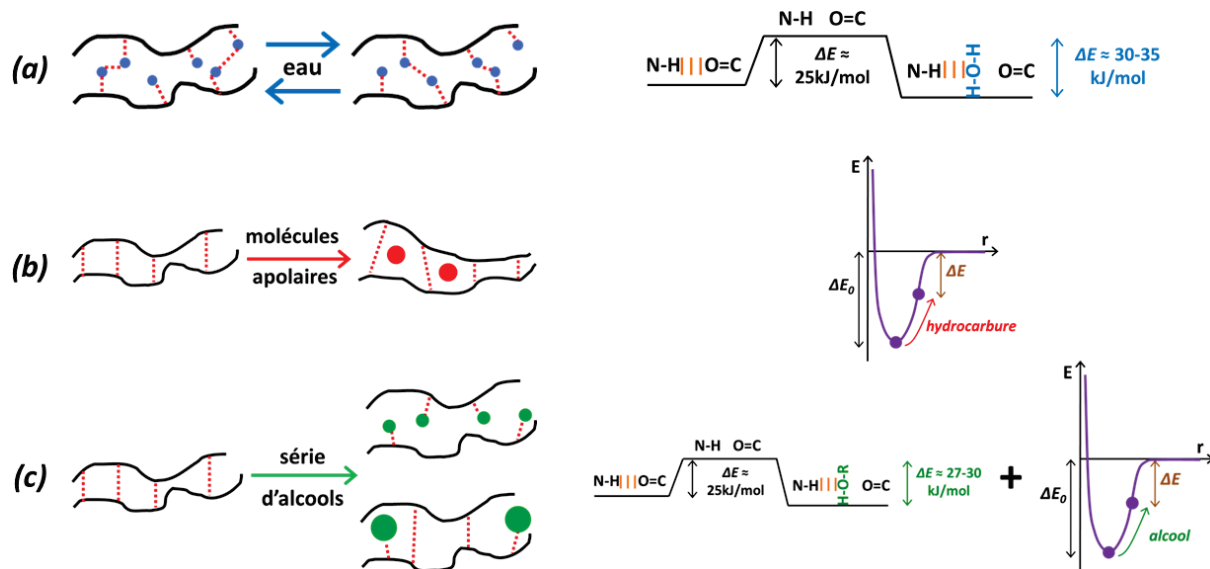


Fig. V: Représentation schématique des effets plastifiants pour (a) l'eau, (b) les solvants apolaires et (c) pour la série d'alcools.

Ensuite des hypothèses sur les mécanismes de plastification de l'eau, de la série d'alcools et des solvants apolaires ont été proposées. Ces hypothèses sont représentées de manière schématique sur la Fig. V. Dans le cas de l'eau, ce solvant peut interagir directement avec le réseau de liaisons H provoquant une diminution de la durée de vie de ces liaisons, ce qui donne une chute de T_g . De plus l'eau peut former deux liaisons H donc il serait possible qu'elle puisse former des ponts entre chaînes PA6,6. Dans le cas des molécules apolaires, ces solvants écarteraient les chaînes du PA6,6, ce qui étirerait les liaisons H du système et provoquerait une diminution des temps de vie de ces liaisons induisant une augmentation de la mobilité moléculaire. Une hypothèse qui expliquerait les effets de plastification différents observés pour les solvants aromatiques et aliphatiques serait que les molécules aromatiques, du fait de leur structure chimique et orientation dans l'espace, pourraient provoquer un écartement des chaînes PA6,6 plus important que les solvants aliphatiques. Finalement, concernant la série d'alcools, ces solvants seraient capables de plastifier le PA6,6 par un « double effet » qui combinerait des interactions directes avec les liaisons amide du fait de leur fonction hydroxyle et un effet de gonflement amené par leur chaîne alkyl.

Les cinétiques de sorption de l'eau, de l'éthanol, et du toluène ont ensuite été étudiées et elles sont montrées sur la Fig. VI. On observe que le toluène semble suivre à priori une cinétique Fickienne et que l'eau et l'éthanol ont un régime de sorption qui varie avec le temps. On observe que l'eau plastifie très rapidement le PA6,6, ce qui induit la diffusion du solvant dans un polymère plastifié selon une cinétique pseudo-Fickienne. Ensuite on observe

que l'éthanol plastifie aussi le PA6,6 mais plus lentement, ce qui conduit à la diffusion de ce solvant selon un régime anormal. Finalement le toluène ne parviendrait pas à plastifier le PA6,6 pendant la sorption, ce qui conduirait la diffusion de ce solvant selon un régime Fickien.

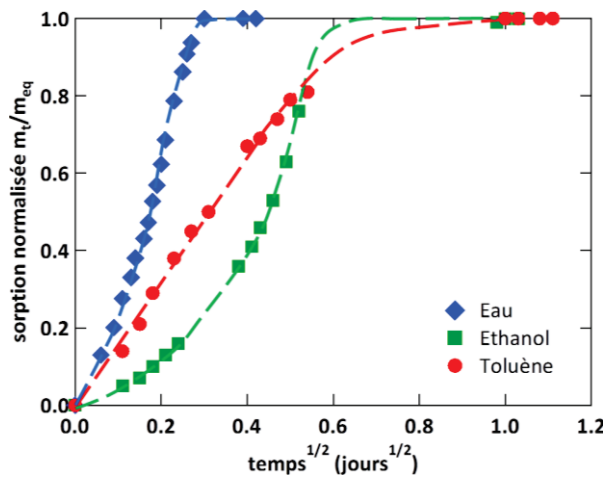


Fig. VI: Cinétiques de sorption de l'eau, de l'éthanol et du toluène dans du PA6,6 à 23°C.

Ensuite, l'effet de l'eau et de l'éthanol sur la structure de la phase cristalline du PA6,6 a été étudié par Diffraction des Rayons X. On observe comme montré sur la Fig. VII qu'après la sorption de ces solvants, la structure cristalline du polymère évolue vers la structure α , plus stable, caractérisée par un écartement plus grand des pics de Bragg correspondant aux plans cristallographiques (100) et (010). Il se peut que du fait que ces solvants augmentent la mobilité moléculaire de la phase amorphe, ils vont permettre à la phase cristalline de se réorganiser pour que cette phase évolue vers la structure la plus stable. Nous pourrions penser alors que si un solvant a un effet sur la phase amorphe il pourrait avoir aussi un effet sur la phase cristalline.

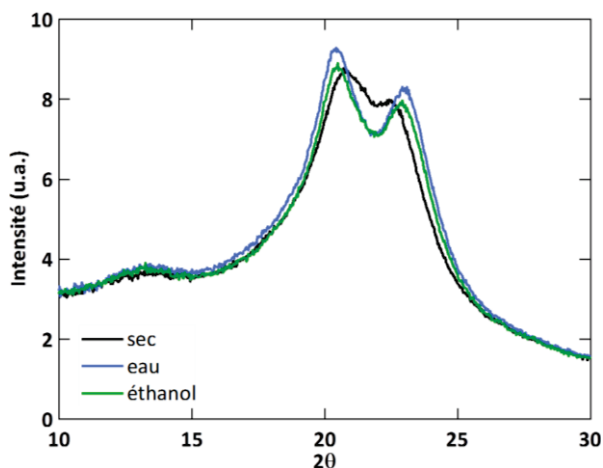


Fig. VII: Spectres de diffraction de Rayons X des films *NeatPA66* sec et après sorption d'eau ou d'éthanol.

De plus il serait intéressant de comparer si l'effet sur la mobilité moléculaire d'un échantillon sec induit par une augmentation de la température est similaire à celui provoqué par la présence de solvants dans le PA6,6.

On a étudié ensuite la sorption par le PA6,6 d'une série de mélanges ternaires composés d'éthanol, toluène et isooctane (EX). Ces mélanges sont fortement non idéaux et donc nous avons déterminé l'activité chimique de chacune des espèces dans ces mélanges car c'est l'activité qui pilote la sorption des solvants. Une GC-FID a été utilisée pour analyser la phase vapeur de ces mélanges et obtenir les activités chimiques d'éthanol, de toluène et d'isooctane. On observe que les activités chimiques de ces espèces sont relativement élevées dû aux effets répulsifs qui existent entre l'éthanol et les hydrocarbures, et ce surtout pour les mélanges contenant ces solvants en faible concentration comme montré sur la Fig. VIII.

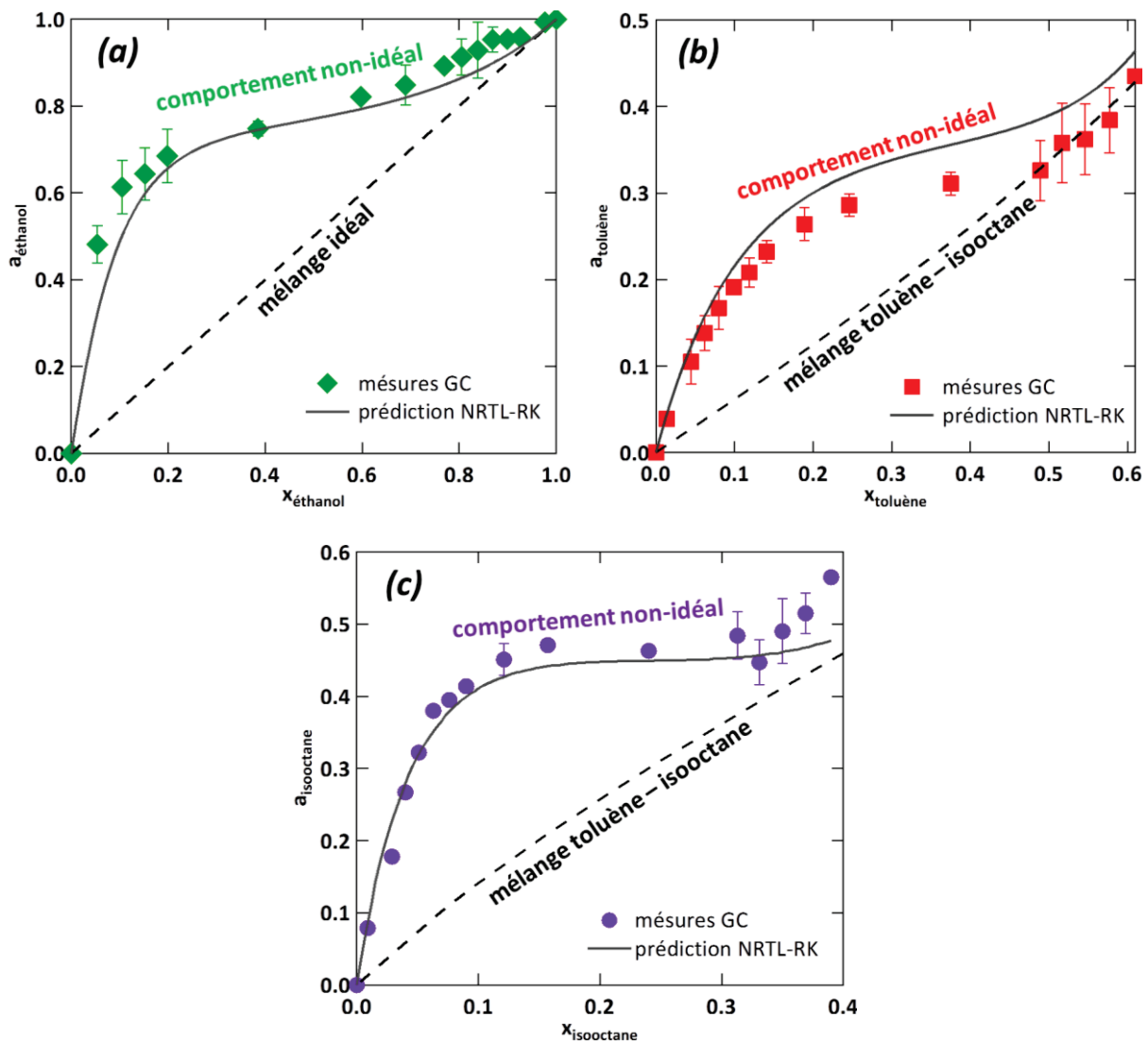


Fig. VIII: Activités chimiques a_i obtenues par GC-FID pour (a) l'éthanol, (b) le toluène, and (c) l'isooctane en fonction de la fraction molaire de ces solvants dans les mélanges EX. Les données obtenues sont comparées à des simulations faites par le modèle NRTL-RK ainsi qu'avec un mélange idéal (pointillés sur le graphe (a)) ou un mélange réel de toluène - isooctane (pointillés sur les graphes (b) et (c)).

Ensuite nous avons comparé la prise en éthanol des films PA6,6 en contact avec ces mélanges EX à la prise en éthanol pur pour les mêmes activités chimiques. On observe que les films en contact avec les mélanges absorbent plus d'éthanol comme montré en Fig. IX.

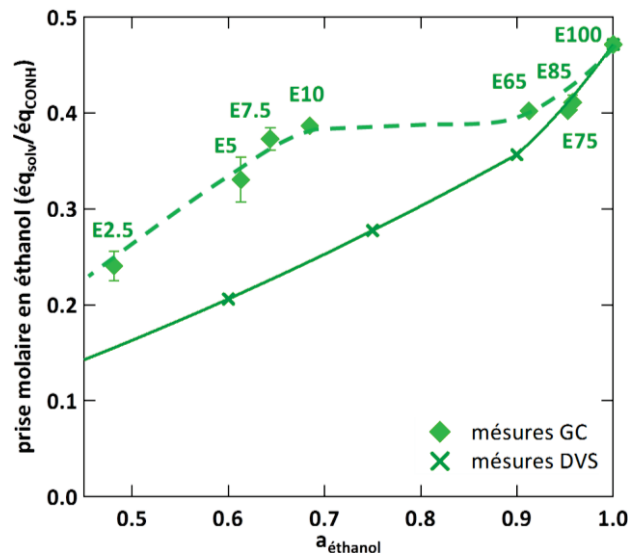


Fig. IX: Comparaison entre la fraction molaire en éthanol obtenue par DVS à plusieurs activités d'éthanol pur (croix et courbe pleine) et la fraction en éthanol pour les films PA66 en contact avec des mélanges EX mesurée par GC-FID (points et courbe pointillé), le tout tracé en fonction de l'activité en éthanol.

Ceci pourrait s'expliquer par un effet provoqué par le toluène, aussi présent dans les films, qui écarterait les chaînes PA6,6 et qui permettrait à plus d'éthanol d'être absorbé par le polymère. Finalement l'effet des mélanges EX sur la mobilité moléculaire du PA6,6 a été étudié. On observe que la chute de T_g provoquée par ces mélanges serait majoritairement due à la présence d'éthanol dans les échantillons et que, même si le toluène y est présent, ce solvant n'induit pas un effet plastifiant supplémentaire comme montré sur la Fig. X.

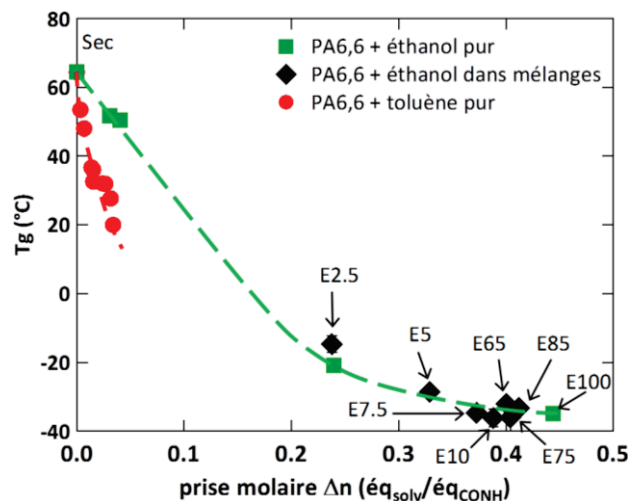


Fig. X: Chute de la T_g du PA6,6 en fonction de la fraction molaire Δn en éthanol pur (points verts), en éthanol dans les mélanges EX (points noirs), et en toluène pur (points rouges).

Chapitre IV. Propriétés des PA6,6 additivés ou modifiés chimiquement

Dans ce chapitre on a abordé l'effet de l'introduction d'un additif ou d'une modification chimique du PA6,6 sur la structure et les propriétés du polymère. Deux formulations additivées (10HA et 10LA), deux copolymères (HIA et AISLI) et un PA6,6 pur (REF) ont été étudiés.

L'effet des modifiants sur la phase cristalline du PA6,6 a tout d'abord été étudié. On observe que les échantillons 10LA et 10HA ont un taux de cristallinité X_C légèrement supérieur et que leurs températures de fusion T_f et de cristallisation T_C sont similaires à REF. Les échantillons HIA et AISLI ont des taux de cristallinité proches de REF mais leurs températures de fusion et cristallisation sont plus basses comme montré sur la Fig. XI. Il se peut que la présence de co-monomères dans le PA6,6 gêne dans une certaine mesure la cristallisation du polymère.

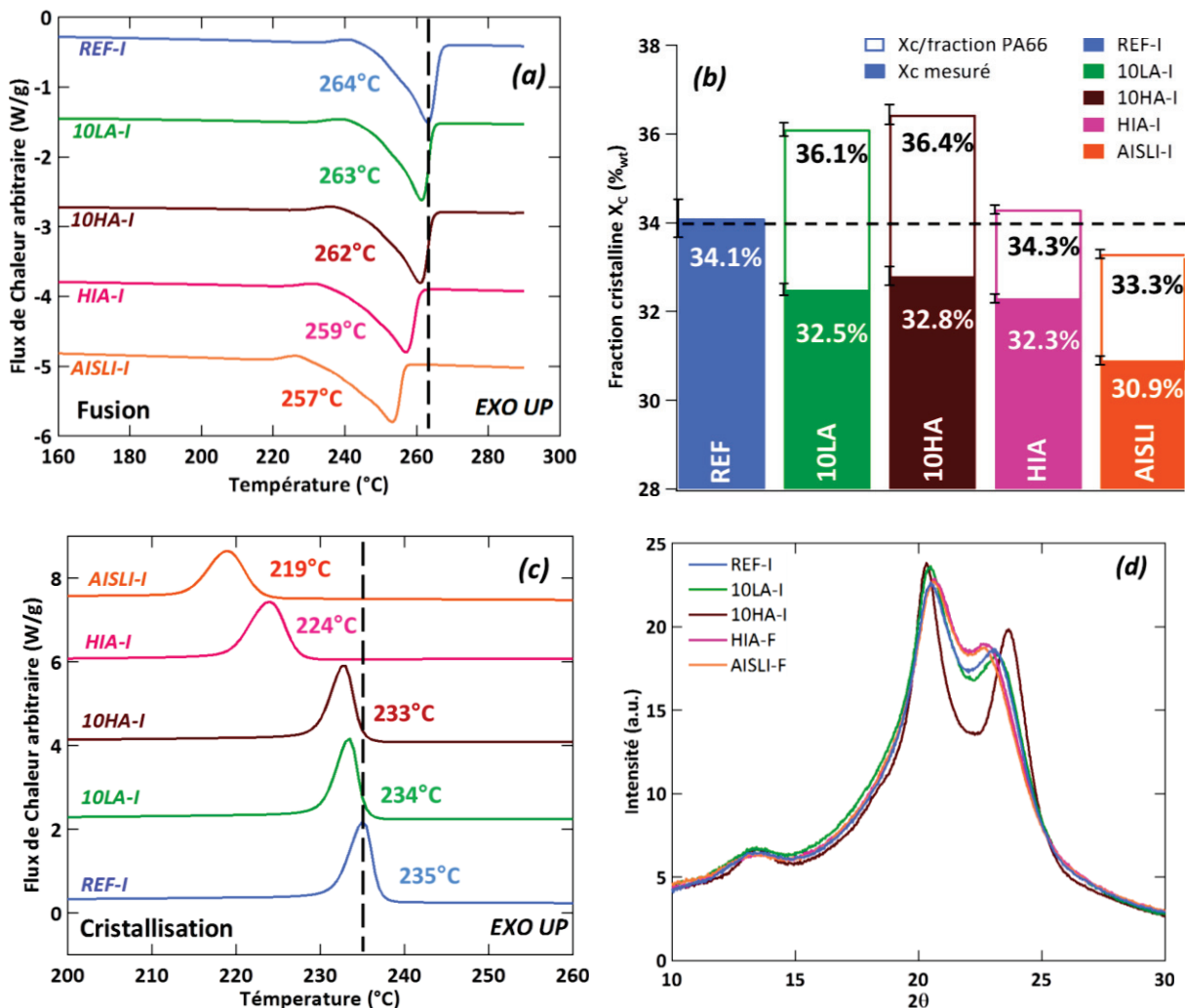


Fig. XI: Données sur la phase cristalline des échantillons REF, 10HA, 10LA, HIA, et AISLI: (a) thermogrammes DSC montrant la fusion, (b) fractions cristallines totales X_C (plein) et corrigées X_{C-PA66} (vide) obtenues par DSC, (c) thermogrammes DSC montrant la cristallisation et (d) spectres de diffraction de Rayons X.

L'effet des modifiants sur la structure cristalline a aussi été étudié par Rayons X. On observe que la présence d'additifs lauryl- et heptanaldéhyde induit une évolution de la phase cristalline du PA6,6 vers la structure α_1 plus stable. Par contre la présence de co-monomères 6HIA et 6AISLI induit une forme cristalline moins parfaite. Cet effet pourrait être lié aussi au procédé de mise en œuvre des échantillons car dans ce travail nous avons étudié des échantillons injectés et extrudés

Ensuite la mobilité moléculaire de la phase amorphe de ces échantillons a été étudiée par DSC, DMA et Spectroscopie Diélectrique. Les résultats sont montrés sur la Fig. XII. Il

semblerait que l'additif heptanaldéhyde et surtout l'additif laurylaldéhyde plastifient le PA6,6. Quant aux copolymères, les échantillons HIA et AISLI ont des T_g plus élevées que REF, ceci est dû au fait que ces copolymères possèdent des groupements aromatiques dans leurs chaînes et dans le cas de AISLI, les fonctions sulfonate de lithium peuvent interagir avec les groupements amide et former des liaisons de complexation plus fortes que les liaisons amide-amide, ce qui réduirait la mobilité moléculaire des chaînes. De plus l'ajout des motifs 6AISLI provoquerait une augmentation de la largeur du pic du module dynamique de perte E'' , ce qui pourrait être lié à une modification ou à une variation des interactions intermoléculaires dans le PA6,6 du fait de la présence de ce co-monomère.

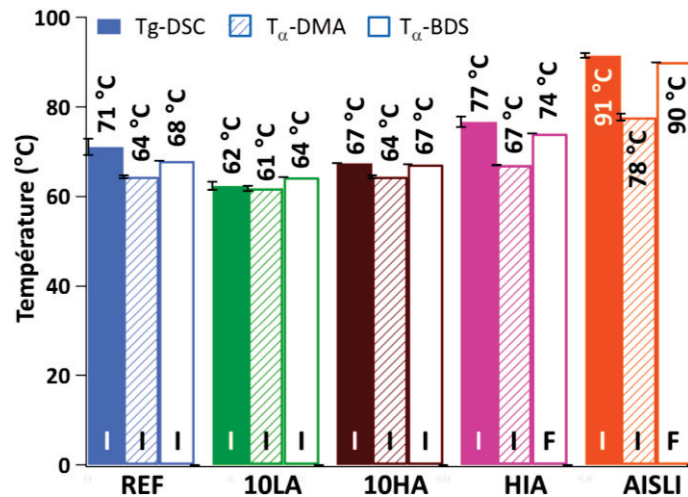


Fig. XII: T_g et T_α (1 Hz) obtenues par DSC, DMA, et BDS pour les formulations REF, 10HA, 10LA, HIA et AISLI sèches.

L'effet des modifiants sur les relaxations moléculaires du PA6,6 a aussi été étudié. On observe que les additifs lauryl- et heptanaldéhyde diminuent la température et l'énergie d'activation de la relaxation β , ce qui laisse penser que ces additifs peuvent interagir et perturber les fonctions amide du PA6,6. Finalement pour la relaxation γ aucun effet provoqué par des modifiants n'a été observé.

Ensuite les propriétés barrière des formulations modifiées sont évaluées. La sorption de l'eau, de l'éthanol et du toluène a tout d'abord été étudiée. On observe que l'eau est absorbée en quantités similaires par toutes les formulations sauf pour AISLI qui absorbe plus d'eau, probablement du fait de la présence des fonctions sulfonate de lithium qui sont très hydrophiles. Concernant l'éthanol, sa prise par 10LA, HIA et AISLI est supérieure à celle de REF, ceci s'explique du fait que les additifs ou co-monomères pourraient écarter les chaînes PA6,6, augmentant l'accessibilité des groupements amide et permettant à l'éthanol d'être absorbé davantage par ces formulations. Cette hypothèse est analogue à celle formulée dans le cas de la sorption des mélanges ternaires décrite précédemment. Par contre ce même effet n'a pas été observé pour 10HA, dont la prise en éthanol est légèrement inférieure à celle de REF. De plus, aucun effet des modifiants sur la prise en toluène n'a été observé, probablement parce que l'espace libéré par les modifiants n'est pas suffisamment grand pour permettre au toluène de s'absorber plus dans le polyamide.

Les cinétiques de sorption de l'eau, de l'éthanol et du toluène ont été étudiées. On observe que l'eau plastifie très rapidement les formulations PA6,6 et qu'elle diffuse selon un régime anormal. Dans le cas de l'éthanol, ce solvant plastifie aussi les formulations étudiées et il

diffuse de la même manière selon une cinétique anormale. De plus on observe que la cinétique de l'éthanol avant la plastification du polymère est Fickienne, et sa vitesse dépend de l'état de mobilité moléculaire de la formulation à l'état sec : si un polymère a une T_g initiale basse la diffusion d'éthanol dans ce matériau serait plus vite que pour un autre polyamide dont sa T_g initiale est plus élevée. Finalement le toluène ne parvient pas à plastifier les formulations pendant la sorption, ce qui conduirait à ce solvant à diffuser avec un régime Fickien.

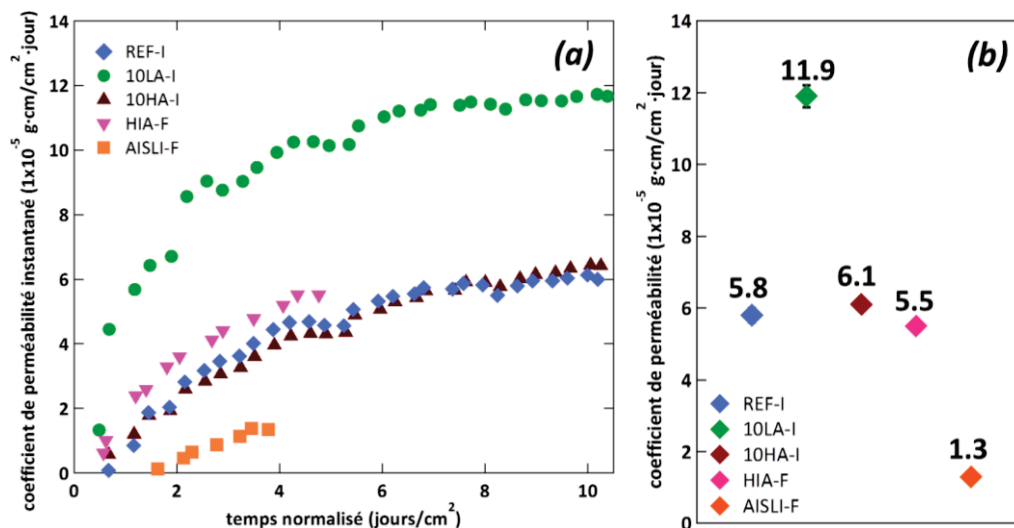


Fig. XIII: Coefficient de perméabilité de l'éthanol (a) instantané en fonction du temps normalisé par l'épaisseur des échantillons et (b) au régime permanent obtenus à 40°C pour les formulations modifiées.

La perméabilité à l'éthanol a ensuite été évaluée. Les résultats sont montrés sur la Fig. XIII. On observe que 10LA a le coefficient de perméabilité le plus élevé, AISLI a le plus bas, et les autres formulations ont des coefficients similaires. Ces différences pourraient s'expliquer par la cinétique de sorption et la sorption à l'équilibre de l'éthanol dans ces matériaux, car la perméabilité dépend de ces deux phénomènes. Dans le cas de 10LA, l'éthanol est plus absorbé par rapport à REF et sa cinétique de sorption dans cette formulation est la plus rapide, ce qui pourrait conduire à une perméation de ce solvant plus importante. Concernant AISLI, ce polymère absorbe plus d'éthanol que REF mais sa cinétique dans ce polymère est la plus lente, ce qui pourrait conduire à une faible perméation de l'éthanol. 10HA et HIA, qui ont des prises et cinétiques de sorption en éthanol similaires à REF, ont aussi des perméations proches.

L'effet des solvants sur la mobilité moléculaire de ces formulations a ensuite été étudié. On observe par Spectroscopie Diélectrique que l'eau a le même effet plastifiant dans toutes les formulations. Ceci est aussi observé pour l'éthanol. Concernant le toluène on observe que ce solvant a le même effet plastifiant dans toutes les formulations sauf pour AISLI, dont l'effet est deux fois plus important. Ceci s'expliquerait du fait que le toluène serait capable de perturber les interactions amide-sulfonate d'AISLI, ce qui induirait un effet plastifiant supplémentaire.

Ensuite nous nous sommes intéressés aux propriétés mécaniques en traction de ces échantillons à l'état sec. Dans le cas du module de Young E et du module dynamique élastique E' de ces échantillons, tracé en fonction de la température, on observe sur la Fig.

XIVa (E') que les valeurs du module dans le plateau vitreux dépend des interactions intermoléculaires entre le PA6,6 et les modifiants. Les co-monomères 6HIA et 6AISLI rigidifient le PA6,6 par ajout des fonctions aromatiques et des interactions fortes, ce qui augmenterait le module. Les additives phénoliques sont capables de plastifier le PA6,6 par des effets stériques, ce qui diminuerait le module du polymère. Concernant la contrainte au seuil σ_Y de ces échantillons, on observe que lorsque celle-ci est comparée à $T-T_g$, une courbe maitresse est obtenue comme montré sur la Fig. XIVb. Ceci qui voudrait dire que pour ces échantillons la contrainte au seuil σ_Y est similaire pour un niveau de mobilité moléculaire donné.

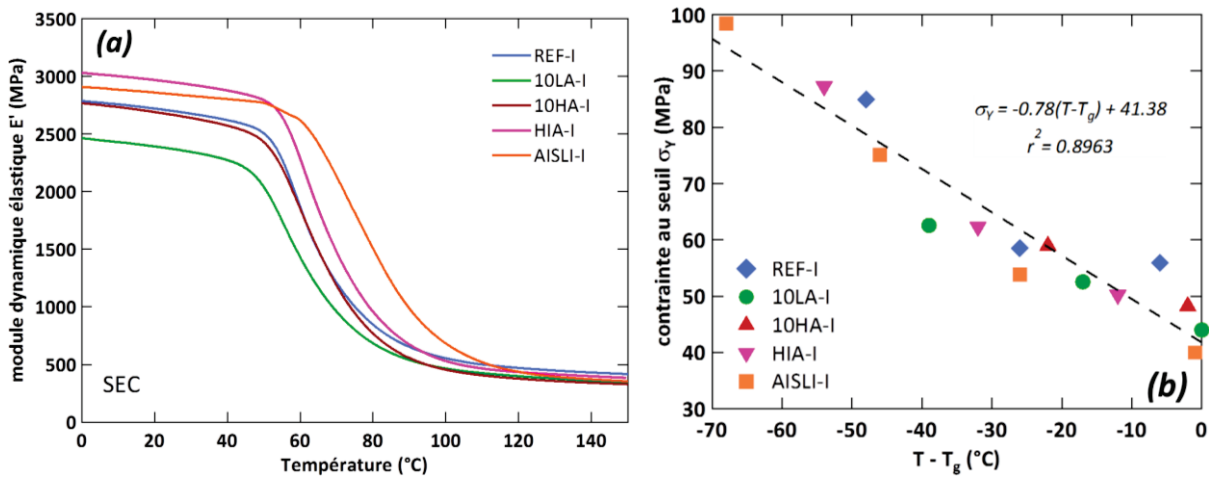


Fig. XIV: (a) module dynamique élastique E' en fonction de la température et (b) contrainte au seuil σ_Y en fonction de $T-T_g$ pour les échantillons modifiés à l'état sec tracés.

Nous nous sommes ensuite intéressés à la résistance en choc de ces échantillons à l'état sec mais aussi à deux états de conditionnement en eau (HR50 et HR100) afin d'obtenir différents états de mobilité moléculaire. Les températures de transition-fragile ductile $T_{F/D}$ ont été obtenues par des essais de choc Charpy instrumentés. Les valeurs de $T_{F/D}$ obtenues ont été comparées à la T_g mesurée par DSC pour ces échantillons comme montré sur la Fig. XVa.

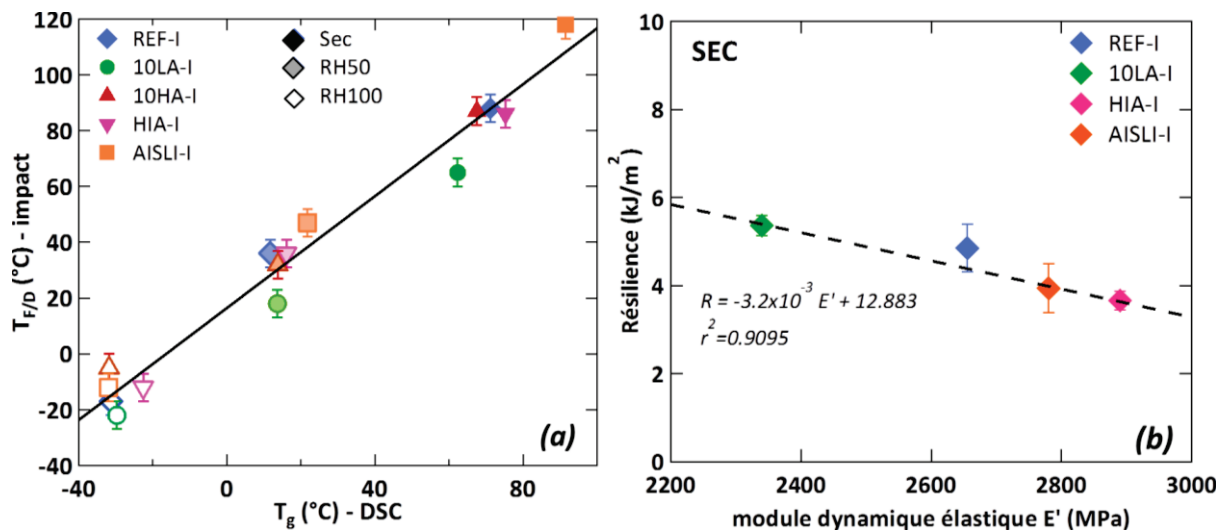


Fig. XV: (a) Température de transition fragile-ductile $T_{F/D}$ tracée en fonction de la T_g pour les échantillons modifiés secs et conditionnés à HR50 et HR100 et (b) résiliences au plateau fragile ($T - T_{F/D} = -30^\circ\text{C}$) pour les échantillons secs en fonction du module dynamique élastique E' à l'état vitreux.

On observe sur la Fig. XVa qu'il y a une globalement corrélation linéaire entre la $T_{F/D}$ et la T_g , ce qui voudrait dire que pour une formulation polyamide donnée la température de transition fragile-ductile est déterminée principalement par la mobilité moléculaire de cette formulation polymère. On observe que les valeurs de $T_{F/D}$ pour 10LA sont inférieures à celles des autres formulations, ceci serait dû à la probabilité que le laurylaldehyde serait capable de former des micelles dans le PA6,6. Ces micelles agiraient comme des concentrateurs de charge, ce qui conduirait à une meilleure distribution de l'effort mécanique pendant le choc et donc à une amélioration de la tenue à l'impact. Finalement, la relation entre module mécanique et résilience au plateau fragile a été étudié comme montré en Fig. XVb. On observe une dépendance linéaire entre la résilience et le module : lorsque le module mécanique augmente la résilience diminue.

Conclusion

Dans ce travail une meilleure compréhension de l'effet de la phase amorphe du PA6,6 sur les propriétés barrière et mécaniques a été développée. Nous avons pu décrire comment la nature d'un solvant conditionne sa sorption et son effet plastifiant dans le PA6,6. On a aussi observé que la nature et les interactions interchaînes de la matrice polymère conditionnent aussi la prise en solvants. De plus, une approche thermodynamique a été proposée pour étudier et comprendre la sorption de mélanges ternaires éthanol-toluène-isooctane et leur effet plastifiant dans le PA6,6. Grâce à cette approche nous avons pu mieux comprendre le comportement thermodynamique de ces mélanges et l'effet de ce comportement sur leur sorption et leur effet plastifiant dans le PA6,6. On a aussi montré que les propriétés mécaniques du PA6,6 dépendent ou sont liées à l'état de mobilité moléculaire de la phase amorphe de ce polymère. La partie applicative de la thèse, qui était l'obtention des formulations PA6,6 pour réservoirs à essence ayant des bonnes propriétés barrière aux solvants tout en gardant une bonne tenue aux impacts, n'est pas vraiment aboutie à ce stade. On observe qu'une formulation qui a des bonnes propriétés barrière n'a pas une tenue en choc adéquate et vice-versa. Les résultats obtenus dans ce travail concernant l'effet des solvants et des modifiants sur les propriétés barrière et mécaniques du PA6,6 nous permettrait de mieux cibler une éventuelle modification structurale de ce polymère pour arriver à une formulation ayant un bon compromis entre ces deux propriétés.

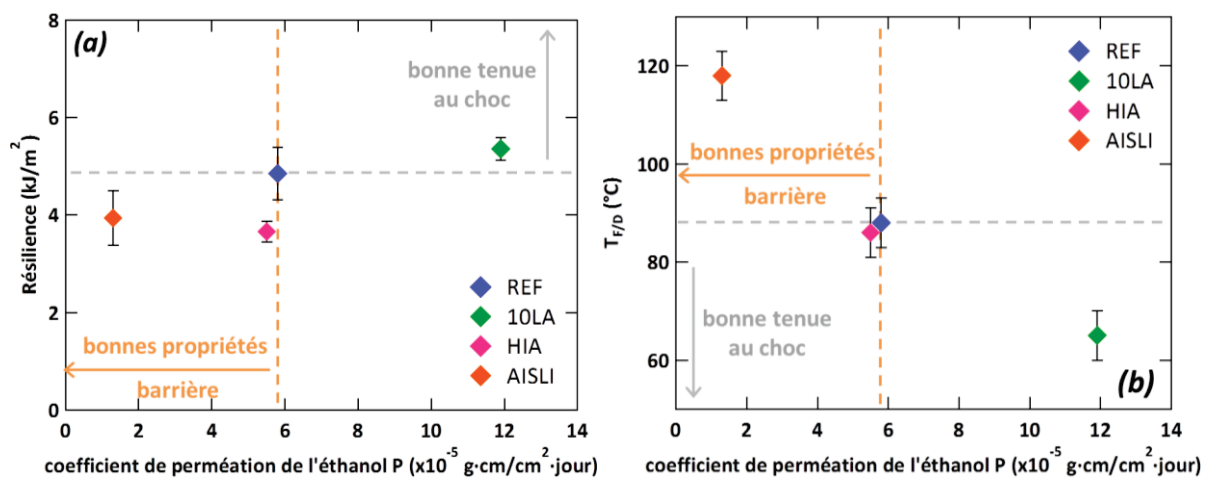


Fig. XVI: (a) Résilience au plateau fragile et (b) $T_{F/D}$ des échantillons secs en fonction du coefficient de perméation de l'éthanol pour les formulations étudiées.